Age and geochemistry of the Staré Sedlo and Mirotice complexes, Bohemian Massif, Czech Republic

by

Jan Košler

This thesis is submitted for the degree of Doctor of Philosophy

The University of Glasgow

June 1993

ProQuest LLC.
789 East Eisenhower Parkway
P.O. Box 1346
Ann Arbor, MI 48106 – 1346

DECLARATION

The material presented in this thesis summarises the results of three years of research carried out in the Department of Geology and Applied Geology of Glasgow University under the supervision of Professor Donald R. Bowes and Professor Bernard E. Leake. This study is based on my own independent research and any previously published or unpublished results of other researchers used in this thesis have been given full acknowledgement in the text.

14th June 1993

ACKNOWLEDGEMENTS

This thesis is the culmination of three years of research carried out in the period 1990 - 1993 from Department of Geology and Applied Geology at Glasgow University to a distance of 1200 miles in southern Bohemia. This research has been made possible due to the financial support from University of Glasgow and the ORS scheme awarded by Committee of Vice-Chancellors and Principals of the Universities of the United Kingdom, for which I am grateful.

I would like to acknowledge the support and guidance of both my supervisors Professor Donald Bowes and Professor Bernard Leake who have been a constant source of inspiration and encouragement while working on this thesis. I am also grateful to Drs Tim Dempster and Colin Farrow who were always generous with their time and advice. At the SURRC I wish to give my special thanks to Dr. Margaret Aftalion for her "Lectures in zirconology" and Dr. Graeme Rogers, not only for teaching me "Principles of neodymium model ages", but also for reading over the isotopic part of the thesis.

I have received kind and invaluable help from Peter Ainsworth, John Ball, George Bruce, Bob Cumberland, Jim Gallagher, Vincent Gallagher, John Gilleece, Sheila Hall, Donald Herd, Joss Jocelyn, Jim Kavanagh, Anne Kelly, Bob MacDonald, Murdoch MacLeod, Douglas Maclean, Roddy Morrison, Tricia Park, Tracy Shimmield and Dougie Turner. Without their expertise the thesis could not ever have been accomplished.

In Prague I would like to thank to Drs Emil Jelínek and Petr Jakeš for reading first draft of parts of the thesis. I also wish to thank to Dr. Magda Pačesová, Zdena Rýdlová and Dr. Martin Mihaljevič for their encouragement and support and for making the facilities of Charles University available to me during my return visits to Prague.

I am grateful to the postgraduate community in Glasgow, particularly Mehmet Arslan, John Hughes, Gary Kitchener and Vojta Janoušek for their companionship.

Above all I thank to my parents and my wife Alena for encouragement, support and patience during the last three years.

CONTENTS

1. INTRODUCTION

1.1 Regional geological setting

Within the eastern Hercynides in the Bohemian Massif of the central and southern Czech Republic there are metamorphic complexes with the gross form of roof pendants in the late Hercynian granitoids of the Central Bohemian Pluton. They consist of meta-sedimentary and meta-igneous (both the meta-volcanic and meta-plutonic) rocks, the former making up most of the Islet zone. Two of the roof pendants, made up largely of deformed granitoid rocks, are referred to as the Staré Sedlo and Mirotice complexes (30 and 300 km^2; *Svoboda, 1966*) and are located ca 80 km S of Prague (Fig.1.1). It is the nature, geochemistry, petrogenesis and age(s) of these complexes that are the object of the present investigations. The evidence for their protoliths being igneous indicated the possibility of elucidating igneous history before the emplacement of the Central Bohemian Pluton in this part of the Bohemian Massif while the variety of previous interpretations, (see Par.1.2), none of which could be sustained on the basis of existing knowledge, pointed to the possibility that geochemical and isotopic study might not only solve several aspects of the evolution of this part of the Bohemian Massif but also provide solutions that would have wide application in the region.

1.1.1 Bohemian Massif

The Bohemian Massif is the largest exposed part of the eastern Hercynides (E - W-trending mid to late Palaeozoic orogenic belt) in central Europe. Other parts of this orogen can be followed to the W and SW, to Austria, Germany, France, Spain and southern England (Fig.1.2). It formed as a result of closure of the Prototethys Ocean and a collision of Baltica and Gondwana during the Hercynian orogeny (in early Devonian to early Carboniferous times) but it also contains older pre-Hercynian relics. The details and mechanism of the collision are yet to be determined as is also the precise timing of individual events (for discussion see *Patočka, 1989*). The internal structure of the orogen shows a number of individual zones which differ from one another in crustal thickness, stratigraphy, composition and structural and metamorphic styles (*Ellenberger and Tamain, 1980*). The Moldanubian zone in which the

Staré Sedlo and Mirotice complexes occur is dominated by polyphase deformed and metamorphosed sediments including those of the Moldanubian and Teplá-Barrandian assemblages (Figs 1.1a; 1.2).

The Bohemian Massif is bounded to the NW by the Thüringer Wald marginal fault and the Franconian, Keilberg and Danubian faults. In the NE its boundary is formed by the Odra fault and in the N by the Triassic and younger Fenosarmatian platform sediments. In the E and SE the margin is the Moldanubian - Ramzovian - Nýznerov Thrust which separates the Bohemian Massif from its Cadomian basement. In the S and SW are the pre-platform complexes of the Bohemian Massif bounded by the Miocene sediments of the Alpine foredeep.

1.1.2 Central Bohemian Pluton

The Central Bohemian Pluton (ca 3200 km^2 at present erosion level) is a NE - SW-trending elongate late Hercynian post-tectonic composite granitoid body. It consists of at least four petrographically and geochemically different rock suites and probably more than 25 separate plutons (types). The emplacement of at least some intrusions at 331 ± 4 Ma (Blatná granodiorite, Rb - Sr whole-rock; *van Breemen et al., 1982*) marks the end of the Bretannian phase in the eastern part of the European Hercynides. The four main rock suites are: tonalite suite, granite - granodiorite suite, durbachite (i.e. melanocratic variety of syenite; cf. *Holub, 1989; Le Maitre, 1989*) suite and gabbro - diorite suite. Chemically the pluton has a calc-alkaline character with the durbachite suite and some of the gabbro - diorite suite intrusions having shoshonitic affinities (*Bowes and Košler, 1993*). Although the evidence for operation of processes like magmatic differentiation, mixing or contamination by crustal (mostly sedimentary) material have previously been reported from various parts of the pluton (e.g. *Vejnar, 1973; Mísař et al. 1983; Bendl and Vokurka, 1989*) the calc-alkaline and shoshonitic suites are likely to have originated in different tectonic environments. While the tonalite, granite - granodiorite and gabbro - diorite suites have been interpreted as representing the products of Andean-type subduction (i.e. a compressional regime; *Palivcová, 1984*), the ascent of K-rich mantle-derived magma and its differentiation in the crust (i.e. variations of compression and extension regimes) are likely to have been the case for durbachite and some members of gabbro - diorite suites (*Bowes and Košler, 1993*). The age relations between the rock suites of the Central Bohemian Pluton are not yet clear but while at least some of the durbachite suite

intrusions are younger, several intrusions of the tonalite suite are older than the ca 331 Ma granite - granodiorite suite (*Andrusov, 1932; Kodym, 1956; Holub and Žežulková, 1978*).

The NE - SW elongation of the Central Bohemian Pluton (CBP) suggests its emplacement in between the rocks of the Moldanubian and Teplá - Barrandian assemblages was tectonically controlled. This however does not hold for the intrusions of durbachite and some of the intrusions of gabbro - diorite suites whose isometric cross-sections at the present erosion level suggest a substantial proportion of ballooning. The elongation of the CBP and the proportion of the pluton-related dyke rocks within it, as well as the spatial relations of granitoid intrusions in its southeastern part, suggest an overall tongue-like shape (*Kettner, 1930b*) with the upper tip curving over towards the SE.

In the NW the Central Bohemian Pluton has a sharp contact with sedimentary sequences of the late Proterozoic and early Palaeozoic rocks of the Teplá - Barrandian assemblage in which a narrow contact aureole evolved. In the N the pluton is covered by the late Carboniferous (Stephanian) sediments. The southeastern contact zone of the CBP with the metasediments of the Moldanubian assemblage (mostly paragneisses) is much wider than the north-western one with various types of migmatites and mixed rocks being present. Along this contact some of the granitoids of the CBP show a planar fabric. The metasedimentary and metavolcanic xenoliths and roof pendants preserved within the granitoids of the CBP (Islet zone; cf. *Svoboda, 1966*) are lithologically and geochemically similar to the rocks of the Teplá - Barrandian late Proterozoic - early Palaeozoic assemblage present along the northwestern margin of the Central Bohemian Pluton.

The time constraints for the crystallization age of the Central Bohemian Pluton are:

(1) the pluton caused contact metamorphism of Cambrian and late Proterozoic sediments of the Teplá - Barrandian assemblage and early to mid Devonian sediments of the Islet zone (*Svoboda, 1966; Chlupáč, 1989*), and

(2) the northeastern part of the pluton is covered by Stephanian basal conglomerates (*Svoboda, 1966*).

This constrains the range for the emplacement of most of the intrusions of the Central Bohemian Pluton as being ca 380 - 295 Ma although both the Rb - Sr and K - Ar data suggest the peak of plutonic and thermal activity in this part of the Bohemian Massif at ca 340 - 310 Ma (cf. *van Breemen et al., 1982*; see also review of K- Ar data in *Zoubek, 1988*).

1.1.3 Islet zone

The Islet zone (cf. *Svoboda, 1966*) consists of 11 separate metasedimentary and metavolcanic roof pendants and numerous blocks - relics of the roof of the Central Bohemian Pluton. As documented by fossils (*Štorch et al., 1984; Chlupáč, 1986*) and lithological and geochemical analogies with the sediments of the Teplá - Barrandian assemblage (*Košler, 1988; Chlupáč, 1989*), the metasedimentary sequence ranges from the late Proterozoic to early Devonian (Daleian) with so far no evidence existing for the occurrence of Cambrian rocks. The rock types present are biotite- and cordierite-bearing hornfelsed schists and hornfelses, metapsammites, quartzites, metaconglomerates, erlans (i.e. calc-silicate vesuvianite-bearing rocks) and marbles. Most metasedimentary and metavolcanic rocks of the Islet zone (if not intensely hornfelsed) display a NE - SW- to NNE - SSW-trending foliation which varies in dip and which in places is mylonitic (*Rajlich, 1988*). Intensive late Hercynian contact thermal metamorphism (amphibole to pyroxene hornfels facies) and, to certain extent also chemical, overprinting associated with various intrusions of the Central Bohemian Pluton, could conceal the possible expressions of a Cadomian metamorphic event such as that documented from various parts of the Bohemian Massif (*Zoubek, 1988*). The relationships of the metasedimentary and metavolcanic rocks of the Islet zone to the nearby Staré Sedlo and Mirotice gneiss complexes is not clear because of paucity of exposure. However like the mylonitic foliation of gneisses, the schistose fabric they display is cross-cut by the igneous masses that bound them.

1.1.4 Staré Sedlo and Mirotice complexes

The Staré Sedlo and Mirotice complexes form separate NE-trending bodies surrounded by granitic intrusions of the Central Bohemian Pluton (Fig.1.1b). Both complexes consist dominantly of strongly foliated biotite- and amphibole-bearing mylonite gneisses whose mineralogical, chemical and isotopic compositions are consistent with them having an igneous protolith (orthogneisses; see Chapters 2, 4, 8). The gneisses are cut by tabular minor intrusions of foliated amphibolite (Fig.1.3a) and meta-aplite that are 0.2 - 10 m and up to 0.5 m thick, respectively. While the intrusions of amphibolite are mostly parallel to the foliation of their host gneisses, no such relation holds between the gneisses and the

intrusions of meta-aplite. The foliation in the rocks of both complexes is cross-cut by igneous masses of the surrounding granitoids of the CBP as demonstrated at the contacts of gneisses of the Staré Sedlo complex exposed in the Vltava river valley ca 2 km S of Staré Sedlo (Fig.1.3b).

In the NW, W and S, the Staré Sedlo complex has a sharp contact with granites and granodiorites (Kozárovice type) which enclose numerous xenoliths of the gneisses (Fig.1.3c). In the E and SE, the gneisses are bounded by an intrusion of durbachite (Čertovo břemeno type) which also cross-cuts their foliation. The NE margin of the complex adjacent to a durbachitic intrusion is not exposed although the interpretation of *Waldhausrová et al. (1986)* suggests it is a tectonic contact. In the N the Staré Sedlo complex is bounded by early Palaeozoic (Ordovician and Silurian) metasediments of the Sedlčany - Krásná Hora islet. Further to the NE the gneisses of the Staré Sedlo complex are exposed in the Lašovice quarry and they are likely to extend further to the NE underneath the late Proterozoic and early Palaeozoic metasediments of the Sedlčany - Krásná Hora islet (*V. Kachlík, pers. com.*).

The Mirotice complex consists of two main parts (Fig.1.1b). The northern part has intrusive contacts with granodiorite (Blatná type) and tonalite (Sázava type) in the NW and N, respectively, while in the SE it is bounded by late Proterozoic metasedimentary and metavolcanic rocks of the Mirovice islet. The southern part has sharp contacts with granodiorite (Blatná type) in the W, S and SE and tonalite (Sázava type) in the NE. In the N it is bounded by Palaeozoic metasediments of the Mirovice islet. Due to the paucity of exposure, no age and genetic interpretations can be made about the relations between the rocks of the Mirotice complex and surrounding units. However on the basis that the age of the granodiorite (Blatná type) which bounds the complex (331 ±4 Ma, Rb - Sr whole-rock; *van Breemen et al., 1982*) is similar to that of the other parts of the composite pluton, the rocks of both the Staré Sedlo and Mirotice complexes and the metamorphic fabric they display, are pre-Visean in age.

1.2 Previous investigations

Previous investigations of the roof pendants of the Central Bohemian Pluton and especially of the Staré Sedlo and Mirotice complexes have mostly been linked to the geological mapping. Although the area has been mapped in the past several times (*Jokély, 1855; Andrusov, 1932; Urban, 1932; Kodym and Suk, 1958; Kodym et al., 1963*) no evidence on the age and affiliations of the meta-plutonic units has

been given. New 1:25000 geological mapping has been recently carried out by the Czech Geological Survey but only part of the results has been published (*Tonika et al., 1980; Žežulková et al., 1985; Waldhausrová et al., 1986*). The importance of the study and understanding the affiliations of the roof pendants for the interpretation of granitoids of the Central Bohemian Pluton and the overall evolution of this part of the Bohemian Massif has been pointed out by *Kettner (1930a)*. A contact of metasediments of the Sedlčany - Krásná Hora islet with gneisses of the Staré Sedlo complex E of Lašovice has been reported by *Mrázek (1963)*. However the lack of palaeontological or other evidence for the age of these metasediments did not allow any constraints to be placed on the intrusion age of the protolith of the gneisses.

In the past both the Staré Sedlo and Mirotice complexes have generally been interpreted as an integral part of the Islet zone or other crystalline units of the Bohemian Massif although they also have been interpreted as a part of a magmatic suite associated with the Central Bohemian Pluton. The following summarizes the interpretations that have been made concerning the age of formation and the regional affiliations of the rocks of both complexes.

(1) The gneisses represent rocks of the Moldanubian assemblage into which the Central Bohemian Pluton was emplaced (*Zelenka, 1929*). This interpretation implies that the protolith of the gneisses is either late Proterozoic and pre-Cadomian or that another hitherto unrecognized group of rocks is present.

(2) The gneisses represent regionally metamorphosed Cadomian granitoid intrusions and related acid to basic dyke rocks with superimposed contact metamorphism related to the emplacement of Central Bohemian Pluton (*Waldhausrová et al., 1986*).

(3) The gneisses represent an early phase of Hercynian plutonism and the fabric they display is the result of solidification under pressure associated with the emplacement of other masses of the Central Bohemian Pluton (*Kettner, 1930a; 1930b*).

(4) The gneisses correspond to lithologically similar rocks of the Kutná Hora - Svratka complex of the Bohemian Massif 80 km to the NE (*Kodym* in *Mísař et al., 1983*).

Each of these interpretations has difficulties associated with it which have precluded general acceptance. The rocks of the Moldanubian assemblage are dominantly metasedimentary, most of the intrusions of the Central Bohemian Pluton are not strongly foliated, there is no widespread regional metamorphism and penetrative foliation formation associated with post-tectonic granite emplacement, and the age and

affiliations within the Bohemian Massif of the Kutná Hora - Svratka Complex are yet not known. In addition no diagnostic or genetic mineralogical, structural, geochemical or isotopic characteristics of the rocks of the Staré Sedlo and Mirotice complexes have been presented to support any of these interpretations.

1.3 Review of existing geochronological framework

Several attempts to summarize geochronological data from the Bohemian Massif have been made in the past (*Dornsiepen, 1978; Bergner et al., 1988; Dudek et al., 1988*). However most of the published geochronological data are not linked to specific geological events using structural relationships etc. and as authors variously do not record the petrography of studied samples, decay constants used for age calculations or realistic error estimations for both the measured and calculated isotopic ratios and the calculated age, previous results and their interpretations have to be evaluated critically. For the purpose of this review, only the ages based upon reliable data and relevant to the present study are taken in account.

(1) The time constraints for the emplacement of most intrusions of the Central Bohemian Pluton are 380 - 295 Ma (see 1.1.2), and the emplacement of, and the formation of the mylonitic foliation in the rocks of the Staré Sedlo and Mirotice complexes was before 331 Ma, the age of Blatná granodiorite (*van Breemen et al., 1982*). Therefore the focus here is particularly on units from which the ages of 331 Ma and older have been reported and special interest is paid to the period c. 380 - 330 Ma as this is likely to represent any time of overlap of the activities in the Staré Sedlo and Mirotice complexes and in the Central Bohemian Pluton.

(2) As many of the K - Ar and Ar - Ar dates reported previously from this part of the Bohemian Massif are clearly influenced by the late Hercynian magmatic and tectonothermal events, it is the Sm - Nd, Rb - Sr, U - Pb and Pb - Pb data which are considered to be more reliable. Even so, much care is needed with the interpretation of Rb - Sr whole-rock data as illustrated by the discussion and interpretations of *van Breemen et al. (1982)*.

(3) When necessary, ages were recalculated according to the decay constants as recommended by *Steiger and Jäger (1977)* and the age uncertainties are quoted at 2 sigma level.

(4) The time scale used is that given in the 1989 Global Stratigraphic Chart of the International Union of Geological Sciences issued as a supplement to *Episodes* 12 (2), June 1989.

The available Sm - Nd, Rb - Sr, U - Pb and Pb - Pb geochronological data from the Moldanubian zone of the Bohemian Massif do not yield a simple explanation for the succession of events in this part of the Hercynides but certain groupings are representative of specific sets of events (see Table 1.1). These data largely reflect Hercynian plutonic and tectonothermal activity with development of at least some eclogites presumed to be associated with subduction of oceanic crustal material that took place in more than one phase of tectonism (380 - 370, 345 - 335 and ?325 Ma). The earliest of these events overlaps, at least in part, the time of volcanism in the Moldanubian assemblage while the 345 - 335 Ma event is temporally associated with c. 350 - 335 Ma granulite - high grade metamorphism which was followed by ductile deformation at c. 335 - 330 Ma and by a period of extensive granitoid plutonism (c. 330 - 300 Ma) that probably continued to c. 285 Ma (*Arnold and Scharbert, 1973*). The presence of cobbles that have been correlated with gneisses and granulites of the Moldanubian zone in mid Visean conglomerates on the eastern margin of the Bohemian Massif suggest a quick uplift, exhumation and erosion (of at least some parts of the Moldanubian zone) which were synchronous with thrusting at 340 - 335 Ma (*Štelcl, 1960*). Evidence for the Cadomian episode in the eastern part of the Bohemian Massif is unequivocal with the time span bridging the Proterozoic - Palaeozoic boundary and ending in early Cambrian times. There is also evidence for igneous and tectonothermal activity in early Ordovician times which had apparently only limited extent and expression which is consistent with the interpretation of post-Cadomian - pre-Hercynian (early Cambrian - late Devonian) period being one during which there was mainly destructive activity (*Bowes, 1992*). However the isotopic data are indicative of a considerable history of plate tectonic, igneous and tectonothermal activity during late Devonian and early Carboniferous times, i.e. during the period before the emplacement of the Central Bohemian Pluton (c. 330 Ma) which cross-cuts the gneisses of the Staré Sedlo and Mirotice complexes.

When considered in the light of the above data, some of the K - Ar and Ar - Ar data can be linked to particular geological events. For example c. 330 Ma hornblende Ar - Ar cooling ages from amphibolites of meta-ophiolite complexes of the Bohemian Massif (*Macintyre et al., 1992*) would be consistent with early Carboniferous metamorphism followed by thrusting and uplift. In addition the same authors record a time of metamorphic recrystallization during mid Ordovician times (464 ± 5 Ma).

However the lack of correspondence in other cases and the large spread of ages presented means that much of the interpretation based on K - Ar and Ar - Ar studies needs to be treated with caution.

Table 1.1
Previously published geochronological data from the Moldanubian zone in the Bohemian Massif

Geological unit	Age [Ma]	Dating method	Analyzed rock	Interpretation	Reference
Cadomian episode					
Brno Pluton	584±5	U-Pb (zircon)	diorite	magmatic age	4
Thaya Pluton	551±6	Rb-Sr (WR)	granodiorite	magmatic age	3
Presumed plutonism in Cadomian episode					
Teplá-Barrandian assemblage	570	U-Pb (zircon)	rhyolite cobble	magmatic age	16
Teplá-Barrandian assemblage	594	U-Pb (zircon)	granite cobble	magmatic age	16
Tectonothermal activity in Cadomian episode					
Gföhl gneiss	570±60	Rb-Sr (WR)	gneiss	metamorphic age	4
Igneous activity in early Ordovician					
Mariánské Lázně complex	496±1	U-Pb (zircon)	gabbro pegmatite	magmatic age	13
Teplá-Barrandian assemblage	491±5 *)	Rb-Sr (WR)	dacite-rhyolite	magmatic age	2
Křizanovice Pluton	483±91	Rb-Sr (WR)	tonalite	magmatic age	6
Tectonothermal activity in early Ordovician					
Moldanubian assemblage	486±11 *)	Rb-Sr (WR)	granulite	metamorphic age	1
Eclogite and garnet pyroxenite formation					
Kutná H.-Svratka complex	377±20	Sm-Nd (Gt-Cpx-WR)	eclogite	metamorphic age	15
Moldanubian assemblage	373±7	Sm-Nd (Gt-Cpx-WR)	garnet pyroxenite	metamorphic age	14
Gföhl nappe	370±15	Sm-Nd (Gt-Cpx-WR)	garnet pyroxenite	metamorphic age	11
Gföhl nappe	344±10	Sm-Nd (Gt-Cpx-WR)	garnet pyroxenite	metamorphic age	11
Gföhl nappe	342±9	Sm-Nd (Gt-Cpx-WR)	eclogite	metamorphic age	15
Gföhl nappe	341±7	Sm-Nd (Gt-Cpx-WR)	eclogite	metamorphic age	14
Kutná H.-Svratka complex	338±6	Sm-Nd (Gt-Cpx-WR)	eclogite	metamorphic age	14
Gföhl nappe	336±16	Sm-Nd (Gt-Cpx-WR)	eclogite	metamorphic age	15
Gföhl nappe	324±5	Sm-Nd (Gt-Cpx-WR)	eclogite	metamorphic age	14
Gföhl nappe	323±7	Sm-Nd (Gt-Cpx-WR)	eclogite	metamorphic age	15
Volcanic and tectonothermal activity in late Devonian					
Moldanubian assemblage	367+18/-20	U-Pb (zircon)	paragneiss	metamorphic age	7
Moldanubian assemblage	367±8	U-Pb (zircon)	granulite	magmatic age	17
Moldanubian assemblage	362±9	U-Pb (zircon)	granulite	magmatic age	17
Tectonothermal activity in Hercynian episode					
Moldanubian assemblage	348±16	U-Pb (zircon)	granulite	metamorphic age	17
Moldanubian assemblage	348±7	U-Pb (zircon)	granulite	metamorphic age	17
Moldanubian assemblage	347+9/-10	U-Pb (zircon)	paragneiss	metamorphic age	7
Moldanubian assemblage	345±5	U-Pb (zircon)	granulite - Lišov	metamorphic age	4
Moldanubian assemblage	345±5	U-Pb (zircon)	granulite - Mobelno	metamorphic age	4
Gföhl gneiss	341±4	U-Pb (zircon)	gneiss	metamorphic age	4
Moldanubian assemblage	339±2	U-Pb (monazite)	granulite - Mobelno	metamorphic age	4
Moldanubian assemblage	338±0.5	U-Pb (zircon-monazite)	granulite	metamorphic age	9
Gföhl gneiss	337±3	U-Pb (monazite)	gneiss	metamorphic age	4
Moldanubian assemblage	335±3	Rb-Sr (WR)	migmatite	metamorphic age	12
Ductile deformation in Hercynian episode					
Moldanubian assemblage	333±3	U-Pb (xenotime)	mylonite	metamorphic age	8
Plutonic activity in Hercynian episode					
Moldanubian Pluton	349±4	Rb-Sr (WR)	granite	magmatic age	5
Central Bohemian Pluton	331±4	Rb-Sr (WR)	granodiorite	magmatic age	4
Central Bohemian Pluton	331±9	Rb-Sr (WR)	granodiorite	magmatic age	10
Bechyně complex	331±5	Rb-Sr (muse)	pegmatite	magmatic /deformation age	4
Křizanovice Pluton	320±4	Rb-Sr (WR)	granite	magmatic age	6
Moldanubian Pluton	318±7	Rb-Sr (WR)	granite	magmatic age	12
Moldanubian Pluton	303±6	Rb-Sr (WR)	granite	magmatic age	12

References:

1 Arnold and Scharbert (1973), 2 Vidal et al. (1975), 3 Scharbert and Batík (1980), 4 van Breemen et al. (1982), 5 Scharbert (1987a), 6 Scharbert (1987b), 7 Krőner et al. (1988), 8 Teufel (1988), 9 Aftalion et al. (1989), 10 Bendl and Vokurka (1989), 11 Carswell and Jamtweit (1990), 12 Scharbert and Veselá (1990), 13 Bowes and Aftalion (1991), 14 Brueckner et al. (1991),15 Beard et al. (1992), 16 Dörr et al. (1992), 17 Wendt et al. (1992).

*) values recalculated according to decay constants recommended by Steiger and Jäger (1977).

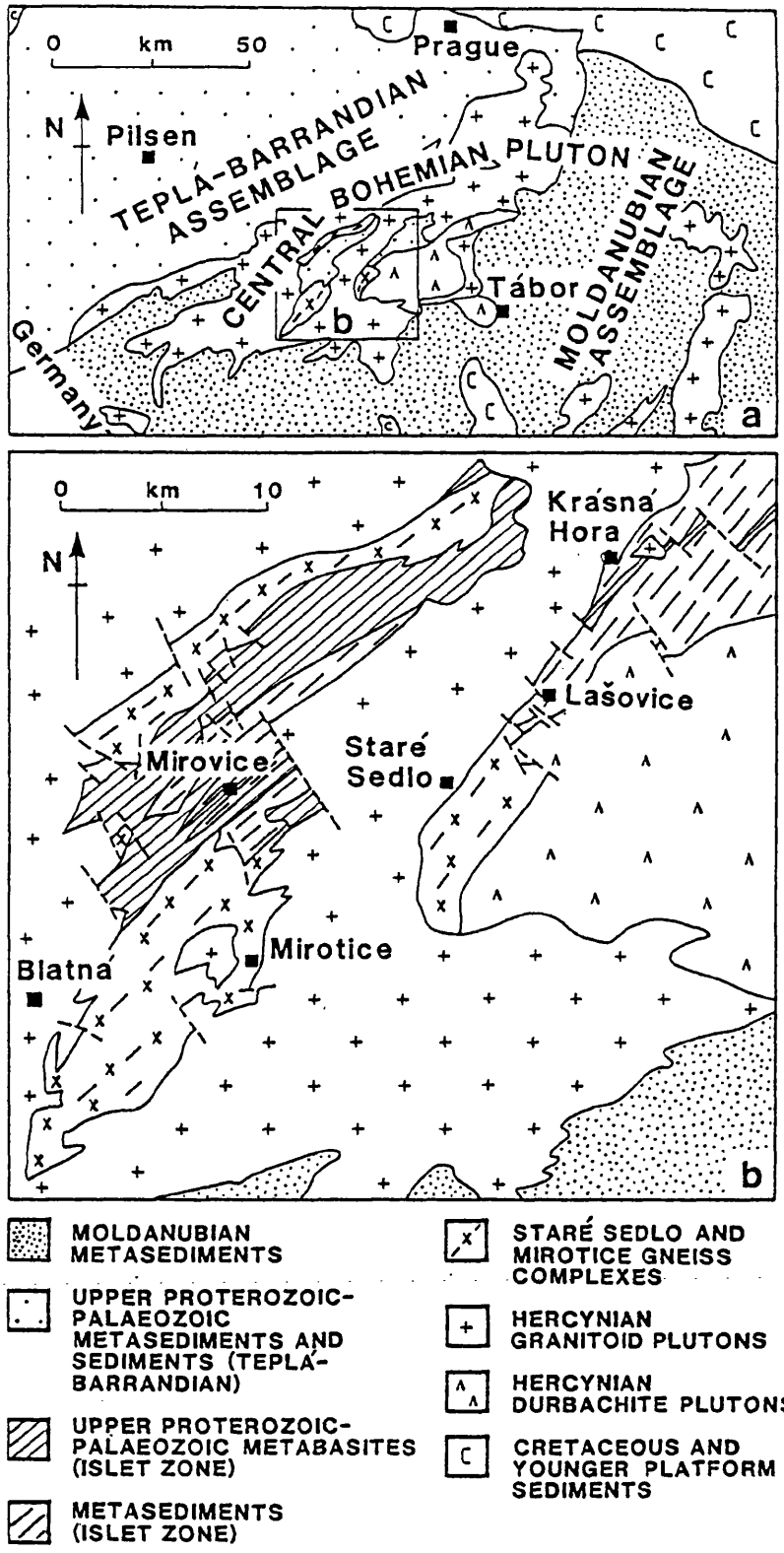

Fig.1.1

(a) Distribution of major rock units within the Czech part of the Bohemian Massif; based on 1:500 000 map of the Czech geological Survey.

(b) Outline geological map of the studied area; based on 1:200 000 map of the Czech Geological Survey.

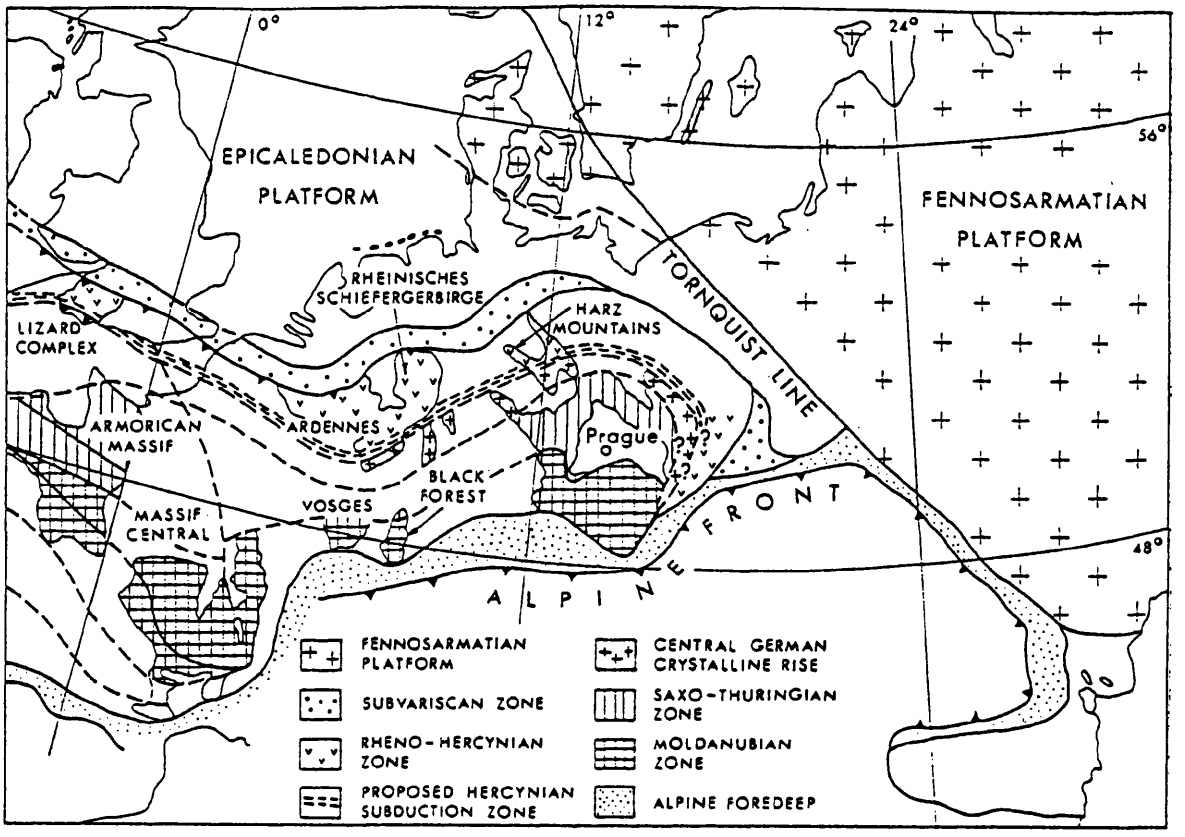

Fig.1.2

Outline geological map showing relics of the Hercynian mountain chain in Central and Western Europe with the delineation of the main structural zones (from van *Breemen et al., 1982*).

Fig.1.3

(a) Minor intrusion of amphibolite (dark) within the amphibole - biotite mylonite gneiss; roadcut 1.5 km SE of Staré Sedlo.

(b) Contact of biotite - amphibole mylonite gneiss (left) with granodiorite (Kozárovice type); Vltava River valley, 2 km S of Staré Sedlo.

(c) Xenolith of mylonite gneiss (dark) enclosed in granodiorite (Kozárovice type); Kozárovice, quarry in the village.


a


b

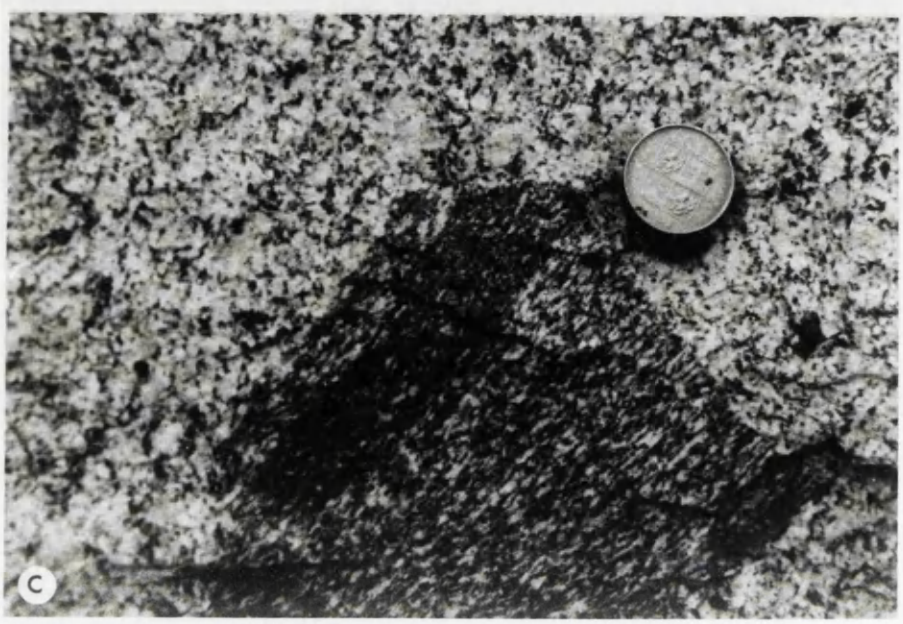
c

2. ROCK UNITS

2.1 Rock units present within the Staré Sedlo and Mirotice complexes

Most of the rock units have mylonitic affinities and are described best as mylonite gneiss, mylonite schist, and ultramylonite that in parts is blastomylonite (*Higgins, 1971; Bell and Etheridge, 1973; Wise et al., 1984*). There are gradations between these rocks (cf. Fig.2.2) but the dominant types are strongly foliated biotite, amphibole - biotite, garnet - biotite and feldspar mylonite gneisses that have the characteristics of augen gneisses with plagioclase, K-feldspar and quartz present as augen minerals (Fig.2.1d,e) and have been referred to as such in literature (e.g. *Waldhausrová et al., 1986*). The protoliths of the mylonite gneisses are cut by minor intrusions of amphibolite and meta-aplite (meta-microgranite) that are affected by the same foliation as their hosts but generally do not show such intense mylonitic characters. The order of emplacement of the minor intrusions (amphibolite followed by meta-aplite) proposed by *Waldhausrová et al. (1986)* on the basis of regional distribution has been confirmed by cross-cutting relations (Fig.2.1a).

On the basis of petrographical and geochemical features the mylonite gneisses have been interpreted as orthogneisses and they and at least some of the mylonite schists and ultramylonites correspond compositionally to tonalites and granodiorites (see Chapter 4). Within the Mirotice complex there are K-feldspar rich mylonite schists (medium- to fine-grained intensely foliated quartzofeldspathic rocks with variable proportions of K-feldspar and quartz porphyroclasts) and ultramylonite - blastomylonite. These occur as lenses up to 3 km long. The fine-grained types with a low proportion of porphyroclasts have been referred to by some authors as leptynites while those with a considerable proportion of porphyroclasts have been referred to as porphyroides (*Tonika at al., 1980*). Their petrographical characters compared to those of the dominant gneisses are considered to reflect differences in mineral composition of their protolith and the related different physical and chemical responses to the deformation. Overall the whole assemblage is indicative of variable responses to deformation of different minerals. Ductile deformation is dominant for some minerals (e.g. quartz) while some minerals (e.g. zircon - see also *Boullier, 1980*) show only few effects of brittle deformation (cf. Chapter 6, Fig.6.3) and some minerals (e.g. feldspars) show the effects of both ductile and brittle deformation. Hence while on a

small scale the mylonitic fabric cannot be attributed solely to either ductile or brittle deformation, the fact that the rocks did not lose their primary coherence means that the deformation on a larger than microscopic scale was essentially ductile.

Most of the samples used in this study come from outcrops and old quarries within the Staré Sedlo and Mirotice complexes (Fig.1.1b). The contents of biotite, amphibole and plagioclase are variable even on a small scale of an outcrop and there is a complete gradation between the different gneiss types proposed by *Tonika et al. (1980)*, *Žežulková et al. (1985)* and *Waldhausrová et al. (1986)*. In addition the variations in biotite, amphibole and plagioclase contents are often not reflected in the chemical compositions of the gneisses (cf. Chapter 4). Accordingly it is considered that grouping based on these variations is arbitrary and not useful in an understanding of the petrogenesis of what is a single rock unit. The grouping preferred is based largely on locality, major petrographical variations and rock relationships (mylonite gneiss of tonalite - granodiorite composition, K-feldspar rich mylonite schists - ultramylonites - blastomylonites and the later minor intrusions of amphibolite and mete-aplite). Because there are particular compositional characteristics in the gneisses of the Lašovice quarry in the northern extension of the Staré Sedlo complex (Fig.1.1), these rocks are treated separately from those of the main part of that complex. The groups (and abbreviations used for analyzed samples) are:

Staré Sedlo complex

Biotite - amphibole - feldspar-bearing mylonite gneisses - Staré Sedlo (STG)

Biotite - feldspar-bearing mylonite gneisses - Lašovice quarry (LG)

Amphibolites - Staré Sedlo (STA)

Meta-aplites - Staré Sedlo (STM)

Mirotice complex

Biotite - feldspar - garnet-bearing mylonite gneisses - Mirotice complex (MIG)

K-feldspar-bearing schists - ultramylonites - blastomylonites - Mirotice complex (MIS)

A few amphibolites and meta-aplites do occur in the Mirotice complex but the exposures are poor and not suitable for collecting specimens for geochemical study. However in petrographical characters they correspond to the analogous rocks of the Staré Sedlo complex.

The nomenclature and classification used throughout this study follows closely the principles for classification of metamorphic rocks recommended by SCMR/IUGS outlined in *Gregerová and Suk (1991).*

2.1.1 Biotite, amphibole - biotite, biotite - amphibole and plagioclase mylonite gneisses

This rock unit includes various types of mylonite gneisses from both the Staré Sedlo (samples STG and LG) and Mirotice (samples MIG) complexes which represent the dominant lithologies present. The gneisses are strongly foliated coarse- to fine-grained rocks (the grain size varies from 2.5 mm to 0.05 mm) and locally show variations from mylonite gneiss to ultramylonite (Fig.2.2) in which variable recrystallization gives some of the fine-grained rocks the characteristics of blastomylonite. They are composed of 35 - 65% quartz, 20 - 50% plagioclase (An_{10-40}), 5 - 20% K-feldspar, 1 - 15% biotite, 0 - 6% hornblende and 0 - 1.5% ore minerals (pyrite and magnetite). Titanite, zircon, apatite, allanite and epidote are accessory minerals. Despite the presence of a well-expressed, penetrative foliation, porphyroclasts (augen) of plagioclase, K-feldspar and quartz are still preserved as pre-tectonic relics in a medium - fine grained quartzofeldspathic matrix with mortar structure along the porphyroclast boundaries. Quartz is present either as flattened, recrystallized porphyroclasts (up to 2.5 mm in size) that represent relics of the pre-deformational assemblage, or in the matrix, as irregular grains with undulose extinction. In the most deformed rocks quartz often forms ribbons or blade-shaped lenses oriented parallel to the foliation planes. Two generations of plagioclase are present in the rock: relics of the assemblage whose crystallization pre-dates the deformation occur as porphyroclasts (often zoned with albite and, or, Carlsbad twinning) and syn- to post-deformational irregular grains are present in the matrix (mainly albite twinned). Deformation, bending and recrystallization of the rims of the plagioclase porphyroclasts is very common (Fig.2.1c,d). K-feldspar occurs as small, irregular and cloudy grains in the matrix and rarely as perthitic porphyroclasts up to 2 mm in size. Symplectitic intergrowth of quartz and feldspar (myrmekite) is sometimes present. Strongly pleochroic brown biotite forms clusters up to 2 mm in size oriented parallel to the foliation planes and bent around the feldspar porphyroclasts (Fig.2.1e). Kink-bands in

biotite indicate that it was affected during later stages of the deformation. Inclusions of apatite and zircon are surrounded by pleochroic haloes. Similar haloes occur in green and strongly pleochroic hornblende that is present in clusters also oriented parallel to the foliation planes.

The fabric of the biotite, amphibole - biotite, biotite - amphibole and plagioclase gneisses matches well the criteria given by *Seyfert (1987)* for mylonite and mylonite gneiss. The following are the most pronounced features.

(1) The volumetric proportion of porphyroclast in the rock (usually formed by feldspars of more than 0.2 mm in size) exceeds 30%.

(2) Quartz shows undulose extinction and often forms flattened lens-shaped grains and ribbons oriented parallel to the foliation of the rock.

(3) Feldspars and quartz grains along the porphyroclast boundaries often show a mortar texture.

(4) Deformation and bending of feldspar porphyroclasts is a common feature.

(5) Some biotite flakes show a weak kink-banding.

As both the mineral and rock compositions (see Chapter 3 and 4) of these mylonite gneisses correspond with those of a tonalite - granodiorite igneous suite, the rocks are interpreted as being orthogneisses with a protolith of tonalite - granodiorite.

2.1.2 Garnet - biotite mylonite gneisses

This rock type (samples MIG) is an integral part of the gneiss suite but as it has been found only within the Mirotice complex and only in that part adjacent to the contact with surrounding granitoids of the Central Bohemian Pluton, it is here described separately. The mineral composition of these gneisses corresponds to that of biotite-, amphibole- and plagioclase-bearing mylonite gneisses except for the garnet which is present as a late- to post-deformational growth that occurs, together with the clusters of brown biotite, as up to 0.2 mm euhedral individual grains or clusters oriented parallel to the foliation of the rock (Fig.2.1f). The garnets show no zoning pattern and no structural features indicative of rock deformation. Most of the biotite is present in clusters oriented parallel to the rock foliation although the individual grains and the flakes within the clusters have a random orientation. The fabric in parts is mylonitic but in parts it approaches being granoblastic. This, and the growth of the garnet over a gneissic

fabric is interpreted as resulting from the local effects of thermal (contact) metamorphism of the dominant type of gneiss.

2.1.3 K-feldspar-bearing mylonite schists - ultramylonites - blastomylonites

This rock unit is present exclusively within the Mirotice complex (samples MIS) and it occurs in NNE-trending lenses within the mylonite gneisses. The mineral constituents of the mylonite schists and the ultramylonites - blastomylonites are the same but they differ in both the proportions of minerals and the size of the porphyroclasts.

The mylonite schists are strongly foliated medium- to fine-grained rocks (the grain size in the matrix varies from 0.03 up to 0.2 mm). The matrix is composed mainly of quartz, feldspar, biotite and muscovite. Flattened augen (porphyroclasts) of quartz, K-feldspar and rare plagioclase are up to 1 cm in size and elongate parallel to the mylonitic foliation (Fig.2.1g). Zircon, apatite titanite and ore mineral occur as accessory minerals. As well as being present as porphyroclasts, quartz is present as irregular grains with undulose extinction in the matrix. It also forms sigmoidal grains and blade-shaped lenses and ribbons oriented parallel to the rock foliation (Fig.2.1g). K-feldspar occurs as small irregular cloudy grains in the matrix and as deformed sericitized augen with Carlsbad twinning. Irregular grains of plagioclase with dominant albite twinning are also often sericitized. Biotite (often green) and muscovite occur as small irregular grains or grain clusters in the matrix oriented parallel to the foliation.

The ultramylonites - blastomylonites are strongly foliated fine-grained rocks (the grain size is up to 0.03 mm) with very few or no porphyroclasts. The minerals present (quartz, K-feldspar, plagioclase, biotite, zircon and apatite) and their proportions correspond to the matrix of the mylonite schists. The varying proportions of recrystallized quartz and feldspar are gradational and increase from ultramylonite to blastomylonite.

On the basis of the mineralogical and chemical characteristics (see Chapters 3 and 4), the K-feldspar mylonite schists - ultramylonites - blastomylonites represent deformed and metamorphosed equivalents of granite (or rhyolite) that was spatially associated with a tonalitic - granodioritic protolith of the mylonite gneisses of the Mirotice complex. They share a common foliation with other mylonitic rocks in the Mirotice complex.

2.1.4 Amphibolites

This rock unit occurs within both the Staré Sedlo (samples STA) and Mirotice complexes. It consists of foliated minor intrusions which cross-cut the protolith of the gneisses but whose fabric was formed together with that in their host gneisses (Fig.2.1a,h). Porphyroclasts of plagioclase up to 3 mm in size are in a matrix that varies in grain size from 0.02 mm up to 1 mm. The rock is composed of 1 - 15% quartz, 40 - 50% plagioclase (An_{29-32}), 0 - 5% K-feldspar, 2 - 15% biotite, 30 - 50% hornblende and 1 - 2% ore minerals. The plagioclase porphyroclasts represent relics of a pre-deformational igneous assemblage and in them Carlsbad and albite twinning are common. In the matrix K-feldspar is present as small irregular cloudy grains. Quartz occurs as irregular or flattened lens-shaped grains with undulose extinction in the matrix and its proportion is very variable. Strongly dimensionally oriented hornblende forms small irregular pleochroic green grains in the matrix and larger (up to 3 mm) irregular grains that are often twinned on [100]. Biotite occurs as small irregular flakes in the matrix oriented parallel to the foliation. Inclusions of apatite with surrounding pleochroic haloes are common in both biotite and hornblende.

The presence of oligoclase - andesine porphyroclasts in the foliated (in parts mylonitic) oligoclase - andesine - hornblende - biotite - quartz matrix is consistent with the geochemical evidence (Chapter 4) suggesting that the protolith of these minor intrusions was tonalitic - dioritic in composition. The continuity of the foliation planes in the amphibolites and their host mylonite gneisses indicate that they shared a common metamorphic history.

2.1.5 Meta-aplites

Dykes of leucocratic medium- to fine-grained (grain size varies from 0.7 to 0.05 mm) foliated rocks (samples STM) which cut the protolith of both the gneisses and amphibolites of the Staré Sedlo complex can be categorized as meta-aplites (Fig.2.1a,b). In parts their fabric is mylonitic. Both the minerals present and their proportions correspond to those of the amphibole- and biotite-bearing mylonite

gneisses. The foliation shows continuity with that in their host mylonite gneisses (Fig.2.1b) indicating intrusion before the intense deformation.

2.2 Origin of rock foliation

The intensity of the effects of the mylonitic deformation varies considerably from rock type to rock type and within individual types it varies considerably within a short distance of a few decimetres (Fig.2.2) as do the proportions of effects resulting from ductile and brittle deformation. The most intense effects are shown by the schists - ultramylonites - blastomylonites and with the chemical and mineralogical evidence indicating that the protolith of these rocks differed from that of the gneisses (or at least the great bulk of the gneisses), a compositional control over the response to deformation is indicated. This is also considered to be a major feature in the generally much less intense expression of the fabric in the amphibolites and particularly the meta-aplites although locally mylonitic foliation in these units is very strongly developed. It is also likely that there was a gross compositional - competence control on the expression of this fabric within both the gneiss and schist rock units. Geochemical studies (Chapter 4) point to the possibility of rocks compositionally comparable to the K-feldspar-bearing schists of the Mirotice complex being present as mylonite gneiss amongst the dominantly plagioclase-rich mylonite gneisses. Likewise there could be small units of plagioclase-rich rocks amongst the mylonite schists - ultramylonites - blastomylonites.

The foliation in the rocks of the Staré Sedlo and Mirotice complexes was interpreted by *Kettner (1930a,b)* to represent a primary magmatic feature resulting from magmatic crystallization in a strain-dominated environment (e.g. shear zone). That a mylonite-looking fabric (crystal-plastic strain fabric) can be developed in granitoids has been established by *Hutton (1988, 1992), Paterson et al. (1989), Hutton et al. (1990)* and *Hutton and Ingram (1992)*. However the continuity of the mylonitic foliation in the gneisses and schists of the Staré Sedlo and Mirotice complexes through the later minor intrusions as well (Fig.2.1b,h) rules out the possibility of its magmatic origin. Consequently the crystallization of the rock protoliths and ductile deformation must represent separate events. Such a conclusion is supported by the U - Pb and Rb - Sr isotopic data (Chapters 6 and 7).

Apart from the mylonitic fabric and corresponding features seen at the mineral grain scale (undulose extinction of flattened quartz grains, quartz blade-shaped lenses and ribbons oriented parallel to the rock foliation, mortar structure in quartz and feldspar along the porphyroclast boundaries and deformation and bending of plagioclase) there are other observations consistent with the superposition of a phase of ductile deformation (probably in a shear zone) on the products of earlier crystallized rock units.

(1) The penetrative mylonitic foliation in both the Staré Sedlo and Mirotice complexes and in all the rock units is generally parallel to the NNE-trending of the gneiss complexes themselves.

(2) The strike of the foliation is usually parallel to the zones of intense mylonitization (especially in the northern part of the Staré Sedlo complex where it varies from NNE- to NE-trending).

(3) The true width of both gneiss complexes, as estimated from those parts of the roof pendants where the foliation is not subhorizontal, is not more than 10 km, i.e. within the range for mylonitic zones (*Davis et al., 1980*).

2.3 Conclusions

1. The Staré Sedlo and Mirotice complexes consist of biotite-, amphibole- and plagioclase-bearing mylonite gneisses (and garnet-bearing varieties in parts adjacent to the later Central Bohemian Pluton), K-feldspar-bearing mylonite schists - ultramylonites - blastomylonites, amphibolites and meta-aplites. All rock units are foliated, and in most the foliation is mylonitic. In them both the presence of feldspar and quartz porphyroclasts and the oscillatory zoning in plagioclase feldspar are consistent with an igneous protolith.

2. The continuity of the foliation through the various rock units suggests the crystallization of their protolith(s) and the ductile deformation represent separate events.

3. The development of mylonitic rocks within a narrow NNE- to NE-trending zone and both the strike and direction of their foliation are accounted for by the operation of ductile deformation along a NNE-trending shear zone.

Fig.2.1

Rock types of the Staré Sedlo and Mirotice complexes and their relations.

(a) Amphibolite (dark, left-hand side) within amphibole - biotite mylonite gneiss (STG-6), cut by meta-aplite (STM-1); length of the scale is 2 cm.

(b) Enlargement of gneiss - meta-aplite relationship from (a); note the continuity of the foliation in the two rock types; scale in mm.

(c) Bent plagioclase grain in a biotite mylonite gneiss (STG-19); XN; x 60.

(d) Zoned plagioclase porphyroclast in a mylonitic matrix consisting of quartz, plagioclase, K-feldspar and biotite; mylonite gneiss (STG-7); XN; x 17.

(e) Clusters of strongly pleochroic biotite bent around a plagioclase porphyroclast and oriented parallel to the foliation in a mylonite gneiss (STG-15); PPL; x 17.

(f) Cluster of euhedral garnet grains and small flakes of biotite oriented parallel to a weakly expressed foliation; garnet - biotite gneiss with some granoblastic features (MIG-11); PPL; x 43.

(g) Sigmoidal and ribbon-shaped deformed and recrystallized porphyroclasts of quartz in a fine-grained mylonite schist (MIS-6) which consists of quartz, K-feldspar, plagioclase and biotite; XN; x 17.

(h) Small amphibolite minor intrusion (STA-6) that cuts an amphibole - biotite mylonite gneiss and shares the same foliation; PPL; x 17.

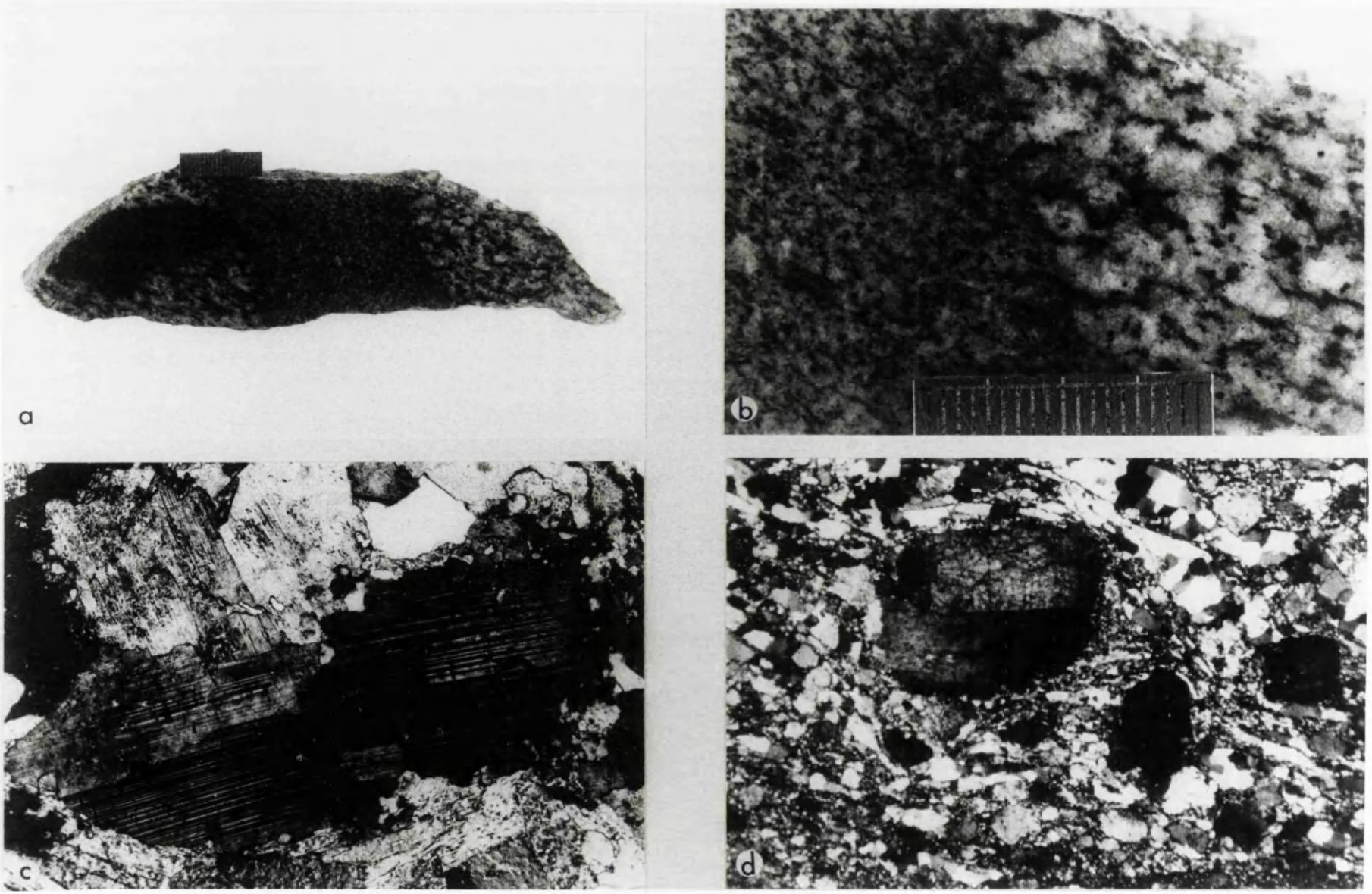
a
b
c
d

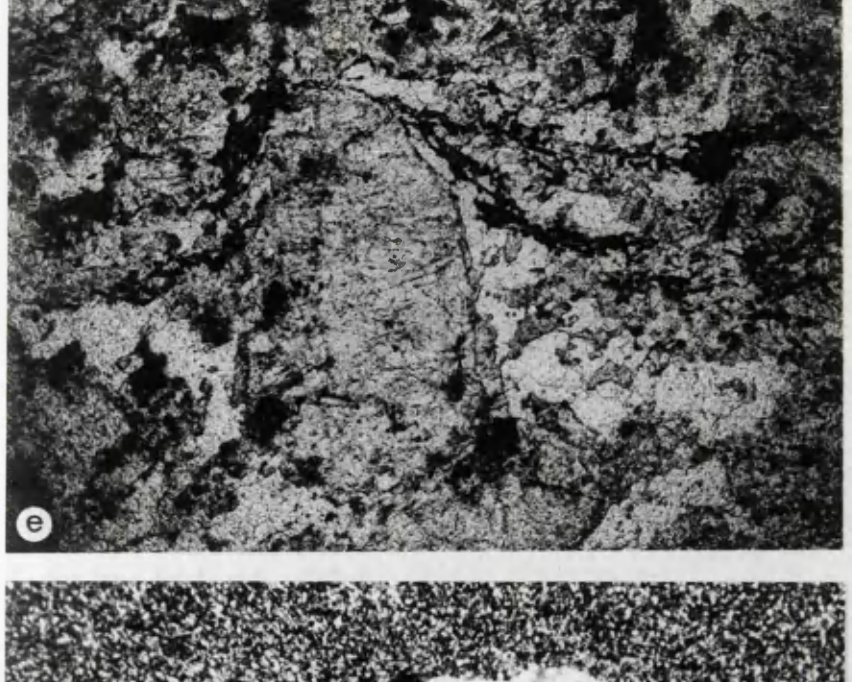
e

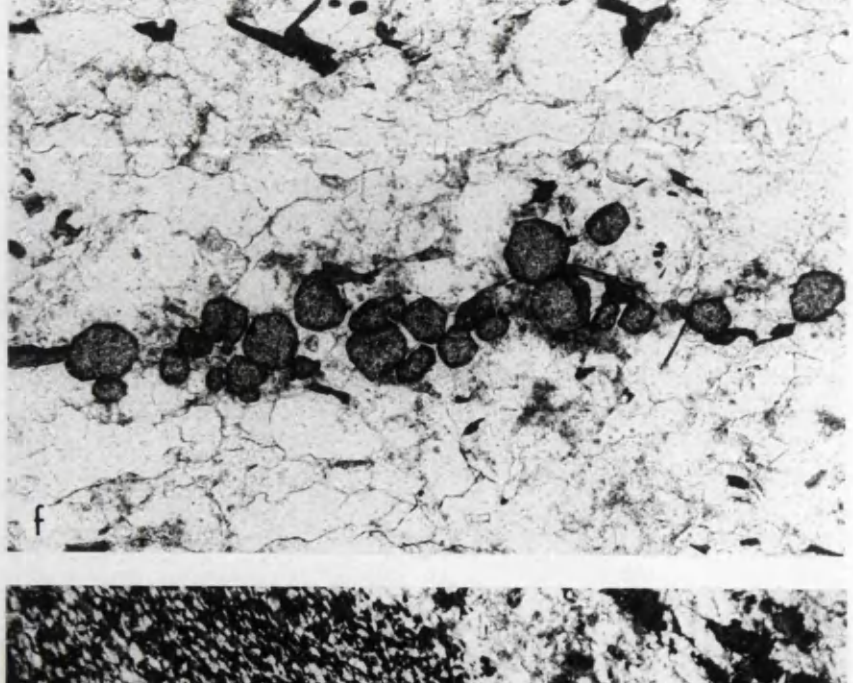
f

g

h

Fig.2.2

Stages of progressive mylonite fabric development in gneisses of the Staré Sedlo and Mirotice complexes; (a) biotite mylonite gneiss (LG-5); (b) biotite mylonite (MIG-2); (c) biotite ultramylonite - blastomylonite (the same locality as STG-15); scale in mm.

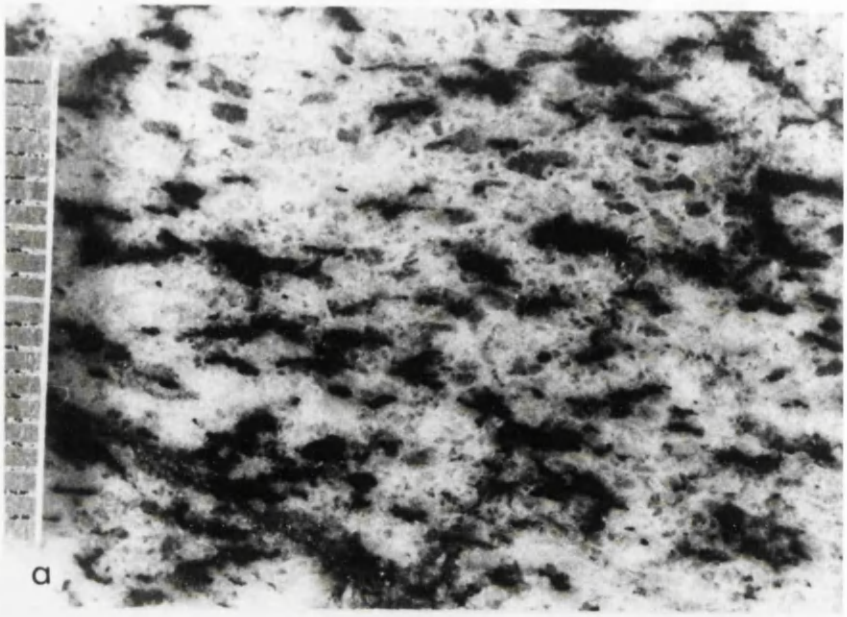
a

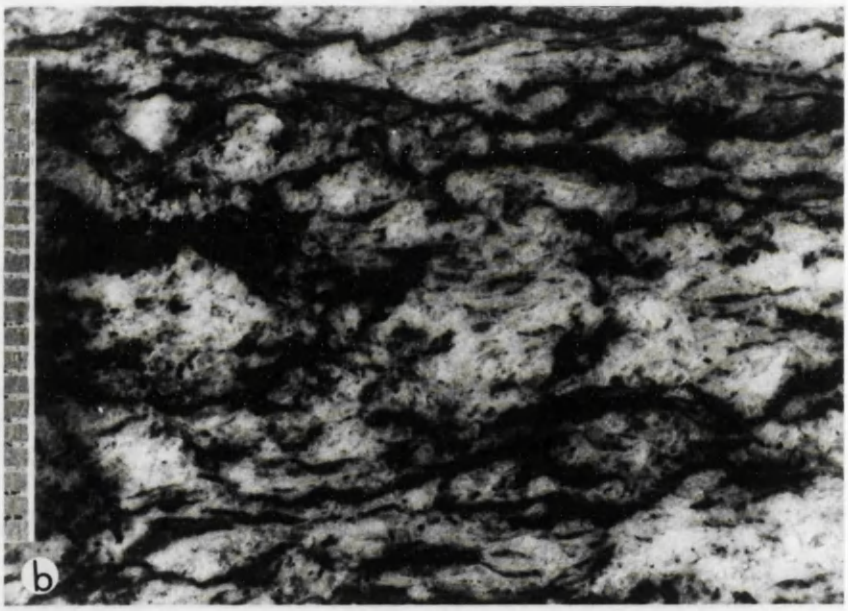
b

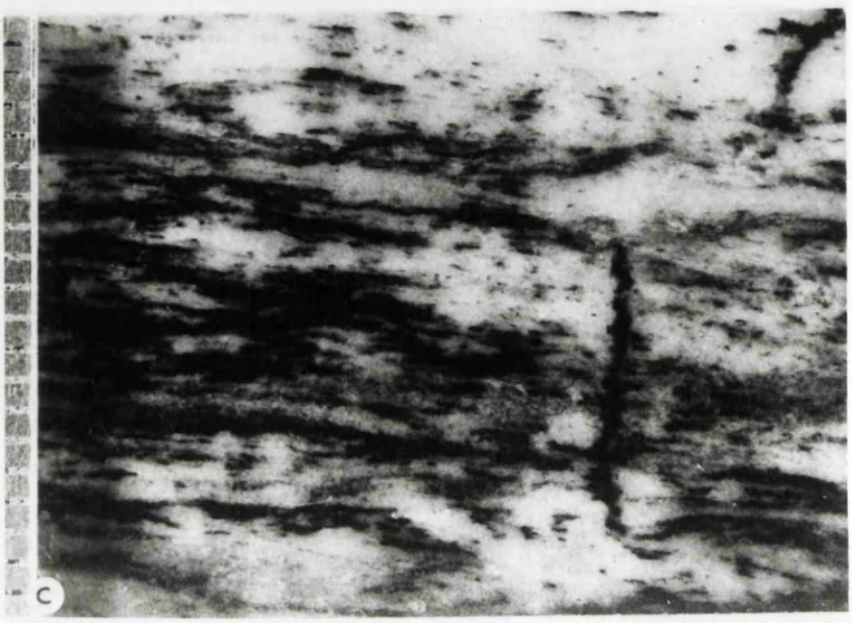
c

3. MINERAL CHEMISTRY

In order to characterize the chemical compositions of the rock-forming minerals of various rock units within the Staré Sedlo and Mirotice complexes and, by doing so, to form a basis for geothermobarometric and isotopic studies, an electron microprobe study of feldspars, biotite, amphibole and garnet has been carried out. The details of the analytical methods are given in Appendix 2 and the analytical data and corresponding mineral formulae are listed in Appendix 3. The particular minerals are dealt with in groups based upon the rock units defined in Chapter 2 (mylonite gneisses, K-feldspar-bearing schists - ultramylonites - blastomylonites and amphibolites). The chemistry of minerals from the meta-aplites of the Staré Sedlo complex has not been dealt with, as both their petrographical and major element compositions generally correspond to those of the mylonite gneisses. In order to make the approach to the analytical data consistent with that in Chapter 4, the geometric average (G) is used rather than the arithmetic average (X), unless there are no zero values present.

3.1 Plagioclase

Two generations of plagioclase are present in the studied mylonite gneisses, schists and amphibolites: (1) porphyroclasts with a well-developed normal oscillatory zoning which represent relics of a pre-deformational assemblage, and (2) younger unzoned grains in the matrix and along the margins of zoned porphyroclasts which are part of the metamorphic (deformational) assemblage. The chemical compositions of the two generations overlap with the An content varying generally from 10 to 47 mol % (oligoclase - andesine). This range of composition represents mainly the core - rim variations in the porphyroclasts while the composition of the plagioclase from the matrix usually corresponds to oligoclase. The summary of some statistical parameters for the composition of plagioclase from various rock types is given in Table 3.1 and Fig.3.1.

For the mylonite gneisses there is no substantial difference in the plagioclase compositions from the Staré Sedlo and Mirotice complex except for the Lašovice gneisses in which the plagioclase composition (An_{30} in average, with no grains of An_{0-20} present) is somewhat more Ca-rich (Table 3.1; Fig.3.1). However this conclusion may be related to the relatively small number of analyzed grains from

the Lašovice gneisses which may not cover completely the whole compositional range. The Ab/An ratio of plagioclase from the Mirotice schists is within the same range as that of plagioclase from the gneisses with most of the grains corresponding to oligoclase but with one analyzed grain being albite. Plagioclase from amphibolites of the Staré Sedlo complex forms a tight cluster which straddles the boundary of oligoclase and andesine. Taking in account the typical p-T-time conditions of plutonic and metamorphic processes controlling the crystallization of plagioclase in the gneisses, schists and amphibolites, the plagioclase is classified as ranging from low andesine through low oligoclase to low albite (*Smith and Brown, 1988*). The average Or content in the plagioclase grains is usually less than 5 mol %, i.e. within the range where Ab, An and Or components form a solid solution (*Smith and Brown, 1988*). There are only a few plagioclase grains with more than 5 mol % Or content (Fig.3.1) suggesting only a limited submicroscopic antiperthite presence.

The maximum Or content does not correspond with the maximum on the histogram of plagioclase composition i.e. with the mass volume crystallization of plagioclase in the gneisses from both the Staré Sedlo and Mirotice complexes (Fig.3.2). This holds also when the data which have Or > 5 mol% (that may correspond to micro-antiperthite) are excluded. The plagioclase composition can be explained on the basis of a study of the Ab/An ratio and Or-content of plagioclase in some orthogneisses and migmatites from the Bohemian Massif (*Lang, 1990*). The results show that the proportion of the Or-component in so called ternary feldspar (plagioclase with an increased content of potassium) in those rocks is complementary to the mass volume crystallization of plagioclase (expressed as maximum on the histogram of plagioclase composition). This is interpreted as the result of dilution of the available amount of potassium with the great volume of rising plagioclase (i.e. crystallization of plagioclase in a closed chemical system). Both the decreasing miscibility of the plagioclase components at low temperatures (the crystallizing plagioclase is Na-rich and K-poor) and the introduction of potassium into the rock from outside would result in a correlation of Or-content with the volume of crystallizing plagioclase feldspar (i.e. crystallization of plagioclase in an open system). Correspondingly the complementary character of the Or-component distribution and the maximum of An-component frequency in plagioclase from the Staré Sedlo and Mirotice gneisses is considered to result from crystallization of plagioclase in a closed system with respect to Na, Ca and K, and also Si and Al, assuming these elements take part in a Na-Si<-->Ca-Al equilibrium. This suggests that the proportion of Or-component in the

plagioclase may reflect both the volume of rising plagioclase and potassium available in the rock (*Lang, 1990*).

The nature of chemical zoning in the plagioclase has been studied on a chemical profile through a zoned porphyroclast (Fig.3.3). The step chosen for this traverse was too large to detect the oscillatory character of zoning. However the chemical profile shows the gradual and almost regular change in composition which varies from a Ca-rich ($CaO > Na_2O$) core of the grain (which represents its original crystallization centre) towards a Ca-poor and Na-rich ($CaO < Na_2O$) rim. The presence of this type of normal chemical zoning (which however holds only for the left-hand side of the diagram in Fig.3.3), together with oscillatory zoning (seen in the cross-polarized light), is attributed to the crystallization of the grain from the melt. The oscillation in chemical composition can result either from oscillatory changes in p and T conditions in the melt during the crystal growth and, or, from periodic reaching of a critical concentration of "crystallochemically unsuitable" components on the surface of a growing crystal (*Putnis et al., 1992*). However on the right-hand side of Fig.3.3 the regular zoning of both CaO and Na_2O have been obliterated and there are no regular trends in the observed chemical composition along the profiles. As the CaO and Na_2O profiles do not match the typical pattern known to result from diffusion within the crystal lattice (*Smith and Brown, 1988*), the obliteration of regular zoning in the rim of porphyroclast is likely to represent a later growth. This growth is related to partial plagioclase recrystallization during ductile deformation and associated metamorphism of the protolith of the mylonite gneisses. The recrystallization is consistent with a common occurrence of small plagioclase grains along the edges of other plagioclase porphyroclasts which often form domains of a mortar texture in the matrix. However a backscattered electron image of this grain did not reveal the core - rim relations, probably due to the small differences in their mean atomic numbers. However as the proportion of the plagioclase metamorphic overgrowth in the rocks is very small, it has only negligible, if any, impact upon the results of isotope study of plagioclase porphyroclasts.

3.2 K-feldspar

Like the plagioclase, K-feldspar occurs as two generations in the mylonite gneisses and the K-feldspar-bearing mylonite schists - ultramylonites - blastomylonites of the Staré Sedlo and Mirotice

complexes: (1) as porphyroclasts which are usually perthitic and chemically unzoned and which are part of the original igneous mineral assemblage, and (2) as small grains in the matrix which have a somewhat lower proportion of perthite. The latter often have a mortar texture and usually occur in domains along the margins of K-feldspar porphyroclasts. No differences in the chemical composition were found between the two generations of K-feldspar and there are no significant differences between the compositions of K-feldspar from the gneisses of the two complexes (see summary of selected statistical values of K-feldspar composition from the mylonite gneisses and K-feldspar-bearing mylonite schists - ultramylonites - blastomylonites of both the Staré Sedlo and Mirotice complexes in Table 3.2). The porphyroclasts of the generation I. are commonly altered to the mixture of K-feldspar and sericite. However K-feldspar from the mylonite schists - ultramylonites - blastomylonites has a somewhat lower proportion of Na_2O and higher proportion of TiO_2 compared to the K-feldspar from the mylonite gneisses. As no inclusions of any Ti-bearing mineral in K-feldspar have been found, this is explained by a more pronounced substitution with a charge compensation of Ti^{4+} for Al^{3+} (based on their similar ionic radii; *Zemann, 1966*) in the crystal lattice of the K-feldspar present in the schists. However more data are clearly needed to further elucidate these relations.

3.3 Biotite

Biotite is present in the mylonite gneisses, K-feldspar-bearing mylonite schists - ultramylonites - blastomylonites and amphibolites of both complexes. It occurs as irregular flakes or clusters that are consistently oriented parallel to the foliation formed as a result of ductile deformation and metamorphism (for p - T conditions see Chapter 5). Accordingly biotite in these rocks is considered to be a part of the metamorphic mineral assemblage. In order to evaluate all aspects of biotite mineral chemistry, recalculations of electron microprobe data were made on the following bases.

1. The crystallochemical formulas are based upon 22 oxygen (F, Cl, ...) atoms; this was done as there is no information available concerning the content of volatile components.

2. The Al^{IV} and Al^{VI} proportions are based on the assumption that $Si+Al^{IV} = 8$.

3. To assess the Fe^{3+}/Fe^{2+} ratio in the formula, biotite separates from samples which are representative of the Staré Sedlo, Lašovice and Mirotice mylonite gneisses were analyzed for FeO (method used was the

same as that for FeO determination in the whole-rock samples - see Appendix 2). Accordingly 32, 11 and 30 wt% of the total Fe-content (expressed as FeO) in biotite were recalculated to Fe_2O_3 in samples of the Staré Sedlo, Lašovice and Mirotice mylonite gneisses, respectively. The recalculation used for biotites from the K-feldspar-bearing mylonite schists - ultramylonites - blastomylonites was the same as that for biotites from the mylonite gneisses of the Mirotice complex.

The main statistical parameters of the chemical composition of biotite from the mylonite gneisses and K-feldspar-bearing mylonite schists - ultramylonites - blastomylonites of the Staré Sedlo and Mirotice complexes are given in Table 3.3 and the projection of the data on to the phlogopite - annite - eastonite - siderophyllite classification diagram is shown in Fig.3.4. Simple statistical evaluation of the data suggests that there are differences in FeO_{tot} and MgO contents in biotite from the Staré Sedlo and Mirotice mylonite gneisses. However the biotites from the Mirotice mylonite gneisses form two separate groups: they plot towards the ends of the overall trend shown by all the biotites so that an average value has no real meaning. In addition, biotites from one mylonite gneiss sample taken close to the margin of the Staré Sedlo complex (ca 5 metres away from the contact with Kozárovice granodiorite of the late Hercynian Central Bohemian Pluton) plot away from the overall trend (having both low Fe/(Fe+Mg) ratio and high Al^{IV} content). Hence for the biotite data from this rock unit the mean statistical values (Table 3.3) have no real meaning.

All studied biotites show the phlogopite - annite <--> eastonite - siderophyllite substitution of the main octahedral (Mg, Fe) and tetrahedral (Al^{IV} and complementary Si) components (Fig.3.4). Biotite from an amphibolite of the Staré Sedlo complex plots at the Mg-end of the overall field.

The ratio of the two main cations (Fe/Mg) of the octahedral layer is an important characteristic of biotite and most of the grains from the mylonite gneisses, K-feldspar-bearing mylonite schists - ultramylonites - blastomylonites straddle the boundary between Mg- and Fe^{2+}-biotites having the Mg/Fe^{2+} ratio close to 1 in the triangular diagram Mg - $Al+Fe^{3+}+Ti$ - $Fe^{2+}+Mn$ (Fig.3.5). Al-rich biotites from the Staré Sedlo mylonite gneisses differ from a somewhat more Fe^{2+}-rich biotites from the Lašovice mylonite gneisses but there is no compositional overlap with biotites from granitoid rocks (*Foster, 1960*). These differences, partially related to the Fe^{3+}/Fe^{2+} ratio, are explained on the basis of different oxidation conditions, especially higher oxygen fugacity during ductile deformation and associated metamorphism of the protolith of the gneisses and schists compared to those of magmatic crystallization.

Consistent with the experimental work of *Rutherford (1973)* the Al^{VI} content in biotites increases with increasing metamorphic grade and the associated increased temperature and oxygen fugacity conditions (cf. *Wenk, 1970; Ramsay, 1973*). However for the Staré Sedlo and Mirotice rocks, the biotites largely plot in the field of magmatic biotites in the Al^{VI} vs Si/Al^{IV} discrimination diagram of *Bea (1980)* (Fig.3.6). The only grains that plot in the field of metamorphic biotites are three grains from rocks adjacent to a plutonic intrusion which also plot as part of a separate cluster on Fig.3.4. The other three from this group plot within the field of magmatic biotites but well away from the main cluster of biotites from the Staré Sedlo gneisses and relatively close to the metamorphic biotites - magmatic biotites boundary.

Whether the scatter of Al^{VI} content in the majority of the Staré Sedlo and Mirotice biotites can be explained on the basis of variable metamorphic conditions across the shear zone or should rather be attributed to variable Al activity in the system at the time of biotite crystallization, is not clear. However as biotite was likely to have been a mineral present in the tonalite - granodiorite protolith of the Staré Sedlo and Mirotice gneisses, it is possible that recrystallization in a closed system (mainly with respect to Al) during ductile deformation of this protolith could have resulted in the compositions of most of the recrystallized biotites being close to those of biotites of magmatic origin.

In the ternary system Fe^{3+} - Fe^{2+} - Mg (annite - phlogopite - $KFe_3^{3+}AlSi_3O_{12}(H_{-1})$; Fig.3.7) biotites from the Staré Sedlo and Mirotice gneisses and biotites from Lašovice gneisses form two separate arrays which correspond to the trends of experimentally synthesized biotite buffered by Fe_3O_4 - Fe_2O_3 and Ni - NiO systems, respectively (*Wones and Eugster, 1965*). The two straight-line patterns of biotite data in Fig.3.7 reflect the fact that only biotites from the representative samples of the Staré Sedlo, Lašovice and Mirotice gneisses were analyzed for FeO, but they do suggest very similar Fe^{3+}/Fe^{2+} ratios in biotites from the Staré Sedlo and Mirotice gneisses which are different from those for biotites from the Lašovice gneisses. *Wones and Eugster (1965)* carried out experiments on biotite synthesis under different temperature conditions using various buffering systems (Fe_3O_4 - Fe_2O_3, Fe_3O_4 - $Fe_{1-x}O$, NiO - Ni and SiO_2 - Fe_2SiO_4 - Fe_3O_4) in order to control the oxygen fugacity. They found that the contents of Fe and Mg in biotite (expressed as $Fe_{tot}/(Fe_{tot}+Mg)$ ratio) are controlled by the independent intensive parameters temperature, water fugacity (fH_2O) and oxygen fugacity (fO_2) during the crystallization of biotite, while the total pressure (p_{tot}) has only a negligible influence upon the biotite composition. They also derived a

series of equations which enabled them to construct a diagram of biotite stability in the fO_2-T system. Such positive correlation of oxygen fugacity and temperature is shown by the data for the biotites recrystallized during ductile deformation that resulted in the formation of the Staré Sedlo and Mirotice mylonite gneisses (Fig.3.8). The presence of both magnetite and hematite in the Staré Sedlo and Mirotice gneisses is consistent with the data plotting along the trend of biotites experimentally synthetized under the Fe_3O_4 - Fe_2O_3 buffering system. The limited data also suggest a somewhat different fO_2 during the growth of biotite in the Staré Sedlo and Mirotice gneisses and in the gneisses from the Lašovice quarry. On this plot the stability fields are contoured with values of constant $100*Fe_{tot}/(Fe_{tot}+Mg)$ and the biotite of a given $Fe_{tot}/(Fe_{tot}+Mg)$ ratio is stable below the corresponding contour. Above that contour the biotite of a particular composition would decompose by the reaction biotite <==> more magnesian biotite + alkali feldspar + magnetite + gas (gas phase is assumed to consist of H_2 and H_2O). The $100*Fe_{tot}/(Fe_{tot}+Mg)$ ratios in biotites from the Staré Sedlo and Mirotice gneisses and from the Lašovice gneisses vary from 42 to 71 and from 45 to 56, respectively (see also Fig.3.4). Assuming constant fH_2O and a pressure of 2.07 kbar, biotites from the Lašovice gneisses would crystallize at higher temperatures than those from the Staré Sedlo and Mirotice gneisses. The suggested fO_2 - T path for the ductile deformation of the protolith of the Staré Sedlo, Lašovice and Mirotice gneisses differs from that associated with magmatic crystallization as illustrated by data for gabbros, tonalites and diorites of the Central Bohemian Pluton given by *Cimbálníková et al. (1976)*: the trend for rocks of this magmatic suite cuts across the line representing the Fe_3O_4 - Fe_2O_3 buffering system suggesting that this crystallization was under conditions of variable fO_2 and fH_2O.

The Fe/(Fe+Mg) ratios in biotites from gneisses and K-feldspar-bearing mylonite schists - ultramylonites - blastomylonites of the Staré Sedlo and Mirotice complexes show neither positive, nor negative correlation with the whole-rock SiO_2 content which has been described by *Czamanske et al. (1981)* as being typical for ilmenite-bearing and magnetite-bearing granitoid suites, respectively (Fig.3.9). This is in accordance with other considerations as the redox path during the ductile deformation-related growth of biotite is not likely to be linked to the whole-rock differentiation (see also *Burkhard, 1991*). However with magnetite being associated with biotite in most of the studied rocks, this does indicate that the redox conditions of the system during biotite crystallization were not only controlled by a magnetite - hematite type of buffer but also that the buffering system was a rather complex one.

3.4 Amphibole

Amphibole is present as oriented clusters of elongate crystals in the gneisses of the Staré Sedlo and Mirotice complexes and it is often associated with biotite, sphene and magnetite. As its growth was clearly controlled by the foliation planes it represents part of the metamorphic mineral assemblage. In the amphibolites of the Staré Sedlo complex amphibole together with plagioclase and biotite form the substantial part of the rock. There also amphibole makes up part of the rock foliation and consequently its growth resulted from metamorphic reconstitution. Both the cores and rims of the amphibole grains were analyzed and no difference was found in their compositions; the main statistical values are given in Table 3.4. The crystallochemical formulae of amphiboles given in Appendix 3 were calculated on the basis of 23 oxygen atoms using a computer program of *Spear and Kimball (1984)* to estimate the proportion of Fe^{3+} and Fe^{2+}. In this recalculation, several estimations of Fe^{3+} content in amphibole were made, assuming the general form of the amphibole formula $A_{0-1}B_2C_5{}^{VI}T_8{}^{IV}O_{22}(OH,F,Cl)_2$. Several methods of normalization based upon the following assumptions were used: (1) Si = 8, (2) Si+Al = 8, (3) Si+Al+Ti+Fe^{3+}+Mg+Fe^{2+}+Mn = 13, (4) Si+Al+Ti+Fe^{3+}+Mg+Fe^{2+}+Mn+Ca = 15, (5) all Na is in the B(M4)-site, (6) A-site is filled. The amphibole formula was then calculated using the average of the highest (in this case based upon 3) and lowest (based upon 4) Fe^{3+} estimations.

The summary of the main statistical parameters of amphibole composition in Table 3.4 suggests that amphiboles from the gneisses of the Staré Sedlo complex have higher Mg relative to those from the Mirotice gneisses which, on the other hand, have higher Al, Fe and Mn. This difference however reflects the Mg-rich composition of the amphiboles in the gneiss occurring close to the contact of the Staré Sedlo complex with an adjacent intrusion of Mg-rich durbachite. Amphiboles from the amphibolites of the Staré Sedlo complex have somewhat higher contents of Ti and Ca compared to those from the gneisses of this complex.

All the amphiboles have $(Ca+Na)_B \geq 1.34$ and $Na_B < 0.67$ which means they belong to the group of calcic amphiboles (*Leake, 1978*). Within this group the majority corresponds to magnesio-hornblende with only a few having the composition of ferro-hornblende (Fig.3.10). Amphiboles from the samples of gneiss occurring close to the contact with the adjacent durbachite intrusion (Čertovo břemeno

type) have the composition of actinolite and actinolitic hornblende. There are also a few amphiboles which, due to somewhat higher Na and K contents in the A-site ($[Na + K]_A > 0.5$) and Fe^{3+} prevailing over Al^{VI}, have compositions corresponding to edenite, ferro-edenite, edenitic hornblende and magnesian hastingsitic hornblende. The close relations that generally exist between the composition of metamorphic amphiboles and the pressure and temperature conditions during their crystallization and, or, the whole-rock composition (e.g. *Leake, 1965; Gilbert et al., 1982; Robinson et al., 1982; Brodie and Rutter, 1985*) mean that the spread in the composition of amphiboles from the gneisses and amphibolites of the Staré Sedlo and Mirotice complexes can be attributed to the variations in the p and T conditions during metamorphic reconstruction of the protoliths as well as to variations in rock composition mainly across the ductile shear zone but also locally in places where the gneisses are adjacent to durbachitic intrusions.

As demonstrated by the Si and Al^{IV} vs Al^{VI} relations (Fig.3.11), the content of Al^{VI} in amphiboles from the gneisses and amphibolites is relatively low and almost uniform but amphiboles from the Mirotice gneisses have a somewhat higher Al^{IV} content than the amphiboles from corresponding rocks of the Staré Sedlo complex. With the content of Al^{VI} having been interpreted as being indicative of both the pressure during amphibole crystallization and the magma or whole-rock chemical composition, respectively (e.g. *Leake, 1965; Leake, 1971*), the overall uniform Al^{VI} content in amphibolites (within the range of 0.03 - 0.31) suggests the crystallization under approximately the same pressure conditions. As this holds also for amphibole from the amphibolite where Al^{VI} content is within the range of amphiboles from the gneisses, the Al^{VI} content in amphiboles in these rocks is unlikely to have been affected by the whole-rock composition. This conclusion is also supported by a somewhat higher Al^{IV} content in amphiboles from the Mirotice gneisses despite their lower whole-rock Al content relative to the Al^{IV} in amphiboles and whole-rock Al content in corresponding rocks from the Staré Sedlo complex (see Table 4.1). Because C(M2)-sites usually prefer Fe^{2+} to Mg^{2+}, amphiboles with high Al^{VI} content tend to be Mg-rich as these sites are filled with Al^{VI} rather than Fe^{2+} (*Ghose, 1965*). Consequently, when Fe^{2+} is replaced by Al^{3+}, the reaction requires charge compensation by means of Al^{3+}-->Si^{4+} substitution which may be responsible for low Fe^{3+} and Ti^{4+} in Al^{VI}-rich calciferous amphiboles (*Leake, 1971*).

Actinolites from gneisses of the Staré Sedlo complex near the contact with the durbachite intrusion have a Si content in the formula of more than 7.5 (Al^{IV} less than 0.5) and a very low Al^{VI}

(some of them have the lowest Al^{VI} from all the studied amphiboles). Therefore the high Mg/Fe ratio of these amphiboles (see also Fig.3.10) cannot be the result of the high Al^{VI} content due to recrystallization under high-pressure conditions. As the corresponding whole-rock analysis does not show any anomalous Mg-enrichment which would indicate a possible effect on the composition of crystallizing amphibole of the whole-rock composition of the gneiss, the likely explanation is that the amphibole recrystallization resulted from the contact heating by the nearby Mg-rich magma. As no relics of an older amphibole were found, this recrystallization had to be complete and probably included an exchange reaction (at least for Mg) between the Mg- and fluid-rich durbachitic magma and the host gneisses. However the extent of the contact influence was probably constrained to a narrow zone (ca 200 - 300 m wide) along the contact.

The Ti content in amphiboles from the gneisses and amphibolites of both complexes (Fig.3.12) is low (less then 0.2) and suggests a metamorphic origin (cf. *Leake, 1965*) for which textural evidence has already been given. Likewise the pressure of amphibole crystallization is reflected by its Al^{VI} content, the Ti content in amphibole is related to the crystallization temperature and indeed to the whole-rock or magma chemical composition. This relationship has been investigated by *Leake (1965)* and subsequently found as valid by many others (see *Robinson et al., 1982* and *Gilbert et al., 1982* for references). Such relations where the Ti content in amphibole decreases with increasing crystallization temperature are rare (e.g. *Cawthorn, 1976*). It has also been noted that Ti content in hornblende depends strongly upon the oxygen fugacity at the time of its crystallization (*Gilbert et al., 1982*). The variations of Ti content in amphiboles from gneisses and amphibolites are within the range of 0.03 - 0.17 and are likely to reflect the fluctuations in temperature, composition and, or, the oxygen fugacity across the shear zone at the time of amphibole crystallization.

The Ca+Na+K content in the amphiboles is fairly close to the limit which *Leake (1971)* considers to represent the upper compositional limit of amphiboles of igneous derivation (Fig.3.13). The somewhat lower Ca+Na+K values for amphibole from the Staré Sedlo amphibolite reflects only depletion of Ca while Na and K contents generally correspond to those in amphiboles from the gneisses (see Table 3.4). Just as the biotites from the mylonite gneisses of the Staré Sedlo and Mirotice complexes (see Section 3.3 for the discussion and Fig.3.6) show igneous affinities so the metamorphic amphiboles appear to reflect a preserved igneous chemical record of their tonalitic - granodioritic protolith. However no relics of igneous amphiboles similar to those reported by *Vrána and Cháb (1981)* from the ductilely

deformed tonalite of the Central Bohemian Pluton were found in the rocks of the Staré Sedlo and Mirotice complexes.

Amphibole mineral chemistry studies from metabasic rocks in several metamorphic terrains indicate that while the mineral assemblage remains constant through a relatively wide range of p-T conditions, the mineral compositions vary continuously as a function of p and T changes (for references see *Brodie and Rutter, 1985*). However as the amphibole composition reflects not only pressure and temperature but also the gas phase fugacity, the fluid phase composition and the whole-rock composition, quantification of these variations is often difficult. *Laird and Abee (1981)* developed a method of pressure estimation within a shear zone based upon the amphibole composition which is independent of the calculation of Fe^{2+}/Fe^{3+} proportion and of the assignment of cations to structural sites. As the composition of amphiboles from amphibolites of the Staré Sedlo complex (despite some small differences in Ca and Ti - see Table 3.4) generally corresponds to that of amphiboles from the gneisses, the total Na/Ca and Al/Si relations proposed by *Laird and Abee (1981)* to be indicative of metamorphic pressure have also been applied to the gneisses. In Fig.3.14 most of the rocks plot along the actinolite - pargasite tie-line representing the medium-pressure metamorphic rocks from Vermont, U.S.A., with only few amphibole samples trending towards the low-pressure rocks. The scatter of points is likely to have resulted from the pressure variation within the shear zone during the ductile deformation of the protoliths of the Staré Sedlo and Mirotice mylonite gneisses.

3.5 Garnet

Garnet is present only in the garnet - biotite mylonite gneisses within a narrow zone along the contact of the Mirotice complex with the granodiorite of Blatná type of the Central Bohemian Pluton. It is present as euhedral grains or clusters often associated with biotite (the analyses are given in Appendix 3). The crystallochemical formulae were calculated on the basis of 24 oxygen atoms using the computer program of *Knowles (1987)* based upon the procedure proposed by *Rickwood (1968)*. In order to estimate the Fe^{3+}/Fe^{2+} proportion, the method similar to that of *Deer et al. (1962)* was employed. The principles of the Fe^{3+}/Fe^{2+} estimation were as follows: if Cr > [Mg + Mn + Fe^{2+}] then all Fe was considered as Fe^{3+}, if Ca > 20, Al < 10 then 95% of all Fe was taken as Fe^{3+}, if Ca > 20, Al > 10 then 50% of all

Fe was taken as Fe^{3+}, if Ca < 20, Al > 12 then 5% of all Fe was taken as Fe^{3+}, if Ca < 20, Al < 12, Mn < 20, Mg > 10 then 5% of all Fe was taken as Fe^{3+}, if Ca < 20, Al < 12, Mn > 20 then all Fe was taken as Fe^{2+} and finally, when none of the previous conditions could be applied, all Fe was recalculated to Fe^{2+}.

Both the cores and the rims of garnet grains were analyzed but no differences in their compositions were found. All the analyses of garnet are within a very narrow compositional range and the variations are likely to be the result of the analytical procedure. The garnet composition expressed by means of average weight percent of its end members is: almandine 54.63, spessartine 35.31, pyrope 5.07, andradite 4.55, grossular 0.38. Together with the coexisting high-alumina biotite that must have crystallized at the same time as garnet, the two minerals are considered to preserve the record of temperature conditions in the thermal aureole of the Blatná granodiorite.

3.6 Conclusions

1. There are three mineral assemblages present in the rocks of the Staré Sedlo and Mirotice complexes that crystallized under different p and T conditions in different times. (1) Porphyroclasts of plagioclase and K-feldspar form part of the oldest (igneous) assemblage. Some of them still have preserved oscillatory compositional zoning. (2) A dynamothermal metamorphic assemblage is represented by biotite and amphibole which, however, still bear some compositional relics of their igneous precursors and by newly formed plagioclase, K-feldspar and quartz. (3) The youngest assemblage, which was formed in response to the thermal metamorphism by adjacent granitoids and durbachites, consists of garnet, high-alumina biotite and actinolite.

2. The ductile deformation and associated metamorphic reconstruction of the protolith of Staré Sedlo and Mirotice complexes took place under medium-pressure conditions. However some pressure as well as temperature and oxygen fugacity fluctuations within the shear zone caused corresponding scatter of the mineral composition of the metamorphic assemblage. These are reflected in the biotite and amphibole compositions.

Table 3.1

Main statistical parameters (wt%) for the composition of plagioclase (porphyroclasts and unzoned grains).

	SiO_2	TiO_2	Al_2O_3	FeO_T	MnO	MgO	CaO	Na_2O	K_2O
				Mylonite gneisses - Staré Sedlo (n=87)					
X	60.63	0.03	24.32	0.09	0.02	0.03	5.94	8.15	0.30
G	60.61	---	24.30	---	---	---	5.81	8.12	0.26
median	60.34	0.01	24.42	0.08	0.00	0.01	6.01	8.05	0.24
min	57.29	0.00	19.35	0.00	0.00	0.00	2.26	6.61	0.10
max	67.93	0.11	26.51	0.45	0.10	0.20	8.54	10.43	2.05
stdev	1.64	0.03	1.04	0.08	0.03	0.04	1.14	0.71	0.28
				Mylonite gneisses - Lašovice (n=9)					
X	58.35	0.02	25.40	0.05	0.01	0.05	7.28	7.30	0.20
G	58.31	---	25.37	---	---	---	7.09	7.23	0.19
median	58.10	0.02	25.51	0.05	0.01	0.01	7.49	7.07	0.20
min	55.75	0.00	22.87	0.00	0.00	0.00	4.24	6.18	0.11
max	61.86	0.08	27.22	0.14	0.06	0.17	9.45	9.27	0.26
stdev	2.14	0.03	1.42	0.05	0.02	0.06	1.67	1.04	0.05
				Mylonite gneisses - Mirotice (n=62)					
X	61.86	0.01	24.37	0.06	0.01	0.08	5.36	8.64	0.22
G	61.80	---	24.31	---	---	---	5.03	8.56	---
median	62.25	0.00	24.10	0.00	0.00	0.00	5.04	8.76	0.12
min	53.69	0.00	22.11	0.00	0.00	0.00	2.52	5.26	0.00
max	66.52	0.17	29.29	0.26	0.13	0.17	11.89	10.78	1.93
stdev	2.63	0.04	1.60	0.07	0.03	0.09	1.96	1.15	0.26
				Mylonite schists - Mirotice (n=17)					
X	62.82	0.01	23.45	0.06	---	0.10	4.32	9.20	0.16
G	62.77	---	23.41	---	---	---	3.86	9.12	---
median	63.53	0.00	23.05	0.00	---	0.17	3.78	9.44	0.12
min	57.54	0.00	20.98	0.00	---	0.00	1.12	6.47	0.00
max	67.59	0.17	26.83	0.13	---	0.33	8.26	11.19	0.48
stdev	2.64	0.04	1.49	0.07	---	0.10	1.81	1.21	0.11
				Amphibolites - Staré Sedlo (n=7)					
X	60.06	0.01	24.83	0.17	0.01	0.04	6.43	8.01	0.22
G	60.06	---	24.83	0.16	---	---	6.43	8.00	0.20
median	60.05	0.00	24.83	0.13	0.00	0.00	6.34	8.04	0.21
min	59.57	0.00	24.55	0.10	0.00	0.00	6.24	7.72	0.11
max	60.41	0.05	24.97	0.25	0.04	0.13	6.74	8.36	0.31
stdev	0.29	0.02	0.14	0.06	0.02	0.05	0.20	0.27	0.08

Table 3.2

Main statistical parameters (wt%) for the composition of K-feldspar.

	SiO_2	TiO_2	Al_2O_3	FeO_T	MnO	MgO	CaO	Na_2O	K_2O
					Mylonite gneisses - Staré Sedlo (n=25)				
X	64.19	0.17	18.55	0.06	0.03	0.06	0.10	1.08	14.87
G	64.19	---	18.55	---	---	---	---	0.95	14.83
median	64.21	0.20	18.46	0.07	0.02	0.05	0.03	0.95	15.13
min	63.38	0.00	18.23	0.00	0.00	0.00	0.00	0.33	10.25
max	64.98	0.41	19.31	0.19	0.14	0.17	0.71	4.01	15.91
stdev	0.34	0.12	0.28	0.05	0.04	0.05	0.18	0.70	1.11
					Mylonite gneisses - Mirotice (n=36)				
X	64.36	0.20	19.00	0.03	0.02	0.04	0.21	1.19	14.84
G	64.35	---	18.98	---	---	---	---	0.93	13.84
median	64.28	0.17	18.90	0.00	0.00	0.00	0.00	0.88	15.24
min	62.46	0.00	18.33	0.00	0.00	0.00	0.00	0.40	0.48
max	65.67	0.33	23.81	0.13	0.13	0.17	4.62	8.90	16.50
stdev	0.64	0.08	0.87	0.05	0.05	0.07	0.79	1.40	2.57
					Mylonite schists - Mirotice (n=14)				
X	63.91	0.29	18.64	0.03	0.00	0.05	0.01	0.88	15.22
G	63.91	0.25	18.64	---	---	---	---	0.83	15.21
median	63.96	0.17	18.71	0.00	0.00	0.00	0.00	0.88	15.36
min	63.32	0.17	18.52	0.00	0.00	0.00	0.00	0.54	14.09
max	64.17	0.67	18.71	0.13	0.00	0.17	0.14	1.35	15.78
stdev	0.31	0.18	0.09	0.06	0.00	0.08	0.04	0.28	0.52

Table 3.3

Main statistical parameters (wt%) for the composition of biotite.

	SiO_2	TiO_2	Al_2O_3	FeO_T	MnO	MgO	CaO	Na_2O	K_2O
	Mylonite gneisses - Staré Sedlo (n=25)								
X	36.12	2.79	15.48	19.25	0.64	11.10	0.05	0.19	9.29
G	36.12	2.77	15.36	19.12	0.60	11.05	---	---	9.29
median	36.07	2.77	14.40	18.86	0.63	11.49	0.06	0.22	9.32
min	35.38	2.26	14.08	15.47	0.32	8.73	0.00	0.00	8.95
max	36.87	3.91	19.72	22.47	1.41	12.49	0.12	0.36	9.56
stdev	0.42	0.36	2.05	2.26	0.24	1.12	0.04	0.12	0.19
	Mylonite gneisses - Lašovice (n=5)								
X	35.70	3.23	15.67	17.07	0.41	10.54	0.04	0.18	9.37
G	35.70	3.20	15.66	16.94	0.40	10.51	0.04	0.18	9.37
median	35.43	3.31	15.37	18.71	0.46	10.55	0.04	0.19	9.42
min	35.22	2.50	15.20	14.55	0.28	9.62	0.02	0.10	8.98
max	36.34	3.67	16.25	18.73	0.49	11.56	0.08	0.24	9.57
stdev	0.52	0.47	0.54	2.26	0.09	0.91	0.03	0.06	0.23
	Mylonite gneisses - Mirotice (n=48)								
X	35.83	2.97	15.98	21.95	0.79	9.37	0.03	0.20	9.36
G	35.82	2.83	15.94	21.75	0.71	9.00	---	---	9.35
median	35.94	2.92	15.50	21.04	0.77	10.70	0.00	0.27	9.40
min	34.44	1.67	14.74	18.14	0.26	5.47	0.00	0.00	8.19
max	37.43	4.50	18.52	26.12	1.29	12.60	0.28	0.40	9.76
stdev	0.94	0.90	1.20	2.95	0.32	2.54	0.07	0.11	0.31
	Mylonite schists - Mirotice (n=9)								
X	35.39	2.97	16.78	21.90	0.79	8.46	0.03	0.18	9.35
G	35.39	2.91	16.77	21.89	0.78	8.44	---	---	9.33
median	35.29	3.17	16.82	21.87	0.77	8.62	0.00	0.13	9.52
min	34.87	2.17	16.25	21.10	0.65	7.63	0.00	0.00	8.07
max	36.15	3.67	17.57	22.90	0.90	8.95	0.14	0.27	9.64
stdev	0.37	0.59	0.43	0.50	0.12	0.45	0.06	0.10	0.49
	Amphibolites - Staré Sedlo (n=1)								
	37.14	3.39	14.49	17.95	0.52	11.99	---	0.29	9.50

Table 3.4

Main statistical parameters (wt%) for the composition of amphibole.

	SiO_2	TiO_2	Al_2O_3	FeO_T	MnO	MgO	CaO	Na_2O	K_2O
	Mylonite gneisses - Staré Sedlo (n=40)								
X	46.86	0.79	6.58	17.04	1.15	11.45	11.59	1.08	0.65
G	46.77	0.74	6.13	16.93	0.99	11.28	11.59	1.02	0.58
median	45.66	0.78	7.45	16.78	1.24	11.28	11.64	1.14	0.76
min	43.65	0.28	2.25	13.88	0.24	7.74	10.93	0.27	0.13
max	52.74	1.25	9.17	21.22	2.02	14.91	12.53	1.57	0.99
stdev	2.89	0.26	2.05	2.02	0.51	1.97	0.36	0.32	0.24
	Mylonite gneisses - Mirotice (n=22)								
X	44.46	0.83	8.46	19.01	1.61	10.02	11.35	1.38	0.82
G	44.43	0.78	8.40	18.82	1.58	9.79	11.35	1.38	0.81
median	45.03	0.67	8.13	17.69	1.68	10.78	11.33	1.35	0.84
min	40.86	0.50	6.99	16.47	1.03	5.64	11.05	0.94	0.60
max	47.06	1.50	11.34	25.09	1.94	12.10	11.61	1.62	1.20
stdev	1.62	0.31	1.11	2.88	0.26	2.01	0.16	0.16	0.15
	Amphibolites - Staré Sedlo (n=6)								
X	45.86	0.95	7.53	16.47	0.81	11.84	11.86	1.22	0.73
G	45.83	0.94	7.45	16.46	0.81	11.82	11.85	1.21	0.71
median	45.55	0.97	7.71	16.60	0.82	11.66	11.84	1.19	0.75
min	43.93	0.73	5.53	15.07	0.69	11.02	11.70	0.93	0.47
max	48.81	1.13	8.89	17.44	0.89	13.44	12.14	1.49	0.94
stdev	1.63	0.15	1.10	0.77	0.07	0.83	0.16	0.21	0.15

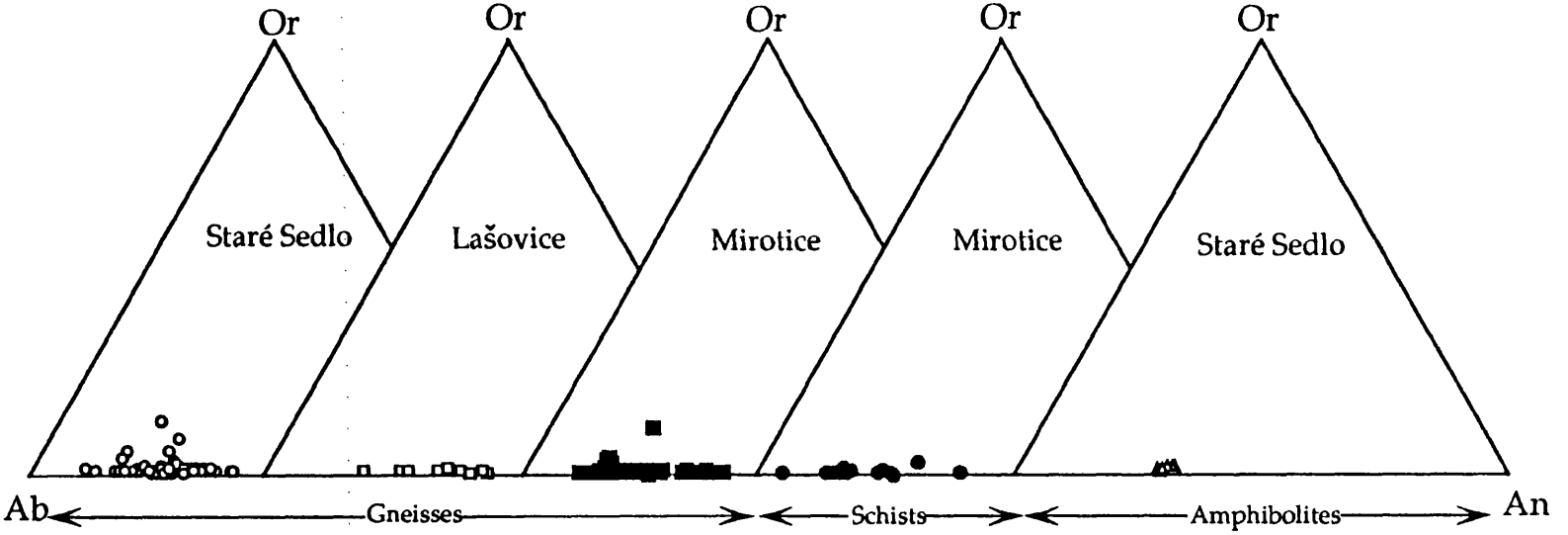

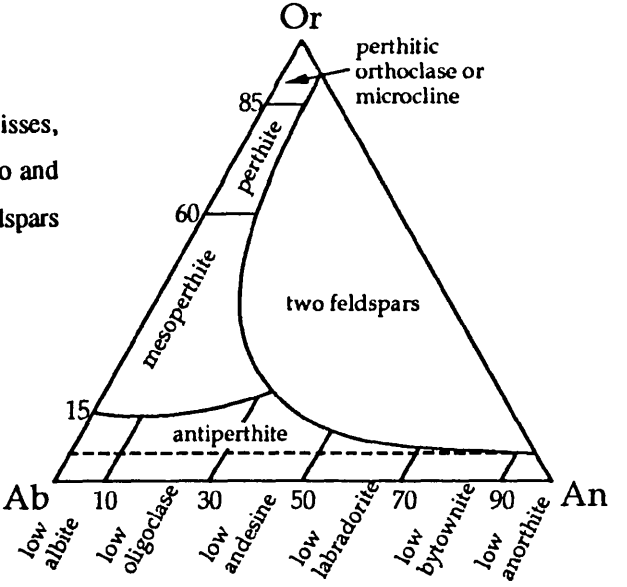

Fig.3.1

Composition of plagioclase from the mylonite gneisses, mylonite schists and amphibolites of the Staré Sedlo and Mirotice complexes; the classification of ternary feldspars is from *Smith and Brown (1988).*

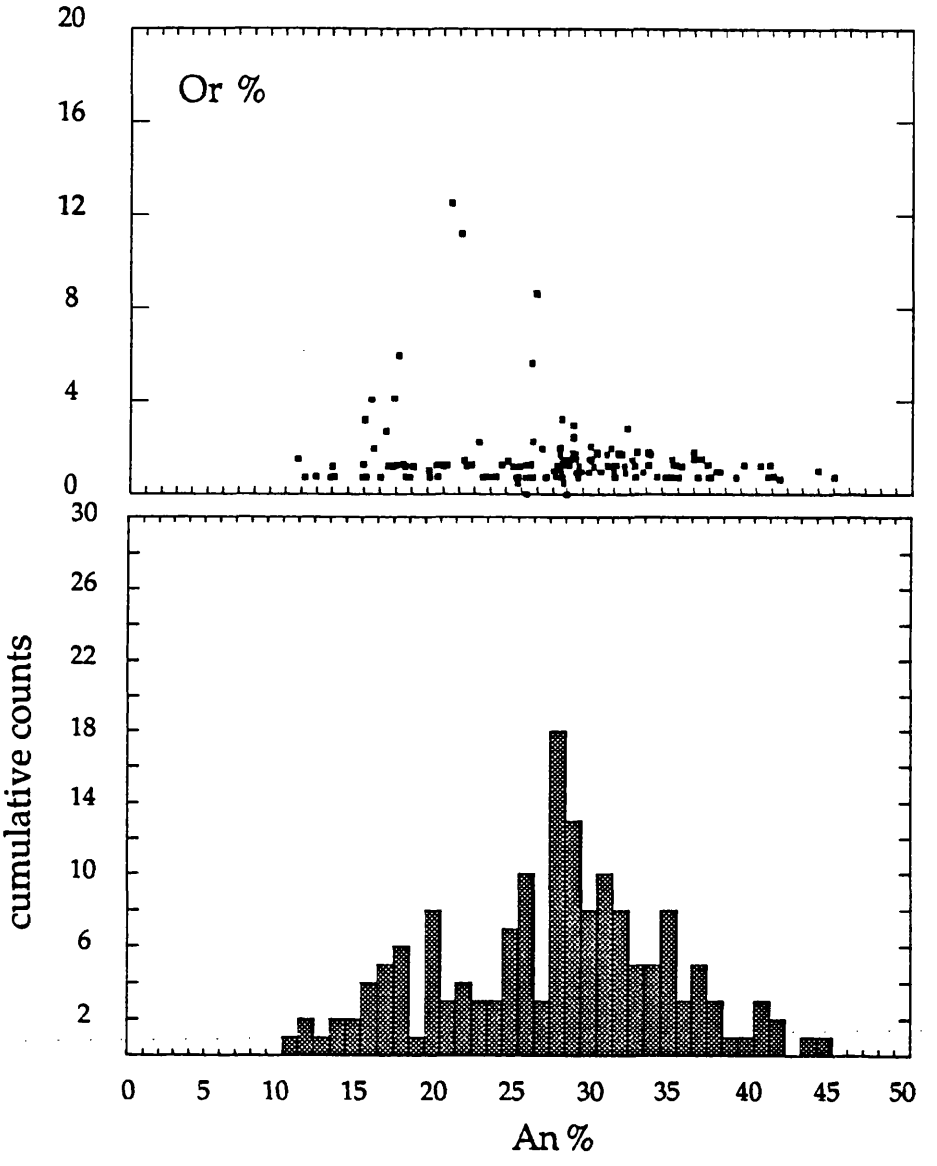

Fig.3.2

Histogram of An [mol%] composition and a corresponding Or [mol%] in plagioclase from mylonite gneisses of the Staré Sedlo and Mirotice complexes.

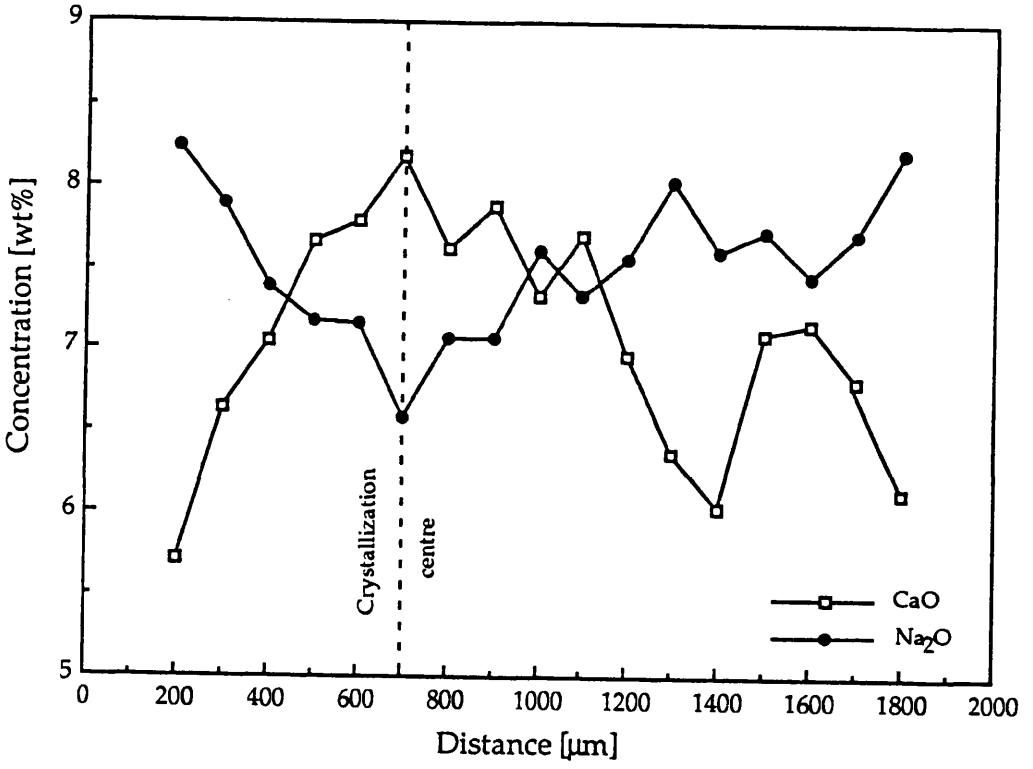

Fig.3.3

CaO and Na_2O chemical profiles across a zoned plagioclase porphyroclast from mylonite gneiss (sample STG-11, Plg16 - Plg 32); Staré Sedlo complex.

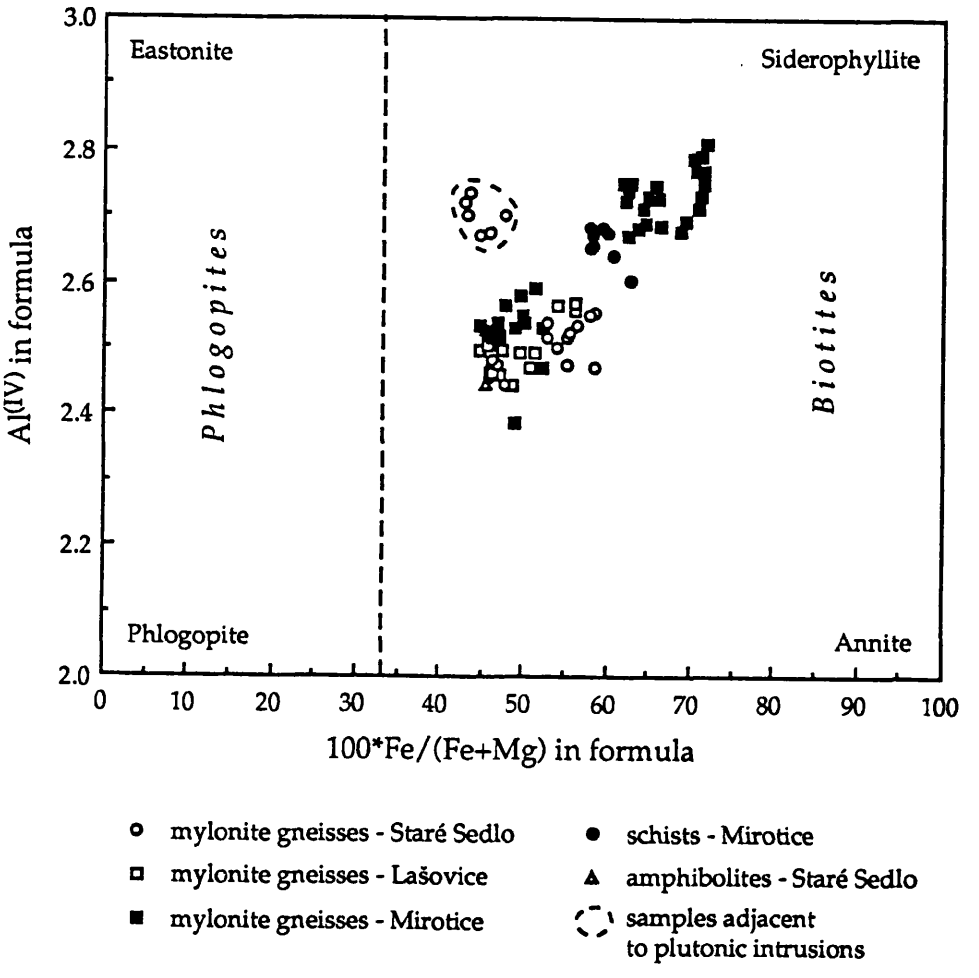

Fig.3.4

Al^{IV} and Fe/(Fe+Mg) composition of biotites from the mylonite gneisses, mylonite schists and an amphibolite of the Staré Sedlo and Mirotice complexes.

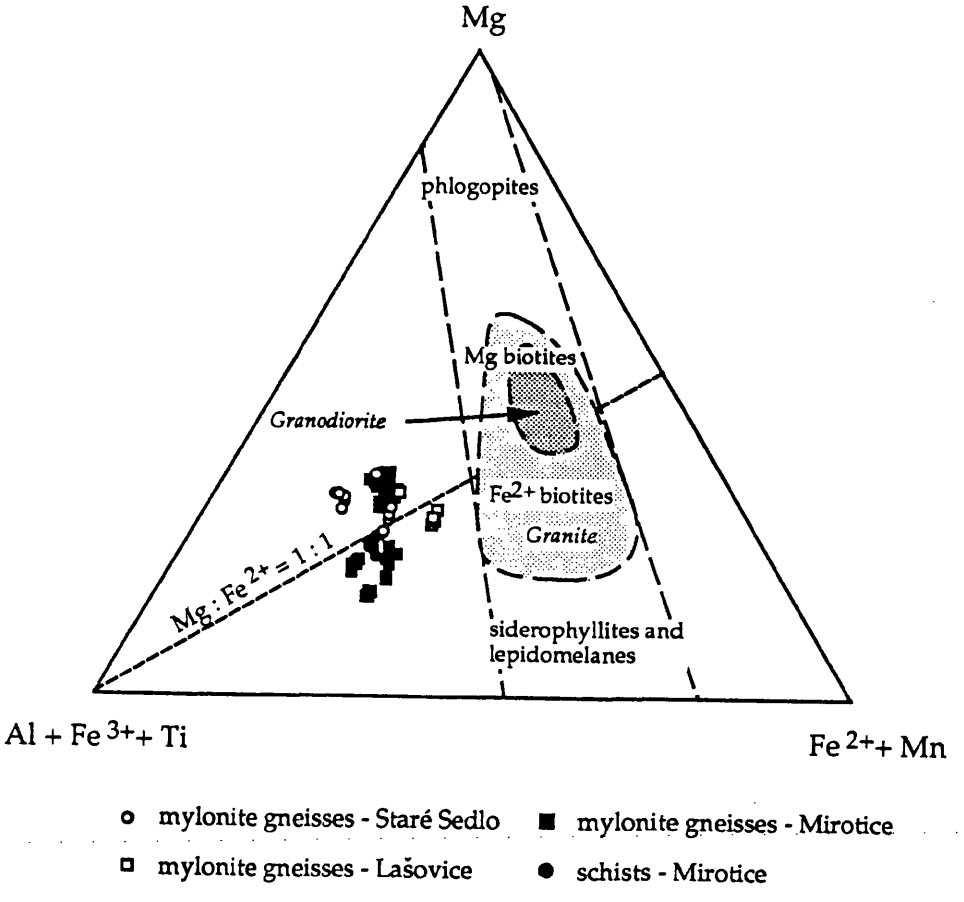

Fig.3.5

The ratio of the main cations (Fe and Mg) of the octahedral layer of biotite from mylonite gneisses and mylonite schists of the Staré Sedlo and Mirotice complexes; fields for biotite from granite and granodiorite are from *Foster (1960)*.

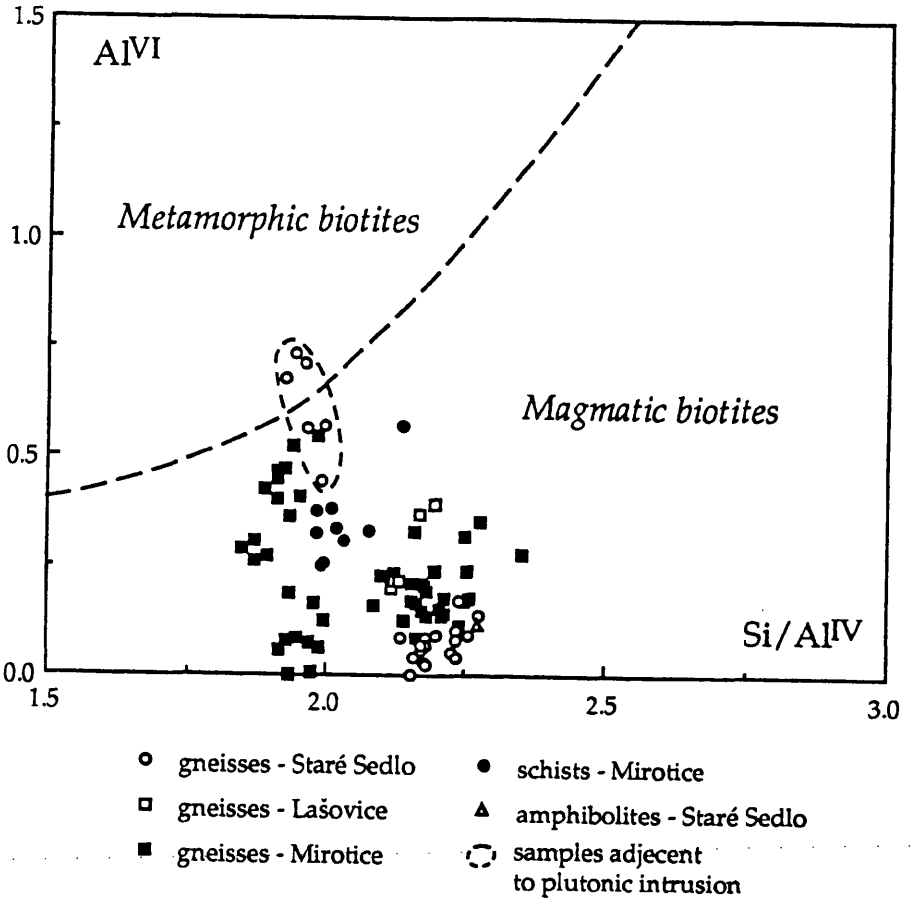

Fig.3.6

Al^{VI} vs Si/Al^{IV} discrimination diagram for biotites from mylonite gneisses, mylonite schists and an amphibolite from the Staré Sedlo and Mirotice complexes; fields for biotites of magmatic and metamorphic origin are from *Bea (1980)*.

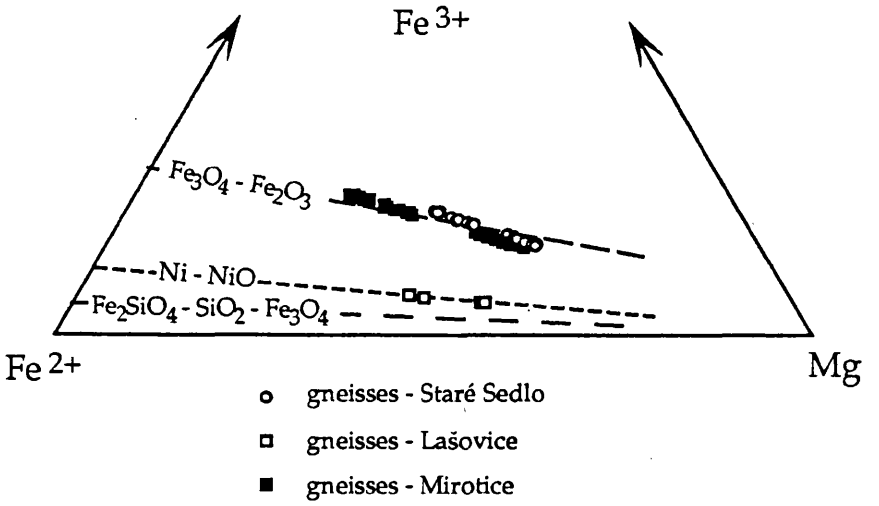

Fig.3.7

The composition of biotites from the mylonite gneisses of the Staré Sedlo and Mirotice complexes in the annite - phlogopite - $KFe_3^{3+}AlSi_3O_{12}(H_{-1})$ system; also shown are the compositions of synthetic biotites from the Fe_3O_4 - Fe_2O_3, Ni - NiO and Fe_2SiO_4 - SiO_2 - Fe_3O_4 buffered systems of *Wones and Eugster (1965).*

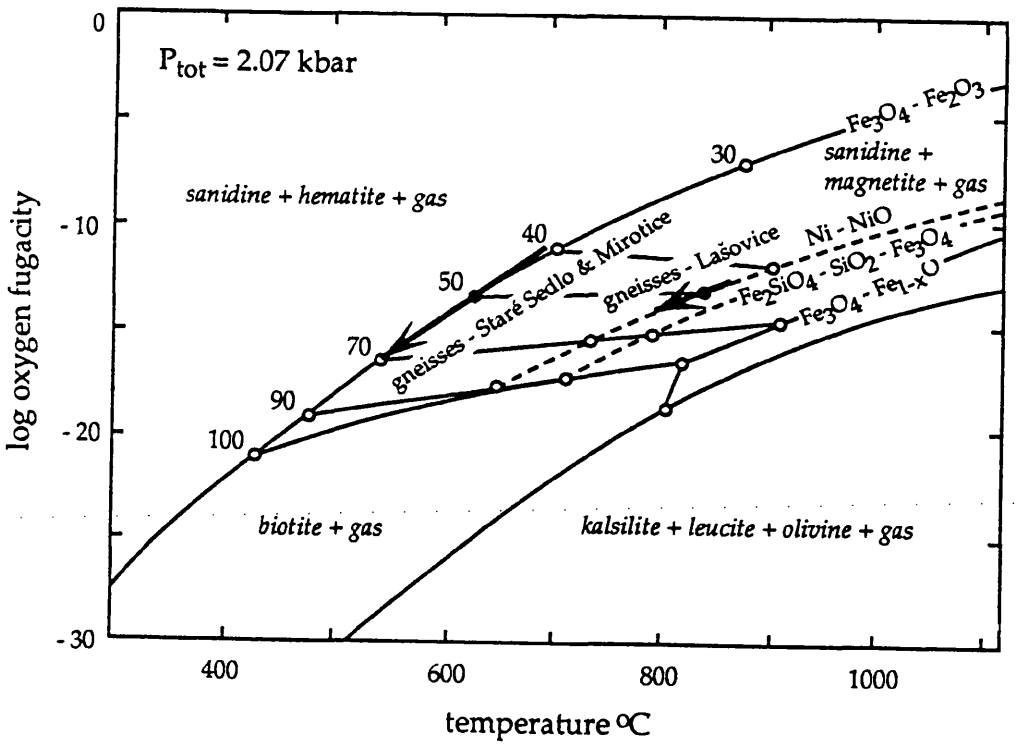

Fig.3.8

Diagram of biotite stability under different temperature and oxygen fugacity at a total pressure of 2.07 kbar (*Wones and Eugster, 1965*); trends for biotites from the mylonite gneisses of the Staré Sedlo and Mirotice complexes are represented by arrows oriented in sense of decreasing temperature; numbers correspond to the constant 100*Fe/(Fe+Mg) values under which is biotite with a given Fe/(Fe+Mg) ratio stable; buffering systems are those from Fig.3.7.

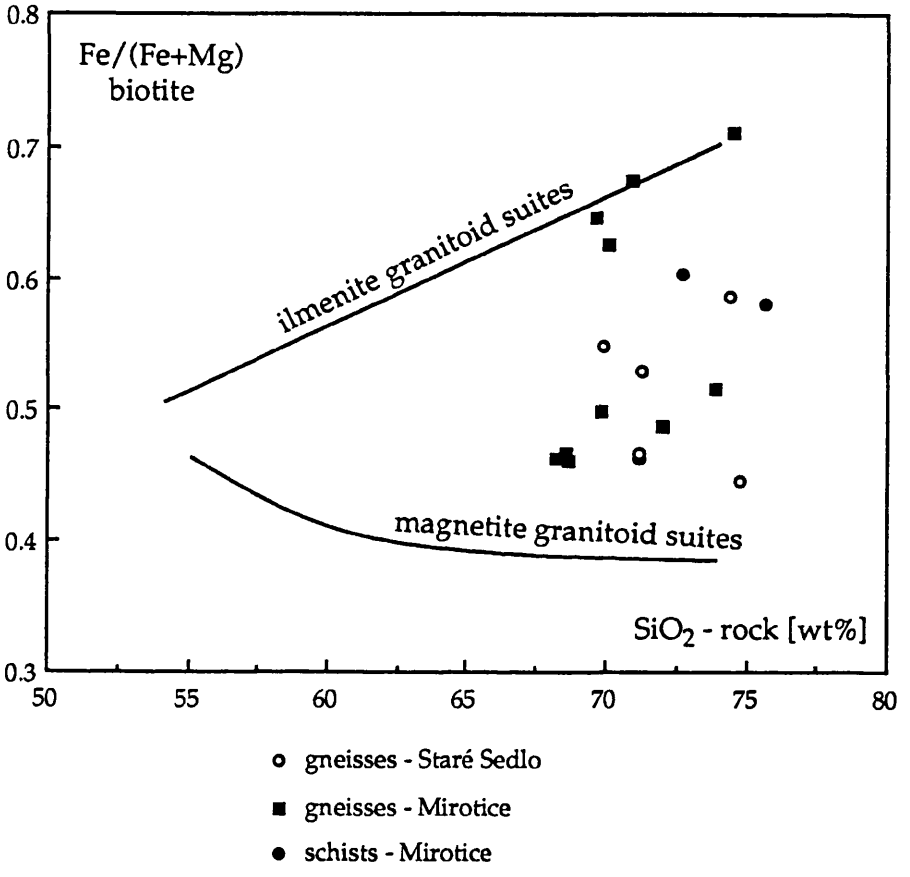

Fig.3.9

Fe/(Fe+Mg) ratio in biotites from gneisses and schists of the Staré Sedlo and Mirotice complexes; trends for ilmenite- bearing and magnetite-bearing granitoid suites are from *Czamanske et al. (1981).*

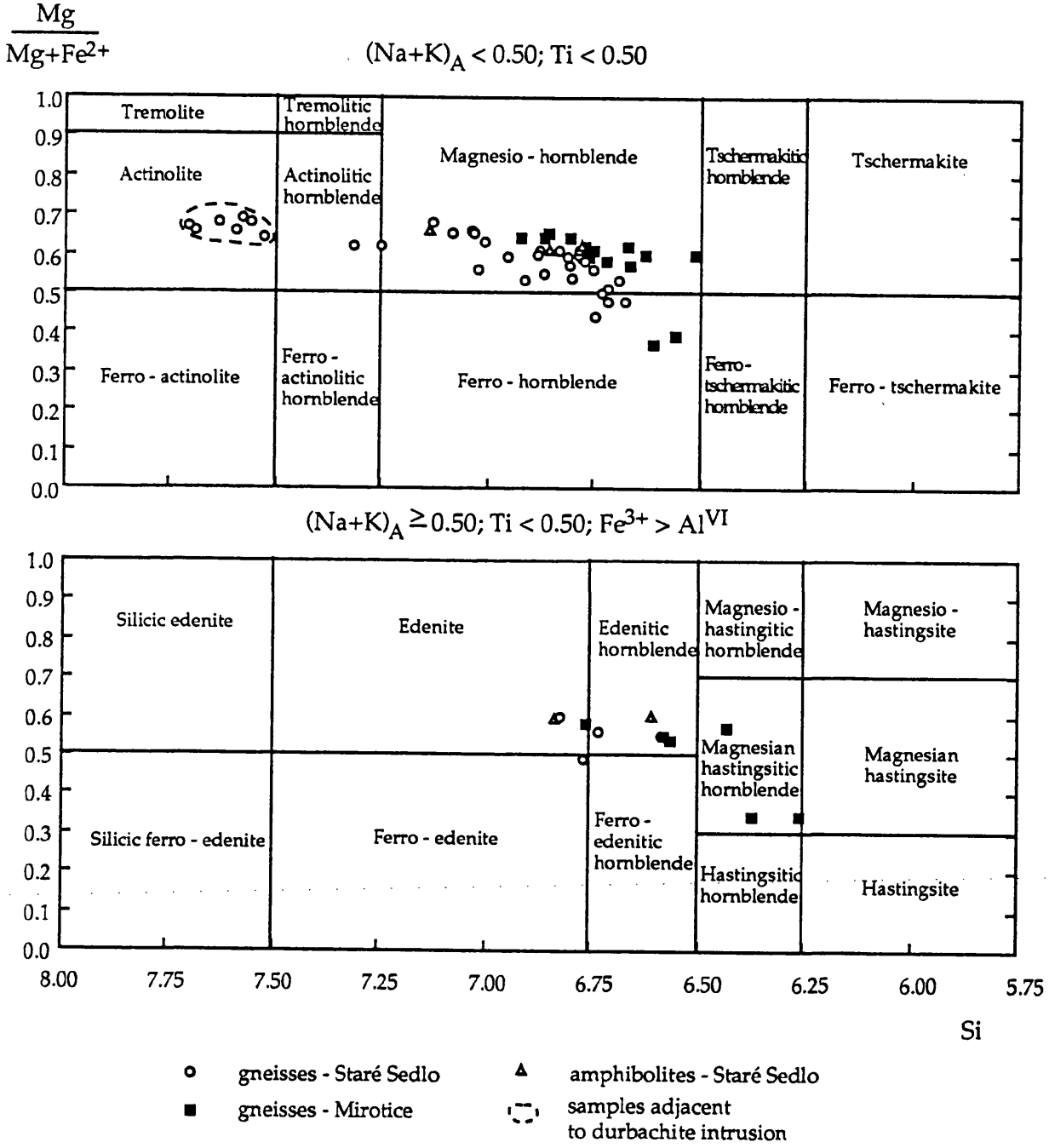

Fig.3.10

Plots of amphibole composition from gneisses and amphibolites of the Staré Sedlo and Mirotice complexes in the classification diagram for calcic amphiboles of *Leake (1978)*.

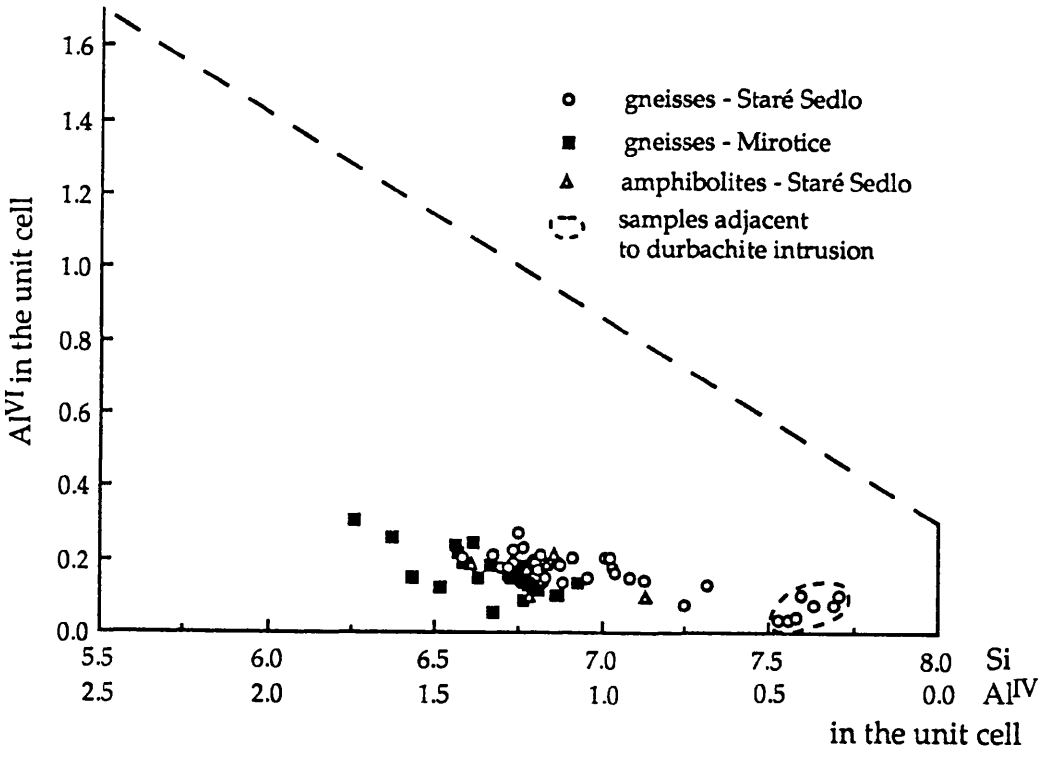

Fig.3.11

Distribution of Al^{VI} in calcic amphiboles from gneisses, schists and amphibolites of the Staré Sedlo and Mirotice complexes; the diagonal line shows the maximum possible Al^{VI} content at a corresponding Si content for calciferous and subcalciferous amphiboles (*Leake, 1965*).

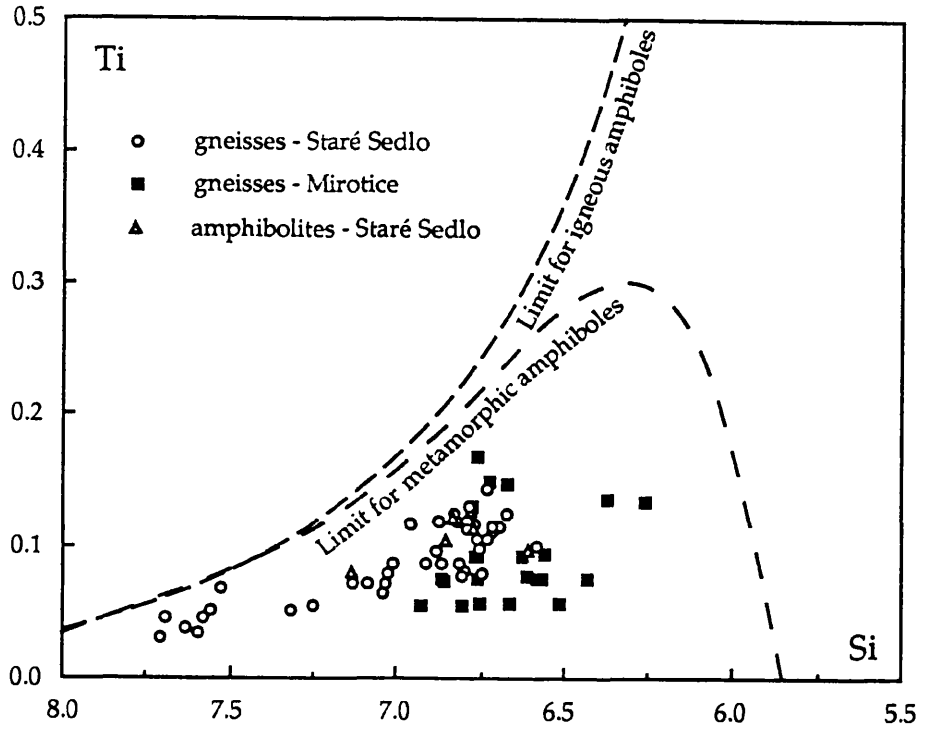

Fig.3.12

Ti content in amphiboles from gneisses and amphibolites of the Staré Sedlo and Mirotice complexes; compositional limits for igneous and metamorphic amphiboles are from *Leake (1965)*.

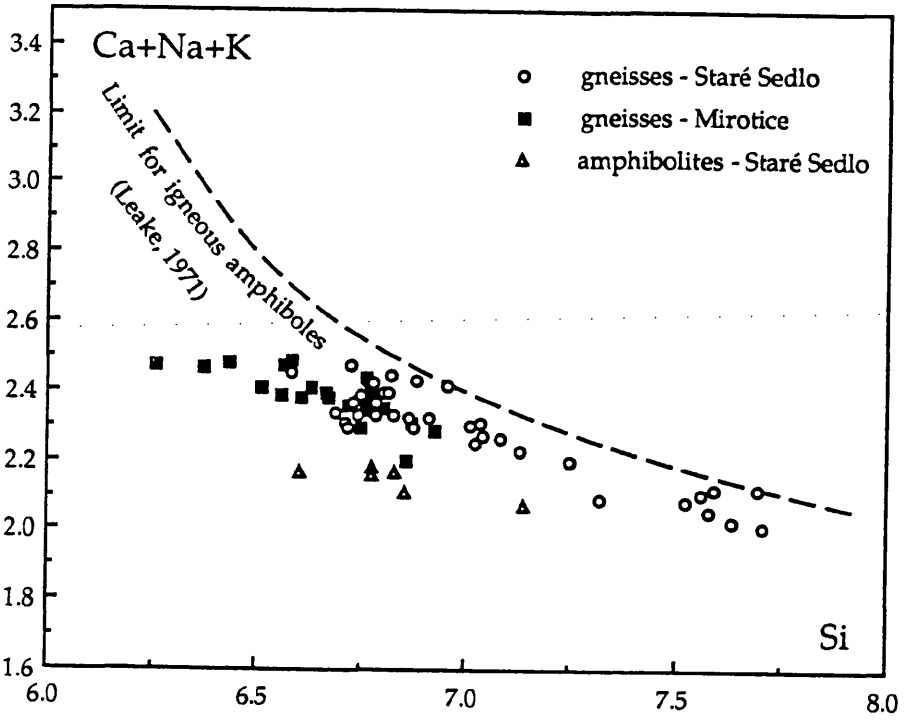

Fig.3.13

Ca+Na+K vs Si contents in calcic amphiboles from mylonite gneisses and amphibolites of the Staré Sedlo and Mirotice complexes.

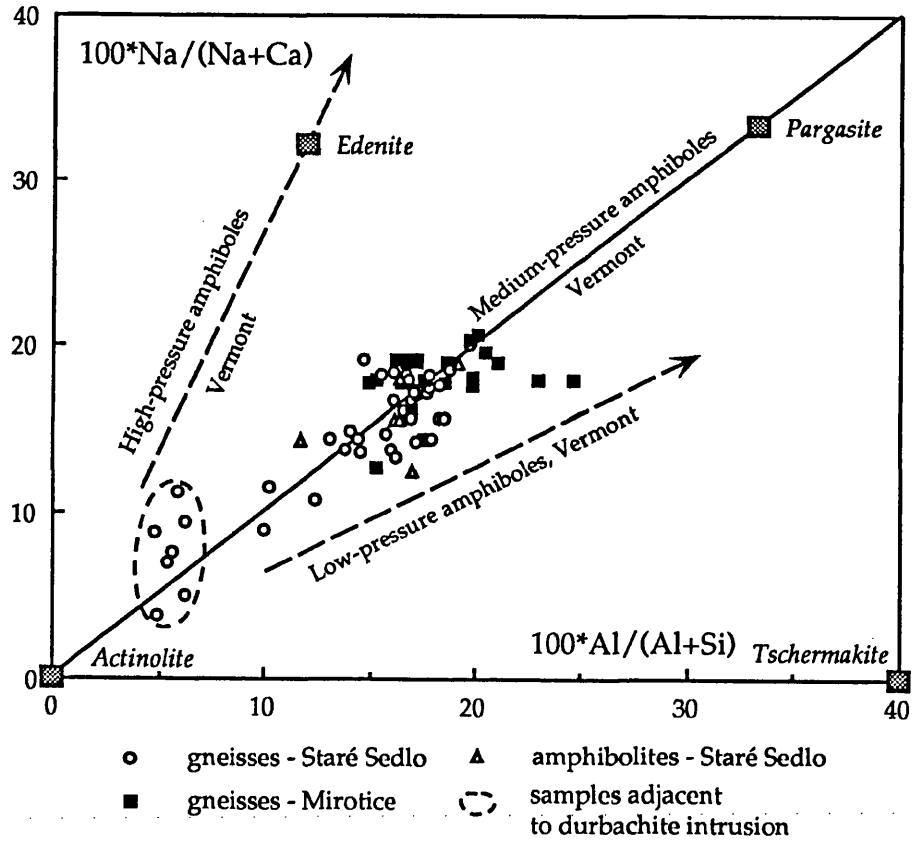

Fig.3.14

Total Na/Ca vs total Al/Si in calcic amphiboles from gneisses and amphibolites of the Staré Sedlo and Mirotice complexes; trends are for high-, medium- and low-pressure amphiboles are from Ivrea shear zone and metamorphic terraines in Vermont, U.S.A. (*Laird and Abee, 1981*).

4. ROCK CHEMISTRY

In order to demonstrate the nature and geotectonic affiliations of rocks from the Staré Sedlo and Mirotice complexes both major and trace element chemical analyses were carried out using x-ray fluorescence (XRF) for most major and trace elements, inductively coupled plasma mass spectrometry (ICP-MS) for rare earth elements and Cs and classical methods for FeO, H_2O and CO_2. The details of particular methods and analytical procedures used for individual elements are described in Appendix 2 and the analytical data are given in Appendix 4. The rocks are dealt with in groups based upon the rock unit and locality. The grouping is as follows.

Staré Sedlo complex

Biotite - amphibole - feldspar-bearing mylonite gneisses - Staré Sedlo (STG) - samples are from the main part of the Staré Sedlo complex E of Staré Sedlo town (see Fig.1.1b).

Biotite - feldspar-bearing mylonite gneisses - Lašovice quarry (LG) - samples are from the single quarry outcrop that represents a northern extension of the Staré Sedlo complex.l

Amphibolites - Staré Sedlo (STA) - samples are from the part of the complex E of Staré Sedlo town.

Meta-aplites - Staré Sedlo (STM) - samples are from the part of the complex E of Staré Sedlo town.

Mirotice complex

Biotite - feldspar - garnet-bearing mylonite gneisses - Mirotice complex (MIG)

K-feldspar-bearing schists - ultramylonites - blastomylonites - Mirotice complex (MIS)

Most attention in this chapter is given to the main rock units - gneisses and schists of both the Staré Sedlo and Mirotice complexes - although some aspects of geochemistry of amphibolites and meta-aplites are also discussed.

4.1 Major element chemistry

Representative statistical values of the major element compositions of gneisses, schists, amphibolites and meta-aplites from both the Staré Sedlo and Mirotice complexes are given in Table 4.1. There are no systematic differences between the arithmetical (X) and geometrical (G) averages suggesting

that the statistical distribution of major elements in the rock suites is generally symmetrical and therefore either can be used to represent the compositions of rock groups. However in order to make the evaluation of major element composition consistent with that of trace element composition, the geometrical average is preferred to the arithmetical average, unless there are no zero values present.

The average major element compositions of the rock suites match well the composition of the Phanerozoic upper continental crust as calculated by *Taylor and McLennan (1985)*. The gneisses from both complexes have a somewhat variable but generally consistent contents of major components (see Table 4.1). Both differ from the schists from the Mirotice complex in their higher CaO content and usually lower K_2O/Na_2O ratio. This feature reflects the proportion of plagioclase to K-feldspar which is larger in the gneisses than in the schists. The compositions of both the gneisses and schists differ substantially from that of the amphibolites which have lower SiO_2 contents and higher contents of other (Fe, Ti, Mg, Ca) cations. As inferred from the petrographical study of the rocks, these differences reflect the larger proportion of mafic minerals (hornblende and biotite) in amphibolites. Although the meta-aplites have a somewhat higher contents of K_2O and Al_2O_3, most of their major element composition corresponds to that of the gneisses.

Consistent with the results of the petrographical study (Chapter 2), major element compositions of most gneisses and schists from both complexes show igneous affinities (cf. Fig.4.1), suggesting these rocks had an igneous protolith. Their position in the F-fm vs qz diagram is consistent with that of some augen gneisses and granulites from the Moldanubian assemblage which were derived from igneous protoliths (*Köhler and Raaz, 1951*). Because there are no basic rocks within the rock suites, the data points do not show any trend and form a tight cluster close to the +qz apex. However some of the gneisses plot away from the main cluster (samples STG-25, MIG-30) but within the igneous field while other (samples LG-4, MIG-20) plot close to, or within the upper part of the field which is assigned to the rocks which have sedimentary affinities. These variations suggest that the parent magma from which the protolith of the gneisses crystallized could have been contaminated by a sedimentary material. This could have been the case especially for the protolith of some gneisses from the Lašovice quarry and this evidence is consistent with at least part of the trace element and isotopic signatures (cf. Par.4.2 and Chapter 8) and the proximity of sedimentary wall-rocks (*Mrázek, 1963*). The assimilation of sedimentary material in a granitoid magma should also be reflected by its trend on AFM diagram (*Robinson and*

Leake, 1975). However the lack of more basic rocks amongst the gneisses and schists does not permit such discrimination (cf. Fig.4.4). Nevertheless all the geological, petrographical and most of the geochemical evidence consistently shows that both the gneisses and schists had an igneous protolith. Accordingly the weak sedimentary affinities shown by some gneisses and schists (e.g. samples LG-4 and MIG-20 in Fig.4.1) are interpreted as the result of a more pronounced assimilation of sedimentary material by their parent magma(s) than was generally the case. This interpretation is consistent with Sr and Nd isotopic signatures of both the gneisses and schists (cf. Chapter 8).

For classification of the gneisses the chemical approximation to the modal QAPF diagram was used. While this approach was proposed by *Streckeisen and Le Maitre (1979)* to facilitate the classification of fine-grained volcanic rocks for which other methods of modal analysis (e.g. point counting) are not suitable, it is also applicable to the fine-grained schists (both the mylonite schists and ultramylonites - blastomylonites). The method is is also suitable for heterogeneous rocks for which a reliable estimation of mineral proportions cannot be achieved by point counting such as mylonitic gneisses for which a thin section is normally not representative. Using the granitic mezonorm of *Mielke and Winkler (1979)* - see Appendix 4 - the mineral norms for the gneisses fall mostly across the fields 2, 3a, 3b, 4 and 5a (Fig.4.2), i.e. corresponding to alkali feldspar granite, syenogranite, monzogranite, granodiorite and tonalite, respectively but with no systematic affiliations for the Staré Sedlo, Lašovice or Mirotice gneisses. However most of the schists plot in the field of syenogranite and alkali feldspar granite (or rhyolite and alkali feldspar rhyolite). The wide range of igneous types corresponding to the normative compositions of the gneisses and schists of both complexes can only partly be attributed to analytical and classification uncertainties and to the way the norms were calculated (*Lyons, 1976; Streckeisen and Le Maitre, 1979; Cambel and Vilinovič, 1987; Le Maitre, 1989*). There are several samples which, in contrast to their petrographical signatures and field occurrences within particular rock units, have chemical affinities indicative of another unit. In most diagrams in this chapter these samples plot away from the main fields for their rock units. This is mostly attributed to the heterogeneities in the composition of the protolith (e.g. due to its local contamination by wall-rock and, or, magma fractionation), although limited metamorphic segregation or otherwise undetected mechanical mixing of different rock units cannot be ruled out. However the overall petrographic (see also Chapter 2) and chemical compositions of most of the gneisses correspond to tonalites and granodiorites.

Within the suite of granitoid rocks, most of the gneisses and schists from both complexes straddle the boundary of peraluminous and metaluminous rocks as well as that of I- and S-type granitoids (*Chappell and White, 1974*). The aluminium saturation index (A.S.I. = mol $Al_2O_3/(CaO+Na_2O+K_2O)$; *Shand, 1927*) for gneisses and schists varies from ca 0.9 to up to 1.9, with the majority being within the range of 0.95 - 1.2 (Fig.4.3). While most of the Staré Sedlo and Mirotice gneisses straddle the limits for I- and S- type granitoids and metaluminous and peraluminous rocks, the majority of the Lašovice gneisses correspond to S-type, peraluminous granitoids. Most of the schists have A.S.I. values > 1.1 (i.e. peraluminous and S-type), but the spread in the composition of the schists is much larger than that for the Lašovice gneisses. There are a few samples which have different compositions from that of most of their rock units (LG-4, MIG-20, MIG-21). This is being attributed to heterogeneity in the compositions of their respective protoliths. However there are also differences shown by Sr contents: the field for the Staré Sedlo gneisses shows no overlap with that for the Lašovice gneisses (which have the lowest Sr contents), but it overlaps considerably the field for Mirotice gneisses. This may reflect a more pronounced contribution of a fractionated material (e.g. sediments) to the magma which formed the protolith of the Lašovice gneisses although the operation of a process of magma fractionation cannot be ruled out.

Geochemically the suites of gneisses and schists of both complexes show calc-alkaline affinity which is demonstrated on AFM and $CaO-Na_2O-K_2O$ diagrams. In the AFM diagram (Fig.4.4) the gneisses and schists form a tight cluster close to the A apex and plot below the tholeiitic - calc-alkaline discrimination line. However the lack of more basic rocks amongst the gneisses and schists does not permit the complete reconstruction of the evolution of their respective magmas in the AFM system. The gneisses generally follow the calc-alkaline trend with most rocks having a K_2O/Na_2O ratio within the range of 0.5 - 1.5 (Fig.4.5). Only a small number of samples are away from the main field and could be interpreted as having some affinity to the tonalitic trend of *Condie (1981)*.

While the AFM diagram does not discriminate between different series of acidic rocks, the overall calc-alkaline affinities of gneisses and schists from both complexes can be further indicated using the calc-alkali ratio (CaO/Na_2O+K_2O) and SiO_2 content (Fig.4.6; *Brown, 1982*). The compositions of most of the gneisses and some schists correspond to normal calc-alkaline andesites with some of them overlapping to the field of the calcic series (represented by the trend of New Zealand Taupo volcanic suite). However the composition of most of the schists correspond to the alkali-calcic series (represented by the volcanic

suite of SE New Guinea). This suggests a considerable shift in the magma composition which formed the respective protoliths of gneisses and schists. In this diagram the SiO_2 content, corresponding to the zero of the logarithm of calc-alkali ratio, represents the alkali - lime index (A.L.I.; *Peacock, 1931*). Accordingly, most of the gneisses and some schists have the alkali - lime index within the range of calc-alkaline rocks (A.L.I. = 56 - 62). The A.L.I. values of rocks having the alkali-calcic affinities and those having the calcic affinities are less than 56 and greater than 62, respectively.

The major element compositions of gneisses from both the Staré Sedlo and Mirotice complexes thus indicate an overall igneous protolith(s) that is mainly calc-alkaline in character and mainly tonalitic - granodioritic in composition. However the schists which form a part of the Mirotice complex differ in their major element characteristics substantially from the adjacent gneisses as well as from those of the Staré Sedlo complex: they correspond to meta-granites (or meta-rhyolites) and represent the most acidic and alkaline part of the complexes. Their relatively low alkali-lime index (mostly less than 56) together with a high SiO_2 content (ca 75 wt%) indicate affinities to the alkali-calcic series whose members are often regarded as originating in an extensional regime (*Brown, 1982*). This contrasts with the calc-alkaline to calcic affinities of gneisses which have the characteristics consistent with development in a compressional regime. Suites of metamorphosed igneous rocks consisting of multiple intrusions which are variable in composition have previously been described from the Svecocarelides of eastern Finland (*Park et al., 1984; Hopgood, 1984*). The presence of multiple intrusions and variability in their compositions there is indicative of an arc-type regime, with repeated phases of compression, rotation, slip and extension having been operative.

4.2 Trace element chemistry

Representative statistical values of the trace element contents (XRF data) in gneisses, schists, amphibolites and meta-aplites from both the Staré Sedlo and Mirotice complexes are given in Table 4.2. The systematic differences between the arithmetical (X) and geometrical (G) averages suggest the asymmetry in the statistical distributions of several trace elements. Systematically lower values of the geometrical average point to the positive skewness that has been interpreted as being typical for trace element distribution in igneous rocks (*Davis, 1973*). The reason for this is due to the statistical

distribution of trace element content in the rocks being restricted by the detection limit of the analytical method used (in this case XRF) towards the lower values, and towards the high values the distribution is limited by the nature of trace elements (present in trace proportions). As these two factors are often unbalanced, the trace element distribution in the rock is asymmetrical. Due to this asymmetry, the geometrical average lies closer to the mean and, unless there are no zero values present, it is used to represent the mean trace element composition.

The mean trace element composition of gneisses, schists, amphibolites and meta-aplites from both complexes matches well the composition of the Phanerozoic upper continental crust (*Taylor and McLennan, 1985*). Both Table 4.2 and Fig.4.7 show that the Staré Sedlo, Lašovice and Mirotice gneisses have somewhat variable but generally consistent contents of most trace elements. However the Lašovice gneisses differ from the other gneisses by having substantially lower average contents of Sr and Ba (87 and 447 ppm, respectively); the average contents of Sr are 387 and 215 ppm, and Ba 829 and 809 ppm in the Staré Sedlo and Mirotice gneisses, respectively. In addition the content of Th in most of the Lašovice gneisses is below the detection limit of XRF method (12 ppm). The composition of the schists generally corresponds to that of the Staré Sedlo and Mirotice gneisses, although the schists have lower average contents of Sr and higher contents of Ba (146 and 1262 ppm, respectively). The trace element signature of amphibolites differs from that of the Staré Sedlo and Mirotice gneisses in Ba, Cr, Co and Ni. The composition of the meta-aplites corresponds to that of most of the gneisses although the meta-aplites show higher average contents of Rb and Y (178 and 8 ppm, respectively). Some rock units show a larger spread in composition than other rock units; this may be an artefact resulting from the number of analyzed samples (cf. Table 4.2 and Fig.4.7).

4.2.1 Large ion lithophile (LIL) and high field strength (HFS) elements

The average K/Rb ratios for the upper continental crust and for the bulk continental crust are 250 and 284, respectively (*Taylor and McLennan, 1985*) while for granitoids of I- and S-type they are 196 and 171, respectively (*Chappell and White, 1983*). The K/Rb ratios of ca 300 (cf. Fig.4.8) for both the gneisses and the schists of the Staré Sedlo and Mirotice complexes are higher than the average values given for granitoids but they generally match the composition of the continental crust. However there are

no major differences in the K/Rb ratios of the Staré Sedlo, Lašovice and Mirotice gneisses and the Mirotice schists. Most of the K/Rb ratios for amphibolites are similar to those for the gneisses and schist. However some are considerably lower (cf. Fig.4.8, sample STA-4). Most of the meta-aplites have K/Rb ratios lower (c. 250) than most of the gneisses. Some samples have K/Rb ratios higher or lower than most of their respective rock units; these are the same samples which plot appart from the main grouping in most diagrams (e.g. Figs 4.3, 4.5. 4.10) and the compositions of which are interpreted as the result of heterogeneity in the composition of their protoliths (cf. Par.4.1). The scatter in the K and Rb data for some samples (K/Rb ratio being almost as low as 150 in some samples while it is close to 500 in others) can also be attributed to a decoupling of these elements during metamorphic reconstruction of the protolith(s). A possible mechanism for such decoupling is that of preferential Rb-loss in the process of biotite recrystallization (*Heier, 1973*).

The K/Rb ratio is often regarded as being indicative of the extent of fractionation processes leading to the formation of the rock or its precursor (igneous protolith(s) in the case of the rocks of the Staré Sedlo and Mirotice complexes; *Heier and Billings, 1978*). The mechanism of K and Rb fractionation towards the lower K/Rb values in the more fractionated rocks is a result of the similar crystallochemical properties of both elements during the fractional crystallization of K-bearing minerals from the magma. As Rb is not present as a major constituent in any rock-forming mineral, the somewhat different ionic radii of K^+ and Rb^+ (0.133 and 0.149 nm, respectively; *Zemann, 1966*), results in preferential incorporation of K into K-bearing minerals. This effectively controls the decoupling of K and Rb leading to the change in the K/Rb ratio. In addition, due to their large ionic radii both K and Rb tend to concentrate in partial melts. There the process of decoupling is also based on the difference in the ionic radii of the two elements. Thus the low K/Rb ratios are indicative of rocks which underwent several stages of fractionation. Accordingly the somewhat higher K/Rb ratios in the gneisses and schists compared with the upper continental crust, bulk continental crust and various types of granitoid rocks are indicative of some contribution of less differentiated material in their protolith(s).

As the most pronounced differences between the feldspar-rich rock units of the Staré Sedlo and Mirotice complexes are in the Ba and Sr contents, the Rb - Ba - Sr triangular diagram is used to assess detailed variations. The compositions of gneisses from both complexes overlap (Fig.4.9) and plot mainly within the fields corresponding to normal granites, anomalous granites, granodiorites and quartz diorites of

El Bouseily and El Sokkary (1975); the composition of most schists corresponds to that of the normal granites. The meta-aplites are plotted for reference, and their Rb, Ba and Sr contents correspond to those of the anomalous granites or they plot on the boundary between these and quartz diorites and granodiorites. While there is considerable overlap, there are also overall increases in the Ba/Sr and the Rb/Ba ratios from the field of the Staré Sedlo gneisses to the field of the Lašovice gneisses. Likewise there is an increase in the Ba/Sr ratio from the gneisses to the field of the schists but with the Rb/Ba ratio in the schists generally corresponding to that of the Staré Sedlo and Mirotice gneisses.

The contents and ratios of these elements in granitoid rocks reflect the major element composition of evolving magma and the order of feldspar crystallization. Sr is depleted in the melt when Ca-rich plagioclase crystallizes. This results in an increase of the Ba/Sr ratio in the melt. At the beginning of crystallization of K-feldspar the melt is relatively enriched in Ba and relatively Ba-rich feldspars crystallize. But when the major crystallization of K-feldspar starts, Rb replaces K in the structure of the K-feldspar and therefore its concentration in the melt decreases (and the Rb/Ba ratio in the crystallizing products increases). The whole process takes place in two steps. The first step is characterized by crystallization of plagioclase and an increase of its Ba/Sr ratio. The second step is characterized by crystallization of K-feldspar and a increase in its Rb/Ba ratio. Accordingly while the Rb - Ba - Sr signature of the Staré Sedlo complex indicates that the Lašovice gneisses (samples LG) represent the more differentiated material relative to the rest of the gneisses from the Staré Sedlo complex (Staré Sedlo gneisses, samples STG), the differences between the gneisses and schists of the Mirotice complex require a different explanation. One such explanation could be that, just as the major element signature of gneisses and the schists is indicative of their derivation in a compressional regime (most of the gneisses) and extensional regime (most of the schists; cf. Par.4.1 and Fig.4.6), their trace element patterns indicate the same duality of development.

The Sr/Pb ratio also reflects magmatic differentiation processes, and this is the reason for most of the Lašovice gneisses (samples LG) having lower Sr/Pb ratios than the rest of the gneisses (Staré Sedlo gneisses, samples STG and Mirotice gneisses, samples MIG; Fig.4.10). The range of Sr/Pb ratios from gneisses and schists overlap but the ratios for most of the schists are relatively low and so show similarities to the Lašovive gneisses. The meta-aplites also have low Sr/Pb but high Rb/Ba ratios (<10 and >0.25, respectively).

Like the behaviour of Sr and Pb in magmatic processes that of Rb and Ba is often controlled by feldspar crystallization. Sr and Pb are both divalent ions with very similar radii (0.127 and 0.132 nm for Sr^{2+} and Pb^{2+}, respectively; *Zemann, 1966*) but as the Pb - O bond has a more covalent nature than the Sr - O bond, Pb is enriched in the feldspars crystallizing in the more fractionated magma. Accordingly in the Lašovice gneisses both the low Sr/Pb and relatively high Rb/Ba indicate that their protolith crystallized from a more fractionated magma and, or, was contaminated by more differentiated material than was the case for the rest of the gneisses.

Sr and Zr contents in most of the Mirotice gneisses show an apparent positive correlation (Fig.4.11a). This however does not hold for the Staré Sedlo and Lašovice gneisses or for the schists. In the case of Ba and Zr there is a lack of correlation in all the rock units (Fig.4.11b) but with some gneisses (LG-9, MIG-30) showing markedly higher contents of Zr than most of the other rocks. This may indicate that these rocks contain larger proportions of inherited zircon than is the case for most of the gneisses (cf. Chapter 6). The content of Zr in magmatic rocks increases with progressive magma fractionation (*Wilson, 1989*) and accordingly its positive correlation with Sr in most of the Mirotice gneisses is indicative of the operation of this process, at least in early stages of feldspar crystallization (cf. Figs 4.9 and 4.10). The lack of corresponding correlation in other rock units is indicative of the operation of more complex processes than just magma fractionation, while the lack of correlation in the Ba - Zr system suggests that the process of magma fractionation was no longer operative when Ba-rich feldspars crystallized. The character of such more complex processes, at least for the Lašovice gneisses, can be explained on the basis of a combination of both the magma fractionation involving Ca (Sr)-bearing mineral(s) and the assimilation of wall-rock sedimentary material (cf. Par.4.1 and Fig.4.1).

4.2.2 Rare-earth elements

The gneisses and amphibolites from both the Staré Sedlo and Mirotice complexes show up to 100 times LREE enrichment and 2 - 10 times HREE enrichment relative to the composition of CI chondrite (*Boynton, 1984*) and most show a negative Eu-anomaly (Figs 4.12 and 4.13). They both have REE patterns which are typical for evolved continental crust (*Taylor and McLennan, 1985*). The Staré Sedlo gneisses have approximately 1.5 times higher total REE content than the Lašovice gneisses

(Fig.4.12). Both have similar LREE/HREE ratios but they differ in the Eu-anomaly with the average Eu/Eu* value being 0.85 and 0.78 for the Staré Sedlo gneisses and Lašovice gneisses, respectively. The chondrite normalized $REE_{(n)}$ patterns of amphibolites from the Staré Sedlo complex (Fig.4.13) differ from those of gneisses having substantially lower LREE/HREE ratios (the average $La_{(n)}/Lu_{(n)}$ ratios are 14.68, 16.43 and 9.92 for the Staré Sedlo gneisses, Lašovice gneisses and the amphibolites, respectively) but a similar average Eu/Eu* value (0.87) to that of the gneisses. Compared to the overall REE composition of the Staré Sedlo complex (Staré Sedlo and Lašovice gneisses), the analogous rocks of the Mirotice complex (Mirotice gneisses) show a generally larger spread in the LREE as well as in the HREE contents with only small depletion in the total content of LREE (Fig.4.13). Schists from the Mirotice complex show large variations in both LREE and HREE compositions (with the enrichment relative to the chondrite composition of 60 - 80 and 2 to 7 times for LREE and HREE, respectively) and a positive Eu-anomaly (the Eu/Eu* 1.38 to 1.47; Fig.4.14). Some of the Mirotice schists (samples MIS-9 and MIS-11) are depleted in Tb, Dy and Ho and relatively enriched in Eu, Tm, Yb and Lu so that the HREE part of chondrite-normalized REE spectrum has an open U-shape.

There is general agreement (see *Jakeš, 1984*; *Humphris, 1984*; *Grauch, 1989*) that during the metamorphic processes up to the beginning of partial melting under granulite facies conditions rocks usually retain their REE compositions unchanged. In the process of metamorphic recrystallization the overall gains and losses of the rare-earth elements are a function of several factors, viz. a) the abundance in the protolith, distribution in its mineral phases and relative stability of these phases, b) the concentration of the rare-earth elements in the fluid and the fluid's ability to transport the REE out of the system and c) the ability of the new minerals to accommodate the rare-earth elements. Accordingly, even though the rocks of the Staré Sedlo and Mirotice complexes have been subjected to both metamorphic reconstruction and ductile deformation, the REE patterns are considered to be representative of, or at least very similar to, the REE patterns of their protolith(s). Consequently they can be used to elucidate the magmatic history of these protoliths.

Within the Staré Sedlo complex the trends of both major and trace element compositions in the Lašovice gneisses suggest the operation of magma fractionation and, or, contamination by wall-rock sediments, while the larger negative Eu-anomaly together with the lower total content of REE in these gneisses are indicative of the operation of fractional crystallization (*Cullers and Graf, 1984*). In both cases

the composition of Lašovice gneisses is indicative of a more advanced stage of magma differentiation than is indicated by the composition of the rest of the complex (Staré Sedlo gneisses). The main difference in the present (metamorphic) mineral assemblages of the Staré Sedlo and Lašovice gneisses is in the presence of amphibole (hornblende) in the former and its lack in the latter rocks. If fractional crystallization is responsible for the differentiation of the protolith of the Lašovice gneisses from the common protolith represented by the composition of the Staré Sedlo gneisses, the composition of the Staré Sedlo gneisses should be obtained by adding a suitable proportion of minerals (in terms of their REE composition) to the composition of the Lašovice gneisses. In order to decide whether this hypothesis is a realistic one, as well as which minerals and in what proportions should fractionate to form a residual liquid which has the REE composition of the Lašovice gneisses, a calculation of mineral proportions based upon their REE contents was carried out. As the graphical methods are restricted to the solution of problems which have only three components, simple mixing equations proposed by *Bryan et al. (1969)* were employed.

The mixing model is designed to solve a number of simultaneous equations in order to obtain the best-fit of the data using a least-square method. In the mixing calculations ${}_{n}\mathbf{X}_{k}$ represents the matrix of composition of the members to be mixed (x_{ij} are the ith composition of jth component, i varies from 1 to n - the number of chemical elements, j varies from 1 to k - the number of components - minerals to be mixed), ${}_{n}\mathbf{Y}_{1}$ is the vector representing the real composition of the final member which resulted from mixing and ${}_{1}\mathbf{B}_{k}$ is the vector of proportions in which mixing gives the best approximation of **Y**. The model is as follows:

$$b_1x_{11}+b_2x_{12}+b_3x_{13}+.....+b_kx_{1k}=y_1$$

$$b_1x_{21}+b_2x_{22}+b_3x_{23}+.....+b_kx_{2k}=y_2$$

$$b_1x_{k1}+b_2x_{k2}+b_3x_{k3}+.....+b_kx_{nk}=y_n.$$

This described in the matrix form is

$${}_{n}\mathbf{X}_{k} * {}_{1}\mathbf{B}_{k} = {}_{n}\mathbf{Y}_{1}.$$

By multiplying both sides of this equation by the transposed matrix **X'**, a matrix

$$\mathbf{X'XB} = \mathbf{X'Y}$$

is obtained, which multiplied again from the left side by $(X'X)^{-1}$ gives the desired estimation of the vector of the least square proportions in which the components were mixed, i.e.

$$B = (X'X)^{-1}X'Y.$$

This equation gives solution only if the number of analyzed chemical elements (k) exceeds the number of components (n) which are to be mixed. A substitution of vector B to the original equation for vector B gives the best fit least square estimation Y of vector Y for which the sum of residues

$$S = \sum_{i=1}^{n}(y-y_i)2$$

is minimal with respect to the original values.

As there are no REE mineral data available for the Staré Sedlo complex, the REE mineral compositions given by *Gromet and Silver (1983)* for the rock-forming minerals of granodiorite were used for this calculation together with the average REE compositions of the Staré Sedlo and Lašovice gneisses. As all the minerals employed in the mixing calculation tend to keep their REE patterns (proportions of elements, not the absolute concentrations) irrespectively of small variations in the whole-rock composition (*Gromet and Silver, 1983*), the error introduced by using the data from literature rather than actual REE mineral compositions can affect only the proportions in which the components (minerals) are mixed and not which minerals should be involved to obtain the best fit approximation.

The results of modelling (Table 4.3) suggest (in terms of the present mineral composition of gneisses, their assumed REE contents and the whole-rock REE contents) that the protolith of the Lašovice gneisses could have resulted from fractional crystallization of parent material that was close in composition (REE) to that of the protolith of the Staré Sedlo gneisses by means of fractionation of hornblende (Hb), epidote (Ep) and zircon (Zir). The small negative value of the coefficient for titanite (Tit) may reflect the lack of complete consistency of the real REE data with those given by *Gromet and Silver (1983)*, operation of processes other than magma fractionation (e.g. contamination of the magma by sedimentary country rocks; cf. Chapter 8) or the fact that the present (metamorphic) mineral assemblage was used to simulate the fractionation process prior to the metamorphic event. In addition igneous epidote is not common in granitoid rocks and if present, it usually crystallizes in later stages of magma evolution (*Zen and Hammastrom, 1984*). Irrespective of these problems the model suggests the possibility of hornblende-, zircon- and epidote-contained proportions of REE to fractionating from the Staré Sedlo

gneisses parent composition to produce an REE composition that is close to that of the Lašovice gneisses. In addition the fractionation of a Ca-bearing mineral (i.e. hornblende) is consistent with the lack of amphibole and the lower content of Sr in the Lašovice gneisses compared to the Staré Sedlo gneisses (Figs 4.5 and 4.9) although some feldspar fractionation is also likely to have taken place.

Contamination of the parent magma of the Lašovice gneisses protolith by sedimentary country rocks (cf. Fig.4.1) can be simulated using the same mixing equations and the REE compositions of metasediments of the adjacent Sedlčany - Krásná Hora islet (*Košler, 1988*). The results (Table 4.3) suggest that the best approximation of the REE composition of the Lašovice gneisses is achieved when the REE composition of the Staré Sedlo gneisses (31 %) is mixed with those of lower Palaeozoic marble (36 %) and amphibole - biotite hornfels (30 %) of the Sedlčany - Krásná Hora islet.

However both the high sum of residues (3.584) in the case of the magma contamination model, and high estimation of the proportion of Lašovice gneisses (1.214) in the case of magma fractionation model, as well as the questionable fractionation of epidote, indicate that neither of these approximations on its own is likely to account for the present composition of the Lašovice gneisses. In addition a granitoid magma is not capable of assimilating such a large amount of sedimentary material. Accordingly the composition of the Lašovice gneisses is explained as being derived from a magma corresponding to the Staré Sedlo gneisses on the basis of both the magma fractionation and assimilation of sedimentary material corresponding to lower Palaeozoic sediments of the Sedlčany - Krásná Hora islet.

The nature of the REE patterns of the Staré Sedlo gneisses and the amphibolites (Fig.4.13) does not rule out the possibility of a common or comparable parent magma for both rock types, although any model must account for a time span indicated by their cross-cutting relations (cf. Chapter 1). The lower $La_{(n)}/Lu_{(n)}$ ratio in the amphibolites could reflect magmatic differentiation prior to the emplacement of the protolith of the gneisses. On the basis of such hypothesis the incompatible element-rich magma could have separated and have formed a plutonic body of a tonalite - granodiorite composition leaving behind a more Mg-, Fe-, Ca- (see Table 4.1) and also HREE-rich restite. The later could have subsequently intruded the tonalitic - granodioritic protolith of the Staré Sedlo gneisses forming minor intrusions of tonalitic - dioritic composition which are now represented by amphibolites. However, to test this idea and to shed more light on the nature and origin of the parent magma(s) of both the gneisses and the amphibolites, further evidence such as the Nd isotope data is needed.

Most of the schists from the Mirotice complex have a positive Eu-anomaly and some show Er -> Lu enrichment; this is indicated by the open U-shape of their chondrite-normalized HREE patterns (cf. Fig.4.14, samples MIS-9 and MIS-11). The Er -> Lu enrichment in these rocks is explained on the basis of the presence of a limited proportion of inherited zircon (cf. Chapter 6). As the total HREE contents are relatively low, the zircon REE pattern dominates the HREE part of the spectrum. Accordingly the REE patterns of schists represent a contribution of two factors, viz. (1) accumulation of a relatively large proportion of feldspars (in which K-feldspar dominates over plagioclase) which results in strong LREE enrichment and a positive Eu-anomaly, and (2) the zircon-dominated HREE pattern. However despite low total REE contents, some schists (samples MIS-2 and MIS-7) do not show the Er -> Lu enrichment. This is taken to be indicative of a low proportion of zircon inheritance in these rocks.

4.3 Tectonomagmatic affiliations of the rocks of the Staré Sedlo and Mirotice complexes

The affinities of most of the gneisses of both the Staré Sedlo and Mirotice complexes with calc-alkaline andesites (cf. Fig.4.6) imply that their protolith has developed in a compressional arc-type regime; the major element composition (alkali-calcic affinities) of most schists from the Mirotice complex is indicative of their derivation from an extensional regime. The diagrams which *Pearce et al. (1984)* use for discriminating the tectonomagmatic affinities of granitoid rocks (Fig.4.15a,b) provide confirmation of this interpretation. The gneisses, schists, amphibolites and meta-aplites from both complexes correspond to the fields of volcanic arc + syn-collision granites in the Nb vs Y diagram (Fig.4.15a), while in Rb vs Y+Nb diagram (Fig.4.15b) most of these rocks plot within or close to the field of volcanic arc granites. The high content of Rb in some gneisses and meta-aplites (samples STG-12, STM-2, STM-3) indicates these samples could have developed in a regime corresponding to that of syn-collision granites, although other explanations for high contents of Rb, such as metamorphic differentiation, cannot be ruled out due to a small number of samples.

Further support for the interpretation of the tectonomagmatic affiliations of the rocks is given by the R1 and R2 discrimination parameters (Fig.4.16; *de la Roche et al., 1980; Batchelor and Bowden, 1985*) for the gneisses and schists from both complexes. These values point to overall preplate-collision

and syn-collision affinities for most of these rocks and also indicate a contribution of mantle-like material to their protolith(s). The evidence for an arc-type compressional regime (gneisses) which was spatially associated with an arc-type extensional regime (schists) is consistent with the evidence for repeated phases of compression, rotation, slip and extension described from a volcanic arc in the Svecocarelides of eastern Finland (*Hopgood, 1984*).

With the available evidence consistently pointing to the existence of a volcanic arc regime from which parent mostly calc-alkaline (but also alkali-calcic and calcic) magma(s) of rocks present in the Staré Sedlo and Mirotice complexes were derived, the contrasting behaviour of large ion lithophile (LIL) and high field strength (HFS) elements can be used to confirm the subduction relationship of the magmas. As in subduction zones those element pairs which normally behave coherently even during the melting processes can be strongly decoupled as a result of the slab dehydration processes (Fig.4.17; *Saunders et al., 1991*). Dominant in terms of its contribution to the arc magmatism is the element flux derived from the mantle wedge, while the subducted slab element flux probably dominates only in the marginal part of the arc (close to the trench). Accordingly in the continent-based arc the proportion of the subducted material involved in the magma formation is likely to be very small. The estimations based upon the Sr isotopic studies suggest that only 3% of subducted material effectively contributes to the formation of the new continental crust (*Hawkesworth and Ellam, 1989*) and that most of the subducted material bypasses the magma-production zone being carried down to the deep mantle. As the arc usually produces large volume of magma over a relatively long period of time, a slab-induced convection in the mantle wedge compensates for the major and trace element changes in the mantle wedge above the subducted slab (*Saunders et al., 1988; Hawkesworth et al., 1990*).

The strong decoupling resulting from the subduction processes concerns large ion lithophile elements (i.e. K, Rb, Ba) on the one hand and the high field strength elements (i.e. Nb, Ti, P, Zr) on the other. The HFS elements are retained in the subducted slab while the LIL elements are preferentially released from the slab and carried by fluids to the overhanging mantle wedge where they contribute to the magma. This process is affected by the nature of fluids and the p and T conditions and therefore the mineral phases present. Slab melting does not result in the decoupling of LIL and HFS elements unless the HFS element-bearing minor phases are present. Consequently the plots of various LIL/HFS element ratios proved to be a tool in discriminating between an oceanic and continental arc with the magmas

produced in an oceanic arc having higher LIL/HFS element ratios (*Saunders et al., 1991*). Plots of Ce/Nb vs Ba/Nb and Ce/Nb vs K/Nb (Fig.4.18) indicate the overall continental arc affinities for both the Staré Sedlo and Mirotice complexes. The rocks have low LIL/HFS element ratios and the overlapping fields of the various rock units form a trend pointing to the field of ocean island basalts (OIB - data from *Saunders et al., 1988*) in the Ce/Nb vs Ba/Nb system. The scatter in the Ce/Nb vs K/Nb diagram is attributed mainly to the variations in the K content of the gneisses, schists, amphibolites and meta-aplites (cf. Pars 4.1 and 4.2). The samples which plot away from the main clusters of their respective rock units (STG-12, STG-13, MIS-9, MIS-11) are indicative of heterogeneities in the composition of their protolith(s). The evidence for the OIB-like mantle affinities of protoliths of both complexes suggest an OIB-related composition of the overhanging mantle wedge which in a continent-based arc would have contributed substantially to the produced magma. This contribution to the parent magma of OIB-like mantle material is also reflected by isotopic compositions of both Sr and Nd in rocks of the Staré Sedlo and Mirotice complexes (cf. Chapter 8) and is consistent with evidence for mantle material contributing to the parent magma indicated by R1-R2 discrimination parameters (Fig.4.16).

As inferred from the study of various arc-related volcanic rocks (e.g. *Jakeš and White, 1972; Wilson, 1989)* there is a relation between the depth and angle of dip the subduction zone and the chemical composition of magma produced. Calc-alkaline igneous suites typically occur in crust of intermediate thickness (20 - 30 km) and over that part of a subduction zone that is 100 - 200 km deep (*Condie, 1973*) and dips at an angle of 20 - 30^{o} (*Harmon et al., 1984*). However it is not only the major element rock composition but also related trace element characteristics (mainly the contents of Rb, Sr, Ba, Zr and Ni) which reflect the character of the subduction zone with *Condie (1973)* using the Rb vs Sr plot as an indicator of crustal thickness above such a zone (Fig.4.19). On this basis the compositions of most of the Staré Sedlo, Lašovice and Mirotice gneisses indicate the existence of the continental crust over the subduction zone from which was the parent magma(s) of their protolith(s) derived. While most of the Staré Sedlo and Mirotice gneisses straddle the limits for crustal thickness of 20 - 30 km and > 30 km, the Lašovice gneisses correspond exclusively to the 20 - 30 km range (Fig.4.19). However as the error of this estimation is ca ± 5 km, or even more, the assessment on the crust thickness can only be regarded as an approximation.

In oceanic volcanic rocks the Rb/Cs ratio is essentially constant at a value of 85 irrespective of their derivation (*Hoffmann and White, 1983*). Accordingly the lower Rb/Cs ratios in corresponding rocks indicate the operation of a process of Rb - Cs decoupling. This is indicated on the Rb/Cs vs K/Rb diagram (Fig.4.20) where the gneisses of both the Staré Sedlo and Mirotice complexes and most of the schists plot below the Rb/Cs value of 85. The scatter of Rb/Cs ratios results mostly from the variations of Rb content in the rocks and may be indicative of heterogeneities in the composition of their protolith(s) although a limited K - Rb decoupling during biotite recrystallization (cf. K - Rb decoupling, Par.4.2) cannot be ruled out.

Decoupling within the group of LIL elements in the subduction zone is explained on the basis of small differences in their overall similar crystallochemical and geochemical properties. Some processes (e.g. limited partial melting) along a subducted slab can result in decoupling and an enhanced Cs component relative to Rb and K in the rocks associated with volcanic arcs (e.g. *Hart et al., 1970*). The mechanism of Cs decoupling from other alkali metals was related by *Hart and Reid (1991)* to high-grade metamorphism and partial melting: alkali metal-bearing phases (mainly K-bearing minerals) preferentially release Cs because of its high incompatibility with the structure of K-bearing minerals (ionic radius of Cs^+ is 0.165 nm while those of Rb^+ and K^+ are 0.149 and 0.133 nm, respectively; *Zemann, 1966*). The fluids and melts rich in Cs then impregnate the overhanging mantle wedge eventually causing the Cs-enrichment of subduction zone-related magmas.

The scatter of data in the Rb/Cs vs K/Rb diagram (Fig.4.20) does not permit any assessment of whether the gneisses and schists would plot along the oceanic sediments - oceanic island basalts mixing line and therefore indicate a corresponding OIB-like mantle affinity of the wedge overhanging the subducted slab. However the existing Rb and Cs data support the evidence suggesting derivation of parent magma(s) of the gneisses and schists of the Staré Sedlo and Mirotice complexes in an arc-type regime. They also suggest a contribution of a slab-derived material to the parent magma(s) of their protolith(s).

While the major and trace element signatures of rocks from the Staré Sedlo and Mirotice complexes provide evidence for the derivation of their protolith(s) from arc type-related compressional and extensional environments, the variations in chemical composition between the rock units are explained on the basis of repeated compression, rotation, slip and extension cycles and of multiple intrusions, features that are typical for arc-type regimes (cf. *Park et al., 1984; Hopgood, 1984*). The variations of rock

composition within individual units are indicative of processes of magmatic fractionation and its contamination by wall-rock sediments. This is also consistent with Sr and Nd isotopic data (cf. Chapter 8). However the available evidence does not indicate whether the parent magma(s) of the protolith(s) of these rocks crystallized in open or closed system. In open system the repeated cycles of magmatic fractionation, tapping, replenishment or of country rock assimilation may account for spatially and temporally associated products which have a wide range of compositions. However further evidence is needed to indicate whether a there was any open system contribution to the variations in the composition of rocks from both the Staré Sedlo and Mirotice complexes.

4.4 Conclusions

1. The gneisses from both the Staré Sedlo and Mirotice complexes had an igneous protolith and show overall tonalitic - granodioritic affinities. The composition of schists from the Mirotice complex corresponds to alkali-feldspar granite (or rhyolite).

2. Both the gneisses and schists straddle the boundary of peraluminous and metaluminous and I- and S-type granitoids, respectively. Most of the gneisses show calc-alkaline affinities corresponding to normal CA andesites; most of the schists show alkali-calcic affinities.

3. Both the major and trace element signatures of gneisses and schists from the Staré Sedlo and Mirotice complexes are indicative of derivation of their parent magma(s) from an arc-type regime with more than one stage of igneous emplacement. The calc-alkaline magmatic products relate to phases of compression and the alkali-calcic magmatic products relate to phases of extension.

4. The major and trace element compositions of gneisses and schists indicate that the parent magma(s) of their protolith(s) was derived from a continent-based arc where there was only a minor contribution of subducted slab to the magma.

5. The composition of parent magma of the Lašovice gneisses was modified by both magmatic fractionation and assimilation of sedimentary material with the later coming from adjacent Sedlčany - Krásná Hora islet.

Table 4.1

Main statistical values (wt %) for the major element composition of rocks from the Staré Sedlo and Mirotice complexes.

	SiO_2	TiO_2	Al_2O_3	Fe_2O_3	FeO	MnO	MgO	CaO	Na_2O	K_2O	P_2O_5
					Gneisses - Staré Sedlo (STG; n=28)						
X	72.17	0.25	14.75	1.00	1.24	0.07	0.65	2.32	4.06	3.12	0.09
G	72.13	0.25	14.71	0.89	1.12	---	---	2.17	4.04	2.77	0.08
median	71.77	0.26	14.98	1.05	1.32	0.08	0.71	2.28	3.98	3.29	0.10
min	66.66	0.11	11.86	0.10	0.24	---	---	0.93	3.16	0.18	0.01
max	78.78	0.30	16.63	1.60	2.17	0.13	0.98	4.39	5.08	6.12	0.13
stdev	2.42	0.04	0.96	0.38	0.48	0.04	0.26	0.83	0.44	1.11	0.03
					Gneisses - Lašovice (LG; n=10)						
X	75.95	0.22	13.65	0.43	1.89	0.06	0.56	1.46	3.21	3.08	0.05
G	75.90	0.20	13.62	0.40	1.79	0.05	0.48	1.28	3.07	2.98	0.04
median	75.34	0.21	13.53	0.49	1.91	0.06	0.54	1.60	3.24	2.93	0.05
min	72.54	0.12	12.06	0.23	1.03	0.02	0.20	0.55	1.56	1.91	0.01
max	81.52	0.33	14.88	0.60	2.77	0.10	1.04	2.63	4.82	4.46	0.09
stdev	3.06	0.10	1.01	0.14	0.63	0.03	0.30	0.72	0.98	0.84	0.03
					Gneisses - Mirotice (MIG; n=32)						
X	72.00	0.22	13.94	1.03	0.85	0.06	0.59	1.90	3.52	3.20	0.06
G	63.22	0.22	12.84	0.98	0.70	0.06	---	1.72	3.35	2.96	0.05
median	72.09	0.19	13.68	1.04	0.70	0.07	0.55	1.93	3.58	3.31	0.04
min	68.21	0.15	11.91	0.42	0.24	0.01	---	0.77	2.26	1.00	0.02
max	76.48	0.39	15.95	1.59	2.58	0.12	1.24	3.36	5.23	4.83	0.14
stdev	2.42	0.06	0.94	0.33	0.55	0.03	0.32	0.76	0.56	0.85	0.03
					Schists - Mirotice (MIS; n=11)						
X	74.52	0.20	12.95	0.80	0.41	0.04	0.56	0.96	3.46	3.80	0.03
G	74.51	0.19	12.94	0.75	0.33	---	0.44	0.85	3.44	3.69	0.03
median	74.49	0.18	13.18	0.83	0.36	0.04	0.63	1.04	3.43	3.86	0.03
min	72.67	0.11	12.16	0.32	0.12	---	0.06	0.42	2.84	1.79	0.01
max	76.54	0.39	13.54	1.14	1.04	0.07	0.99	2.06	4.15	5.55	0.05
stdev	1.23	0.07	0.52	0.26	0.28	0.02	0.30	0.49	0.41	0.87	0.01
					Amphibolites - Staré Sedlo (STA; n=6)						
X	50.36	0.85	17.04	2.78	6.29	0.20	5.85	8.77	2.75	2.42	0.39
G	50.26	0.83	16.83	2.63	6.21	0.19	5.52	8.46	2.64	2.21	0.33
median	49.12	0.90	17.80	3.01	6.69	0.20	5.74	9.14	2.81	1.98	0.29
min	47.08	0.62	11.91	1.38	4.69	0.14	3.24	5.17	1.52	1.56	0.20
max	55.38	1.01	19.53	3.73	7.32	0.25	8.97	11.19	3.93	5.11	0.98
stdev	3.37	0.16	2.74	0.92	1.07	0.04	2.14	2.39	0.82	1.33	0.29
					Meta-aplites - Staré Sedlo (STM; n=3)						
X	72.78	0.24	15.21	0.58	0.93	0.04	0.62	1.26	4.02	4.83	0.14
G	72.76	0.24	15.19	0.52	0.91	0.04	0.61	1.12	3.98	4.82	0.13
median	71.73	0.26	14.89	0.98	1.32	0.08	0.65	2.17	3.95	3.33	0.10
min	70.69	0.20	14.25	0.33	0.72	0.03	0.46	0.63	3.56	4.50	0.09
max	74.18	0.28	16.02	0.98	1.07	0.05	0.78	2.09	4.80	5.13	0.16
stdev	1.84	0.04	0.89	0.35	0.18	0.01	0.16	0.75	0.68	0.32	0.04

Table 4.2

Main statistical values (ppm) for the trace element composition of rocks from the Staré Sedlo and Mirotice complexes.

	Rb	Sr	Ba	La	Ce	Y	Th	Zr	Ga	Co	Ni	Cr	Cu	Pb	Zn	Nb
								Gneisses - Staré Sedlo (STG)								
n	27	28	28	28	28	28	10	28	28	23	5	28	10	10	28	27
X	96.8	394.5	904.9	28.7	60.4	17.6	15.6	124.3	12.9	4.5	6.0	22.4	14.3	22.5	25.6	4.0
G	88.8	386.9	829.0	27.8	59.3	16.9	14.5	121.6	12.8	4.3	5.9	19.1	12.2	20.8	21.0	---
med	91.5	394.5	825.0	29.0	59.0	17.0	14.0	121.6	13.0	4.0	6.0	21.0	11.0	20.0	21.0	4.0
min	19	205	241	11	31	6	12	77	9	3	5	2	8	12	6	---
max	159	503	2114	48	96	29	39	196	15	8	8	47	45	41	104	8
stdev	36.0	74.6	385.4	7.0	11.7	4.9	8.3	27.3	1.3	1.6	1.2	10.9	11.2	9.6	21.6	2.2
								Gneisses - Lašovice (LG)								
n	10	10	10	10	10	10	---	10	10	8	3	10	1	9	10	10
X	79.1	93.2	454.2	15.7	36.3	19.6	---	157.9	12.7	5.1	5.3	24.8	6.0	27.0	31.1	4.4
G	78.0	87.3	446.8	15.5	36.2	19.2	---	155.7	12.6	4.9	5.3	23.2	6.0	25.8	27.7	3.8
med	83.0	95.5	424.0	16.0	36.5	20.0	---	150.5	13.0	5.0	5.0	21.0	6.0	26.0	31.0	4.5
min	58	39	340	12	31	14	---	136	10	3	5	12	6	17	13	1
max	96	133	632	20	43	25	---	244	15	8	6	44	6	46	52	10
stdev	13.6	32.6	90.0	2.7	3.0	3.9	---	31.4	1.7	1.6	0.6	9.8	---	9.2	14.7	2.4
								Gneisses - Mirotice (MIG)								
n	32	32	32	32	32	32	25	32	32	8	6	31	12	13	32	32
X	94.3	233.4	858.5	29.9	49.7	18.1	12.8	147.8	13.1	3.8	6.0	23.3	11.8	19.1	23.3	6.4
G	89.3	215.4	808.6	28.8	47.3	17.3	12.3	144.7	13.0	3.6	5.9	17.7	9.7	17.4	17.1	5.6
med	96.5	198.0	849.0	30.0	47.5	17.0	12.0	139.0	13.0	3.0	5.5	17.0	9.0	15.0	22.0	6.0
min	44	74	247	10	13	9	7	98	10	3	5	5	5	13	3	1
max	219	383	2340	48	102	31	26	237	18	7	9	88	37	56	99	13
stdev	33.1	91.7	330.7	7.5	15.0	5.6	3.7	32.0	1.8	1.4	1.6	18.8	9.1	11.4	20.4	3.1
								Schists - Mirotice (MIS)								
n	11	11	11	11	11	11	8	11	11	---	2	10	2	9	11	11
X	105.1	159.7	1375.5	22.3	33.4	13.0	17.8	118.8	11.1	---	5.5	16.6	9.5	21.3	14.0	7.2
G	100.4	146.1	1261.6	21.3	30.5	12.0	7.8	116.9	11.0	---	1.4	10.6	1.5	11.4	11.9	6.3
med	115.0	147.0	1646.0	23.0	34.0	13.0	19.5	116.0	11.0	---	5.5	15.5	9.5	18.0	12.0	8.0
min	50	88	412	11	13	5	8	90	9	---	5	4	9	14	4	1
max	143	307	2090	33	51	25	23	166	13	---	6	33	10	49	41	12
stdev	30.1	71.8	517.2	6.6	13.2	5.4	4.9	23.0	1.2	---	0.7	10.3	0.7	11.2	9.7	2.7
								Amphibolites - Staré Sedlo (STA)								
n	6	6	6	6	6	6	2	6	6	6	6	6	6	2	6	6
X	94.7	584.5	1318.5	24.7	48.0	24.0	33.5	89.3	16.5	19.8	29.7	188.8	20.0	29.5	75.7	5.2
G	77.9	561.7	1219.0	24.1	47.5	23.9	25.7	78.1	16.5	18.7	19.3	100.3	13.8	25.7	74.8	3.8
med	75.5	636.5	1217.0	26.0	50.5	23.5	33.5	71.0	17.0	19.0	16.5	81.0	11.5	29.5	77.5	3.5
min	35	283	634	16	37	21	12	45	14	10	7	30	6	15	55	1
max	227	689	2385	31	55	28	55	199	18	32	100	717	68	44	88	14
stdev	70.1	150.1	588.8	5.4	7.2	2.8	30.4	57.1	1.4	7.4	35.3	264.5	23.6	20.5	12.4	4.6
								Meta-aplites - Staré Sedlo (STM)								
n	3	3	3	3	3	3	2	3	3	2	3	3	2	3	3	3
X	183.7	262.0	876.3	23.0	58.3	7.7	25.5	126.0	19.3	5.0	5.7	21.3	7.0	34.0	16.3	7.3
G	178.1	251.7	818.8	22.5	57.0	7.5	24.9	122.6	18.7	4.9	5.6	21.1	6.3	30.8	15.7	6.9
med	201.0	208.0	705.0	23.0	49.0	7.0	25.5	136.0	18.0	5.0	5.0	23.0	7.0	30.0	14.0	6.0
min	125	206	579	17	49	6	20	88	14	4	5	17	4	18	12	5
max	225	372	1345	29	77	10	31	154	26	6	7	24	10	54	23	11
stdev	52.2	95.3	410.7	6.0	16.2	2.1	7.8	34.1	6.1	1.4	1.2	3.8	4.2	18.3	5.9	3.2

Table 4.3

Fractionation and contamination models for the gneisses of the Staré Sedlo complex; LGA - the average composition of the Lašovice gneisses (n=4); STGA - the average composition of the Staré Sedlo gneisses (n=5); LIM - the composition of marble (Sedlčany - Krásná Hora islet); PEL - the composition of metapelite (Sedlčany - Krásná Hora islet); LSES, LSEL - the least square estimation of the STGA and LGA compositions, respectively; the sums of residues are 0.0115 and 3.584, respectively; values in ppm.

Fractionation (reversed mixing)

Element	Hb	Ep	Tit	Zir	LGA	STGA	LSES
Ce	22.50	152.00	3305	42.3	35.25	58.91	58.91
Nd	27.50	58.50	2680	14.9	16.87	21.89	21.91
Sm	8.67	9.45	655	5.4	2.97	3.61	3.52
Eu	1.38	3.38	165	1.3	0.73	1.02	1.00
Dy	8.29	5.67	470	56.9	1.34	2.20	2.25
Er	4.18	2.69	237	116.0	0.69	1.34	1.32
Yb	3.18	2.10	207	253.0	0.79	1.50	1.50
Proportion	0.224	0.307	-0.005	0.003	0.685	-----	1.214

Contamination (mixing)

Element		LIM	PEL	STGA	LGA	LSEL
La		18.10	9.10	31.29	18.06	18.83
Ce		27.50	23.80	58.91	35.25	35.12
Nd		15.00	12.60	21.89	16.87	15.90
Sm		3.20	5.00	3.61	2.97	3.77
Eu		0.58	1.35	1.02	0.73	0.93
Tb		0.61	1.20	0.40	0.27	0.71
Ho		0.36	1.60	0.39	0.22	0.73
Tm		0.33	0.51	0.20	0.10	0.33
Yb		1.10	2.80	1.50	0.79	1.70
Lu		0.12	0.45	0.22	0.12	0.25
Proportion		0.359	0.303	0.306	-----	0.968

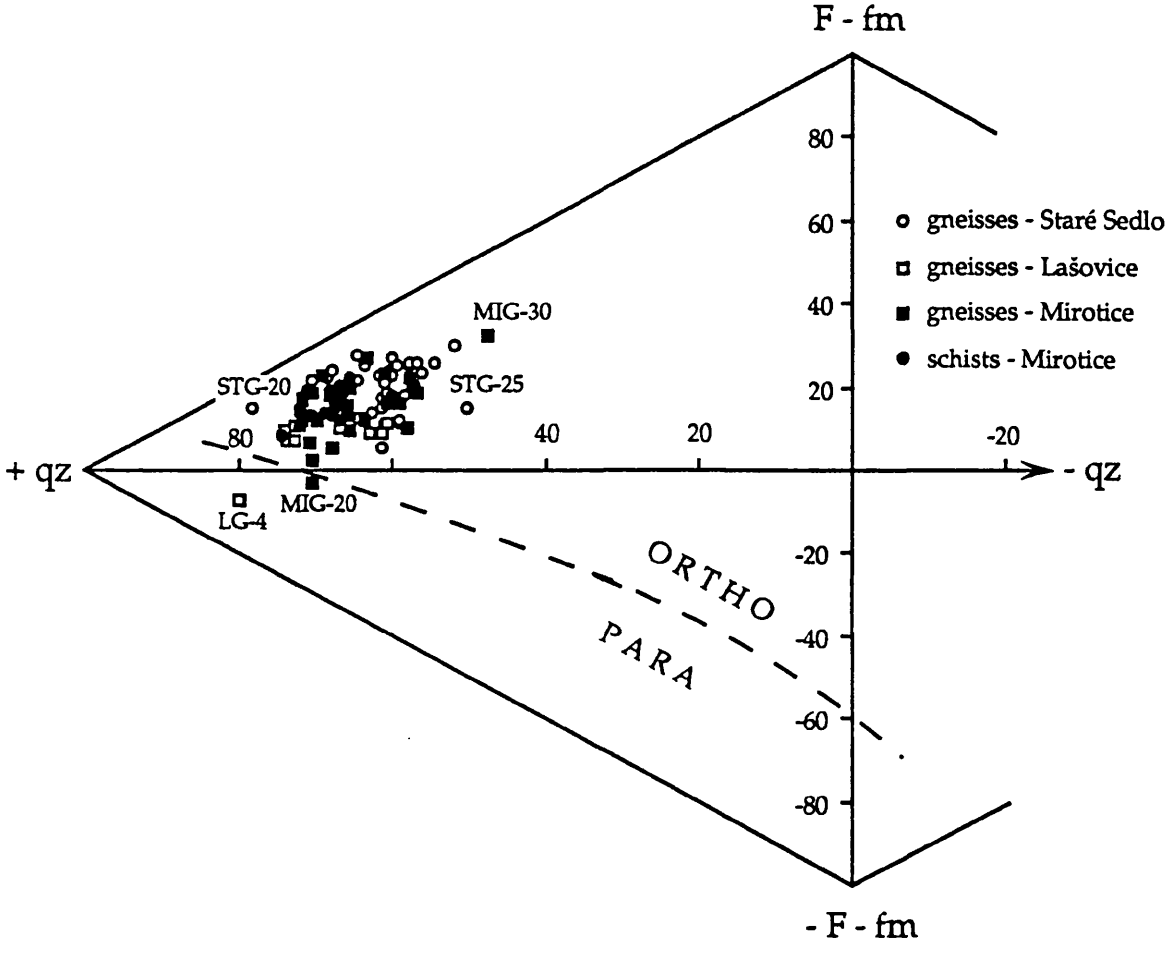

Fig.4.1

F - fm and qz values for gneisses and schists from the Staré Sedlo and Mirotice complexes calculated from the whole-rock major element composition; the ortho - para discrimination line is from *Bouška (1968).*

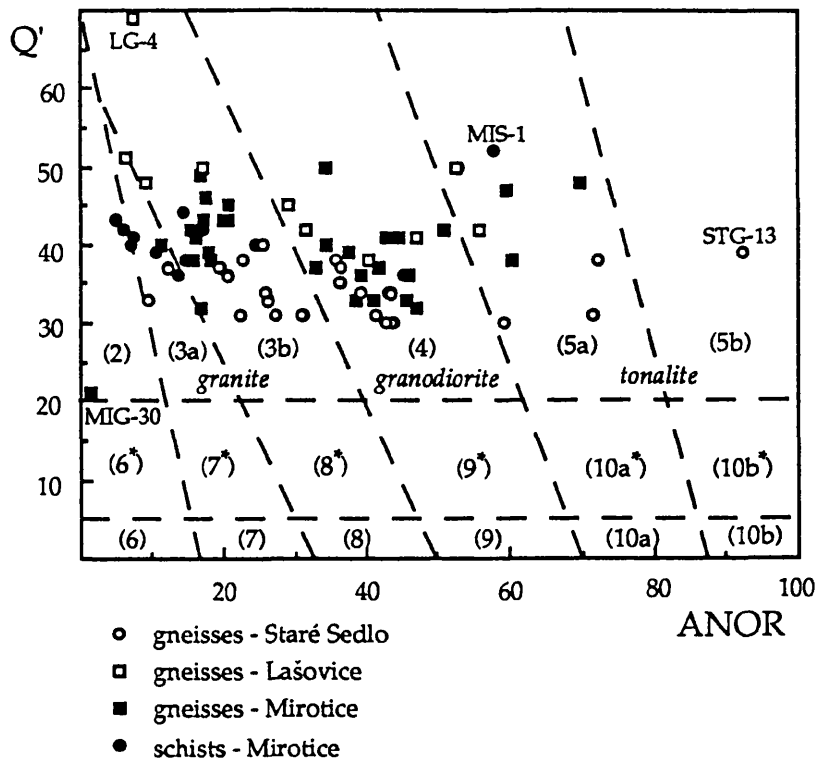

Fig.4.2

Plots on a Q' vs ANOR classification diagram of the normative values calculated from the major element composition of gneisses and schists from the Staré Sedlo and Mirotice complexes using granitic mesonorm of *Mielke and Winkler (1979)*. 2: alkali-feldspar granite; 3a,b: granite; 4: granodiorite; 5a,b: tonalite; 6: alkali-feldspar syenite; 7: syenite; 8: monzonite; 9: monzonite - monzogabbro; 10a,b: diorite - gabbro - anorthosite; * refers to the quartz variety.

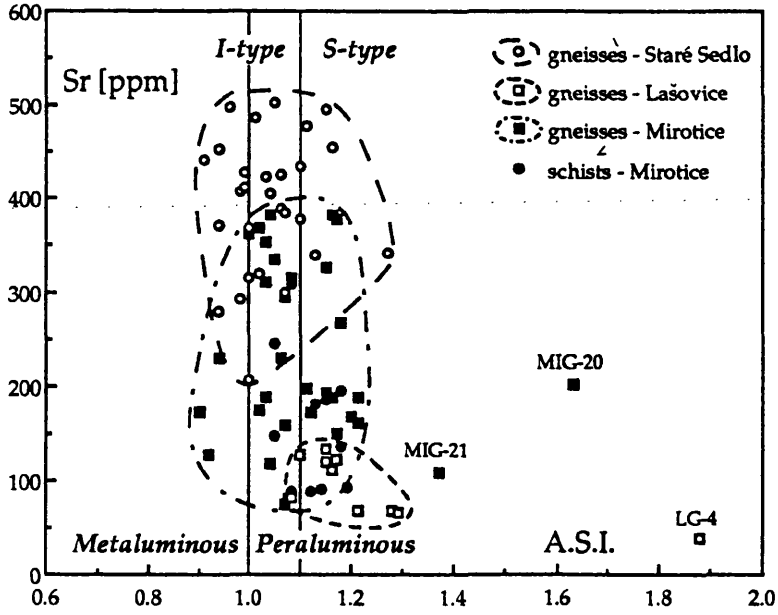

Fig.4.3

A.S.I. vs Sr diagram showing the peraluminous to metaluminous and I- to S-type affinities of rocks from the Staré Sedlo and Mirotice complexes.

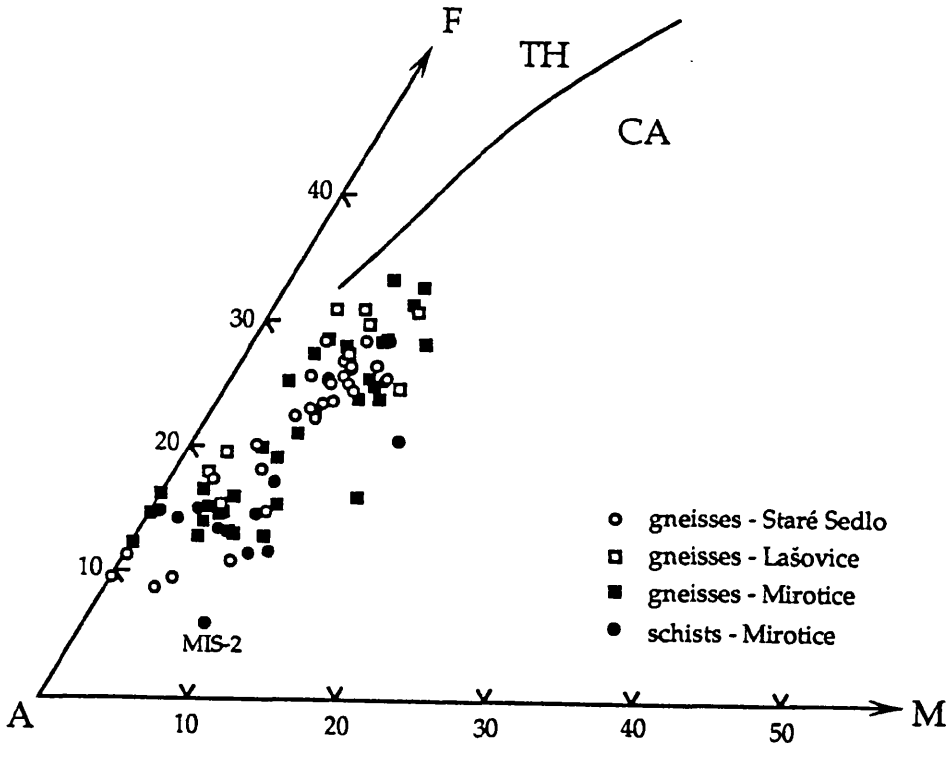

Fig.4.4

Plots for gneisses and schists of the Staré Sedlo and Mirotice complexes on an AFM diagram; TH - tholeiitic series, CA - calc-alkaline series.

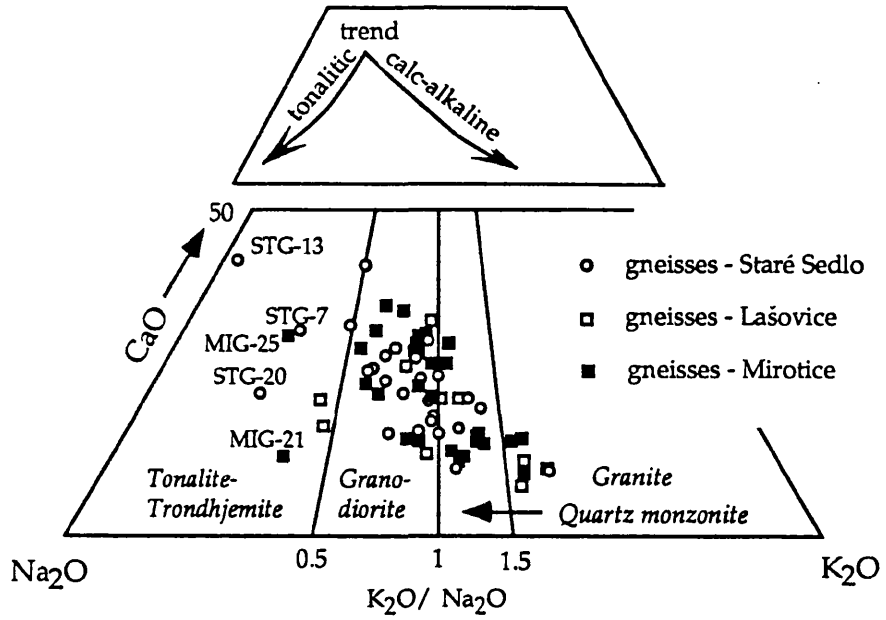

Fig.4.5

Plots for the Staré Sedlo, Lašovice and Mirotice gneisses on the CaO - Na_2O - K_2O classification diagram of *Condie (1981)*.

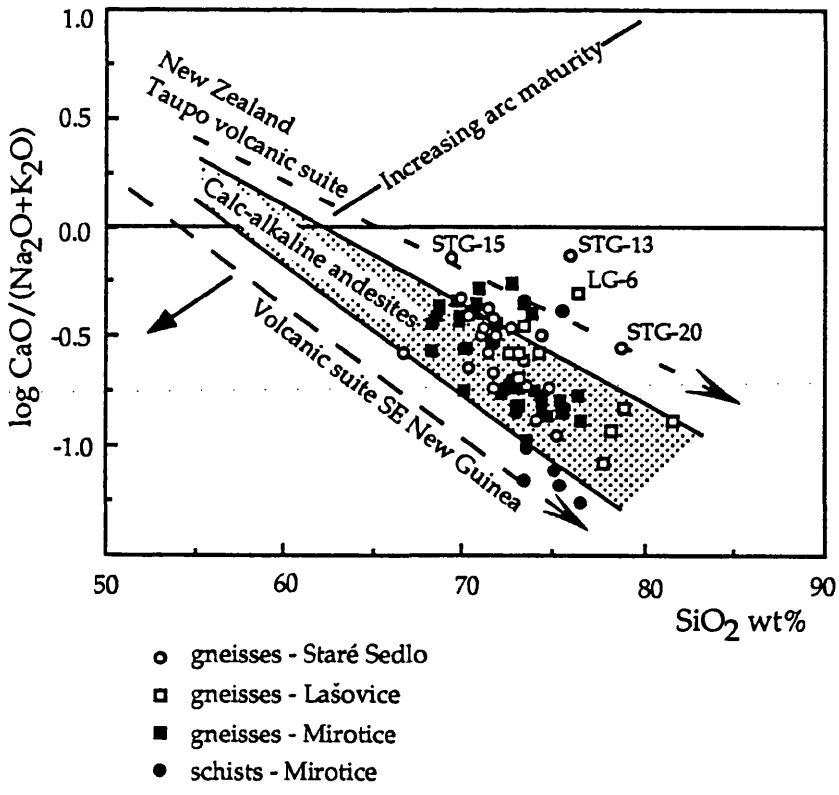

Fig. 4.6

Plots for the Staré Sedlo, Lašovice and Mirotice gneisses and schists on the log calc-alkali ratio vs SiO_2 diagram.

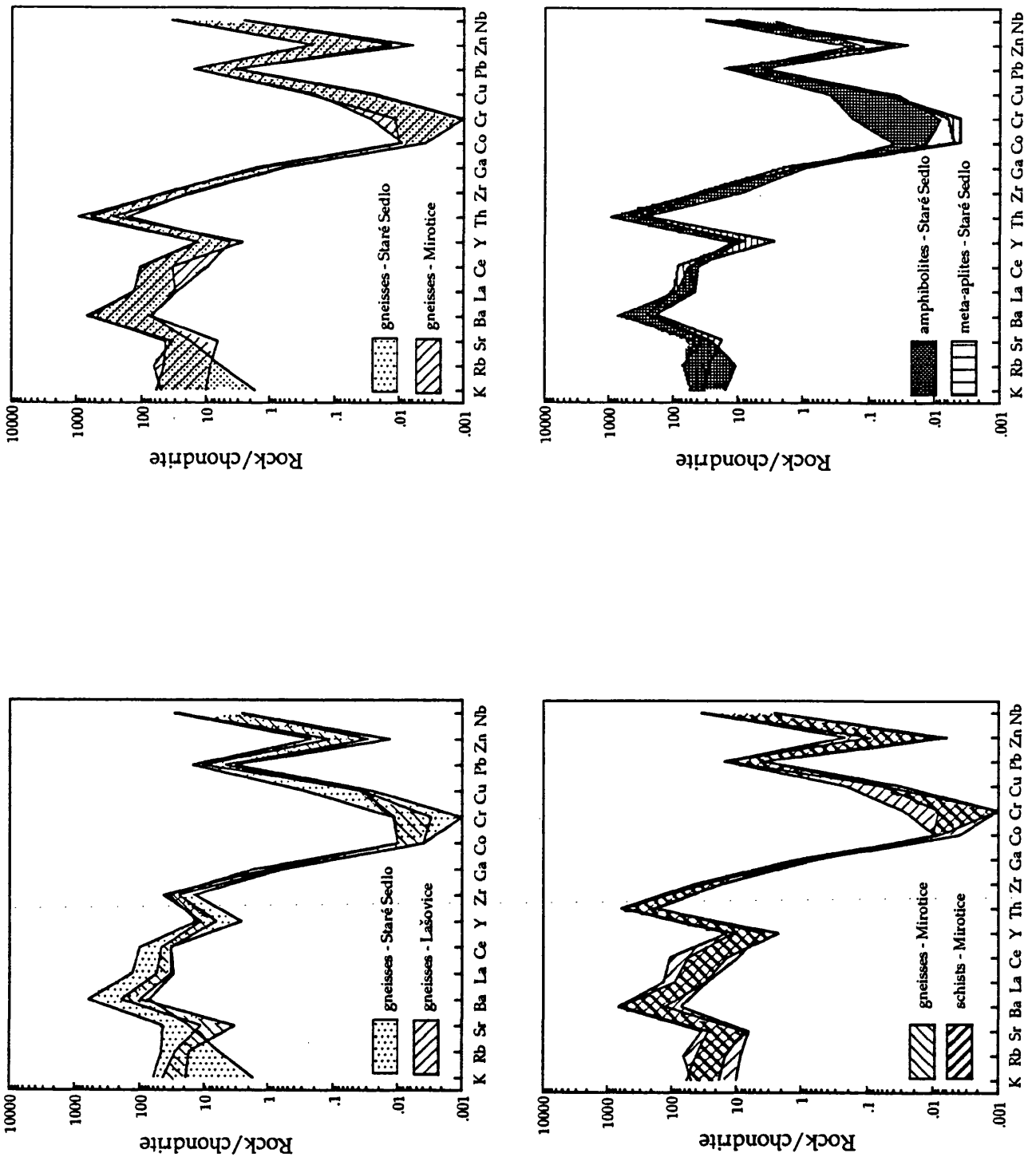

Fig.4.7

Chondrite-normalized trace element (and K) spidegrams of rocks from both the Staré Sedlo and Mirotice complexes.

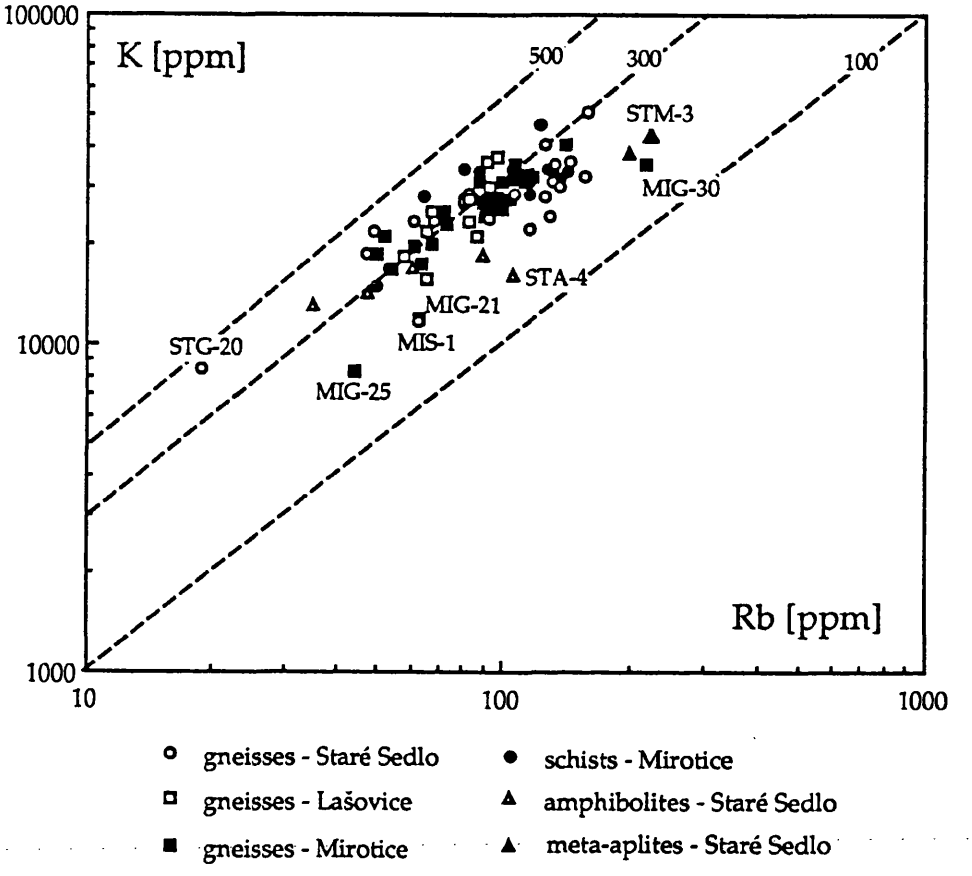

Fig.4.8

K vs Rb diagram for the rocks of the Staré Sedlo and Mirotice complexes.

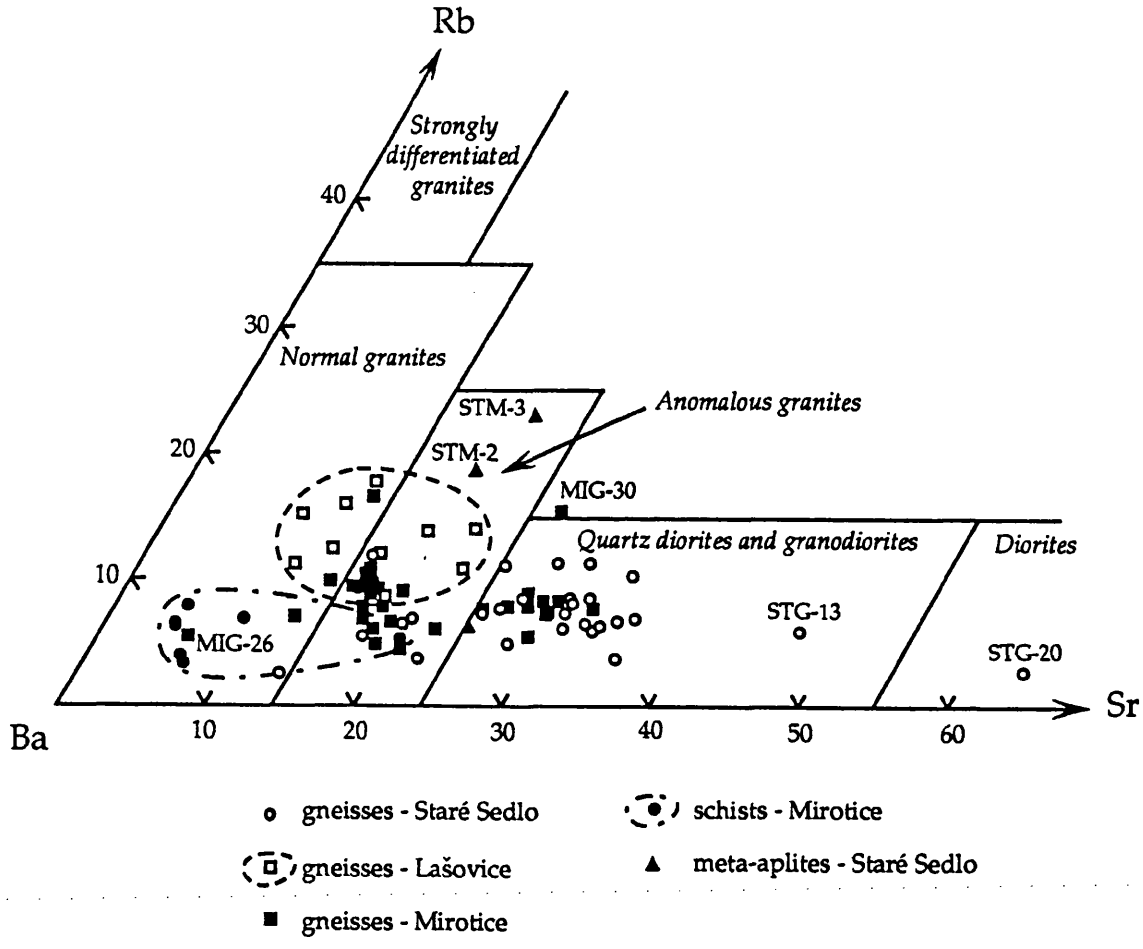

Fig.4.9

Data for the rocks of the Staré Sedlo and Mirotice complexes plotted on Rb - Ba - Sr triangular diagram (*El Bouseily and El Sokkary, 1975*).

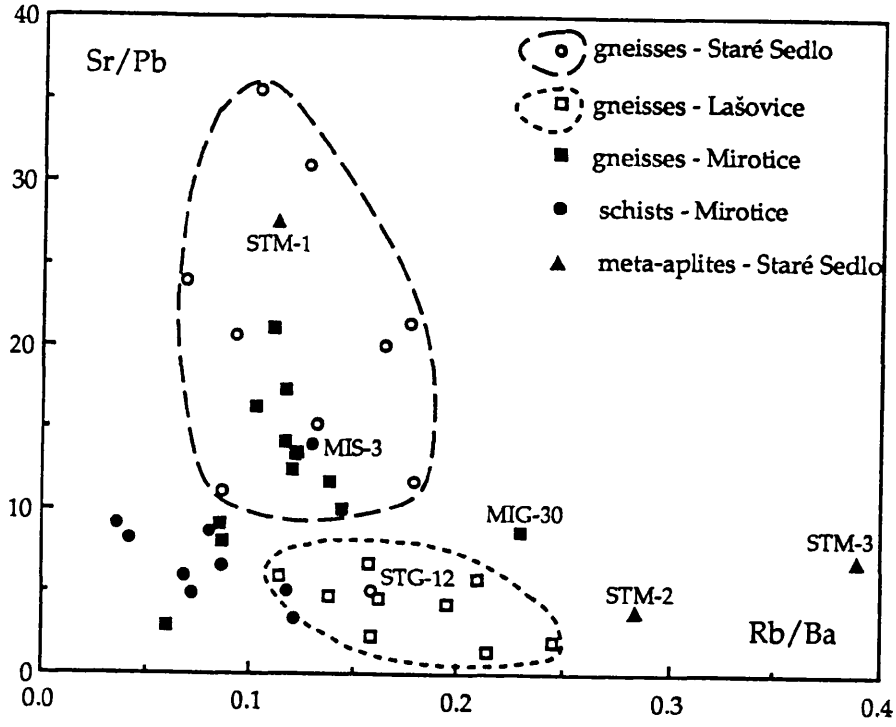

Fig.4.10

Sr/Pb vs Rb/Ba diagram for rocks from the Staré Sedlo and Mirotice complexes.

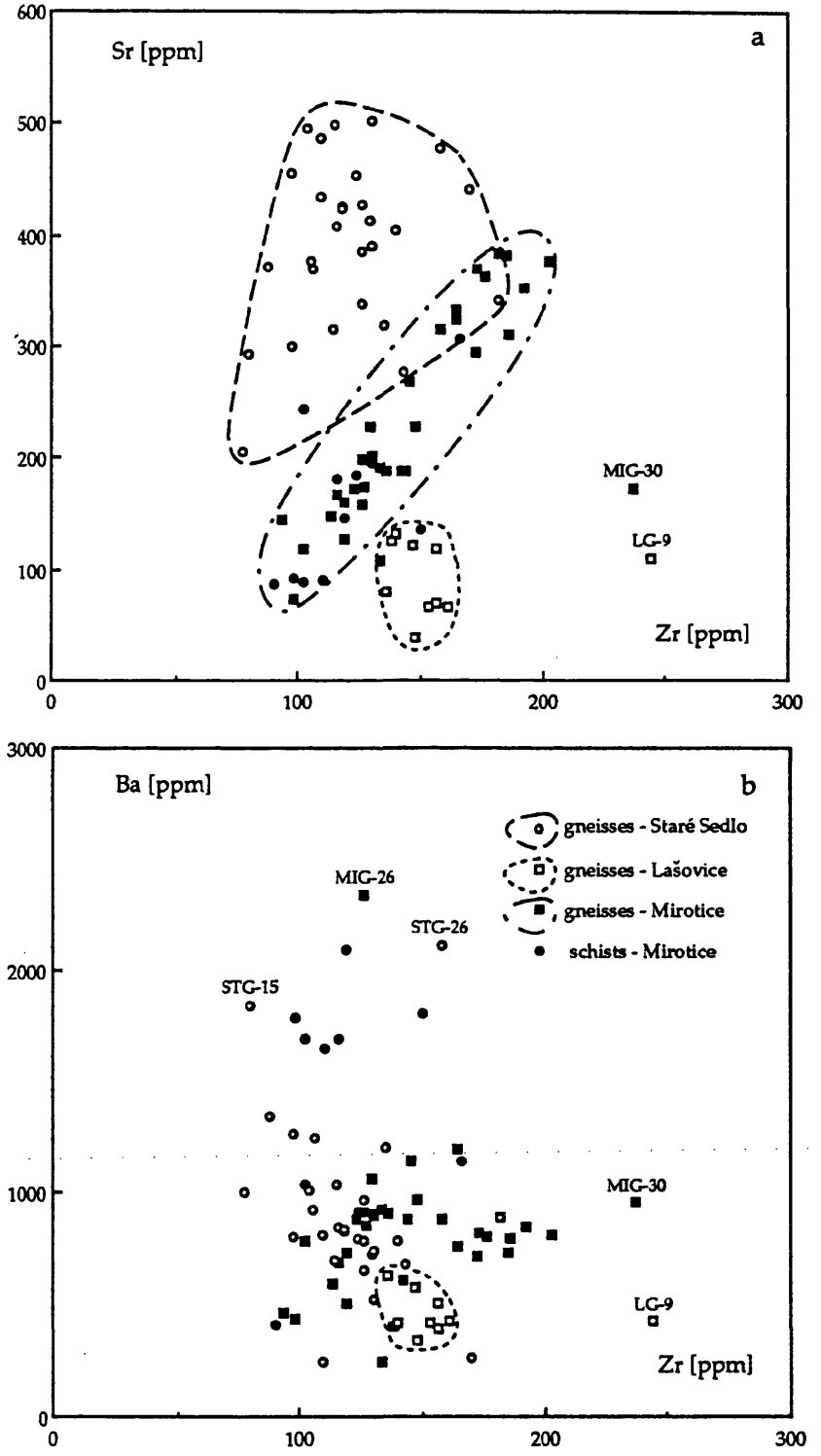

Fig.4.11

Zr vs Sr and Zr vs Ba diagrams for gneisses and schists from the Staré Sedlo and Mirotice complexes.

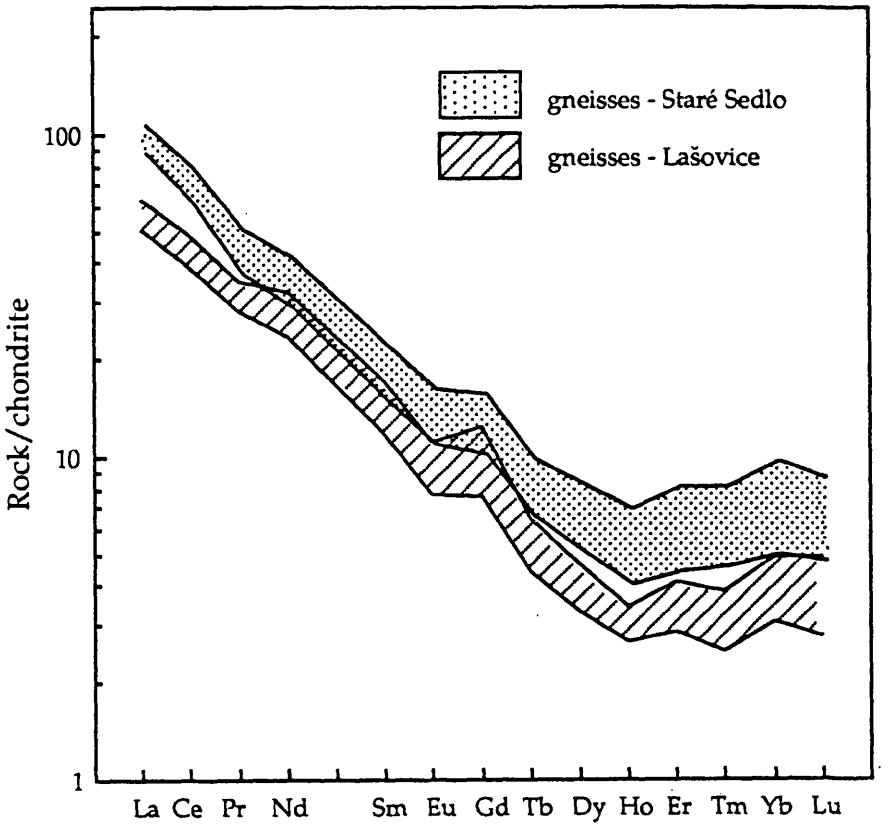

Fig.4.12

Chondrite-normalized REE patterns of Staré Sedlo and Lašovice gneisses of the Staré Sedlo complex.

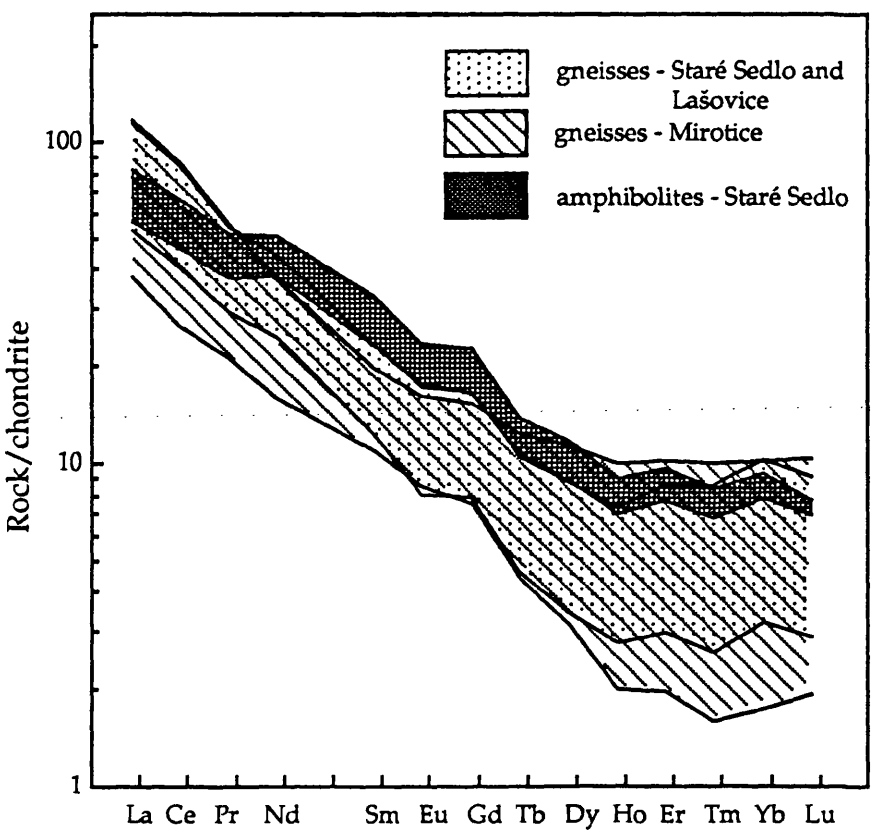

Fig.4.13

Chondrite-normalized REE patterns for the gneisses from the Staré Sedlo and Mirotice complexes and for amphibolites of the Staré Sedlo complex.

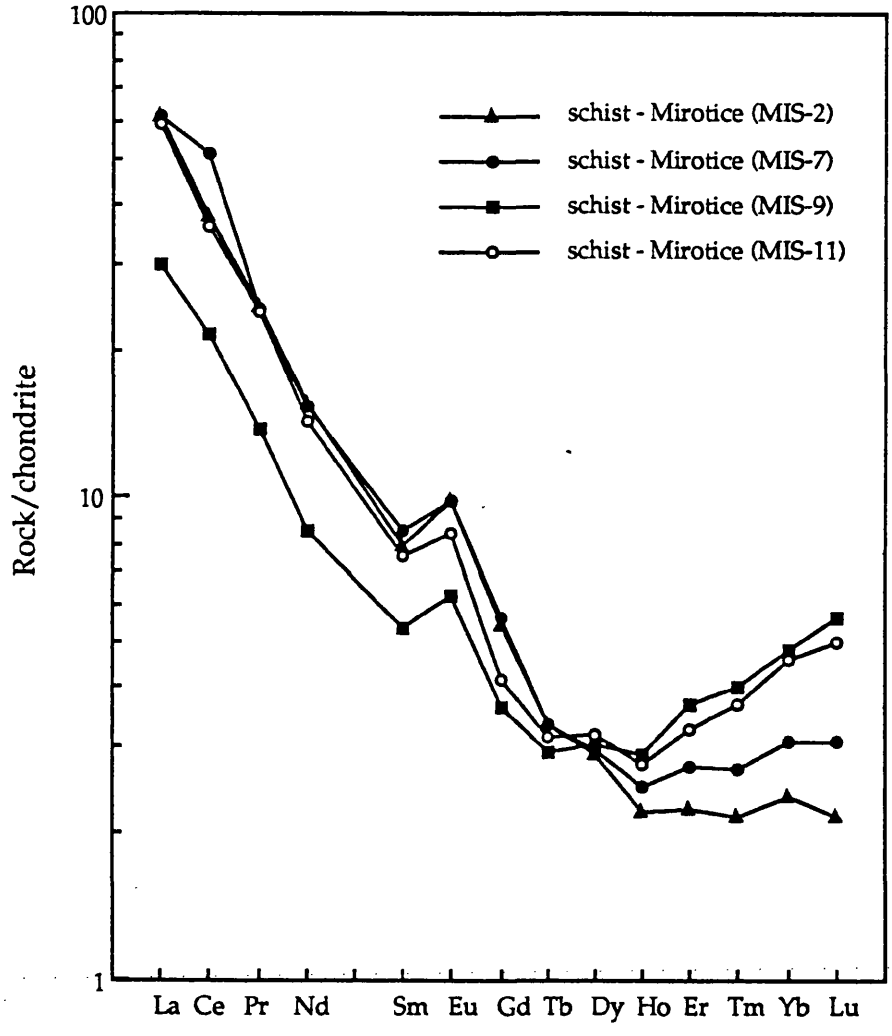

Fig.4.14

Chondrite-normalized REE patterns for schists of the Mirotice complex.

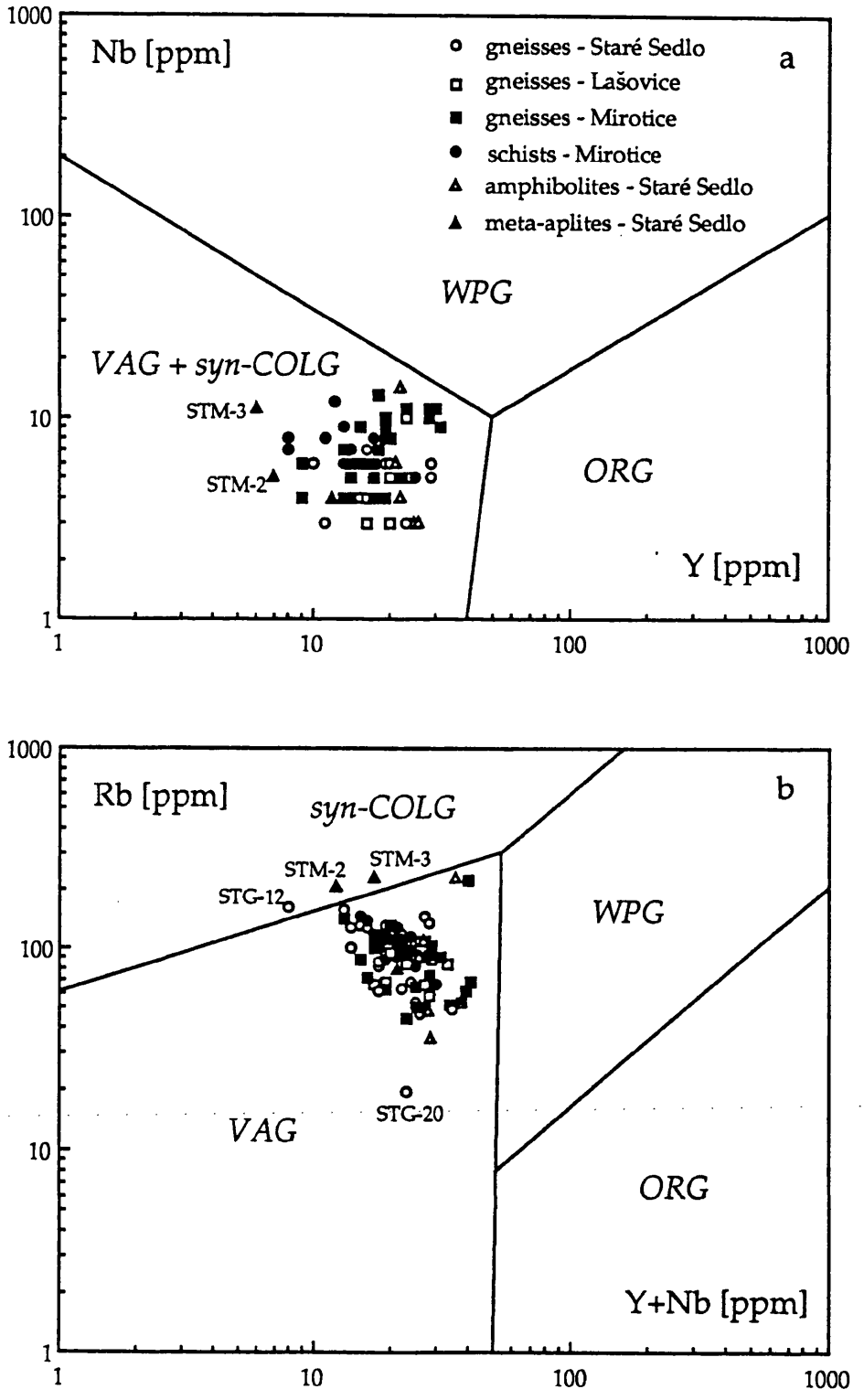

Fig.4.15

Data for rocks from both the Staré Sedlo and Mirotice complexes plotted in the discrimination diagrams for granitoid rocks (*Pearce et al., 1984*); VAG - volcanic arc granite, ORG - ocean ridge granite, WPG - within-plate granite, syn-COLG - syn-collision granite.

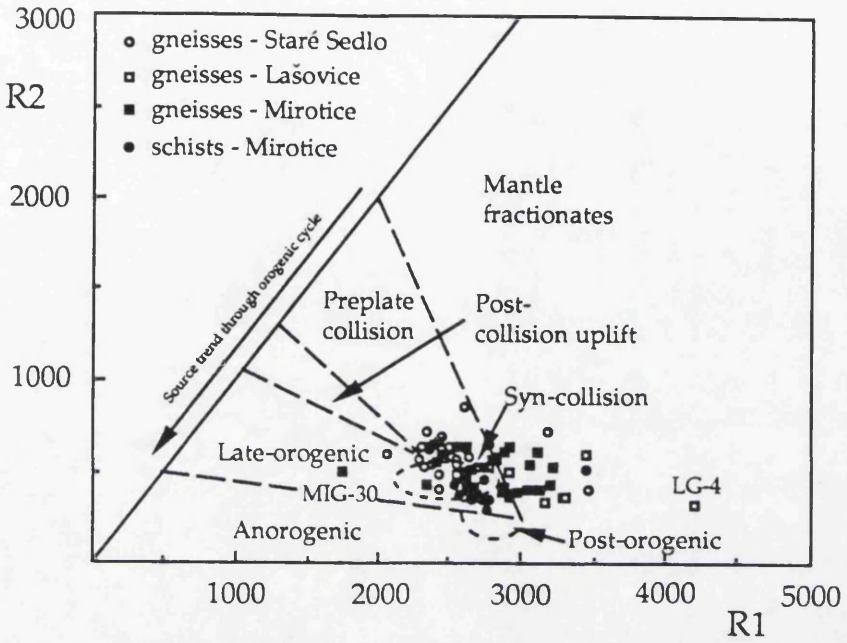

Fig.4.16

Tectonomagmatic affinities of rocks from the Staré Sedlo and Mirotice complexes on the basis of R1 - R2 discrimination functions (after *Batchelor and Bowden, 1985*).

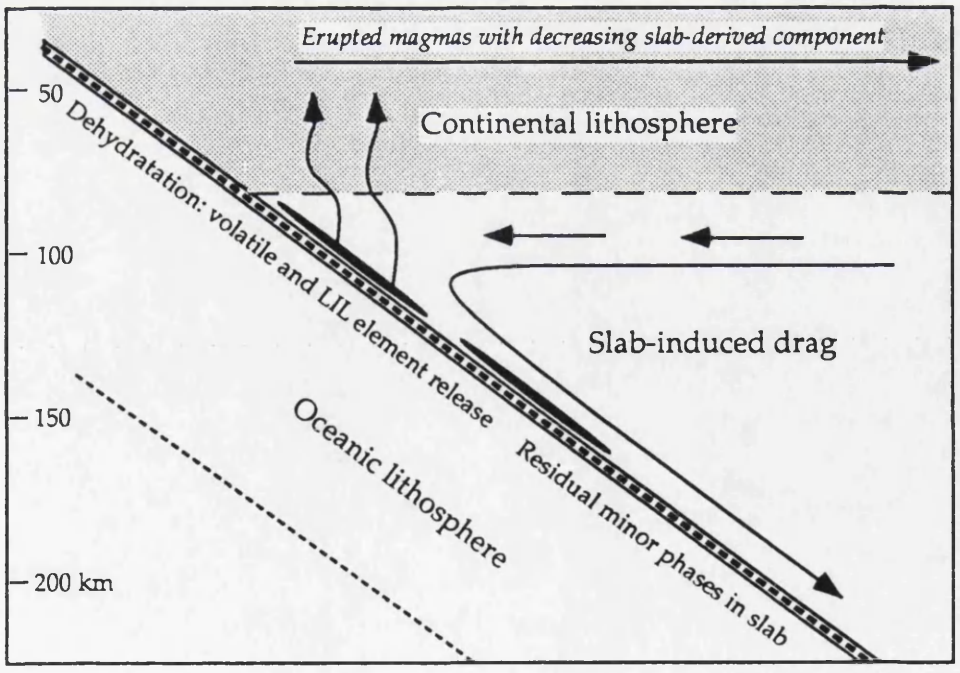

Fig.4.17

Schematic diagram of a continent-based volcanic arc (adapted from *Saunders et al., 1991*).

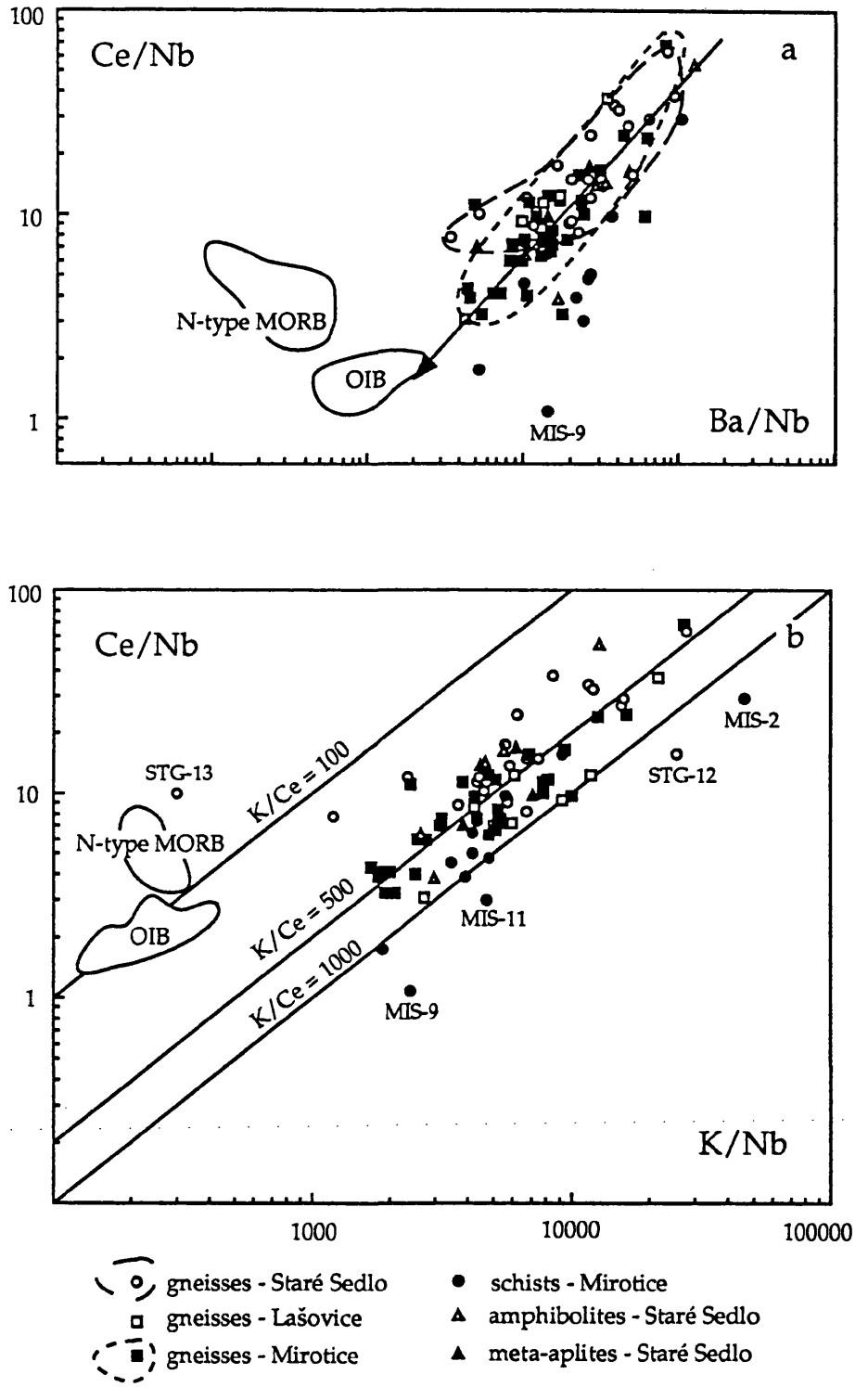

Fig.4.18

LIL/HFS element diagrams for rocks from the Staré Sedlo and Mirotice complexes; fields for mid ocean ridge basalts (MORB) and ocean island basalts (OIB) are from *Saunders et al. (1991)*.

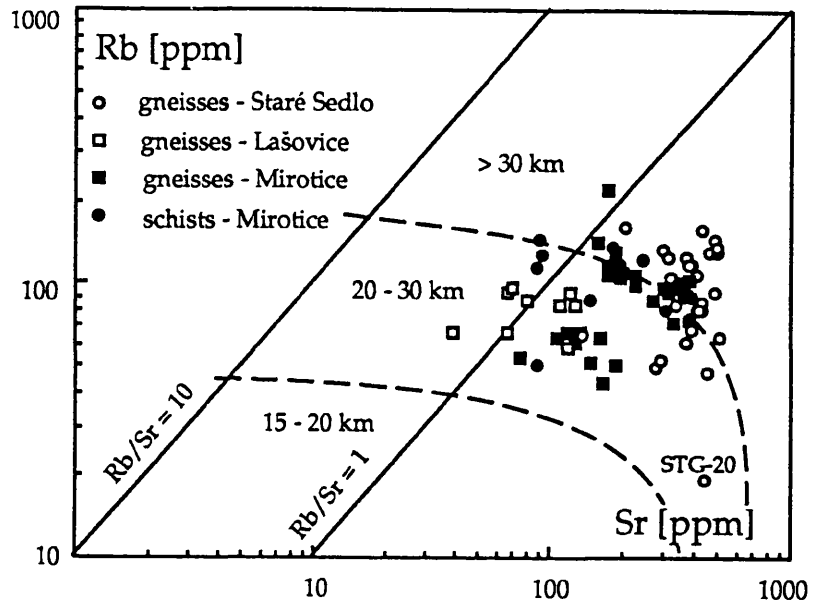

Fig.4.19

Rb and Sr contents in the rocks from both the Staré Sedlo and Mirotice complexes related to the thickness of crust above a subduction zone (after *Condie, 1973*).

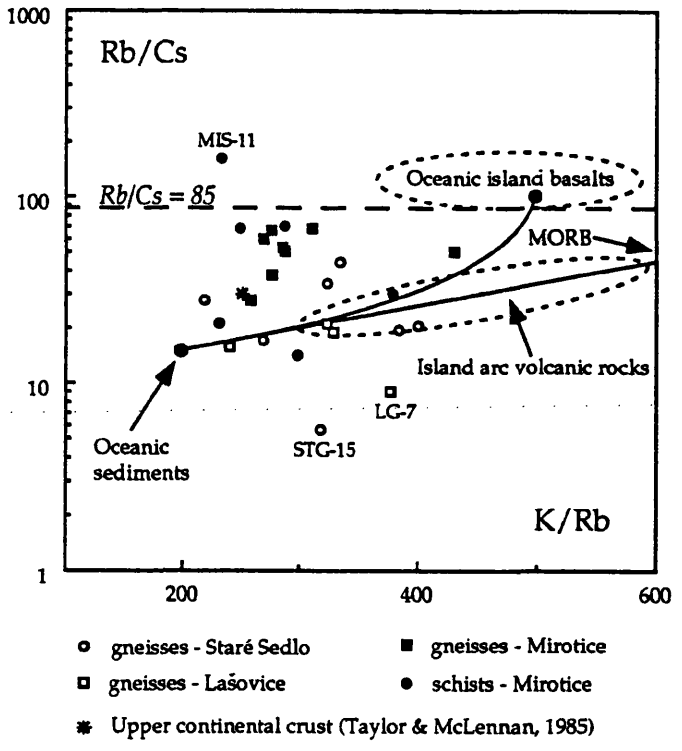

Fig.4.20

Rb/Cs vs K/Rb plots for rocks from the Staré Sedlo and Mirotice complexes. The solid lines represent mixing between an average composition of oceanic sediments; for data sources of mid ocean ridge basalts (MORB) and oceanic island basalts see *Hart and Reid (1991)*.

5. PRESSURE AND TEMPERATURE CONSTRAINTS ON THE THREE-STAGE DEVELOPMENT OF THE STARÉ SEDLO AND MIROTICE COMPLEXES

The study of both the rock-forming minerals in various rock units of the Staré Sedlo and Mirotice complexes and their chemical compositions (Chapters 2 and 3) has shown the existence of three different mineral assemblages which formed at different times and under different p and T conditions, viz. (1) the products of magmatic crystallization in the protolith(s) of the two complexes (2) the products of metamorphic reconstruction associated with ductile deformation that resulted in the development of the dominant rock fabric and (3) the products of a local thermal overprint in the contact zone of later emplaced plutons. The chemical signatures of these three mineral assemblages shed light on changes of pressure and temperature during the polyphase history of these complexes. The data used for this purpose are those obtained from electron microprobe studies of the main rock-forming minerals of the mylonite gneisses (Chapter 3) and the zircons (Chapter 5), together with some previously published results.

5.1 P and T constraints on the magmatic stage

The evidence from the oscillatory zoning (which is considered to have resulted exclusively from the crystallization of a particular zoned mineral from the melt), together with the presence of porphyroclasts in a mylonitic matrix of the gneisses, suggests that the only minerals of the magmatic assemblage that remained extant are feldspars (porphyroclasts of both plagioclase and K-feldspar) and zircon. Although these minerals do not provide a record of pressure at the time of crystallization of the protolith, the depth of the protolith at the time of solidification can be estimated from both the field relations and the evidence relating to the thickness of the adjacent Teplá - Barrandian sedimentary assemblage. The protolith of the gneisses of the Staré Sedlo complex intrudes early Palaeozoic metasediments of the southern part of the Sedlčany - Krásná Hora islet (Fig.1.1; *Mrázek, 1963*) which have been correlated with the Ordovician sediments of the Teplá - Barrandian assemblage (*Chlupáč, 1989*). As the age of the protolith crystallization of the Staré Sedlo and Mirotice gneisses straddles the boundary of mid - late Devonian (Chapter 6) and the maximum thickness of Ordovician to mid - late Devonian sediments of the adjacent Teplá - Barrandian assemblage is estimated to be ca 4000 m (*Mísař, 1983; Suk,*

1984), the minimum corresponding pressure at the top surface of the protolith of the Staré Sedlo and Mirotice gneisses is estimated to be less than 1.5 kbar.

5.1.1 Thermometry based on Zr-saturation in the magma

Although the limited number of zircon grains studied does not permit meaningful statistical evaluation, various conclusions concerning the temperature of crystallization of the protolith (and therefore the possibility of zircon inheritance) may be drawn. The zircons of the gneisses of both complexes occur as subhedral to euhedral grains or grain fragments with {100} and {110} prisms and {101} and {211} pyramids variably present. They correspond to S8 - S10 typological groups of *Pupin (1980)*. As the zircon crystal shape is generally dependent upon the chemical composition of the melt from which it crystallizes (and the physical conditions of the magma), each typological group of zircons can be related to a corresponding magma composition and therefore to the temperature of crystallization. The S8 to S10 typological groups correspond to granitic magma of calc-alkaline character for which the temperature of 700 ± 50 °C is generally accepted (*Pupin, 1980*); evidence for the calc-alkaline character of the Staré Sedlo and Mirotice gneisses protolith is given in Chapter 4.

The experimental work of *Watson and Harrison (1983)* on zircon saturation and the effect of magma composition upon the zircon solubility has shown that crustal magmas with high zirconium concentrations are often incapable of dissolving any additional zircons which results in zircon inheritance (cf. *Paterson et al., 1992; van Blackenburg, 1992*). The solubility function for zircon is

$$\ln D^{zircon/melt}_{(Zr)} = -3.80-[0.85*(M-1)]+1290/T$$

where $D^{zircon/melt}_{(Zr)}$ is the concentration ratio of Zr in a stochiometric zircon to that in the melt, M is the ratio of cations (Na+K+2Ca)/(Al*Si) in the magma and T is the temperature in K (*Watson and Harrison, 1983*). This method makes it possible either to assess the probability of older refractory zircon grains being present in the magma or to calculate the zircon saturation temperature in a magma of a particular chemical composition and the results of such estimations for a sample of mylonite gneiss from

both the Staré Sedlo and the Mirotice complexes (samples RC 2274 and RC 2284) are summarized in Table 5.1.

The negligible proportion of primary crystallized cores in zircon grains from both the Staré Sedlo and Mirotice gneisses as revealed by the BSE imagery (see Chapter 6) suggests the possibility of whole-rock Zr content being used with confidence for calculation of Zr saturation temperatures. For this calculation both the ideal Zr content in stochiometric $ZrSiO_4$ and the real Zr content in zircons from the electron microprobe study (Table 5.1) were used. The resultant estimations show the differences between the two saturation temperatures to be within the error of the method (± 30 °C, *Harrison et al., 1987*). Accordingly mean figures for the protolith of the Staré Sedlo and Mirotice mylonite gneisses (stochiometric zircon composition) are 793 ± 30 and 795 ± 30 °C, respectively. The limited proportion of primary crystallized cores in the grains and the estimate of magma temperature on the basis of zircon typology (700 ± 50 °C) suggests that the best figure for the temperature of the protolithic magma could be near the lower end of this temperature range, i.e. possibly in the order of 765 - 795 °C.

5.1.2 Two-feldspar thermometry

The two-feldspar thermometer based upon the correlation of the distribution of the albite component between coexisting plagioclase and K-feldspar with temperature has been revised several times since its application was first proposed (for review see *Brown and Parsons, 1981*). Progressively over the subsequent 40 years it has become clear that the activities of all three components (Or, Ab and An) in both plagioclase and K-feldspar have an important influence on the equilibrium between the composition of potassium feldspar and plagioclase

$$X(KF)_{Ab} = X(PLG)_{Ab}$$

where $X(KF)_{Ab}$ and $X(PLG)_{Ab}$ are the molar proportions of albite in K-feldspar and plagioclase, respectively. This has been utilized by *Price (1985)* who derived the thermometric equation

$$T(K)=[(X(KF)_{Or})^2\{18810+17030X(KF)_{Ab}+0.364P(bar)\}-\{(X(PLG)_{An})^2(28230-39520X(PLG)_{Ab}\}]/$$
$$[10.3(X(KF)_{Or})^2+8.3143\ln K_D]$$

where

$K_D=[X(PLG)_{Ab}\{2-X(PLG)_{Ab}-X(PLG)_{Or}\}\{X(PLG)_{Ab}+X(PLG)_{Or}\}]/[X(KF)_{Ab}\{2-X(KF)_{Ab}-X(KF)_{Or}\}\{X(KF)_{Ab}+X(KF)_{Or}\}]$.

In these equations $X(Y)_Z$ represents the molar proportion of the phase Z in the phase Y. The uncertainty given by *Price (1985)* for the range of 650 to 900 °C is ± 50 °C.

The temperature ranges derived from this equation for the cores of K-feldspar and plagioclase porphyroclasts from the gneisses of both complexes are 291 - 473 °C, 301 - 485 °C and 312 - 498 °C at pressures of 2, 3 and 4 kbar, respectively. The relatively low temperatures together with the large temperature variations even for the feldspar cores suggest that the feldspar equilibration was below the solidus. Accordingly the calculated temperatures can be linked to post-magmatic process(es), possibly to an equilibration related to a subsolidus feldspar unmixing.

5.2 P and T constraints on metamorphic reconstruction associated with the ductile deformation

The petrographic study of the Staré Sedlo and Mirotice gneisses has shown that both biotite and amphibole form part of the gneissic foliation and evidence for their development associated with mylonitization resulting from dominantly ductile deformation is given in Chapter 2. Accordingly this mineral pair is likely to preserve a p - T record of metamorphism associated with ductile deformation and add to the qualitative data from the chemical composition of amphibole pointing to the existence of medium-pressure conditions in the later stages of this reconstitution (cf. Fig.3.14).

As the scatter of both the biotite and amphibole compositions is larger between samples than within an individual sample, and in order to form a more reliable base for p and T calculations, the average biotite and amphibole compositions from each sample were used for calculations.

5.2.1 NaM4 content in amphibole

The correlation of NaM4 content (the proportion of crossite component) in Ca-amphiboles and pressure of metamorphism has been proposed by *Shido and Miyashiro (1959)* and modified into an empirical comparative geobarometer by *Brown (1977)*. The proposed exchange reaction is

Ca-amph + Ab + Chl + Fe-oxide = Na-amph + Ep.

The exact stochiometry and possible involvement of other phases depends on the particular compositions of the minerals involved. Where it coexists with albite, chlorite and iron oxide the Ca-amphibole should have a constant NaM4 content at any given pressure (and temperature). The influence of temperature upon the amphibole composition is reflected in a negative slope of isobars in the NaM4 vs Al^{IV} diagram (Fig.5.1). This barometer was originally calibrated against coexisting mineral assemblages in rocks of the aureole of the Sierra Batholith in California, the Otago terrain in New Zealand and the Mt Shuksan Belt in the Cascade Range, Washington. Its accuracy cannot exceed those of the estimates of pressure for these areas (for discussion see *Brown, 1977*).

The NaM4 contents of amphiboles from the gneisses of the Staré Sedlo and Mirotice complexes vary from 0.02 to 0.12 and they straddle the 2 kbar isobar on the NaM4 vs Al^{IV} diagram (Fig.5.1). Amphiboles from the Mirotice complex plot systematically above this isobar, while amphiboles from the Staré Sedlo mylonite gneisses are scattered both sides of it. This may indicate pressure variations within the shear zone at the time of amphibole crystallization although the differences are far less than the accuracy of this barometer (approx. $\pm$ 1 kbar). However the data do indicate low- to medium-pressure conditions at least in the later stages of ductile deformation and associated metamorphism of the protolith of the Staré Sedlo and Mirotice mylonite gneisses. This conclusion is consistent with the evidence given on the basis of total Na/Ca and total Al/Si ratios in the studied amphiboles (Chapter 3, Fig.3.14).

5.2.2 Amphibole - biotite pairs

The distribution of mg (mg=Mg/[Mg+Fe+Mn]) between coexisting biotite - amphibole pairs and its correlation with temperature has been studied by *Perchuk (1970)* who found that with increasing temperature the mg value in amphibole increases at the expense of the coexisting biotite. This lead to a formulation of an empirical thermometer (in the form of isotherms in the bi(mg)-amph(mg) system). An alternative form of this thermometer also includes the Ti content in both biotite and amphibole. While the correlation of Ti content in calcic amphiboles with temperature of their crystallization has been documented by *Leake (1965)*, the relation of crystallization temperature and Ti content in biotite has not been established unequivocally. However study of coexisting amphibole - biotite pairs in tonalitic rocks

of the late Hercynian Central Bohemian Pluton (*Lang et al., 1978*) has shown the strong Ti-affinity of biotite which results in a somewhat higher calculated crystallization temperatures of amphibole - biotite pairs when Ti is included in the mg value. In addition, the assumption of total Fe being present as Fe^{2+} and, or, the proportion of Fe^{2+} being equal in both amphibole and biotite certainly has some effect upon the resulting temperature.

The amphibole - biotite pairs from the gneisses of both the Staré Sedlo and Mirotice complexes straddle the 600 ^{o}C isotherm on the bi(mg) vs amph(mg) diagram (Fig.5.2a) and this provides an estimate of the temperature of the closure of mg in the amphibole - biotite pair. When Ti is included in both amph(mg) and bi(mg) (Fig.5.2b), the corresponding temperatures are 50 - 70 ^{o}C higher. However for the reasons given above, the temperature derived from amph(mg) - bi(mg) pairs which do not include Ti are likely to be more realistic but as this thermometer has not yet been calibrated on naturally-occurring assemblages, and its reliability is still subject to much discussion (*Lang et al., 1978*), the temperatures obtained by this method can only be regarded as approximate estimations.

5.2.3 Al content in amphibole

The relation between Al^{VI} content in both magmatic and metamorphic amphiboles and pressure conditions of their crystallization has previously been set out (*Leake, 1965, 1971*) and already discussed in Chapter 3. Subsequent studies aimed at quantifying this relation has lead to the formulation of various empirical geobarometers based upon the total aluminium (Al^{T}) content in hornblende:

P ($\pm$ 3 kbar) = - 3.92 + 5.03Al^{T} (*Hammastrom and Zen, 1986*);

P ($\pm$ 1 kbar) = - 4.76 + 5.64Al^{T} (*Hollister et al., 1987*);

P ($\pm$ 0.5 kbar) = - 3.46($\pm$0.24) + 4.23($\pm$0.13)Al^{T} (*Johnson and Rutherford, 1989*);

P ($\pm$ 1 kbar) = - 6.23 + 5.34Al^{T} (*Thomas and Ernst, 1990*).

These barometers have been defined for calc-alkaline plutonic and volcanic complexes and the calibration covers the range of 2 to 12 kbar (see *Thomas and Ernst, 1990* for discussion). Clearly the limitation of these barometers to rocks of a specific (calc-alkaline) composition, together with the large uncertainty in the pressure calculation, rules out any possible temperature influence upon the hornblende composition. On the other hand the temperature correlation with the Al^{IV} content of amphibole coexisting with

plagioclase in silica-saturated rocks has recently lead to the formulation of an amphibole - plagioclase thermometer (*Blundy and Holland, 1990*) and consequently to numerous discussions on whether it is the pressure or the temperature that is reflected by the aluminium content in hornblende (*Blundy and Holland, 1992a,b; Hammastrom and Zen, 1992; Poli and Schmidt, 1992; Rutherford and Johnson, 1992*). *Blundy and Holland (1990, 1992a,b)* gave evidence for both pressure and temperature having an influence on the Al content of amphibole together with evidence for the insensitivity of Al^{IV} content in amphibole to silica activity in the system above 700 °C. They have also shown the effect of sub-solidus re-equilibration of amphibole - plagioclase pairs upon the amphibole composition which makes the thermometer applicable to metamorphic rocks.

The amphibole - plagioclase thermometer is based on calibration of the reactions:

edenite + 4 quartz = tremolite + albite, and

pargasite + 4 quartz = hornblende + albite.

The equilibrium of both reactions leads to the temperature-sensitive expression:

$$T(K) = (0.677 * P(kbar) - 48.98 + Y) / (-0.0429 - 0.08134 * \ln K)$$

where $K = [(Si-4)/(8-Si)]*XPLG(Ab)$. Y represents plagioclase non-ideality $RT\ln\gamma_{Ab}$ ($Y=0$ for $X_{Ab}>0.5$ and $Y=-8.06+25.5*(1-X_{Ab})^2$ for $X_{Ab}<0.5$).

In order to calculate the temperature of amphibole crystallization in gneisses of the Staré Sedlo and Mirotice complexes the average compositions of amphibole and coexisting plagioclase from the matrix of the gneisses were calculated for each sample. The derived values calculated at a pressure of 2 kbar, vary from 708 to 771 °C (Table 5.2) with the uncertainty (± 75 °C) being that given by *Blundy and Holland (1990)*. The arbitrarily chosen pressure of 2 kbar is likely to correspond to the late stages of ductile deformation (see 5.2.1 and Fig.5.1) and is likely to be unrealistic for the peak of ductile deformation at deeper levels. As pressures of up to 6 kbar have been reported from mylonitic zones elsewhere (e.g. *Beach, 1973*), recalculation of the data for amphiboles at this pressure yields metamorphic recrystallization temperatures of 652 - 711 °C. Even this estimation must be viewed with considerable caution. However the composition of amphibole in the mylonite gneisses of the Staré Sedlo and Mirotice complexes does indicate that ductile deformation was associated with temperatures corresponding at least to mid-amphibolite facies and probably upper amphibolite facies metamorphism.

Assuming a crystallization temperature of 600 - 700 ^{o}C (or any temperature in the lower span of the calc-alkaline crystallization temperatures), the corresponding pressure can be calculated using barometric equations of *Hammastrom and Zen (1986)*, *Hollister et al. (1987)* and *Johnson and Rutherford (1989)*. The results yield the pressure of amphibole crystallization ranging from ca 1.2 kbar to as much as 4.4 kbar (Table 5.3). However the uncertainty is of the same order as the results.

5.3 P and T constraints on the thermal overprint

The intensity and extent of the thermal overprint of already ductilely deformed mylonite gneisses of the Staré Sedlo and Mirotice complexes by the surrounding late Hercynian granitoids of the Central Bohemian Pluton is difficult to assess as the products of mineral reactions induced by the increased temperature in the tonalitic orthogneisses are not common. In addition there are several separate granitoid intrusions adjacent to the complexes which might have had different thermal and not necessarily contemporaneous effects on the gneisses. To accommodate these constraints, at least in part, the influence of granitoid and durbachitic intrusions are considered separately.

Estimation of pressure during the thermal overprint event(s) is difficult. The main contribution to the total pressure during the contact metamorphism is likely to be by the lithostatic pressure and based on the field observations from uranium mines in Central Bohemia, the estimated depth of emplacement of the upper parts of the granitoid intrusions of the Central Bohemian Pluton was likely to be at 2 - 3 km, i.e. corresponding to less than 1 kbar (*Vlašímský, 1986*). Pressure calculated for granitoid intrusions adjacent to the Staré Sedlo and Mirotice complexes using the amphibole composition data given by *Poubová (1971, 1974)*, and the barometric equations of *Hammastrom and Zen (1986)*, *Hollister et al. (1987)* and *Johnson and Rutherford (1989)*, is within the range of 1 - 2.4 kbar but the uncertainty is of the same order as the results.

5.3.1 Thermal overprint by adjacent granitoids

Various changes in the chemical composition of minerals (i.e. biotite and amphibole) in samples of mylonite gneiss taken close to the contact with adjacent granitoids have already been discussed in

Chapter 3. Samples from the southwestern part of the Mirotice complex taken approximately 150 m (at present erosion level) from the contact with the Kozárovice granodiorite contain the assemblage garnet - biotite. Petrographic evidence has been given for Fe-Mn garnet growing statically as a result of heating from the adjacent granodiorite. Therefore the garnet - biotite pair is likely to preserve the record of the temperature conditions in this contact aureole.

The partitioning of Fe and Mg between coexisting garnet and biotite is strongly correlated with temperature and often used in thermometry. The experimental results of *Ferry and Spear (1978)* at 2.07 kbar and 550 - 800 ^{o}C yield the equation

$$[(Mg/Fe)garnet/(Mg/Fe)biotite] = - 2109/T(K) + 0.782$$

which transformed into

$$12452 - 4.662T(K) + 0.057P(bar) + 3RTlnK = 0$$

is used for temperature calculation of Mg - Fe equilibration in the garnet - biotite pair. As the equilibration temperature is influenced by both the garnet and biotite compositions, corrections for Mn and Ca content in garnet (when (Ca+Mn)/(Ca+Mn+Mg+Fe)>0.2) and Al^{VI} and Ti in biotite (when $(Al^{VI}+Ti)/(Al^{VI}+Ti+Fe+Mg)>0.15$) must be employed. While the studied biotite is just acceptable for the thermometry (in terms of both the Al^{VI} and Ti contents), garnet from the mylonite gneiss (spessartine 35.31%) must be corrected for its high Mn content.

In order to do this correction, various methods were employed. Assuming the ideality of Fe - Mg mixing in garnet (*Mueller, 1972*), *Hodges and Spear (1982)* developed a correction procedure based upon the assumption of ideal behaviour of the almandine - spessartine and grossular - spessartine binaries. They constrained the mixing properties of pyrope - spessartine from the mineral assemblage in pelitic schists of Mt Moosilauke, New Hampshire, U.S.A. The final temperature calculation is then the same as that of *Ferry and Spear (1978)* but the equilibrium constant is multiplied by the ratio of activity coefficients of pyrope and almandine:

$$\gamma_{py}/\gamma_{al} = EXP\ [(3300-1.5*T(K))*(X^2_{gr}+X_{al}X_{gr}+X_{gr}X_{sp}+X_{py}X_{gr})]/[RT(K)]$$

where X is the molar fraction of grossular (gr), almandine (al), spessartine (sp) and pyrope (py). The corresponding values for the free energy of interaction for all garnet end-members (Margules parameters) are given in *Hodges and Spear (1982)*.

Another approach recently employed by *Bhattacharya et al. (1992)* uses the updated mixing parameters for pyrope - almandine solution of *Ganguly and Saxena (1984)* and *Hackler and Wood (1989)*. Assuming a non-ideal mixing in the phlogopite (ph) - annite (ann) binary they derived the following equations for the temperature of garnet - biotite equilibration:

$T(K)=[20286+0.0193P(bar)-\{2080(X_{py})^2-6530(X_{al})^2-13807X_{gr}(1-X_{sp}) +$

$8540X_{al}X_{py}(1-X_{sp}+4125X_{gr}(X_{py}-X_{al})\}+4441(2X_{ph}-1)]/[13.138+8.3143\ln K_D+6.276X_{gr}(1-X_{sp})]$

- based upon the data of *Hackler and Wood (1989)* - and

$T(K)=[13538+0.0193P(bar)-\{837(X_{py})^2-10460(X_{al})^2-13807X_{gr}(1-X_{sp})+19246X_{al}X_{py}(1-X_{sp}) +$

$5649X_{gr}(X_{py}-X_{al})\}+7972(2X_{ph}-1)]/[6.778+8.3143\ln K_D+6.276X_{gr}(1-X_{sp})]$ - based upon the mixing parameters of *Ganguly and Saxena (1984)*.

Using the above equations the temperature of Fe - Mg equilibration between coexisting garnet and biotite in a sample of mylonite gneiss from the Mirotice complex at an arbitrarily chosen pressure of 2 kbar was calculated. The results (Table 5.4) suggest equilibration at 604 - 662 °C (*Ferry and Spear, 1978*) or 625 - 681 °C (*Hodges and Spear, 1982*). However the correct (and scarcely used) form of the equilibrium constant for the exchange reaction between garnet and biotite is

$$K_D = [(Mg/Fe^{2+})\text{garnet}]/[(Mg/Fe^{2+})\text{biotite}],$$

i.e. only Fe^{2+} rather than total content of Fe is considered in the calculation. Using the Fe^{2+}/Fe^{3+} estimation for both garnet and biotite (see Chapter 3) substantially lowers the calculated equilibrium temperatures for the garnet - biotite pair to 507 - 553 °C and 528 - 572 °C, respectively (see Table 5.4). In addition, considering the non-ideal mixing on the phlogopite - annite binary (*Bhattacharya et al., 1992*), temperature ranges of 369 - 404 °C and 331 - 359 °C are obtained using total Fe and Fe^{2+}, respectively. The error imposed on this calculation is apparently strongly dependent upon the uncertainty of the Fe^{2+}/Fe^{3+} estimation in both garnet and biotite. Assuming the maximum likely temperature of the intrusion of granodiorite (Kozárovice type of the Central Bohemian Pluton) to be 750 - 800 °C and the distance from the contact in the present erosion level to be 150 m, a realistic temperature estimation lies within the interval of ca 405 - 530 °C, i.e. between the upper limit of Bhattacharya's and lower limit of Hodges and Spear's estimation (using Fe^{2+} only). The relatively constant compositions of both garnet and biotite is likely to have resulted from almost complete equilibration within the rock. No chemical

differences suggesting a possible retrograde exchange were found between core and rim of the studied garnet or between biotite adjacent to garnet and that from the matrix, respectively.

5.3.2 Thermal overprint by adjacent durbachites

Durbachitic rocks (which form the eastern contact of the Staré Sedlo complex) represent a high K and Mg (and also Cr, Ni, U, Th etc.) rocks emplaced probably shortly after the emplacement of most of the granitoid intrusions of the late Hercynian Central Bohemian Pluton (*Holub and Žežulková, 1978*). They undoubtedly crystallized from a volatile-rich magma in a multi-stage process consisting of several crystallization - remelting cycles (i.e. *Minařík et al., 1988; Bowes and Košler, 1993*). This makes any geothermometry based on mineral equilibria in durbachitic rocks extremely difficult. In addition no mineral pairs suitable for the temperature estimation of the overprint were found in orthogneisses of the Staré Sedlo complex adjacent to the durbachitic intrusion. Accordingly the chemical changes in the early Palaeozoic sediments of the Islet zone (ca 15 km NNE of the Staré Sedlo complex) induced by the contact heating of the durbachitic rocks (Čertovo břemeno type) had to be used in order to shed some light on the thermal overprint of the mylonite gneisses.

The equilibrium of isotopic exchange between coexisting calcite and graphite provides a useful tool for temperature estimation based upon the difference in ^{13}C contents between these minerals (*Valley and O'Neil, 1981; Wada and Suzuki, 1983*). Using this thermometer a temperature of ca 650 ^{o}C has been reported from a Devonian graphitic marble occuring ca 500 metres (at present erosion level) from the contact (*Košler, 1988*). However the very shallow dip of the marbles suggests that the true distance is probably less than 100 metres. Accordingly it is likely that part of the Staré Sedlo complex adjacent to durbachite intrusion was subject to a thermal overprint at temperatures of c. 650 ^{o}C. The results are consistent with previously published data suggesting the true width of the contact aureole is c. 300 - 500 m (*Suk, 1973*).

5.4 Conclusions

1. Field observations and stratigraphic correlations suggest a shallow emplacement of the magmatic protolith of the Staré Sedlo and Mirotice gneisses at a depth of less than 4 km. Temperatures of 765 - 795 ^{o}C are likely for this protolithic magma on the basis of both its chemical composition and Zr saturation.

2. Ductile deformation of the protolith of the Staré Sedlo and Mirotice gneisses was associated with temperatures corresponding to mid to upper amphibolite facies metamorphism. Temperatures of 600 - 700 ^{o}C and 600 - 650 ^{o}C were estimated using the bi(mg) - amph(mg) geothermometer of *Perchuk (1970)* and the Al^{IV} content in amphibole geothermometer of *Blundy and Holland (1990)*, respectively. NaM4 and Al^{T} contents of amphiboles indicate low-pressure metamorphism but they are not considered to correspond to peak pressure conditions.

3. Chemical changes in gneisses adjacent to late Hercynian plutonic rocks are associated with a thermal overprint. Estimated temperatures in the contact aureole c. 150 m and less than 100 m away from the contact with granodiorite (Kozárovice type) and with durbachite (Čertovo břemeno type) are 405 - 530 ^{o}C and 650 ^{o}C, respectively.

Table 5.1

Zr saturation temperatures calculated for mylonite gneisses from the Staré Sedlo (RC 2274) and Mirotice (RC 2284) complexes; sample numbers correspond to those in Chapter 6.

Sample/ analysis no.	zircon ZrO_2 (wt%)	rock Zr (ppm)	T(°C) ideal	T(°C) real
RC 2274/1	63.30	177	793	801
RC 2274/2	63.77	177	793	800
RC 2274/3	61.16	177	793	804
RC 2274/4	64.32	177	793	800
RC 2284/5	65.59	172	795	800
RC 2284/6	65.32	172	795	800
RC 2284/7	67.79	172	795	797
RC 2284/8	65.85	172	795	799
RC 2284/9	65.75	172	795	799
RC 2284/10	65.03	172	795	800
RC 2284/11	66.27	172	795	799
RC 2284/12	63.85	172	795	802
RC 2284/13	65.31	172	795	800

	RC 2274 (wt%)	RC 2284 (wt%)
SiO_2	69.52	70.54
TiO_2	0.28	0.29
Al_2O_3	14.62	13.70
Fe_2O_3(tot)	2.80	2.75
MnO	0.08	0.10
MgO	2.33	0.80
CaO	2.56	2.55
Na_2O	3.36	2.94
K_2O	3.17	3.11
P_2O_5	0.10	0.10

Table 5.2

Temperature estimations based on the amphibole - plagioclase thermometer (*Blundy and Holland, 1990*).

Sample	Si-amph	X(Ab)	K	T (°C) @2kbar	T (°C) @6kbar
STG-4	6.955	0.70	1.974	708	652
STG-5	6.824	0.68	1.631	741	683
STG-10	6.694	0.69	1.416	767	708
STG-11	6.825	0.71	1.707	733	676
MIG-5	6.743	0.75	1.629	741	684
MIG-6	6.854	0.64	1.588	746	688
MIG-10	6.552	0.79	1.390	771	711
MIG-22	6.733	0.65	1.409	768	709

Table 5.3

Pressure estimations based on the total Al-content (AlT) in amphiboles;
results in kbar; H+Z (*Hammastrom and Zen, 1986*), H et al. (*Hollister et al., 1987*),
J+R (*Johnson and Rutherford, 1989*).

Sample	Al(T)	H+Z	H et al.	J+R
STG-4	1.175	2.0	1.9	1.5
STG-5	1.360	2.9	2.9	2.3
STG-10	1.506	3.7	3.7	2.9
STG-11	1.343	2.8	2.8	2.2
MIG-5	1.399	3.1	3.1	2.5
MIG-6	1.271	2.5	2.4	1.9
MIG-10	1.620	4.2	4.4	3.4
MIG-22	1.373	3.0	3.0	2.3

Table 5.4

Garnet - biotite thermometry for gneisses of the Mirotice complex (sample MIG-11).

C = core; R = rim; H-W (*Hackler and Wood, 1989*); G-S (*Ganguly and Saxena, 1984*); for other symbols see text.

Hodges and Spear (1982) - based on Fe_{tot}.

	X(al)	X(py)	X(gr)	X(sp)	X(ann)	X(ph)	K_D	T (°C)
Gt-1C/Bi-2	0.560	0.046	0.052	0.342	0.609	0.241	0.2053	640
Gt-1R/Bi-1	0.563	0.045	0.052	0.340	0.606	0.247	0.1973	625
Gt-2/Bi-3	0.565	0.052	0.042	0.340	0.596	0.248	0.2221	667
Gt-3C/Bi-6	0.567	0.052	0.046	0.336	0.607	0.245	0.2277	678
Gt-3R/Bi-6	0.564	0.052	0.046	0.339	0.607	0.245	0.2290	681
Gt-4/Bi-5	0.568	0.052	0.045	0.334	0.597	0.238	0.2294	681

Hodges and Spear (1982) - based on Fe^{2+}

	X(al)	X(py)	X(gr)	X(sp)	X(ann)	X(ph)	K_D	T (°C)
Gt-1C/Bi-2	0.547	0.047	0.054	0.352	0.521	0.295	0.1516	538
Gt-1R/Bi-1	0.548	0.047	0.054	0.351	0.519	0.302	0.1465	528
Gt-2/Bi-3	0.552	0.054	0.044	0.350	0.508	0.302	0.1640	559
Gt-3C/Bi-6	0.554	0.054	0.047	0.346	0.520	0.300	0.1681	568
Gt-3R/Bi-6	0.550	0.054	0.047	0.349	0.520	0.300	0.1691	570
Gt-4/Bi-5	0.554	0.054	0.047	0.346	0.509	0.290	0.1703	572

Bhattacharya et al. (1992) - based on Fe_{tot}.

	X(al)	X(py)	X(gr)	X(sp)	X(ph)	Gt Mg/Fe	Bi Mg/Fe	K_D	H-W T(°C)	G-S T(°C)
Gt-1C/Bi-2	0.560	0.046	0.052	0.342	0.241	0.081	0.397	4.872	499	374
Gt-1R/Bi-1	0.563	0.045	0.052	0.340	0.247	0.080	0.408	5.070	492	369
Gt-2/Bi-3	0.565	0.052	0.042	0.340	0.248	0.092	0.416	4.502	518	397
Gt-3C/Bi-6	0.567	0.052	0.046	0.336	0.245	0.092	0.404	4.391	525	404
Gt-3R/Bi-6	0.564	0.052	0.046	0.339	0.245	0.092	0.404	4.366	525	404
Gt-4/Bi-5	0.568	0.052	0.045	0.334	0.238	0.091	0.399	4.360	524	401

Bhattacharya et al. (1992) - based on Fe^{2+}

	X(al)	X(py)	X(gr)	X(sp)	X(ph)	Gt Mg/Fe	Bi Mg/Fe	K_D	H-W T(°C)	G-S T(°C)
Gt-1C/Bi-2	0.547	0.047	0.054	0.352	0.295	0.086	0.566	6.596	445	333
Gt-1R/Bi-1	0.548	0.047	0.054	0.351	0.302	0.085	0.583	6.826	441	331
Gt-2/Bi-3	0.552	0.054	0.044	0.350	0.302	0.098	0.595	6.097	461	352
Gt-3C/Bi-6	0.554	0.054	0.047	0.346	0.300	0.097	0.577	5.949	467	359
Gt-3R/Bi-6	0.550	0.054	0.047	0.349	0.300	0.098	0.577	5.913	468	359
Gt-4/Bi-5	0.554	0.054	0.047	0.346	0.290	0.097	0.569	5.873	467	355

Ferry and Spear (1978) - based on Fe_{tot}.

	Gt Mg/Fe	Bi Mg/Fe	K_D	T (°C)
Gt-1C/Bi-2	0.081	0.397	0.205	618
Gt-1R/Bi-1	0.080	0.408	0.197	604
Gt-2/Bi-3	0.092	0.416	0.222	649
Gt-3C/Bi-6	0.092	0.404	0.228	659
Gt-3R/Bi-6	0.092	0.404	0.229	662
Gt-4/Bi-5	0.091	0.399	0.229	662

Ferry and Spear (1978) - based on Fe^{2+}

	Gt Mg/Fe	Bi Mg/Fe	K_D	T (°C)
Gt-1C/Bi-2	0.086	0.566	0.152	517
Gt-1R/Bi-1	0.085	0.583	0.147	507
Gt-2/Bi-3	0.098	0.595	0.164	541
Gt-3C/Bi-6	0.097	0.577	0.168	549
Gt-3R/Bi-6	0.098	0.577	0.169	551
Gt-4/Bi-5	0.097	0.569	0.170	553

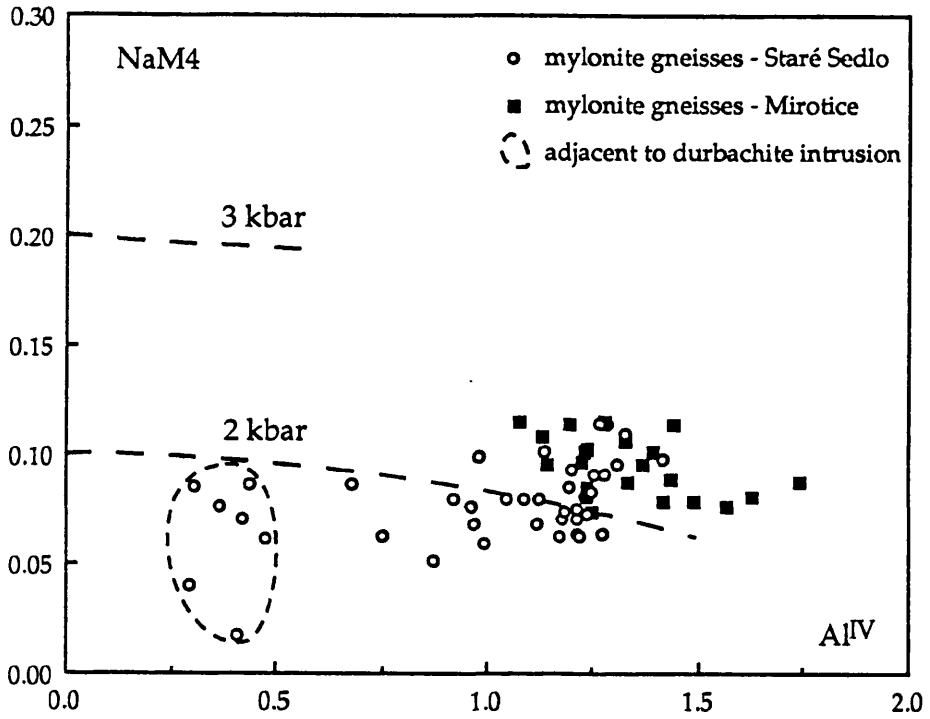

Fig.5.1

NaM4 vs Al^{IV} content in amphiboles from gneisses of the Staré Sedlo and Mirotice complexes; isobars from *Brown (1977)*.

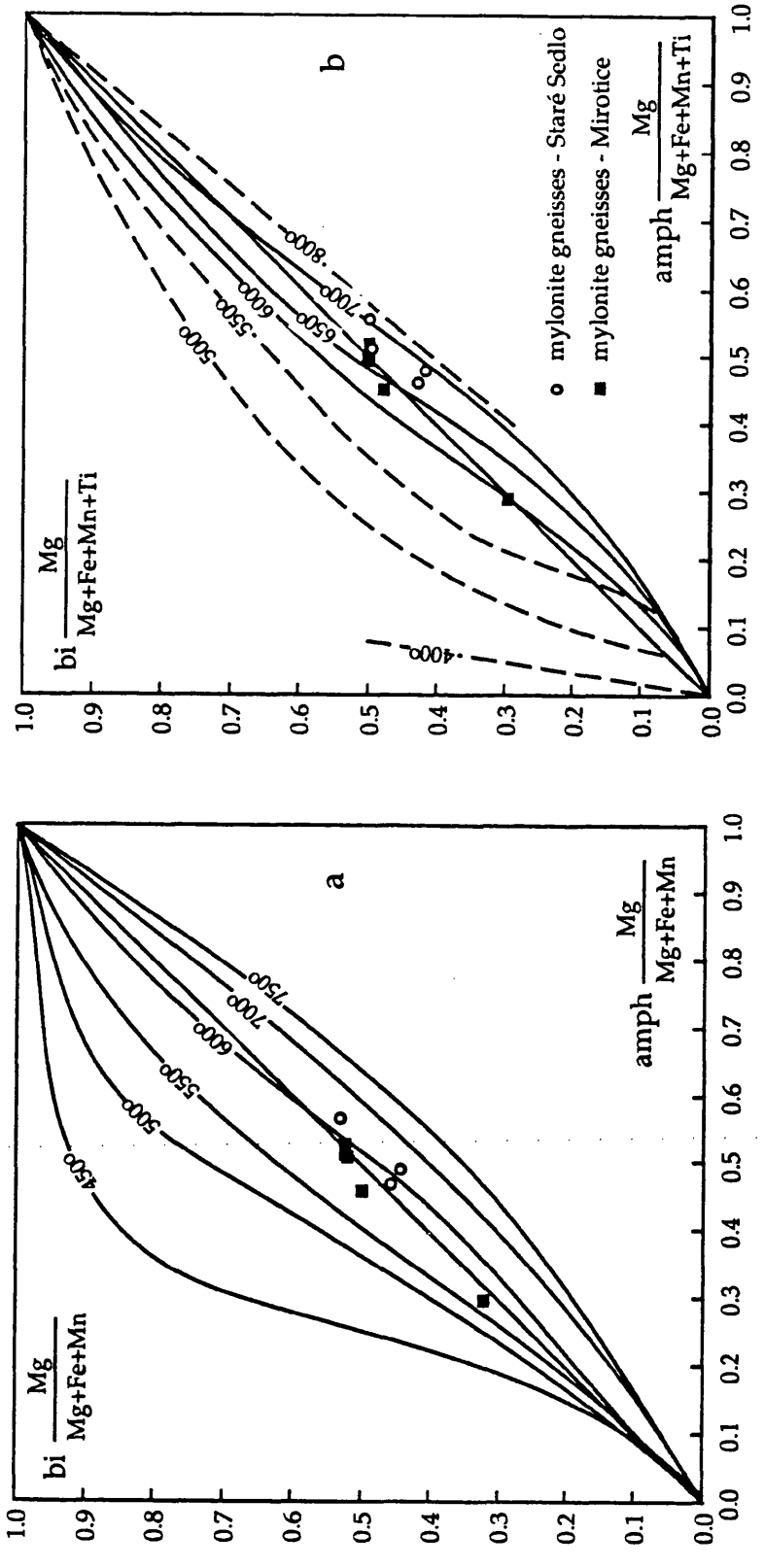

Fig.5.2

a. Distribution of mg (Mg/[Mg+Fe+Mn]) between coexisting amphibole and biotite from gneisses of the Staré Sedlo and Mirotice complexes; isotherms from *Perchuk (1970)*.

b. The same as (a) for mg = Mg/[Mg+Fe+Mn+Ti].

6. U - Pb ZIRCON ISOTOPIC STUDY OF GNEISSES FROM THE STARÉ SEDLO AND MIROTICE COMPLEXES

This chapter has been submitted as a paper for publication in Neues Jahrbuch für Mineralogie Monatshefte. Accordingly its format corresponds to that required by the journal but the numbering of the headings, tables and figures is consistent with the thesis and some of the information which has already been given earlier in this study is repeated here, particularly in the introductory part. The references given at the end of this chapter are incorporated in the main reference list at the end of this thesis.

Mid - late Devonian plutonic activity in the Bohemian Massif: U - Pb zircon isotopic evidence from the Staré Sedlo and Mirotice gneiss complexes, Czech Republic.

By **J. Košler, M. Aftalion and D.R. Bowes,** Glasgow

With 3 figures and 3 tables in the text

Košler, J., Aftalion, M. & Bowes, D.R.: Mid - late Devonian plutonic activity in the Bohemian Massif: U - Pb zircon isotopic evidence from the Staré Sedlo and Mirotice gneiss complexes, Czech Republic.- N. Jb. Miner. Mh., 1993, H.XX, XXX-XXX; Stuttgart 1993.

Abstract: A crystallization age of the plutonic protolith of the gneisses of the Staré Sedlo and Mirotice complexes in the range 380 - 365 Ma (mid - late Devonian) is indicated by an upper intercept U - Pb zircon age of 373 ± 5 Ma for the former and upper concordia intercept and $^{206}Pb/^{204}Pb$ vs $^{207}Pb/^{204}Pb$ isochron ages of 369 ± 4 and 375 ± 5 Ma, respectively, for zircon populations from both complexes. Oscillatory zoning in many zircons is consistent with igneous crystallization while primary crystallized cores and late overgrowths present in a small proportion of grains are unlikely to have had a significant influence on the U - Pb isotopic system. The data points from both zircon populations group within the upper 16 % of their chords and at least some of the

small Pb-loss is related to fracturing and leaching along cracks, mainly during the ductile deformation of the gneiss protolith.

K e y w o r d s: electron microscopy, gneiss, Hercynides, isotopes, oscillatory zoning, plutonism, protolith, zircon.

6.1 Introduction

Within the Central Bohemian Pluton of the Bohemian Massif in southern Bohemia are metamorphic complexes with the gross form of roof pendants, parts of which (the Staré Sedlo and Mirotice gneiss complexes) consist of strongly foliated biotite- and amphibole-bearing gneisses (Fig.6.1). Other parts consist of metasedimentary and metavolcanic rocks (the Mirovice and Sedlčany-Krásná Hora metamorphic islets - KETTNER, 1930a; SUK, 1973). The mineralogical and chemical compositions and petrographical features of the gneisses are consistent with having an igneous protolith of tonalitic - granodioritic composition and so they have been referred to as orthogneisses or metatonalites (1:25000 22-232 Czech Geological Survey map and comments). To establish the age of these rocks, a U - Pb zircon isotopic study, together with a study of the internal fabric of the zircons, have been carried out on samples of both gneiss complexes (Fig.6.1). The rocks are variably biotite-, amphibole - biotite-, biotite - amphibole- and feldspar-bearing and commonly contain augen of plagioclase and K-feldspar as pre-deformational mineral relics in a strongly foliated cataclastic to mylonitic matrix that is indicative of ductile deformation (KOŠLER et al., 1993).

Regionally the foliation of the Staré Sedlo and Mirotice complexes shows discordance to the boundary of the igneous masses of the Central Bohemian Pluton with such a relationship between a granodiorite (Kozárovice type) of the Central Bohemian Pluton and the gneissic foliation of the Staré Sedlo complex displayed in the Vltava River valley 2 km S of Staré Sedlo. On the basis of (1) a corresponding relationship between the Mirotice gneiss complex and granodiorite of Blatná type (Fig.6.1) and (2) the 331 ±4 Ma Rb - Sr whole-rock age for this part of the Central Bohemian

Pluton (VAN BREEMEN et al., 1982) being similar to that of other parts, the metamorphic fabric of the Staré Sedlo and Mirotice gneiss complexes must be pre - mid-Visean in age.

For this study *c.* 10 kg samples were taken from both gneiss complexes (for sample locations see Fig.6.1). The samples were crushed, ground and heavy minerals separated using a Wilfley table, heavy liquids and a Frantz isodynamic separator. Zircon was sieved into size fractions and again split according to magnetic susceptibility. The least magnetic fractions, chosen for analysis, were hand-picked to 99% purity and acid washed. The zircons are honey- to brown-coloured with the smaller grains usually being clear. They occur as subhedral to euhedral grains or grain fragments with dominating {100} and {110} prisms and with {101} and {211} pyramids being present in variable proportions. Their crystal shapes correspond generally with S_{8-10} typological groups (PUPIN, 1980). Fracturing parallel to the c-axis often occurs although some radial fractures were also observed. Inclusions of apatite were found mainly in the large zircon grains.

6.2 U-Pb isotopic study

The digestion of the hand-picked and acid-washed samples (10 - 30 mg in each size fraction) and the analytical techniques used to extract Pb and U closely followed those of KROGH (1973). The recovered radiogenic Pb was loaded in diluted H_3PO_4 on to silica gel on a Re-single filament; U was loaded in *c.* 1% HNO_3 onto Ta_2O_5 in diluted H_3PO_4 on a W-single filament. The isotopic ratios were measured using a VG MM30 semi-automatic mass spectrometer. The ratios of the NBS standards SRM 983 and U-500, respectively, gave the following results:

$^{207}Pb/^{206}Pb = 0.071205 \pm 0.000032$ $^{208}Pb/^{206}Pb = 0.013643 \pm 0.000019$

$^{206}Pb/^{204}Pb = 2758 \pm 14$ $^{238}U/^{235}U = 0.99975 \pm 0.00025$

agreeing, within errors, with the values given by the NBS. The ages were calculated using the decay constants given by JAFFEY et al. (1971). A modified regression analysis (YORK, 1969), together with 2σ blanket errors of $\Delta^{207}Pb/^{206}Pb = 0.1$, $\Delta^{207}Pb/^{235}U = 0.6\%$ and $\Delta^{206}Pb/^{238}U = 0.4\%$, and a correlation factor of 0.8, were used to calculate the isochron and concordia intercepts, respectively. The measured Pb isotopic ratios were corrected for common Pb using the Pb

composition of the nitric acid ($^{206}Pb/^{204}Pb$ = 17.640, $^{207}Pb/^{204}Pb$ = 15.582 and $^{208}Pb/^{204}Pb$ = 37.664), considered to be the main contaminant.

The isotopic results are presented in Tables 6.1 and 6.2 and Figure 6.2. In the concordia diagram the data points of both zircon populations are discordant and group within the upper 16% of their chords. The data points of zircons from the Staré Sedlo gneiss complex are well aligned. However the lower intercept is somewhat negative (- 20 ± 114 Ma, MSWD = 0.27), indicating a slight rotation of the discordia. To compensate for this rotation it was passed through 0 Ma as suggested by DUNNING & KROGH (1985). The upper intercept age is then 373 ± 5 Ma (MSWD = 0.19).

Within the analytical errors the data points of zircon fractions from the Mirotice gneiss complex are slightly above the discordia of the Staré Sedlo complex data points but yield a similar upper intercept age (365 ± 5 Ma, MSWD = 1.5).

A $^{206}Pb/^{204}Pb$ vs $^{207}Pb/^{204}Pb$ isochron from the data for both zircon populations (6 points, Table 6.2) yields an age corresponding to its slope of 375 ± 5 Ma and this agrees well, within errors, with the upper intercept age of 369 ± 4 Ma (MSWD = 1.5). These values suggest a crystallization age for the protolith(s) of the Staré Sedlo and Mirotice gneisses within the 380 - 365 Ma range, a range that straddles the mid - late Devonian boundary.

6.3 Zircon internal fabric and composition

As large zircon grains are sparse the isotopic properties of zircon grains (such as any inherited older Pb component) would be expected to have only an extremely limited, or even negligible, influence on the overall isotopic analytical results. However an electron microscope and microprobe study of the internal fabric and chemical composition of representatives of the coarse fraction from both the Staré Sedlo and Mirotice gneisses has provided information concerning (1) magmatic conditions during their crystallization, (2) the effects of subsequent fluid movement and (3) their reaction to the development of the gneissic rock fabric.

For this work, separated individual zircon grains were mounted in epoxy resin and polished. The internal textures were observed using a backscattered electron detector (BSE) on a Cambridge

Stereoscan 360 electron microscope at the University of Glasgow following the principles of BSE imagery described in LLOYD (1987) and PATERSON et al. (1989). The elemental analysis was carried out on the same samples using a JEOL JCXA-733 electron microprobe at the University of St Andrews. The method used was the same as that of PATERSON et al. (1992). The focused beam of 20 kV and 50 nA was used to produce spot analyses. The samples were measured for Si, Zr and Hf against a natural zircon standard, and for U, REE and Y against UO_2 and REE-doped glass standards of DRAKE & WEILL (1972), respectively.

The backscattered electron imagery revealed a well-preserved oscillatory zoning in most (*c.* 90%) of the studied population (Fig.6.3a, c). However in some cases (*c.* 10%) bright cores and patches in the zircon grains indicate inhomogeneities of a relatively higher mean atomic number $\bar{Z}$ (LLOYD, 1987). Four different types of inhomogeneities were distinguished (Fig.6.3b-e) in addition to the oscillatory zoning. The electron microprobe data from zones with different $\bar{Z}$ are given in Table 6.3 and locations of analyzed points are shown in Figure 6.3.

a) Oscillatory zoning (Fig.6.3a)

This is a common feature of igneous zircons and is generally ascribed to crystallization from a silicate melt. As zircon tends to crystallize as pure $ZrSiO_4$, it pushes all the impurities ahead until they reach a critical concentration on the crystal surface, at which stage they are incorporated into the zircon lattice. This applies mainly to the large tetravalent cations U^{4+}, Th^{4+}, Ce^{4+} and Hf^{4+} which replace Zr^{4+} via isomorphous substitution. It also holds for trivalent cations like Y^{3+} and REE^{3+} for which a charge-compensated substitution involving P^{5+} and Si^{4+}, or replacement of O^{2-} by OH^-, were proposed by ROMANS et al. (1975) and VINOKUROV et al. (1971), respectively. As the process of crystallization is kinetically controlled, the small P - T changes due to the magma movements result in oscillatory changes in the zoning pattern. The higher Y, U and Yb concentrations in the brighter parts of the zoning pattern (analyses no. 1 and 2) are consistent with the operation of this process.

b) Cores (Fig.6.3b)

Sub-round high-$\bar{Z}$ cores represent primary crystallized zircon surrounded by a later-formed rim of zoned zircon. The radial fractures in the rim terminate at the interface between the rim and core (cf. WAYNE & SINHA, 1992, fig.6) suggesting that they are likely to have resulted from progressive

radiation damage caused by the U-rich cores which also show high concentrations of Hf, Y and Yb (see analyses no. 3 and 4). The partial resorption of outer parts of the cores was probably due to Zr undersaturation at some stages during the magmatic evolution (WATSON & HARRISON, 1983). At other stages Zr oversaturation resulted in zircon overgrowth.

c) Overgrowths (Fig.6.3c)

Unzoned Hf-rich cores are overgrown by a high-$\overline{Z}$ rim of a relatively U, Y and Yb-rich zircon (see analyses no. 5 and 6). As the rim itself is zoned, its crystallization is likely to have taken place in a late magmatic stage rather than during superimposed ductile deformation. As there are no other Zr-bearing phases present in the rock, the requisite Zr oversaturation is accounted for by resorption of other zircon grains.

d) Alteration along cracks (Fig.6.3d)

Elongate alteration zones occur along the cracks within the zircon crystals. As most of the cracks are parallel to the c-axis, they cross-cut the oscillatory zones and could have acted as channels for postmagmatic and, or, metamorphic fluids, associated with the leaching of impurities (mainly U, Pb, Hf and REE) from the zones. The extent of leaching for the different elements would have been related to the extent of fracturing in the particular grain, the amount of radiation damage and solubility and instability of each element in the zircon crystal lattice. As an example analyses no. 7 to 10 suggest the loss of Y and Yb. There may also have been loss of other (not analyzed) elements including Pb and this would be reflected in the U-Pb isotopic system.

e) Unzoned irregular patches (Fig.6.3e)

Within some of the zoned zircon grains there are unzoned high-$\overline{Z}$ irregularly-shaped patches similar to those described by WAYNE & SINHA (1988, fig.7) as resulting from zircon deformation during prograde mylonitization, a process that these authors suggest involves fracturing, disaggregation, element leaching, overgrowth, refaceting and annealing of cores, leading to the obliteration of igneous zoning. An alternative explanation is that of recrystallization due to the instability of zoned (trace-element rich) parts of the zircon, a process which PIDGEON (1992) links to the depletion of U and Th in the unzoned parts. However relatively high U concentrations in the unzoned high-$\overline{Z}$ patches and high but variable contents of REE and Y in the zoned low-$\overline{Z}$ parts of grains from the Staré Sedlo and Mirotice gneisses (analyses no. 11, 12 and 13), together with the overgrowths typical

of zircons from mylonitic rocks not being porous (WAYNE & SINHA, 1988), is not consistent with the process described by these authors. With the oscillatory zoning being present, the irregular high-$\bar{Z}$ patches are more likely to result from an incomplete zircon recrystallization with the preferential loss of some trace elements leading to a relative increase of U-proportion in the unzoned part of grains. This explanation is supported by the variations in Hf, REE and Y contents shown in the low-$\bar{Z}$ parts of the grains (analyses 6 and 7), suggesting that the process is linked to alteration of the radiation damaged parts of the crystals associated with the movement of postmagmatic and, or, metamorphic fluids.

6.4 Discussion

The evidence for mid - late Devonian crystallization at *c.* 380 - 365 Ma and subsequent ductile deformation including mylonitization of the tonalitic - granodioritic protolith of the Staré Sedlo and Mirotice gneisses (see also KOŠLER et al., 1993) is consistent with the petrographic evidence for the existence of relics of pre-metamorphic coarse mineral grains in gneisses. Like the zircon crystals, these feldspars often have a well preserved oscillatory zoning that is interpreted as being indicative of igneous crystallization. Accordingly, interpretations of the foliation being an igneous lamination (KETTNER, 1930a, b) cannot be sustained.

The evidence for only a limited Pb-loss from the zircon crystals is consistent with the internal fabric as revealed by the BSE and electron microprobe study. The superposed deformation that had such marked effects on the rock fabric has only limited expression in the zircon crystals, particularly the larger ones, as cracks and fractures mainly parallel to the c-axis and as partial recrystallization of some of the zoned crystals (cf. WAYNE & SINHA, 1992). Limited leaching of some chemical elements (cf. Fig.6.3d) would account for some of the Pb-loss (up to 16 %), but as the lower concordia intercept is close to zero (Fig.6.2), Pb-loss is likely to have occurred in more than one event since magmatic crystallization. However the limited nature of the discordance means that the crystallization age of the protolith can be established with confidence. Neither any minor inheritance from any primary crystallized cores that may have remained, nor the gain from the overgrowths (Figs 6.3b, c) are likely to have significantly affected the U - Pb isotope system.

However slightly different changes in the trace-element content during these processes may have caused the somewhat different loss factors in the two zircon populations and account for the lack of exact correspondence in positions of the two chords (cf. ALLÈGRE et al., 1974).

The isotopic evidence extends the time range of plutonic activity within the Hercynides of this part of the Bohemian Massif back to the late part of middle and the early part of the late Devonian. This is consistent with the stratigraphic evidence recorded for the islet zone where the break in sedimentation is at the very late part of the early Devonian and preceded by the development of the Skoupý conglomerates in the Sedlčany - Krásná Hora metamorphic islet (CHLUPÁČ, 1981, 1989). Further to the N and NW (in the present configuration) sedimentation in the Barrandian assemblage continued for a further *c.* 15 Ma before it was interrupted in the later part of the mid Devonian (Givetian) associated with uplift preceding abundant early Carboniferous granitic magmatism.

A generally analogous geological history is recorded in the North Cascade Range in Washington and British Columbia (HAUGERUD et al., 1991). There also gneissic plutons having features indicative of the superposition of ductile deformation on a plutonic igneous protolith occur within younger higher level undeformed granitic masses. Evidence is presented for an oceanic arc and volcanic arc provenance for the initial plutonism and for the mylonitic - cataclastic fabric of the gneisses being the result of major transcurrent movement leading to unroofing. Geochemical, isotopic and structural studies in the gneiss complexes and granitoid bodies of the Central Bohemian Pluton to be published elsewhere form the basis for assessing whether analogous geotectonic environments also reflect analogous geological histories. One line of evidence supporting the analogy, but from as yet limited data base, is that initial $^{87}Sr/^{86}Sr$ ratios indicate that both the protolith of the Staré Sedlo complex and the Central Bohemian Pluton did not have a long crustal history (KOŠLER et al., 1993).

Elsewhere within the Bohemian Massif of the Hercynides of Central Europe there are isotopic data indicating mid - late Devonian tectonothermal activity. Metamorphism at 370 ± 8 Ma (Rb - Sr, mineral - whole-rock) is reported from the Münchberg augen gneisses, NE Bavaria (SÖLLNER et al., 1981, see also STOSCH & LUGMAIR, 1990). Eclogitization of a tholeiitic protolith within gneisses in the Münchberg gneiss massif at 380 (+14/-22) Ma (U - Pb zircon) is

recorded by GEBAUER & GRÜNENFELDER (1979), while the K-Ar isotope data of KREUZER et al. (1989) for the northwestern margin of the Bohemian Massif (Münchberg upper nappes and Erbendorf-Vohenstrauss zone) could indicate thermal activity at *c.* 380 Ma. However, whether these data represent cooling ages from amphibolite facies metamorphism or a partial resetting of an older K - Ar system is not clear. A 380 Ma (U - Pb, monazite) age reported from a paragneiss in the Erbendorf-Vohenstauss zone also indicates a metamorphic overprint there in mid-Devonian times (TEUFEL, 1988). KRÖNER et al. (1988) interpret U - Pb zircon lower intercept ages of 367 (+18/-20) and 347 (+9/-10) Ma in metasedimentary Moldanubian assemblages of southern Bohemia and western Moravia, respectively, as indicative of Hercynian activity while VAN BREEMEN et al. (1988) give 381 ± 2 (U - Pb, monazite) and 370 - 360 Ma (Rb - Sr, biotite - whole rock) ages of amphibolite facies metamorphism and cooling to greenschist facies metamorphism temperatures, respectively, from the Sowie Góry gneisses, SW Poland. Sm - Nd mineral - whole rock ages of 370 ± 15, 373 ± 7, 379 ± 9 and 377 ± 20 Ma for eclogite facies metamorphism in the Moldanubian zone in Moravia and Lower Austria (garnet pyroxenites) and in western and eastern Bohemia (eclogites), respectively, are reported by CARSWELL & JAMTWEIT (1990), BRUECKNER et. al. (1991), BEARD et al. (1991) and BEARD et al. (1992).

The spatial and temporal relations of the events to which these dates correspond have yet to be determined and any possible links with the emplacement of the protolith of the Staré Sedlo and Mirotice gneisses have still to be established. However the data presented here clearly indicate that tonalitic - granodioritic plutonism took place in mid - late Devonian times in at least part of the disparate assemblage now making up the Bohemian Massif.

6.5 Conclusions

1. An upper intercept U - Pb zircon age of 373 ± 5 Ma for the Staré Sedlo gneisses and upper intercept and $^{206}Pb/^{204}Pb$ vs $^{207}Pb/^{204}Pb$ isochron ages of 369 ± 4 and 375 ± 5 Ma, respectively, for zircon populations from both the Staré Sedlo and Mirotice gneisses indicate a crystallization age of the plutonic protolith in the range of 380 - 365 Ma (mid - late Devonian).

2. The common occurrence of oscillatory zoning present in zircons is consistent with an igneous crystallization.

3. Some zircons from both complexes contain primary crystallized cores and late overgrowths but because of their small proportions, they are unlikely to have had a significant influence upon the U-Pb isotopic system.

4. Fracturing of zircons and leaching along the cracks mainly during the ductile deformation of the gneiss protolith resulted in only a small loss of Pb.

Acknowledgements

We thank Peter Ainsworth, John Ball, Donald Herd, Emil Jelínek, Julian Jocelyn, Bruce Paterson and Ed Stephens for their assistance and B.T. Hansen and an anonymous referee for their helpful comments.

6.6 References

ALLÈGRE, C.J., ALBARÈDE, F., GRÜNENFELDER, M., KÖPPEL, V. (1974): $^{238}U/^{206}Pb$ - $^{235}U/^{207}Pb$ - $^{232}Th/^{208}Pb$ zircon geochronology in alpine and non-alpine environment.- Contrib. Mineral. Petrol., **43**, 163-194.

BEARD, B.L., MEDARIS, L.G., JOHNSON, C.M., MÍSAŘ, Z. & JELÍNEK, E. (1991): Nd and Sr isotope geochemistry of Moldanubian eclogites and garnet peridotites, Bohemian massif, Czechoslovakia.- Terra Abstracts, **6**, 4.

BEARD, B.L., MEDARIS, L.G., JOHNSON, C.M., BRUECKNER, H.K. & MÍSAŘ, Z. (1992): Petrogenesis of Variscian high-temperature group A eclogites from the Moldanubian Zone of the Bohemian Massif, Czechoslovakia.- Contrib. Mineral. Petrol., **111**, 468-483.

BRUECKNER, H.K., MEDARIS, L.G. & BAKUN-CZUBAROW, N. (1991): Nd and Sr age and isotope patterns from Variscian eclogites of the eastern Bohemian Massif.- N. Jb. Miner. Abh., **163**, 169-196.

CARSWELL, D.A. & JAMTWEIT, B (1990): Variscian Sm-Nd ages for the high-pressure metamorphism in the Moldanubian Zone of the Bohemian Massif, Lower Austria.- N. Jb. Miner. Abh., **162**, 69-78.

CHLUPÁČ, I. (1981): Stratigraphy and facial evolution of metamorphosed Palaeozoic in the Sedlčany-Krásná Hora metamorphic islet (in Czech).- Věst. Ústř. Úst. Geol., **56**, 225-232.

CHLUPÁČ, I. (1989): Stratigraphy of the Sedlcany-Krásná Hora metamorphic islet in Bohemia (Proterozoic? to Devonian).- Čas. Mineral. Geol., **34**, 1-16.

DRAKE, M.J. & WEILL, D.F. (1972): New rare earth element standards for electron microprobe analysis.- Chem. Geol., **10**, 179-181.

DUNNING, G.R. & KROGH, T.E. (1985): Geochronology of ophiolites of the Newfoundland Appalachian.- Can. J. Earth Sci., **22**, 1659-1670.

GEBAUER, D. & GRÜNENFELDER, M. (1979): U-Pb zircon and Rb-Sr dating of eclogites and their country rocks. Example: Münchberg gneiss massif, Northeast Bavaria.- Earth Planet. Sci. Lett., **42**, 35-44.

HAUGERUD, R.A., VAN DER HEYDEN, P., TABOR, R.W., STACEY, J.S. & ZARTMAN, R.E. (1991): Late Cretaceous and early Tertiary plutonism and deformation in the Skagit Gneiss Complex, North Cascade Range, Washington and British Columbia.- Geol. Soc. Am. Bul., **103**, 1297-1307.

JAFFEY, A.H., FLYNN, K.F., GLENDENIN, L.E., BENTLEY, W.C. & ESSING, A.M. (1971): Precision measurement of half-lives and specific activities of ^{235}U and ^{238}U.- Phys. Rev. C**4**, 1889-1906.

KETTNER, R. (1930a): The position of metamorphic islets within the Central Bohemian Granitic Massif (in Czech).- Sbor. Stát. Geol. Úst. Čs. rep., **9**, 301-332.

KETTNER, R. (1930b): Geology of the Central Bohemian Granitic Massif (in Czech).- Příroda , **23**, 431-437.

KOŠLER, J., ROGERS, G. & BOWES, D.R. (1993): Rb-Sr isotopic evidence for early Carboniferous ductile deformation in the Hercynides of the southern part of the Bohemian Massif, Czech Republic.- MS submitted for publication.

KREUZER, H., SEIDEL, E., SCHUSSLER, U., OKRUSCH, M., LENZ, K.L. & RASCHKA, H. (1989): K-Ar geochronology of different tectonic units at the northwestern margin of the Bohemian Massif.- Tectonophysics, **157**, 149-178.

KROGH, T.E. (1973): A low contamination method for hydrothermal decomposition of zircon and extraction of U and Pb for isotopic age determinations.- Geochim. Cosmochim. Acta, **37**, 485-494.

KRÖNER, A., WENDT, I., LIEW,T.C., COMPSTON, W., TODT, W., FIALA, J., VAŇKOVÁ, V., VANĚK, J. (1988): U - Pb zircon and Sm - Nd model ages of high-grade Moldanubian metasediments, Bohemian Massif, Czechoslovakia.- Contrib. Mineral. Petrol., **99**, 257-266.

LLOYD, G.E. (1987): Atomic number and crystallographic contrast images with the SEM: a review of backscattered electron techniques.- Mineral. Mag., **51**, 3-19.

PATERSON, B.A., STEPHENS, W.E., & HERD, D.A. (1989): Zoning in granitoid accessory minerals as revealed by backscattered electron imagery.- Mineral. Mag., **53**, 55-61.

PATERSON, B.A., STEPHENS, W.E., ROGERS, G., WILLIAMS, I.S., HINTON, R.W. & HERD, D.A. (1992): The nature of zircon inheritance in two granite plutons.- Trans. R. Soc. Edinburgh Earth Sci., **83**, 459-471.

PIDGEON, R.T. (1992): Recrystallization of oscillatory zoned zircon: some geochronological and petrological implications.- Contrib. Mineral. Petrol., **110**, 463-472.

PUPIN, J.P. (1980): Zircon and granite petrology.- Contrib. Mineral. Petrol., **73**, 207-220.

ROMANS, P.A., BROWN, L.L. & WHITE, J.C. (1975): An electron microprobe study of yttrium, rare earth and phosphorus distribution in zoned and ordinary zircon.- Am. Mineral., **60**, 475-480.

SÖLNER, F., KÖHLER, H. & MÜHLER-SOHNIUS, D. (1981): Rb-Sr dating of rocks from the Münchberg Gneiss Massif (MM), NE Bavaria (Germany)-part 2, mineral dating (in German).- N. Jb. Miner. Abh., **142**, 178-198.

STOSCH, H.G. & LUGMAIR, G.W. (1990): Geochemistry and evolution of MORB-type eclogites from the Münchberg Massif, southern Germany.- Earth Planet. Sci. Lett., **99**, 230-249.

SUK, M. (1973): Reconstruction of the mantle of the Central Bohemian Pluton.- Čas. Mineral. Geol., **18**, 345-364.

TEUFEL, S. (1988): Comparative U-Pb and Rb-Sr age determinations on rocks of the Saxothuringian/Moldanubian transition zone, NE Bavaria (in German).- Göttinger Arb. Geol. Paläont., **35**, 1-87.

VAN BREEMEN, O., AFTALION, M., BOWES, D.R., DUDEK, A., MÍSAŘ, Z., POVONDRA, P. & VRÁNA, S. (1982): Geochronological studies of the Bohemian Massif, Czechoslovakia, and their significance in the evolution of Central Europe.- Trans. R. Soc. Edinburgh Earth Sci., **73**, 89-108.

VAN BREEMEN, O., BOWES, D.R., AFTALION, M. & ŻELAŹNIEVICZ, A. (1988): Devonian tectonothermal activity in the Sowie Góry gneissic block, Sudetes, southwestern Poland: evidence from Rb-Sr and U-Pb isotopic studies.- Ann. Soc. Geol. Polon., **58**, 3-19.

VINOKUROV, V.M., GAINULLINA, N.M., EVGRAFOVA, L.A., NIZAMUTDINOV, N.M. & SUSLINA, A.N. (1971): Zr^{4+}-Y^{3+} isomorphism in zircon and associated charge compensation.- Soviet Physics Crystallography, **16**, 262-265.

WATSON, B.E. & HARRISON M.T. (1983): Zircon saturation revisited: temperature and composition effects in a variety of crustal magma types.- Earth Planet. Sci. Lett., **64**, 295-304.

WAYNE, D.M., & SINHA, K.A. (1988): Physical response of zircons to deformation.- Contrib. Mineral. Petrol., **98**, 109-121.

WAYNE, D.M., & SINHA, K.A. (1992): Stability of zircon U-Pb systematics in a greenschist-grade mylonite from the Rockfish Valley Fault Zone, Central Virginia, USA.- J. Geol., **100**, 593-603.

YORK, D. (1969): Least squares fitting of a straight line with correlated errors.- Earth Planet. Sci. Lett., **5**, 320-324.

Manuscript received by the editor December 16, 1992; ready for publication March 8, 1993.

Authors' addresses:

J. KOŠLER, Department of Geology and Applied Geology, University of Glasgow

Glasgow G12 8QQ, Scotland.

M. AFTALION, Isotope Geology Unit, Scottish Universities Research and Reactor

Centre, East Kilbride, Glasgow G75 0QU, Scotland.

D.R. BOWES, Department of Geology and Applied Geology, University of Glasgow,

Glasgow G12 8QQ, Scotland.

Table 6.1. U-Pb isotopic data and model ages for zircons from amphibole-biotite orthogneisses of the Staré Sedlo and Mirotice gneiss complexes, southern Bohemia.

Size fractions (nm)	Pb (p.p.m.)	U (p.p.m.)	$\frac{^{206}Pb}{^{204}Pb}$	Atom percent radiogenic lead			Atomic ratios			Apparent ages (Ma)		
				^{206}Pb	^{207}Pb	^{208}Pb	$\frac{^{207}Pb}{^{206}Pb}$	$\frac{^{207}Pb}{^{235}U}$	$\frac{^{206}Pb}{^{238}U}$	$\frac{^{207}Pb}{^{206}Pb}$	$\frac{^{207}Pb}{^{235}U}$	$\frac{^{206}Pb}{^{238}U}$
Staré Sedlo gneiss complex (RC 2274)												
+85 NM 2°	32.3	623	2855	83.3079	4.5044	12.1878	0.054069	0.37437	0.050214	374	322	316
-85+65 NM 2°	27.8	488	3897	83.4512	4.5111	12.0377	0.054057	0.41157	0.055216	373	350	346
-65 +53 NM 2°	43.5	772	5134	83.4213	4.5037	12.0750	0.053988	0.40725	0.054706	370	347	343
Mirotice gneiss complex (RC 2284)												
+100 NM 2°	35.5	632	1115	81.3739	4.3815	14.2446	0.053844	0.39367	0.053024	365	337	333
-85+65 NM 2°	41.3	731	2420	81.6896	4.4057	13.9048	0.053932	0.39831	0.053561	368	340	336
-53 NM 2°	46.0	817	2572	81.0325	4.3565	14.6110	0.053762	0.39290	0.053000	361	336	333

RC 2274 and RC 2284 correspond to the catalogue numbers of the Isotope Geology Unit, Scottish Universities Research and Reactor Centre, East Kilbride.

Table 6.2. Pb - Pb isochron for zircons from the Staré Sedlo and Mirotice gneiss complexes.

Size fraction (nm)	$^{206}Pb/^{204}Pb$	$^{207}Pb/^{206}Pb$	$^{207}Pb/^{204}Pb$
		Staré Sedlo gneiss complex (RC 2274)	
+85 NM 2°	2855	0.059194	168.9989
-85+65 NM 2°	3897	0.057812	225.2933
-65+53 NM 2°	5134	0.056838	291.8063
		Mirotice gneiss complex (RC 2284)	
+100 NM 2°	1115	0.066970	74.6716
-85+65 NM 2°	2420	0.059979	145.1492
-53 NM 2°	2575	0.059453	153.0915

Isochron: 6 points, slope: 0.054101, correlation factor: 0.999984, corresponding age: 375 ± 5 Ma.

Table 6.3. Electron microprobe analyses of zircons from the Staré Sedlo and Mirotice gneiss complexes.

Analysis	1	2	3	4	5	6	7	8	9	10	11	12	13
SiO_2	31.29	31.15	32.02	32.50	32.94	33.24	34.22	33.17	32.88	32.09	33.25	32.73	32.51
ZrO_2	63.30	63.77	61.16	64.32	65.59	65.32	67.79	65.85	65.75	65.03	66.27	63.85	65.31
HfO_2	2.27	2.44	4.19	2.29	2.12	1.88	2.62	2.78	2.34	2.40	2.33	2.14	2.24
Y_2O_3	0.31	0.07	0.50	0.11	b.d.l.	0.07	b.d.l.	b.d.l.	0.29	0.10	b.d.l.	1.07	0.07
UO_2	0.12	0.04	1.33	0.05	b.d.l.	0.07	b.d.l.	b.d.l.	0.12	b.d.l.	0.36	0.09	b.d.l.
Yb_2O_3	0.11	b.d.l.	0.27	b.d.l.	b.d.l.	0.04	0.03	b.d.l.	0.12	b.d.l.	0.06	0.09	0.04
Suma	97.40	97.47	99.47	99.27	100.65	100.62	104.66	101.80	101.50	99.62	102.27	99.97	100.17
Zr/Hf	24.34	22.82	12.74	24.52	27.01	30.33	22.59	20.68	24.53	23.66	24.83	26.05	25.45

Values are in wt%. Numbers of analyses correspond to the numbers in Figure 6.3. Analysis number 12 includes 0.38 wt% of Nd_2O_3.

Analyses 1-4 are from zircons of the Staré Sedlo complex orthogneisses (RC 2274), analyses 5-13 are from zircons of the Mirotice complex orthogneisses (RC 2284).

b.d.l. - below detection limit

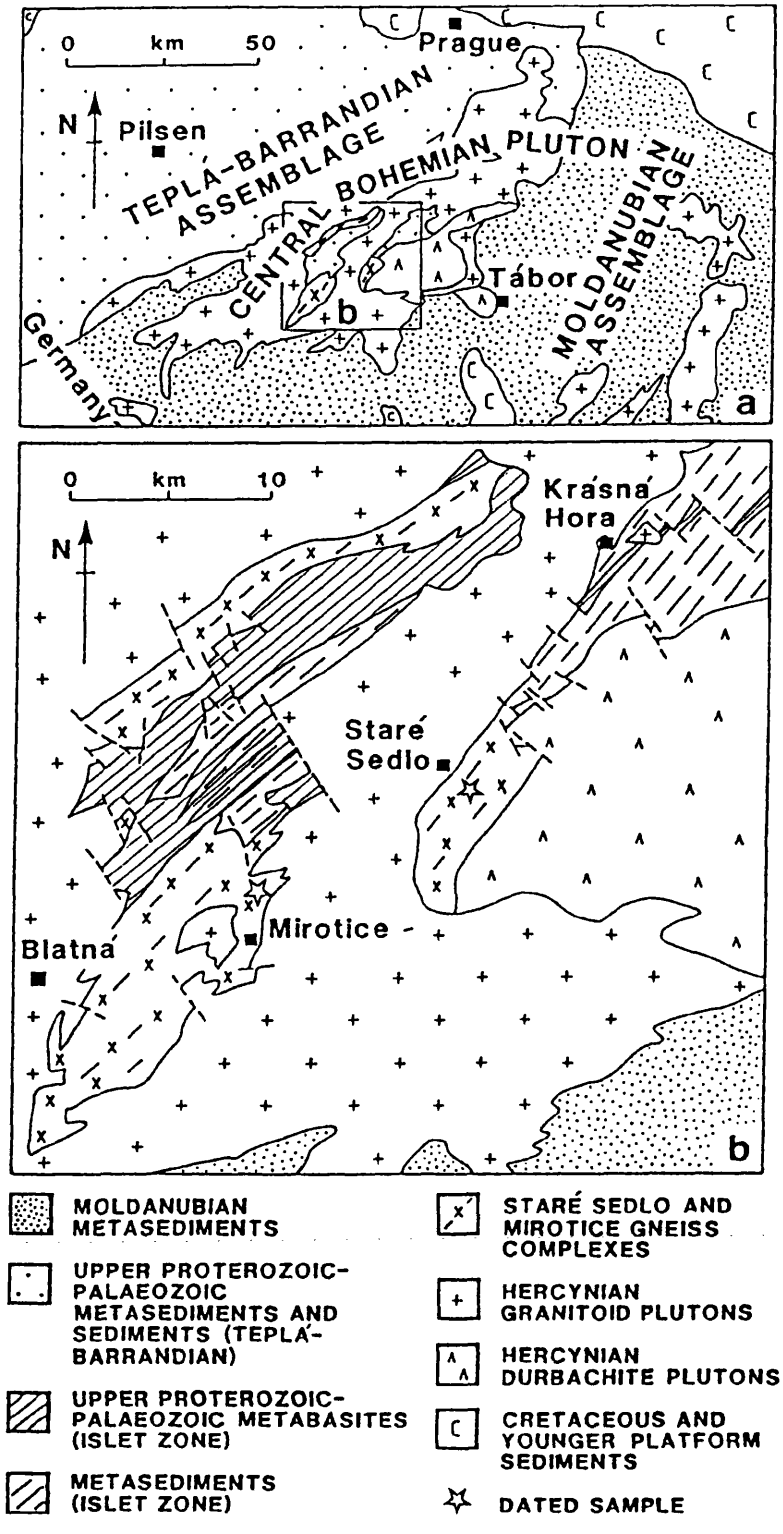

Fig.6.1

(a) Distribution of major units within the Czech part of the Bohemian Massif; based on 1:500 000 map of Czech Geological Survey.

(b) Outline geological map of the Staré Sedlo and Mirotice complexes with the locations of dated samples; based on 1:200 000 map of Czech Geological Survey.

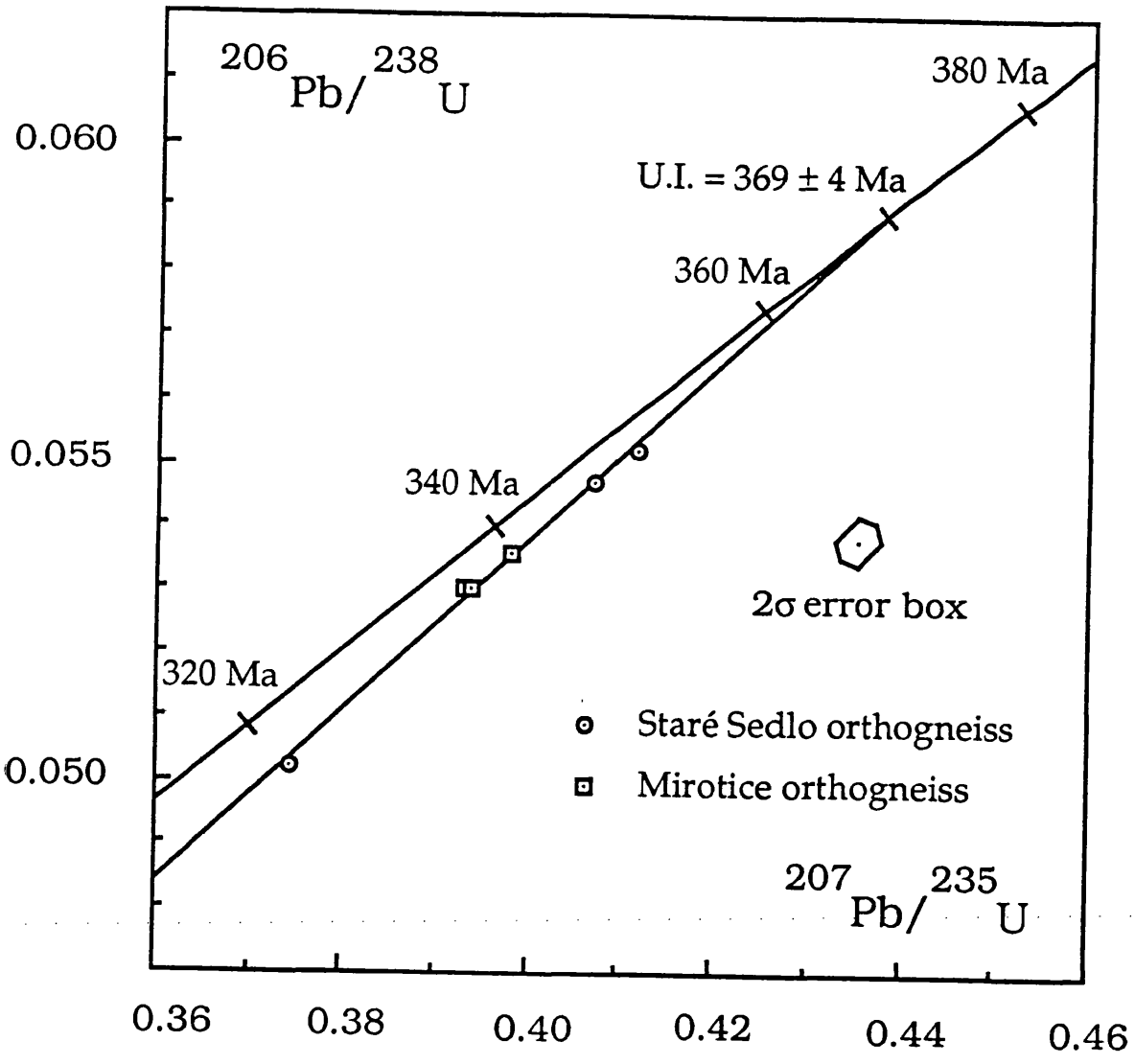

Fig.6.2

U - Pb concordia diagram for zircon fractions from gneisses from the Staré Sedlo and Mirotice complexes, Czech Republic.

Fig.6.3

BSE images of zircon grains from gneisses from the Staré Sedlo (RC 2274) and Mirotice (RC 2284) complexes.

(a) Oscillatory zoning (RC 2274); x 640.

(b) Primary crystallized core (RC 2274); x 640.

(c) Overgrowth (RC 2284); x 340.

(d) Alteration along cracks (RC 2284); x 200.

(e) Unzoned irregular patches (RC 2284); x 200.

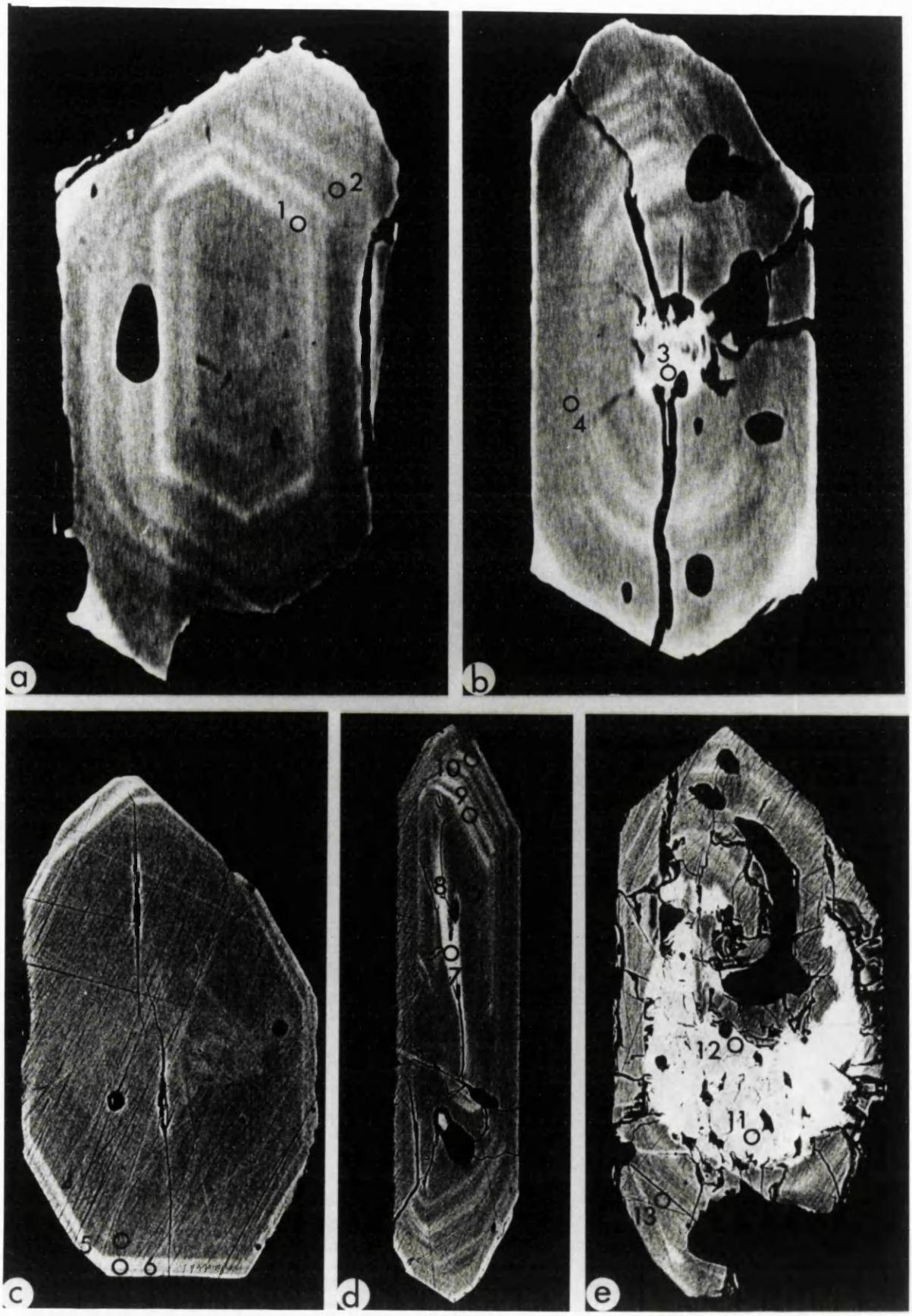
1
2
3
4
5
6
7
8
9
10
11
12
13
a
b
c
d
e

7. Rb - Sr MINERAL - WHOLE-ROCK ISOTOPIC STUDY OF GNEISSES FROM THE STARÉ SEDLO COMPLEX

This chapter has been submitted as a paper for publication in Geological Magazine. Accordingly its format corresponds to that required by the journal but the numbering of the headings, tables and figures is consistent with the thesis and some of the information which has already been given earlier in this study is repeated here, particularly in the introductory part. The references given at the end of this chapter are incorporated in the main reference list at the end of this thesis. Other possible interpretations of presented data and error calculations are discussed in Addendum at the end of this chapter.

Rb - Sr isotopic evidence for early Carboniferous ductile deformation in the Hercynides of the southern part of the Bohemian Massif, Czech Republic

J. KOŠLER*, G. ROGERS+ & D.R. BOWES*

* Department of Geology and Applied Geology, University of Glasgow, Glasgow G12 8QQ, Scotland, U.K.

+ Isotope Geology Unit, Scottish Universities Research and Reactor Centre, East Kilbride, Glasgow G75 0QU, Scotland, U.K.

Abstract

Biotite - plagioclase - whole-rock isotopic data give an early Carboniferous age of mylonitic foliation development in the Staré Sedlo gneisses whose tonalitic protolith crystallized in mid - late Devonian times. The ages of 338 ± 2.5, 335 ± 2 and 331 ± 2.5 Ma are interpreted as representing the closure of the Rb - Sr system in biotite and to indicate the times of the final stages of ductile deformation and metamorphism in different parts of a thrust regime. Low whole-rock $(^{87}Sr/^{86}Sr)_{373}$ ratios confirm the short previous crustal history of the Staré Sedlo gneisses.

7.1. Introduction

Within the Central Bohemian Pluton of the Bohemian Massif in the eastern Hercynides there are metamorphic complexes with the gross form of roof pendants, some of which consist of strongly foliated mylonitic biotite- and amphibole-bearing gneisses (Fig.7.1). The mineralogical and chemical compositions of these gneisses that make up the Staré Sedlo and Mirotice complexes (Fig.7.1b) are consistent with their having an igneous protolith (they have been referred to as orthogneisses or metatonalites, e.g. Waldhausrová, 1986) for which a mid - late Devonian crystallization age (c. 370 Ma) has been determined using U - Pb and Pb - Pb zircon isotopic data (Košler *et al.*, 1993). Both regionally, and as seen in outcrop, the gneissic foliation is discordant to the margins of igneous granitoid complexes of the Central Bohemian Pluton that bound the metamorphic complexes. As the Blatná granodiorite of this composite pluton was emplaced at 331 ± 4 Ma (Rb - Sr whole-rock; van Breemen *et al.*, 1982), the development of the metamorphic fabric must have been between c. 370 (mid - late Devonian) and c. 330 Ma (early Carboniferous).

In order to determine the age of metamorphic recrystallization, and in so doing the age of ductile deformation, a biotite - plagioclase - whole-rock Rb - Sr isotopic study was carried out on gneisses from the Staré Sedlo complex. In these gneisses the prominent foliation is mylonitic and augen (porphyroclasts) of plagioclase and K-feldspar are common (Fig.7.2). Some of the plagioclase feldspars show oscillatory zoning, which is interpreted as being a relict igneous feature like the oscillatory zoning in the dated zircons. The intensely foliated matrix consists largely of strongly dimensionally oriented biotite and amphibole, together with plagioclase and K-feldspar and a smaller proportion of flattened quartz showing undulose extinction. Mortar textures are shown by both quartz and the feldspars along porphyroclast boundaries. The presence of bent feldspars and biotite flakes showing kink-banding indicates that conditions approaching those near the ductile - brittle deformation boundary pertained during the later stages of deformation following a decline in temperature. However the dominant fabric represents the product of ductile deformation.

7.2. Sampling and analytical techniques

The paucity of outcrops and the very limited variation in Rb/Sr ratio precluded the collection of a suite of specimens from which a well-constrained whole-rock isochron could be derived. Accordingly three 40 - 50 kg samples were taken for a mineral - whole-rock study (for sample locations see Fig.7.1b). Biotite and plagioclase were separated from the rocks using a Frantz isodynamic separator, heavy liquids and sieving (in the case of biotite). Checks of the purity of the mineral fractions were carried out using XRD methods. Rb and Sr were separated from the whole-rock powders and mineral separates using the standard cation exchange techniques after acid decomposition in Savillex® PFA digestion vessels. The isotopic ratios were measured on VG MM30 (Rb) and VG 54E (Sr) thermal ionization mass spectrometers using the isotope dilution method. Sr isotopic ratios were corrected for mass fractionation using $^{86}Sr/^{88}Sr = 0.1194$. Replicate analyses of NBS 987 give $^{87}Sr/^{86}Sr = 0.71028 \pm 3$ (2σ); analytical results are reported relative to NBS 987 $^{87}Sr/^{86}Sr = 0.71022$. All ages were calculated using the decay constants recommended by Steiger & Jäger (1977). The regression analysis is according to York (1969). For the isochron calculations the experimental 2σ errors were used for $^{87}Sr/^{86}Sr$ whereas for $^{87}Rb/^{86}Sr$ an overall 2σ error of 0.7% (based on the long term standard results) was employed. All errors on ages and initial $^{87}Sr/^{86}Sr$ ratios are quoted at the 2σ level.

7.3. Results

A summary of the analytical results is given in Table 7.1, and isochron diagrams are shown in Fig.7.3. The three biotite - plagioclase - whole-rock isochrons yield early Carboniferous ages of 338 ± 2.5, 335 ± 2 and 331 ± 2.5 Ma with initial $^{87}Sr/^{86}Sr$ ratios of 0.70493 ± 4, 0.70481 ± 3 and 0.70493 ± 3, respectively (Fig.7.3b). In effect these are only two point isochrons controlled by the biotite and whole-rock compositions as the plagioclase is very close to the whole-rock in both its $^{87}Rb/^{86}Sr$ and $^{87}Sr/^{86}Sr$ ratios (Fig.7.3a). As even a very small loss or gain of Rb or Sr in the biotite could cause a significant shift of the obtained age, the consistent nature of these results permits them to be related to the same event and to be linked to the time when the temperature dropped below the Rb - Sr biotite closure temperature (c. 300 °C - Jäger, 1979).

The regression analysis of the whole-rock data gives an age of 316 ± 46 Ma with an $^{87}Sr/^{86}Sr$ initial ratio of 0.7050 ± 4 and MSWD of 12.64. The $^{87}Sr/^{86}Sr$ ratios of whole-rock and plagioclase samples recalculated at 373 Ma (mid - late Devonian U - Pb zircon age of the crystallization of the Staré Sedlo gneisses protolith - Košler *et al.*, 1993) are within the range of 0.7045 - 0.7047 (Table 7.1), whereas those for biotite samples yield unrealistic values of 0.6949, 0.6432 and 0.6649, respectively. Such a pattern is consistent with Sr isotopic homogenization within the whole-rock system subsequent to initial crystallization, with biotites losing radiogenic Sr during this process. Assuming that the whole-rock Rb/Sr ratios did not change and that the $^{87}Sr/^{86}Sr$ ratios were not substantially reduced during the metamorphic event, the low calculated $(^{87}Sr/^{86}Sr)_{373}$ ratios of the whole-rocks indicate that the protolith of the gneisses did not have a long crustal history. The three whole-rock data points can only be considered to define an errorchron, but they do indicate that the whole-rock Rb - Sr system (for 40 - 50 kg samples) had been reset following igneous crystallization.

7.4. Discussion

The c. 340 - 330 Ma biotite cooling ages for the Staré Sedlo gneiss complex are considerably closer in time to the emplacement of the Central Bohemian Pluton than to the crystallization of the gneiss protolith. While the 338 ± 2.5 Ma age is outside the known age of the plutonic activity in this part of the Bohemian Massif, the 335 ± 2 and, particularly, the 331 ± 2.5 Ma Rb - Sr ages fall within the errors of the 331 ± 4 Ma (Rb - Sr whole-rock) age of Blatná granodiorite and therefore might be interpreted as reflecting re-equilibration related to heat from the Pluton. However at the present level of erosion the nearest plutonic mass to the dated gneiss samples is 1 km away, and the width of the contact zone has been reported to be within the range of 300 - 500 m (Suk, 1973). Accordingly the 331 and 335 as well as the 338 Ma ages are interpreted as representative of the time of an extended phase of ductile deformation during early Carboniferous times with the textural evidence indicative of decreasing temperature which is related to a considerable decrease in crustal depth associated with upward tectonic transport.

Further support for the ages representing the timing of ductile deformation is provided by regional considerations. There is evidence from the Bohemian Massif in southern Bohemia that the latter stage of granulite facies metamorphism at 338 ± 0.5 Ma (U - Pb zircon, monazite: Aftalion *et al.*, 1989)

was followed by movement of the granulites to higher crustal levels, associated with the tectonic emplacement into middle and upper crustal levels of eclogite and mantle-type peridotite (Vrána, 1989). Corresponding evidence for upward movement of eclogitic and peridotitic material from mantle depth in the Bohemian Massif is also recorded in NE Bavaria (O'Brien *et al.*, 1992). In Moravia 345 ± 5 Ma (U - Pb zircon) products of granulite facies metamorphism are intensely foliated with much blastomylonite development (van Breemen *et al.*, 1982); their juxtaposition with both mantle and crustal materials from different levels resulted from Hercynian thrusting (Hopgood & Bowes, 1987) to which van Breemen *et al.* (1982) assigned an age of 338 ± 3 Ma (U - Pb monazite). Accordingly, the phase of ductile deformation which produced the mylonitic fabric of the Staré Sedlo gneisses is linked to an apparently widely expressed early Carboniferous phase of thrust tectonism which followed the peak of metamorphism and preceded a major phase of granitoid emplacement. The concordant 333 ± 3 Ma (U - Pb xenotime) age for a quartz mylonite from a shear zone between the Moldanubian and Erbendorf - Vohenstrauss zones in Germany (Teufel, 1988) could date corresponding thrust tectonism there.

The present sub-horizontal disposition of the gneissic - mylonitic foliation in most of the Staré Sedlo and Mirotice complexes is consistent with development associated with thrusting. Elsewhere within the roof pendants of the Central Bohemian Pluton, both metavolcanic and metasedimentary units exhibit a foliation which in some places is mylonitic and which varies in its disposition from generally flat in the SE to steep in the NW, being usually parallel to the NE- to NNE-trending margins of these elongate bodies. In addition, in the country rock outside the pluton there is a NE-trending, and generally steeply-disposed, planar fabric that in parts is mylonitic and which represents ductile deformation due to simple shear (Rajlich, 1988; Rajlich *et al.*, 1988). This latter evidence suggests the presence of a NE- to NNE-trending sub-vertical lineament that was a significant factor in controlling the emplacement of at least some of the early Carboniferous granitoid masses of the composite pluton. The difference in its disposition to that of the sub-horizontal planar fabric in the Staré Sedlo gneisses can be explained on the basis of ramping, a common feature in major listric thrusts. Such thrusts generally have a staircase-like trajectory with long flats in ductile horizons and shorter ramps through competent units (cf. Elliott & Johnson, 1980, fig.10). Likewise variations in the intensity of foliation development in the roof pendants, from greenschist facies schists seen in the NE to the mylonitic gneisses present in the Staré Sedlo and Mirotice complexes in the SW, can be explained by the existence of zones of lower and higher

strain in rocks of varying competence, and, or, as the result of variable upward movement of different units, rather than by simple variations in temperature leading to a gradational change of metamorphic facies (cf. Suk, 1973; Waldhausrová, 1984).

A model of magmatic emplacement during and after the later stages of shear zone formation is consistent with the foliated and even mylonitic fabric of parts of some of the early intrusions of the Central Bohemian Pluton (Vrána & Cháb, 1981; Palivcová & Franke, 1982), and with the unfoliated nature of the later intrusions. It is also consistent with the evidence for the successive emplacement of plutonic masses in a NE-trending zone and with the overall tongue shape of the composite pluton proposed by Kettner (1930): the base of the elongate pluton corresponds to a major ramp (or series of ramps) with the upper tip curving over towards the SE where flats predominate over ramps. The emplacement mechanism is likely to have been similar to that described by Hutton *et al.* (1990) for an early Proterozoic granite intrusion into an active extensional shear zone while the juxtaposition of bodies of ductilely-deformed orthogneisses within younger undeformed granitoids is similar to that reported from the Mesozoic Skagit gneiss complex in Washington, U.S.A. and adjacent British Columbia, Canada (Haugerud *et al.*, 1991). There, too, the granitoids were intruded along a shear zone, relics of which are still preserved in the gneisses which form roof pendants to the pluton.

7.5. Conclusions

1. Foliation development associated with the ductile deformation and mylonitization during early Carboniferous times is recorded by 338 ± 2.5, 335 ± 2 and 331 ± 2.5 Ma Rb - Sr biotite - plagioclase - whole-rock isochrons which effectively represent the closing of Rb - Sr isotopic system in biotite in the Staré Sedlo gneiss complex in the southern part of the Bohemian Massif, Czech Republic.

2. Whole-rock Rb - Sr isotopic data for 3 samples only define an errorchron (316 ± 46 Ma), but they do indicate that the whole-rock Rb - Sr system (for 40 - 50 kg samples) had been reset.

3. Initial $^{87}Sr/^{86}Sr$ ratios of 0.70493 ± 4, 0.70481 ± 3 and 0.70493 ± 3 derived from the mineral - whole-rock isochrons and 0.7050 ± 4 initial ratio derived from the whole-rock errorchron indicate that the protolith of the Staré Sedlo gneisses had only a short crustal history before rehomogenization of the Rb -

Sr system. This is consistent with the mid - late Devonian crystallization age determined from U - Pb and Pb - Pb data and the early Carboniferous age for ductile deformation.

4. The generally sub-horizontal disposition of the mylonitic - gneissic fabric in the Staré Sedlo complex is interpreted as being on a flat within more ductile horizons in a major listric thrust zone with a staircase-like trajectory. The emplacement and gross shape of the Central Bohemian Pluton are interpreted as having been controlled by a steeply-disposed ramp (or several ramps) through more competent units, with the earlier intrusions of this composite body overlapping in time the later part of the phase of ductile deformation.

Acknowledgements. G. Bruce, S. Hall, D. Maclean and P. Park are thanked for technical assistance. The Isotope Geology Unit at the SURRC is funded by the Scottish Universities and NERC.

7.6.References

AFTALION, M., BOWES, D.R. & VRÁNA, S. 1989. Early Carboniferous U - Pb zircon age for garnetiferous, perpotassic granulites, Blanský les massif, Czechoslovakia. *Neues Jahrbuch für Mineralogie Monatshefte* **H.4**, 145-152.

ELLIOTT, D. & JOHNSON, M.R.W. 1980. Structural evolution in the northern part of the Moine thrust belt, NW Scotland. *Transactions of the Royal Society of Edinburgh: Earth Sciences* **71**, 69-96.

HAUGERUD, R.A., VAN DER HEYDEN, P., TABOR, R.W., STACEY, J.S. & ZARTMAN, R.E. 1991. Late Cretaceous and early Tertiary plutonism and deformation in the Skagit gneiss complex, North Cascade Range, Washington and British Columbia. *Geological Society of America Bulletin* **103**, 1297-1307.

HOPGOOD, A.M. & BOWES, D.R. 1987. Structural succession and tectonic history of the gneiss - amphibolite - granulite - mantle peridotite association near the eastern margin of the Moldanubian zone, Central European Hercynides. *Acta Universitatis Carolinae Geologica*, 51-88.

HUTTON, D.H.W., DEMPSTER, T.J., BROWN, P.E. & BECKER, S.D. 1990. A new mechanism of granite emplacement: intrusion in active extensional shear zones. *Nature* **343**, 452-455.

JÄGER, E. 1979. Introduction to geochronology. In *Lectures in isotope geology* (eds. E. Jäger and J.C. Hunziker), pp 1-12. Berlin, Heidelberg, New York: Springer.

KETTNER, R. 1930. The position of metamorphic islets within the Central Bohemian Granitic Mass. *Sborník Státního Geologického ústavu československé republiky* **9**, 301-322.

KOŠLER, J., AFTALION, M. & BOWES, D.R. 1993. Mid - late Devonian plutonic activity in the Bohemian Massif: U-Pb zircon isotopic evidence from the Staré Sedlo and Mirotice gneiss complexes, Czechoslovakia. *Neues Jahrbuch für Mineralogie Monatshefte*, in press.

O'BRIEN, P.J., RÖHR, C., OKRUSCH, M. & PATZAK, M. 1992. Eclogite facies relics and a multistage breakdown in metabasites of the KTB pilot hole, NE Bavaria: implications for the Variscian tectonometamorphic evolution of the NW Bohemian Massif. *Contributions to Mineralogy and Petrology* **112**, 261-278.

PALIVCOVÁ, M. & FRANKE, W. 1982. Shear zones in granitoids as a structural control of the development of leucodioritic bodies (Central Bohemian Pluton). *Krystalinikum* **16**, 755-786.

RAJLICH, P. 1988. Tectonics of the NW border of the Central Bohemian Pluton and the Variscian transpression of the Bohemicum block structure. *Sborník Geologických Věd Geology* **43**, 9-81.

RAJLICH, P., SCHULMANN, K. & SYNEK, J. 1988. Strain analysis on conglomerates from the Central Bohemian Shear Zone. *Krystalinikum* **19**, 119-134.

STEIGER, R.H. & JÄGER, E. 1977. Subcommission on geochronology: convention on the use of decay constants in geo- and cosmochronology. *Earth and Planetary Science Letters* **36**, 359-362.

SUK, M. 1973. Reconstruction of the mantle of the Central Bohemian Pluton. *Časopis pro Mineralogii a Geologii* **18**, 345-364.

TEUFEL, S. 1988. Vergleichende U - Pb- and Rb - Sr-Altersbestimmungen an Gesteinen des Übergangsbereiches Saxothuringikum/Moldanubikum, NE Bayern. *Göttinger Arbeiten zur Geologie und Paläontologie* **35**, 3-87.

VAN BREEMEN, O., AFTALION, M., BOWES, D.R., DUDEK, A., MÍSAŘ, Z., POVONDRA, P. & VRÁNA, S. 1982. Geochronological studies of the Bohemian massif, Czechoslovakia, and their significance in the evolution of Central Europe. *Transactions of the Royal Society of Edinburgh: Earth Sciences* **73**, 89-108.

VRÁNA, S. 1989. Perpotassic granulites from southern Bohemia - a new rock type derived from partial melting of crustal rocks under upper mantle conditions. *Contributions to Mineralogy and Petrology* **103**, 510-522.

VRÁNA, S. & CHÁB, J. 1981. Metatonalite - metaconglomerate relation: the problem of the upper Proterozoic sequence and its basement in the NE part of the Central Bohemian Pluton. *Sborník Geologických Věd Geology* **35**, 145-185.

WALDHAUSROVÁ, J. 1984. Proterozoic volcanites and intrusive rocks of the Jílové zone in Central Bohemia. *Krystalinikum* **17**, 77-97.

WALDHAUSROVÁ, J. ed. 1986. *1:25000 geological map of ČSSR: 22-232 Kostelec nad Vltavou: Comments.* pp. 1-62, Prague: Geological Survey.

YORK, D. 1969. Least squares fitting of a straight line with correlated errors. *Earth and Planetary Science Letters* **5**, 320-324.

Table 1. Rb - Sr data for amphibole - biotite orthogneisses from the Staré Sedlo complex

Sample	Rb (ppm)	Sr (ppm)	$^{87}Rb/^{86}Sr$	$^{87}Sr/^{86}Sr \pm 2\sigma$	$(^{87}Sr/^{86}Sr)_{373}$
			Sample 1 (age 338 ± 2.5 Ma)		
Bi-1	408.2	59.6	19.9971	0.80107±5	0.6949
Plg-1	31.5	389.3	0.2339	0.70605±5	0.7048
WR-1	75.8	422.7	0.5191	0.70742±4	0.7047
			Sample 2 (age 335 ± 2 Ma)		
Bi-2	543.2	14.6	113.0217	1.24338±10	0.6432
Plg-2	48.7	463.0	0.3040	0.70627±4	0.7047
WR-2	86.6	365.5	0.6856	0.70807±4	0.7045
			Sample 3 (age 331 ± 2.5 Ma)		
Bi-3	342.6	15.3	66.6516	1.01884±13	0.6649
Plg-3	24.5	378.8	0.1873	0.70582±4	0.7048
WR-3	47.1	431.3	0.3159	0.70641±5	0.7047

Note: ages calculated from biotite - plagioclase - whole-rock regression.

7.7 Addendum to Chapter 7

The Rb - Sr ages calculated for biotite - whole-rock pairs are within the errors of ages calculated from biotite - plagioclase - whole-rock and so are also the ages for biotite - plagioclase pairs (which may be interpreted as the age of Sr equilibration of this mineral pair only in the case if the Rb - Sr system in biotite remained closed, or did not substantially change after the Rb - Sr closure in plagioclase). The corresponding biotite - whole-rock, biotite - plagioclase and biotite - plagioclase - whole-rock ages suggest the slope of the respective isochrons is effectively controlled by the composition of biotite and

hence the ages obtained represent biotite cooling ages. While the biotite - whole-rock and biotite - plagioclase ages for two samples of the Lašovice gneiss (LG-A and LG-B, cf. Chapter 8) are 318 ± 2, 318 ± 2 and 324 ± 2, 323 ± 2, respectively, the ages of 316 ± 11 and 324 ± 92 Ma were calculated from the biotite - plagioclase - whole-rock data. In the latter the unrealistically large errors represent the artefact of isochron calculation (error magnification): in the case when the scatter of data is likely to be attributed to other than purely analytical factors (MSWD > 1, cf. Table 8.1), the errors on both the age and initial ratio are multiplied by the square root of MSWD value. Although this procedure has been proven useful for cases when data are dispersed regularly along the isochron (*Kullerud, 1991*), it may yield unrealistically high error estimation when used for calculation of mineral ages where the slope of the regression line is effectively controlled by a single point.

The evidence from Rb - Sr biotite cooling ages for cooling from ductile deformation of the protolith of the Staré Sedlo gneisses at ca 340 - 330 Ma is also supported by Rb - Sr biotite cooling age for one sample of Lašovice gneiss (339 ± 2.5 Ma, sample LG-C, cf. Chapter 8 and Table 8.1). However the biotite - plagioclase - whole-rock Rb - Sr data for other samples of the Lašovice gneiss (LG-A and LG-B) correspond to substantially lower ages of 316 ± 11 and 324 ± 92 Ma. The maximum biotite ages calculated for samples LG-A and LG-B (assuming the minimum $(^{87}Sr/^{86}Sr)_0$ of 0.710) are 320 and 324 Ma, respectively. Accordingly the ages obtained for Lašovice gneisses (LG-A and LG-B) are interpreted as resulting from a post 340 - 330 Ma disturbance of the Rb - Sr system in biotite. Such interpretation of the biotite - plagioclase - whole-rock data from both the Staré Sedlo and Mirotice gneisses assumes (1) the Rb - Sr isotopic system on the scale of whole-rock samples was homogenized during the ductile deformation and associated metamorphism before ca 340 - 330 Ma (for which the temperatures of ca 600 - 650 °C are reported in Chapter 5), (2) rapid cooling from ca 550 °C (closure temperature for Sr in plagioclase; *Giletti, 1991*) to ca 300 ± 50 °C (closure temperatures of the Rb - Sr system in biotite; *Jäger, 1979*) and (3) the Rb - Sr system in biotite, plagioclase and whole-rock samples of the Staré Sedlo gneisses and Lašovice gneiss (sample LG-C) remained closed after the 340 - 330 cooling episode.

The alternative explanations of the Rb - Sr data for samples LG-A and LG-B are (1) the Rb - Sr systems in biotite, plagioclase and whole-rock did not equilibrate during the cooling episode which followed the ductile deformation of the protolith of the gneisses and (2) cooling did not take place within a short time span. This however contradicts the evidences for temperatures of ca 600 - 650 °C during the metamorphism associated with ductile deformation of the protolith of the gneisses (cf. Chapter 5) and a quick uplift documented from other parts of Moldanubian zone in the Bohemian Massif (cf. Štelcl, 1960; Chapter 1). In addition, although the episode of ca 340 - 330 Ma cooling after ductile deformation corresponds to similar events elsewhere in the Moldanubian zone, the possibility of subsequent reheating of gneisses as a result of multiple intrusion of granitoids and durbachites of the Central Bohemian Pluton which followed and, or, overlapped the cooling episode after ductile deformation must be accounted for. However this problem cannot be properly addressed before the timing of individual intrusions is known with sufficient precision.

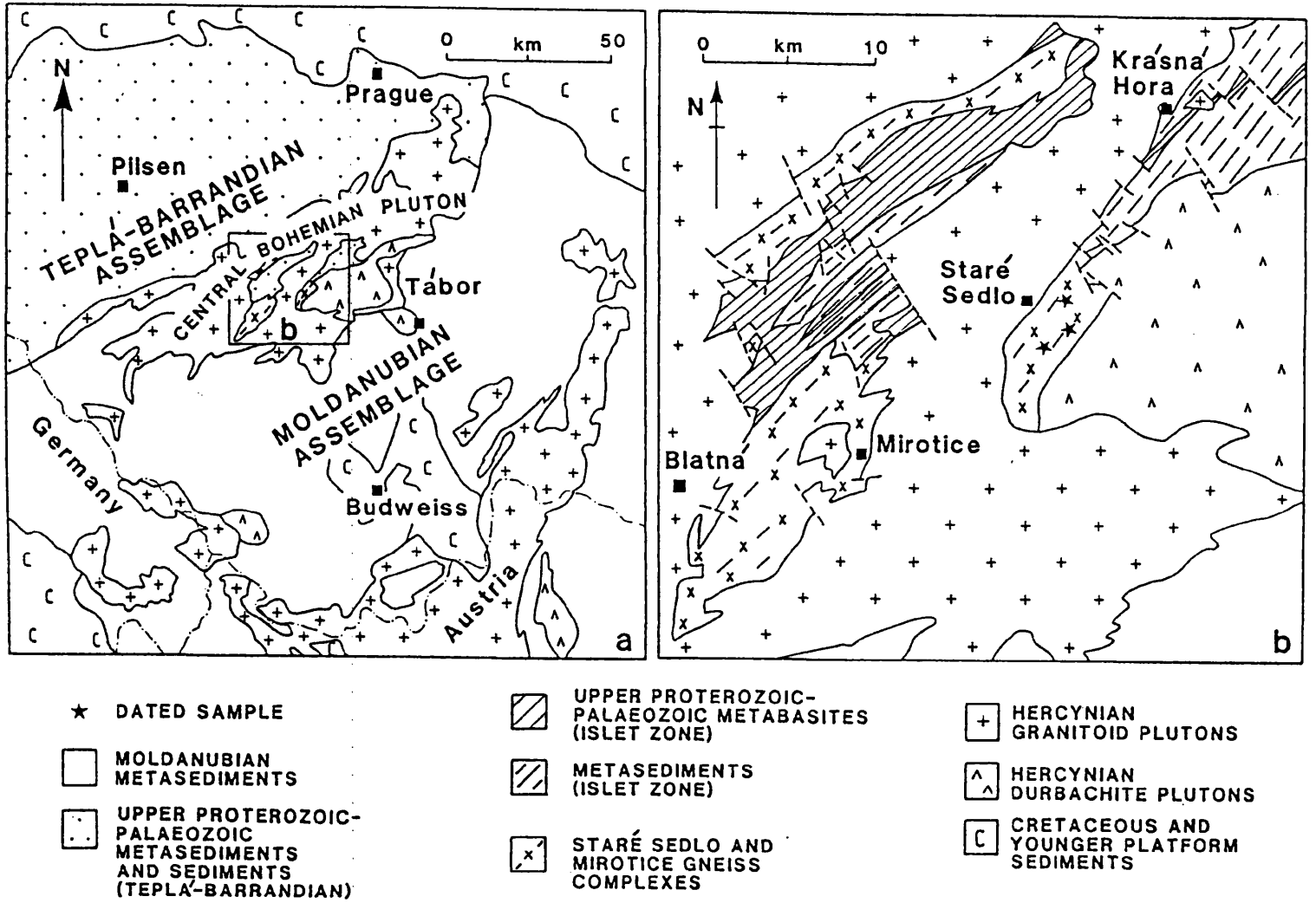

Fig.7.1

(a) Distribution of major units within the Czech part of the Bohemian Massif; based on 1:500 000 map of the Czech Geological Survey.

(b) Outline geological map of the Staré Sedlo and Mirotice complexes with the locations of dated samples; based on 1:200 000 map of the Czech Geological Survey.

Fig.7.2

Plagioclase porphyroclasts (augen) in the mylonitic matrix consisting of quartz, biotite, plagioclase and K-feldspar (x 12, PPL); biotite orthogneiss from the Staré Sedlo complex, southern Bohemia.

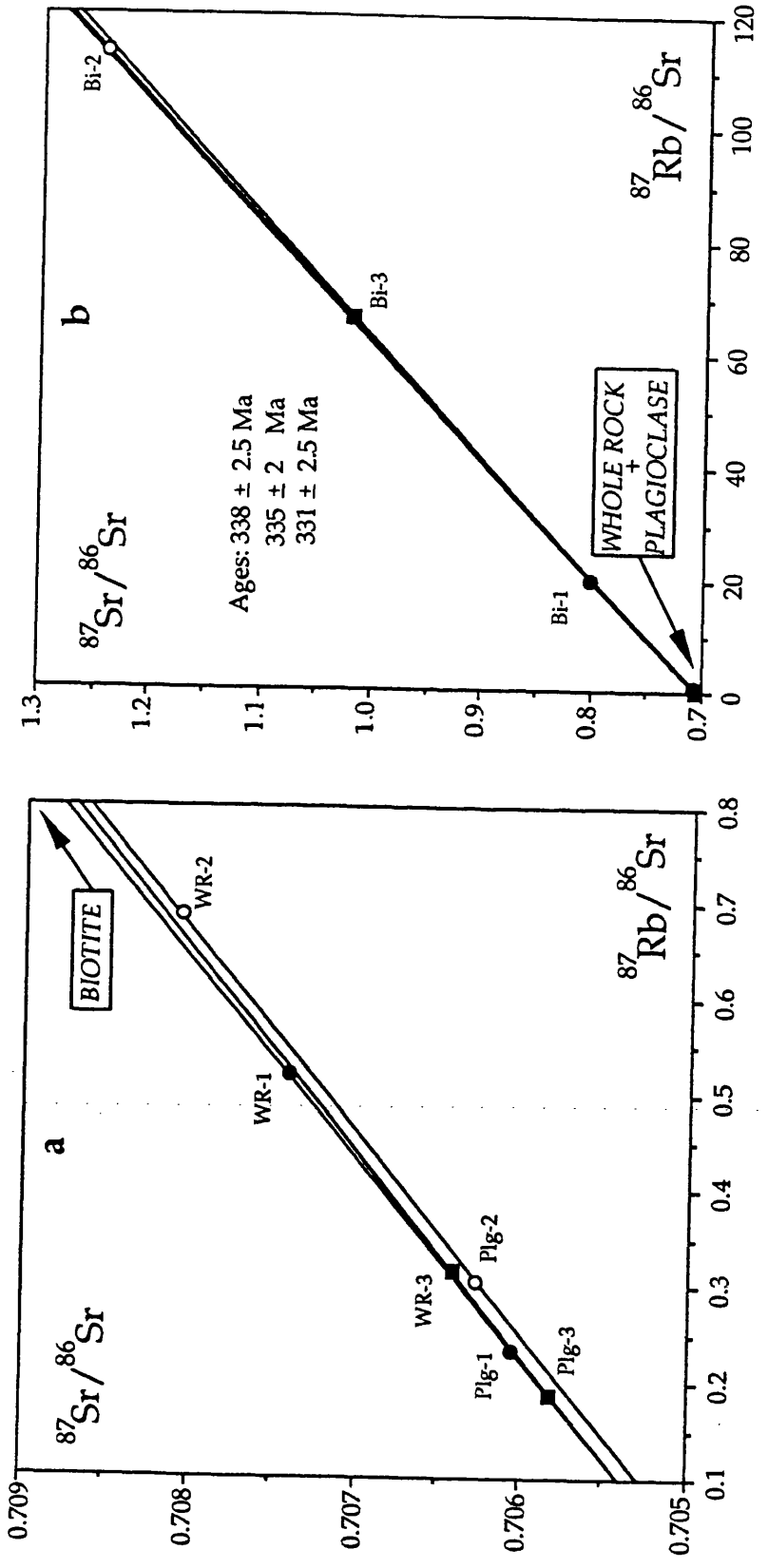

Fig.7.3

Rb - Sr biotite - plagioclase - whole-rock isochrons for three orthogneiss samples from the Staré Sedlo complex, southern Bohemia.

8. MAGMA PETROGENESIS

In order to determine the origin of the protolith(s) of gneisses and schists from the Staré Sedlo and Mirotice complexes, and also to shed more light on the processes responsible for variations in both their major and trace element compositions (cf. Chapter 4), Sr and Nd isotopic studies of the whole-rock samples from the main units of both complexes were carried out. These amplify, from a more extensive sample base, the evidence for the origin and magmatic evolution of the protolith(s) of the rocks of the complexes deduced from consideration of a limited number of $^{87}Sr/^{86}Sr$ initial ratios (see Chapter 7). Samples 1, 2 and 3 from Chapter 7 correspond to samples STG-A, STG-B and STG-C, respectively in this Chapter. Sampling and analytical procedures are described in Appendix 2. The regression analysis is according to *York (1969)* and the ^{87}Rb and ^{147}Sm decay constants are those recommended by *Steiger and Jäger (1977)*. All errors are quoted at the 2 sigma level. The recalculations and notations used for Sr and Nd isotopes are as follows.

1) Recalculation of measured (0) isotopic ratios at a given time (T):

$[^{87}Sr/^{86}Sr]_T = [^{87}Sr/^{86}Sr]_0 - [^{87}Rb/^{86}Sr]_0 * (e^{\lambda RbT} - 1)$

$[^{143}Nd/^{144}Nd]_T = [^{143}Nd/^{144}Nd]_0 - [^{147}Sm/^{144}Nd]_0 * (e^{\lambda SmT} - 1)$;

λRb and λSm are decay constants of ^{87}Rb and ^{147}Sm, respectively.

2) Epsilon values at a given time (T) relative to the uniform reservoir (Sr_{UR}) and chondritic uniform reservoir (Nd_{CHUR}):

$\varepsilon Sr_T = \{([^{87}Sr/^{86}Sr]sample_T / [^{87}Sr/^{86}Sr]UR_T) - 1\} * 10^4$

$\varepsilon Nd_T = \{([^{143}Nd/^{144}Nd]sample_T / [^{143}Nd/^{144}Nd]CHUR_T) - 1\} * 10^4$.

The values used for the present-day composition of the Sr uniform reservoir and the Nd chondritic uniform reservoir are those of *Jacobsen and Wasserburg (1980)*:

$[^{87}Sr/^{86}Sr]UR_0 = 0.7047$ $\qquad$ $[^{143}Nd/^{144}Nd]CHUR_0 = 0.512638$

$[^{87}Rb/^{86}Sr]UR_0 = 0.0847$ $\qquad$ $[^{147}Sm/^{144}Nd]CHUR_0 = 0.1967$.

3) Nd model ages calculated relative to chondritic uniform reservoir $T_{Nd(CHUR)}$ and depleted mantle $T_{Nd(DM)}$:

$T_{Nd(CHUR)} = \lambda Sm^{-1} * \ln \{1 + ([^{143}Nd/^{144}Nd]sample_0 - [^{143}Nd/^{144}Nd]CHUR_0)/ ([^{147}Sm/^{144}Nd]sample_0 - [^{147}Sm/^{144}Nd]CHUR_0)\}$

$T_{Nd(DM)} = \lambda Sm^{-1} * \ln \{1 + ([^{143}Nd/^{144}Nd]sample_0 - [^{143}Nd/^{144}Nd]DM_0)/([^{147}Sm/^{144}Nd]sample_0 - [^{147}Sm/^{144}Nd]DM_0)\}$.

The values used for the present-day isotopic composition of the depleted mantle are those of *Michard et al. (1985)*:

$[^{143}Nd/^{144}Nd]DM_0 = 0.513114$ $[^{147}Sm/^{144}Nd]DM_0 = 0.222$.

8.1 Sr and Nd isotopic systems

A summary of Rb - Sr and Sm - Nd analytical results for the whole-rock samples from the Staré Sedlo and Mirotice complexes as well as the Rb - Sr data for the biotite and plagioclase separates from the Staré Sedlo gneisses are given in Table 8.1. The measured $^{87}Sr/^{86}Sr$ whole-rock ratios show variations between the Staré Sedlo gneisses (0.7064 - 0.7081), Lašovice gneisses (0.7093 - 0.7190), Mirotice gneisses (0.7080 - 0.7081) and Mirotice schist (0.7122). Despite a considerable range of their Rb/Sr ratios (0.1 - 0.8) the nine whole-rock samples can only define an errorchron, the slope of which corresponds to an age of 377 ± 120 Ma with an initial ratio of 0.7043 ± 17 (Fig.8.1). The six biotite - plagioclase - whole-rock Rb - Sr isochrons yield early - late Carboniferous ages of 339 ± 2.5, 338 ± 2.5, 335 ± 2, 331 ± 2.5, 324 ± 92 and 316 ± 11 Ma, respectively. In effect these are only two point isochrons controlled by the biotite and whole-rock compositions as the plagioclase is very close to the whole-rock in both its $^{87}Rb/^{86}Sr$ and $^{87}Sr/^{86}Sr$ ratios (cf. Table 8.1). The consistent nature of four of these results permits them to be related to the same event and to be linked to the time when the temperature dropped below the Rb - Sr biotite closure temperature (ca 300 °C; *Jäger, 1979*). Accordingly these data are interpreted as indicating the times of the final stages of ductile deformation of the protolith of the gneisses at ca 340 - 330 Ma (cf. Chapter 7). The two regressions for biotite - plagioclase - whole-rock Rb - Sr data for samples LG-A and LG-B which yield the lowest and poorly defined ages of ca 324 and 316 Ma are interpreted as indicating the disturbance of the Rb - Sr system not only in plagioclase and biotite but also on the scale of ca 40 - 50 kg whole-rock samples. Such disturbance must have followed the ca 340 - 330 Ma phase of ductile deformation and associated metamorphism indicated by biotite cooling ages in most of the gneisses of the Staré Sedlo complex (cf. Chapter 7) and may be related to the late- and, or, post-magmatic activity in the adjacent Central Bohemian Pluton. Accordingly, these mineral

- whole-rock Rb - Sr ages are assessed as having no geological (chronological) significance. There is however an apparent correlation between the biotite - plagioclase - whole-rock ages and the corresponding measured $^{87}Sr/^{86}Sr$ whole-rock ratios: those regressions of mineral - whole-rock data from the Lašovice gneisses (samples LG-A and LG-B) which show the highest whole-rock $^{87}Sr/^{86}Sr$ ratios of 0.7190 and 0.7160 correspond to ages which are considerably lower and, or, poorly defined compared to most of the mineral - whole-rock ages from gneisses of the Staré Sedlo complex (ca 340 - 330 Ma). Although no mineral separates from the gneisses and schists from the Mirotice complex were analyzed for Rb and Sr isotopes, the high measured $^{87}Sr/^{86}Sr$ ratio of 0.7122 in one sample of schists (MIS-A) suggests similarities of Rb - Sr isotopic systems at least between some of the Mirotice schists and the Lašovice gneisses. The $^{87}Sr/^{86}Sr$ ratios of the whole-rock samples (excluding samples LG-A and LG-B which are indicative of a post 340 - 330 Ma disturbance of Rb - Sr system) recalculated at 369 Ma (mid - late Devonian age of crystallization of the protolith(s) of both the Staré Sedlo and Mirotice gneisses; cf. Chapter 6) are within the range of 0.7025 - 0.7075 which corresponds to the range of εSr_T values of -24.7 - +38. The whole-rock $^{87}Sr/^{86}Sr$ ratios of the Lašovice gneisses (samples LG-A and LG-B) recalculated at 330 Ma yield values of 0.7087 and 0.7049, which correspond to εSr_T values of +63.3 and +7.8, respectively. Corresponding ratios for samples LG-A and LG-B calculated at 369 Ma are 0.7075 and 0.7035 with εSr_T values of +46.7 and -10.2, respectively.

The whole-rock Sm - Nd data for samples from the Staré Sedlo and Mirotice complexes do not define an isochron (Fig. 8.2). The measured $^{143}Nd/^{144}Nd$ ratios in both the Staré Sedlo and Mirotice gneisses are consistent (0.51256 - 0.51257) but differ substantially from those in the Lašovice gneisses (0.51225 - 0.51226). The measured $^{143}Nd/^{144}Nd$ ratio in the sample of Mirotice schist (0.51252) is within the range of that determined for the Staré Sedlo and Mirotice gneisses. Recalculated $^{143}Nd/^{144}Nd$ ratios at 369 Ma show a similar pattern of consistent values for the Staré Sedlo gneisses, the Mirotice gneisses and the Mirotice schist (0.51299 - 0.51232) but all are considerably higher than those from the Lašovice gneisses (0.51196). The recalculated ratios correspond to εNd_T values of +2.6 - +3.1 and -4.0 - -4.1 for the Staré Sedlo gneisses, the Mirotice gneisses, the Mirotice schist and the Lašovice gneisses, respectively. Calculated $T_{Nd(DM)}$ model ages for the Staré Sedlo and Mirotice gneisses and the Mirotice schist (0.69 - 0.74 Ga) are considerably lower than those for the Lašovice gneisses (1.31 - 1.34 Ga, cf. Table 8.1).

Different valency of Rb^{+} and Sr^{2+} ions together with their different ionic radii (0.149 and 0.127 nm; *Zemann, 1966*), as well as the presence of radiogenic and non-radiogenic Sr in different sites of the crystal lattice and, or, in different minerals, result in decoupling of Rb and Sr during metamorphic process. Such a decoupling is even more pronounced when fluids are involved in metamorphic reactions (*Cliff, 1985*). In contrast Sm and Nd are more resistant and their decoupling during metamorphism (if it does not reach partial melting in the granulite facies) is considered to be negligible (cf. *McCulloch and Wasserburg, 1978; DePaolo, 1988*). Assuming that (1) only in some of the Lašovice gneisses (samples LG-A and LG-B) could the whole-rock Rb - Sr systems have been disturbed in response to the post-magmatic activity in the adjacent Central Bohemian Pluton (after ca 340 - 330 Ma) and (2) the whole-rock Rb/Sr and Sm/Nd ratios in samples of the Staré Sedlo gneisses and the Mirotice gneisses and schist and in other Lašovice gneisses (sample LG-C) were not substantially changed after the crystallization of their protolith(s), both the low $(^{87}Sr/^{86}Sr)_{369}$ and high $(^{143}Nd/^{144}Nd)_{369}$ ratios indicate that this protolith(s) was derived from material which could not have had a long, if any, crustal history (assuming the high Rb/Sr and low Sm/Nd ratios in the crust of the Moldanubian zone within the Bohemian Massif; cf. *Vidal et al., 1975; Gorokhov et al., 1979; Liew and Hofmann, 1988; Kröner et al., 1988*). The Lašovice gneiss samples LG-A and LG-B have relatively low $(^{87}Sr/^{86}Sr)_{330}$ ratios (0.7087 and 0.7049, respectively) which do not substantially differ from their $^{87}Sr/^{86}Sr$ ratios recalculated at 369 Ma (0.7075 and 0.7035, respectively). Although they overlap the $(^{87}Sr/^{86}Sr)_{369}$ ratios of other gneisses and schist from the Staré Sedlo and Mirotice complexes (0.7025 - 0.7075), they also differ from the $(^{87}Sr/^{86}Sr)_{369}$ ratio of 0.7069 for the other Lašovice gneiss sample (LG-C). Accordingly, the Rb - Sr systems in the Lašovice gneiss samples LG-A and LG-B must have been disturbed on the scale of whole-rock samples in response to a post 340 - 330 Ma event and their Rb/Sr ratios must have been changed.

In εNd_T vs εSr_T diagram (Fig.8.3) the Staré Sedlo and Mirotice gneisses and the Mirotice schist plot in the depleted field and their Sr and Nd isotopic compositions correspond to that of most modern oceanic island basalts and show affinities to some of the I-type Palaeozoic granitoids of SE Australia. In addition their Sr and Nd isotopic signature is similar to that of some high-temperature (HT) A-group eclogites from the Moldanubian zone in the Central European Hercynides which have transitional OIB - MORB isotopic signatures (*Beard et al., 1992*). This is consistent with the evidence from LIL and HFS trace element patterns (cf. Chapter 4) which suggests that OIB-like mantle-derived material was the main

source for the protolith(s) of most of the rocks of the Staré Sedlo and Mirotice complexes. The limited Sr and Nd isotopic data from Palaeozoic basalts (*Vokurka and Kober, 1992; Bendl et al., 1993*) also suggest an OIB-like isotopic composition of the upper mantle reservoir beneath the Moldanubian zone within the Bohemian Massif. Accordingly the isotopic results support the trace-element evidence for the existence of a continent-based magmatic arc in mid - late Devonian times in this part of Hercynides (cf. Chapter 4) where the contribution of subducted sedimentary material to the newly formed magma was very small (*Hawkesworth and Ellam, 1989*). In addition, the interpretation of the Sr and Nd depleted high-temperature eclogites of the Moldanubian zone as being derived from heterogeneous mantle (*Beard et al., 1992*), and the corresponding isotopic compositions of most of the gneisses and schist of the Staré Sedlo and Mirotice complexes, suggest a considerable contribution to the newly-formed magma of material from an overhanging mantle wedge in a continent-based arc system (cf. Chapter 4 and Fig.4.17). The evidence for a very small contribution of crustal material to the parent magma of the Staré Sedlo and Mirotice gneisses and schist(s) is also supported by distinctive crustal isotopic and chemical signatures of both sedimentary and metasedimentary rocks of the Moldanubian zone (*Liew and Hofmann, 1988*) as assimilation of only a small amount of such material would probably considerably change the isotopic composition of both Sr and Nd in the gneisses and schists (cf. Fig.8.1, samples LG-B and LG-C).

In order to illustrate the effect on the Nd isotopic composition of assimilation of crustal (sedimentary) material by primitive mantle-derived magma, the process is modelled using the simple binary mixing equation (*DePaolo, 1988*). Assuming that (1) the Nd isotopic composition of the mantle-derived parent magma of the gneisses and schists was similar to the Sr and Nd depleted HT eclogite from the Moldanubian zone in the Bohemian Massif (sample CZ-6E; Nd = 1.19 ppm, $(^{143}Nd/^{144}Nd)_{369}$ = 0.512461; *Beard et al., 1992*), and (2) the composition of the assimilated material was similar to that of the Moldanubian paragneiss (sample AA-1; Nd = 32.11 ppm, $(^{143}Nd/^{144}Nd)_{369}$ = 0.511519; *Kröner et al., 1988*), then assimilation of less than 1 wt% of paragneiss by magma of eclogite composition would result in a $^{143}Nd/^{144}Nd$ ratio corresponding to that of the Staré Sedlo and Mirotice gneisses and schist (samples STG-A, MIG-A, MIG-B, MIS-A; cf. Table 8.1).

In contrast to the samples of the Staré Sedlo and Mirotice gneisses and schist, the samples of the Lašovice gneiss have negative εNd_T and plot below the bulk earth composition on the εNd_T vs εSr_T diagram (Fig.8.3). They have essentially the same initial Nd isotopic compositions but show

considerable differences in the composition of Sr isotopes. Assuming a similar mantle source to the Staré Sedlo and Mirotice gneisses and schist, the negative εNd_T values indicate a contribution from crustal material (possibly sediments or their partial melts) to their parent magma and this is consistent with the major and trace element signature of at least some of the Lašovice gneisses (cf. Chapter 4). A calculation of mixing proportions similar to that used for the Staré Sedlo and Mirotice gneisses requires an assimilation of ca 4 wt% of Moldanubian paragneiss by magma of eclogite composition to account for the $^{143}Nd/^{144}Nd$ ratio of the Lašovice gneisses (samples LG-B and LG-C). The differences in the εSr_T values for samples LG-B and LG-C can be explained either on the basis of assimilation of material of different composition (i.e. the two samples lie on different mixing lines in the εNd_T vs εSr_T diagram), or on the basis of a shift in Sr isotopic composition in either of these rocks. However both the correspondence of εNd_T values and the scale of the outcrop (the Lašovice quarry is 300 x 200 x 15 m) suggest that the former can be ruled out. The differences in the εSr_T values may reflect the considerably lower plagioclase - biotite - whole-rock Rb - Sr ages (cf. Table 8.1) than for other gneisses from the Staré Sedlo complex (that for sample LG-A is 316 ± 11 Ma) and their poor definition (the error for LG-B is ± 92 Ma). These features are interpreted as the result of disturbance of the Rb - Sr system which must have followed the c. 340 - 330 Ma phase of ductile deformation and associated metamorphism indicated by biotite cooling ages in most of the gneisses of the Staré Sedlo complex (cf. Chapter 7) and may be related to the late- and, or, post-magmatic activity in the adjacent Central Bohemian Pluton. Accordingly, while both the mineral - whole-rock Rb - Sr ages of ca 324 and 316 Ma for samples LG-A and LG-B and their εSr_T values are assessed as having no geological (chronological) significance, the corresponding mineral - whole-rock age of ca 339 Ma for sample LG-C is considered to indicate the final stages of ductile deformation of the protolith of the Lašovice gneisses and its εSr_T value is interpreted as reflecting the Sr isotopic composition of the protolith of the Lašovice gneisses.

8.2 Magmatic evolution of the protolith(s) of the Staré Sedlo and Mirotice gneisses and schists

The strong mantle affinities and depleted Sr and Nd isotopic compositions such as are shown by rocks of the Staré Sedlo and Mirotice complexes, are rare in granitoids of the European Hercynides (cf.

Bernard-Griffiths et al., 1985; Liew and Hofmann, 1988; Peucat et al., 1988; Holl et al., 1989; Liew et al., 1989, Pin and Duthou, 1990; Turpin et al., 1990). However granitic rocks which contain a substantial proportion of a mantle-derived component have been described elsewhere (e.g. the Lachlan Fold Belt of southeastern Australia: for review see *Chappell and White, 1992*; North Chilean Andes: *Rogers and Hawkesworth, 1989*) and such rocks are also known to form parts of assemblages associated with arc-type regimes (e.g. granitoids in the Svecokarelides of SE Finland; *Patchett and Kouvo, 1986*) where the phases of compressional and extensional tectonism account for variations in the bulk composition of generated magma (cf. Chapter 4; *Hopgood, 1984*). The depleted Sr and Nd isotopic compositions of some calc-alkaline andesites and rhyolites (e.g. rocks from the Andean Volcanic Province; *Thorpe et al., 1984; Hickey et al., 1986; Rogers and Hawkesworth, 1989*) are also indicative of a substantial mantle-derived component. However their compositions cannot be accounted for simply by partial melting of a mantle wedge or contamination of mantle-derived magma by the continental crust through a process of bulk mixing. Rather they are considered to be result of combined fractional crystallization of mantle-derived magma and concurrent contamination by crustal material (*Thorpe et al., 1984*).

The major and trace element compositions of the gneisses and schists from the Staré Sedlo and Mirotice complexes also cannot be accounted for by either simple fractional crystallization of their parent magma or by bulk assimilation by the parent magma of Palaeozoic sediments of the Islet zone (cf. Chapter 4). However as illustrated by the results of modelling (cf. Par.4.2.2), the simultaneous operation of fractional crystallization and wall-rock (or its partial melt) assimilation could account for the composition of at least some of the gneisses of the Staré Sedlo complex. Accordingly, in order to explain at least some of the chemical and isotopic variations in the gneisses and schists from the Staré Sedlo and Mirotice complexes, the trace element and isotopic data, together with the composition of material which may have contributed to the parent magma of their protolith(s), is used for modelling the assimilation and fractional crystallization (AFC) processes.

8.2.1 Theoretical modelling of AFC processes

The model describing the isotopic and trace element consequences on magma composition of concurrent assimilation and fractional crystallization (AFC) has been developed by *DePaolo (1981)*. The underlying assumption is that the composition of resulting magma can be predicted from the compositions of both the parent magma and material assimilated, provided the bulk distribution coefficients of the fractionating phases and the rates of both the fractional crystallization and assimilation can be estimated with a sufficient accuracy. The reversed model (*Powell, 1984*) permits estimation of the composition of wall-rock contaminants from known compositions of parent and resulting magmas. The model emphasizes time dependence and magma mass to allow assimilation and crystallization rates to be related to the physical parameters of the magma (temperature contrast between magma and wall-rock, rate of magma ascent, fusion temperature of wall-rock and crystallization temperature of magma). The model also stresses the fact that both the progress of wall-rock assimilation and heat loss by conduction at the margins of a magma chamber are intimately linked to the extent of magmatic crystallization.

The complete mathematical basis for modelling the assimilation and concurrent fractional crystallization processes and its typical applications are given in *DePaolo (1981)*. Here only the final equations and their applicability to the rocks of the Staré Sedlo and Mirotice complexes are used and the results are discussed.

A magma body which has mass M_m assimilates wall-rock at a rate M_a (mass/time unit) and crystallizes at a rate M_c (the rate of effective separation of crystals from the magma). The initial concentration of an element in a magma and its concentration in wall-rock are C_m^0 and C_a, and the corresponding isotopic ratios are ε_m^0 and ε_a, respectively. D is the bulk solid/liquid distribution coefficient for any chemical element in the fractionating phase. Different equations for the calculation of both the concentration of an element in magma C_m and its isotopic ratio ε_m at any stage of an AFC process are used for cases where the rates of fractionation and assimilation are equal ($M_m = M_c$) or different ($M_m <> M_c$). Accordingly when ($M_m = M_c$), the concentration of an element in the magma is

$$C_m = \{(C_a/DC_m^0) * [1 - \exp(-DM_a/M_m)] + \exp(-DM_a/M_m)\} * C_m^0,$$

and the corresponding isotopic ratio in the magma is

$$\varepsilon_m = \{(C_a/D) * [1 - \exp(-DM_a/M_m)] * \varepsilon_a + C_m^0 * \exp(-DM_a/M_m) * \varepsilon_m\} /$$

$$\{(C_a/D) * [1 - \exp(-DM_a/M_m)] + C_m^0 * \exp(-DM_a/M_m)\}.$$

If, however, the rate of assimilation is different from that of magma fractionation ($M_m <> M_c$), the concentration of an element in a magma is

$$C_m = \{F^{-z} + [r/(r - 1)] * (Ca/zC_m^0) * (1 - F^{-z})\} * C_m^0,$$

and the corresponding isotopic ratio in the magma is

$$\varepsilon_m = \{[r/(r - 1)] * (C_a/z) * (1 - F^{-z}) * \varepsilon_a + C_m^0 * F^{-z} * \varepsilon_m^0\}/$$

$$\{[r/(r - 1)] * (C_a/z) * (1 - F^{-z}) + C_m^0 * F^{-z}\},$$

where r represents the ratio of assimilation and fractional crystallization rates,

$$r = M_a/M_c,$$

$$z = (r + D - 1)/(r - 1)$$

and F is the relative mass of remaining magma, i.e. the ratio of total mass of magma at any stage of the AFC process and total initial mass of magma,

$$F = M_m/M_m^0$$

and represents effectively the progress of magmatic crystallization. For elements with $D > 1$ the AFC model differs from simple fractional crystallization most noticeably as F becomes small, whereas for elements with $D << 1$ the AFC model approaches a simple binary mixing especially in early phases of magma crystallization (high F values). For small rates of assimilation the process essentially becomes one of fractional crystallization.

The application of an AFC model to a real suite of rocks can only be successful provided all the independent parameters (D, F and r), as well as the compositions of parent magma and wall-rock or melt thereof, can be estimated with sufficient accuracy or if there are any additional independent geological constraints available.

8.2.2 Assimilation and fractional crystallization model for gneisses and schists of the Staré Sedlo and Mirotice complexes

The selection of end-members for the AFC model for the parent magma of the gneisses and schists from the Staré Sedlo and Mirotice complexes must satisfy the following conditions: (1) the "mantle end-member" must be represented by Palaeozoic igneous or meta-igneous rock which has a Sr

and Nd depleted composition, shows mantle affinities and occurs within the Moldanubian zone of the Bohemian Massif, (2) the "crustal end-member" must be represented by Palaeozoic or older sedimentary or meta-sedimentary rock from the Teplá - Barrandian assemblage and (3) both the trace element and isotopic compositions of both end-members must be accurately known. The "mantle end-member" is best represented by a high-temperature A-type eclogite from the Kutná Hora complex in the northeastern part of the Moldanubian zone of the Bohemian Massif (Table 8.2; sample CZ-6E) to which *Beard et al. (1992)* assign a garnet - whole-rock Sm - Nd age of 377 ± 20 Ma. This rock belongs to a group of eclogites which has been interpreted as being derived directly from the upper mantle and emplaced into the continental crust during the Hercynian episode. Not only does this rock represent the most chemically and isotopically primitive material available, but also both its chemical signature and $(^{87}Sr/^{86}Sr)_{369}$ ratio correspond to those of early Palaeozoic olivine basalts present in the Teplá - Barrandian assemblage which are also interpreted as mantle derivatives (*Vokurka and Kober, 1992; Bendl et al., 1993*). The choice of "crustal end-member", however, encounters difficulties due to both the scarcity and heterogeneity of isotopic data available from sediments of the Teplá - Barrandian assemblage, and the lack of isotopic data from the metasediments of the Islet zone. Accordingly, based on the lithological and geochemical correlations of Palaeozoic metasediments from the Islet zone with those from the Železné hory Mountains (northeastern part of the Moldanubian zone of the Bohemian Massif) and with Palaeozoic sediments of the Teplá - Barrandian assemblage (*Svoboda, 1966; Matějka, 1980; Košler, 1988*), a sample of an early Palaeozoic metapelite from the Železné hory Mountains (Table 8.2; sample CE-18; *Gorokhov et al., 1979*) has been chosen as being representative of wall-rock material. An alternative choice of a Cambrian shale from the Teplá - Barrandian assemblage (CSH; *Vidal et al., 1975*) would have only a small influence on the results of the AFC model (mostly on F values) as it plots close to the mixing line for eclogite and metapelite (cf. Fig.8.4).

The modelling of AFC processes for the Staré Sedlo and Mirotice gneisses and schist is based on the whole-rock $^{87}Sr/^{86}Sr$ ratios at 369 Ma (mid - late Devonian U - Pb zircon age of crystallization of the Staré Sedlo and Mirotice gneisses protolith) and their Rb/Sr ratios (Fig.8.4). The results suggest that the composition of most of the analyzed gneisses and that of the analyzed schist can be explained on the basis of a concurrent fractional crystallization of a depleted mantle-like parent magma (represented by an eclogite - sample CZ-6E) and assimilation of Palaeozoic sedimentary wall-rock corresponding to a

metapelite (sample CE-18). However there are differences in both the ratio of assimilation and fractional crystallization rates (r) and the character of fractionated material between the individual rock units. For some rock units (Mirotice gneisses MIG-A, MIG-B and schist MIS-A) the constantly low r values are indicative of the fractional crystallization being the most important process which modified the composition of the parent magma. In addition, the model suggests that the main fractionating phase was dominated by plagioclase and that in the parent magma of the schists, plagioclase fractionation was even more pronounced than in the parent magma(s) of the gneisses (cf. Fig.4.11). The Lašovice gneiss samples LG-A and LG-B are plotted for reference only, as it has been shown that their Rb - Sr isotopic systems are consistent with the superposition of a post 340 - 330 Ma disturbance and that they may thus not be representative of their protolith (see above). However the composition of the other Lašovice gneiss sample (LG-C) is consistent with the operation of both the assimilation and fractional crystallization with the main fractionating phase being rich in biotite (or any mineral with $D^{Rb} >> D^{Sr}$). The compositions of the Staré Sedlo gneisses are consistent with the fractionation of phases with a variable proportions of plagioclase, biotite and, or, clinopyroxene (or amphibole). The variations of mineral proportions in the bulk composition of the fractionating phase(s) would account for different fractionation patterns in the $(^{87}Sr/^{86}Sr)_{369}$ vs Rb/Sr diagram. This is illustrated by a fractionation curve calculated for r = 0.3 using the bulk Rb and Sr distribution coefficients $D^{(\text{Lašovice gneisses/Staré Sedlo gneisses})}$ of 0.80 and 0.22, respectively (Fig.8.4) An alternative explanation is that the variations in the composition of the Staré Sedlo, Lašovice and Mirotice gneisses and schists reflect the assimilation of materials with different compositions by the parent magma of each rock type (e.g. assimilation by magma corresponding to HT eclogite CZ-6E of metapelites CE-18 and CE-41; cf. Fig.8.4). The lack of corresponding isotopic data does not permit the metasediments of the Islet zone to be used as end-members in an AFC model. Also, the lack of Nd isotopic data from (meta)sediments of the Teplá - Barrandian assemblage does not allow the Nd and Sr isotopic compositions to be used together in the AFC model for the rocks of the Staré Sedlo and Mirotice complexes. However the corresponding results of modelling the REE composition of the gneisses (cf. Chapter 4), the bulk mixing based on $(^{143}Nd/^{144}Nd)_{369}$, and the AFC model based on $(^{87}Sr/^{86}Sr)_{369}$ and Rb/Sr ratios, consistently show that the composition of the Lašovice gneiss sample (LG-C) is indicative of larger proportion of assimilated sedimentary material compared to that for most of the gneisses from the Staré Sedlo complex.

8.3 Nd model ages

The interpretation of $T_{Nd(DM)}$ model ages (Table 8.1) as crustal formation ages assumes that (1) the isotopic composition of the mantle source is known with sufficient precision, (2) only a short time elapsed between emplacement of the material into the continental crust and the acquisition of a continent-like Sm/Nd ratio, (3) the Sm/Nd ratio of the material has not been modified by subsequent intracrustal events and (4) all the material in the sample must have come from the mantle of a chosen composition during a single event (*Arndt and Goldstein, 1987*). However, the evidence presented above indicates that condition (4) is not fulfilled for samples LG-B and LG-C of the Lašovice gneiss. Accordingly the corresponding $T_{Nd(DM)}$ model ages of 1.31 and 1.34 Ga reflect the isotopic composition of Nd in the mantle-derived material and assimilated crustal material and the proportions in which they were mixed. They can thus only be interpreted as representing mixed (average) ages which may not necessarily have any geological meaning. The Nd and Sr isotopic compositions of the analyzed samples of the Staré Sedlo and Mirotice gneisses and Mirotice schist point to only a small proportion of crust-derived material having been added to their parent magma. Although this evidence approaches compliance with condition (4), the corresponding $T_{Nd(DM)}$ model ages of 0.74 - 0.69 Ga cannot be interpreted as crust-formation ages as neither the length of time which elapsed between emplacement into the crust and the acquisition of crustal Sm/Nd ratio nor the isotopic composition of the mantle source are known.

Although there is considerable uncertainty about the composition of the upper mantle reservoir underneath the Moldanubian zone in the Bohemian Massif in Palaeozoic times, most of the available data suggest that its isotopic composition corresponds to that of OIB or enriched MORB (*Beard et al., 1992; Vokurka and Kober, 1992; Bendl et al., 1993*). Accordingly, assuming that the gneisses and schists were derived from the eclogitic mantle corresponding in composition to the HT eclogites, the grossly corresponding crystallization ages of 369 ± 4 and 377 ± 20 Ma for the Staré Sedlo and Mirotice gneisses and HT eclogites (*Beard et al., 1992*), and their corresponding OIB-like isotopic compositions, indicate the growth of continental crust in Moldanubian zone in the Bohemian Massif in mid - late Devonian times. If the composition of HT eclogite (sample CZ-6E; $^{147}Sm/^{144}Nd = 0.2209$, $^{143}Nd/^{144}Nd = 0.512995$; *Beard et al., 1992*) is used as best-representing the composition of the mantle source, the

calculated $T_{Nd(Eclogite)}$ model ages of 0.59 - 0.54 Ga for gneisses and schist represent mixed T_{Nd} model ages of both their mantle and crustal sources.

8.4 Conclusions

1. The depleted whole-rock Sr and Nd isotopic compositions for most gneisses and schists from the Staré Sedlo and Mirotice complexes indicate that their protolith(s) did not have a long crustal history before their crystallization at mid - late Devonian times.

2. Both the low εSr_{369} and positive εNd_{369} values for the Staré Sedlo gneisses, the Mirotice gneisses and a sample of Mirotice schist suggest that their protolith(s) were derived from a depleted mantle source which was isotopically similar to OIB - enriched MORB.

3. Most of the variations in the composition of gneisses and schists from the Staré Sedlo and Mirotice complexes can be accounted for by concurrent magmatic fractional crystallization and wall-rock assimilation (less than 1 wt%) processes, which operated in variable proportions in parent magma(s) of individual rock units. For the Lašovice gneisses the Sr and Nd isotopic compositions are consistent with a contribution of a larger proportion (ca 4 wt%) of crustal material to their parent magma.

4. The calculated $T_{Nd(DM)}$ model ages for the gneisses and schist cannot be related to any geological event. However, assuming the composition of HT eclogites from the Moldanubian zone corresponds to that of mantle source of the Staré Sedlo and Mirotice gneisses and schists, their corresponding crystallization ages and OIB-like isotopic compositions indicate the growth of continental crust within the Moldanubian zone in the Bohemian Massif in mid - late Devonian times.

Table 8.1
Whole-rock and mineral Rb - Sr and Sm - Nd data from gneisses and schists of the Staré Sedlo and Mirotice complexes.
Blanket 2σ errors for $^{87}Rb/^{86}Sr$ and $^{147}Sm/^{144}Nd$ are 0.7% and 0.1%, respectively; εSr and εNd are calculated at 369 Ma.

	Rb ppm	Sr ppm	$^{87}Rb/^{86}Sr$	$^{87}Sr/^{86}Sr$ ±2σ	$^{87}Sr/^{86}Sr$ @ 369 Ma	Sm ppm	Nd ppm	$^{147}Sm/^{144}Nd$	$^{143}Nd/^{144}Nd$ ±2σ	$^{143}Nd/^{144}Nd$ @ 369 Ma	ε_{Sr}^{369}	ε_{Nd}^{369}	T_{CHUR}^{Nd} (Ga)	T_{DM}^{Nd} (Ga)
Whole-rock data														
STG-A	75.8	422.7	0.5191	0.70742±4	0.70469	4.067	24.15	0.101797	0.512570±6	0.512324	6.2	3.1	0.11	0.69
STG-B	86.6	365.5	0.6856	0.70807±4	0.70447						3.0			
STG-C	47.1	431.3	0.3159	0.70641±5	0.70475						7.0			
LG-A	74.9	99.2	2.1882	0.71904±4	0.70754						46.7			
LG-B	109.9	134.6	2.3651	0.71596±5	0.70353	4.356	21.59	0.121966	0.512250±10	0.511955	-10.2	-4.1	0.79	1.31
LG-C	44.1	286.7	0.4449	0.70927±5	0.70693	4.502	21.69	0.125477	0.512263±6	0.511960	38.0	-4.0	0.80	1.34
MIG-A	88.4	285.7	0.8951	0.70797±4	0.70327	3.118	18.10	0.104128	0.512570±14	0.512318	-14.0	3.0	0.11	0.70
MIG-B	90.7	246.9	1.0628	0.70810±2	0.70252	2.428	13.45	0.109133	0.512563±6	0.512299	-24.7	2.7	0.13	0.74
MIS-A	107.4	181.6	1.7113	0.71221±3	0.70322	2.879	19.38	0.089811	0.512515±8	0.512298	-14.7	2.6	0.18	0.69

Biotite and plagioclase data

	Rb ppm	Sr ppm	$^{87}Rb/^{86}Sr$	$^{87}Sr/^{86}Sr$ ±2σ
Bi/STG-A	408.2	59.6	19.9971	0.80107±5
Bi/STG-B	543.2	14.6	113.0217	1.24338±10
Bi/STG-C	342.6	15.3	66.6516	1.01884±13
Bi/LG-A	689.6	5.4	447.0236	2.73481±38
Bi/LG-B	781.6	7.4	352.3388	2.32802±35
Bi/LG-C	422.5	3.6	409.5253	2.68106±35

	Rb ppm	Sr ppm	$^{87}Rb/^{86}Sr$	$^{87}Sr/^{86}Sr$ ±2σ
Plg/STG-A	31.5	389.3	0.2338	0.70605±5
Plg/STG-B	48.7	463.0	0.3040	0.70627±4
Plg/STG-C	24.5	378.8	0.1872	0.70582±4
Plg/LG-A	21.9	114.0	0.5546	0.71114±5
Plg/LG-B	54.1	168.0	0.9327	0.71197±5
Plg/LG-C	33.8	410.0	0.2313	0.70821±5

Whole-rock - mineral age Ma	Initial ratio ± 2σ	MSWD
338 ± 2.5	0.70493±4	0.00
335 ± 2	0.70481±3	0.34
331 ± 2.5	0.70493±3	0.19
316 ± 11	0.70937±3	32.20
324 ± 92	0.7068±30	2131.7
339 ± 2.5	0.70711±4	0.50

Table 8.2

Isotope and trace element whole-rock data for HT eclogites (*Beard et al., 1992*), metasediments and sediments (*Gorokhov et al., 1979; Vidal et al., 1975*).

		Rb [ppm]	Sr [ppm]	$^{87}Rb/^{86}Sr$	$^{87}Sr/^{86}Sr$	$^{87}Sr/^{86}Sr$ at 369 Ma
Eclogite	CZ-6E	0.92	35.5	0.0729	0.703261	0.70287
Metapelite	CE-18	106.9	79.7	3.928	0.7423	0.7217
Metapelite	CE-41	99.6	132.5	2.184	0.7371	0.7256
Shale	CSH	99.66	93.87	3.070	0.7311	0.7150

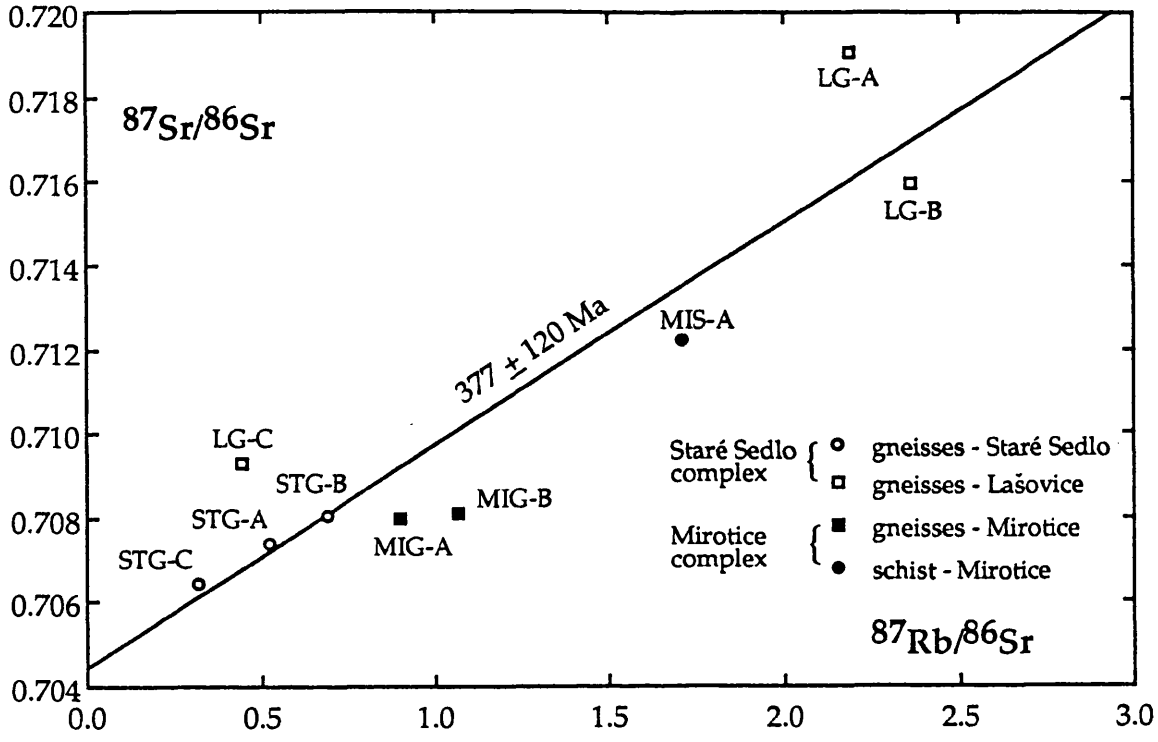

Fig.8.1

Rb - Sr isotope data for gneisses from the Staré Sedlo and Mirotice complexes and schist from the Mirotice complex.

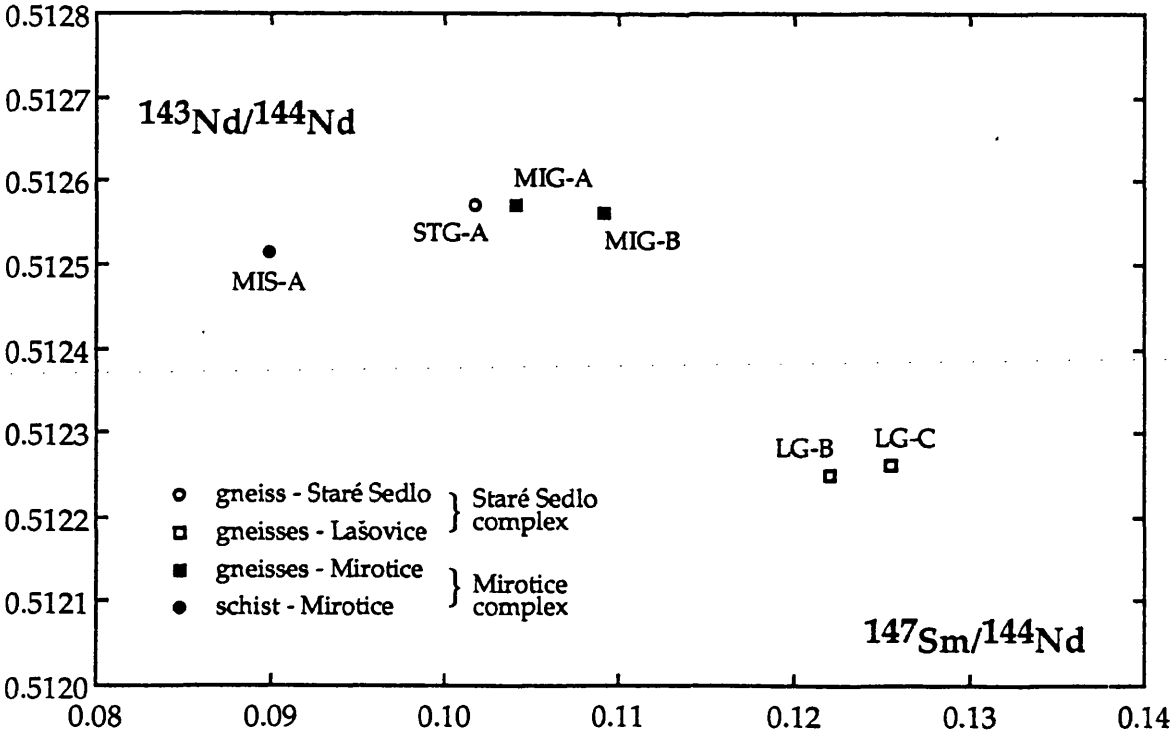

Fig.8.2

Sm - Nd isotope data for gneisses from the Staré Sedlo and Mirotice complexes and schist from the Mirotice complex.

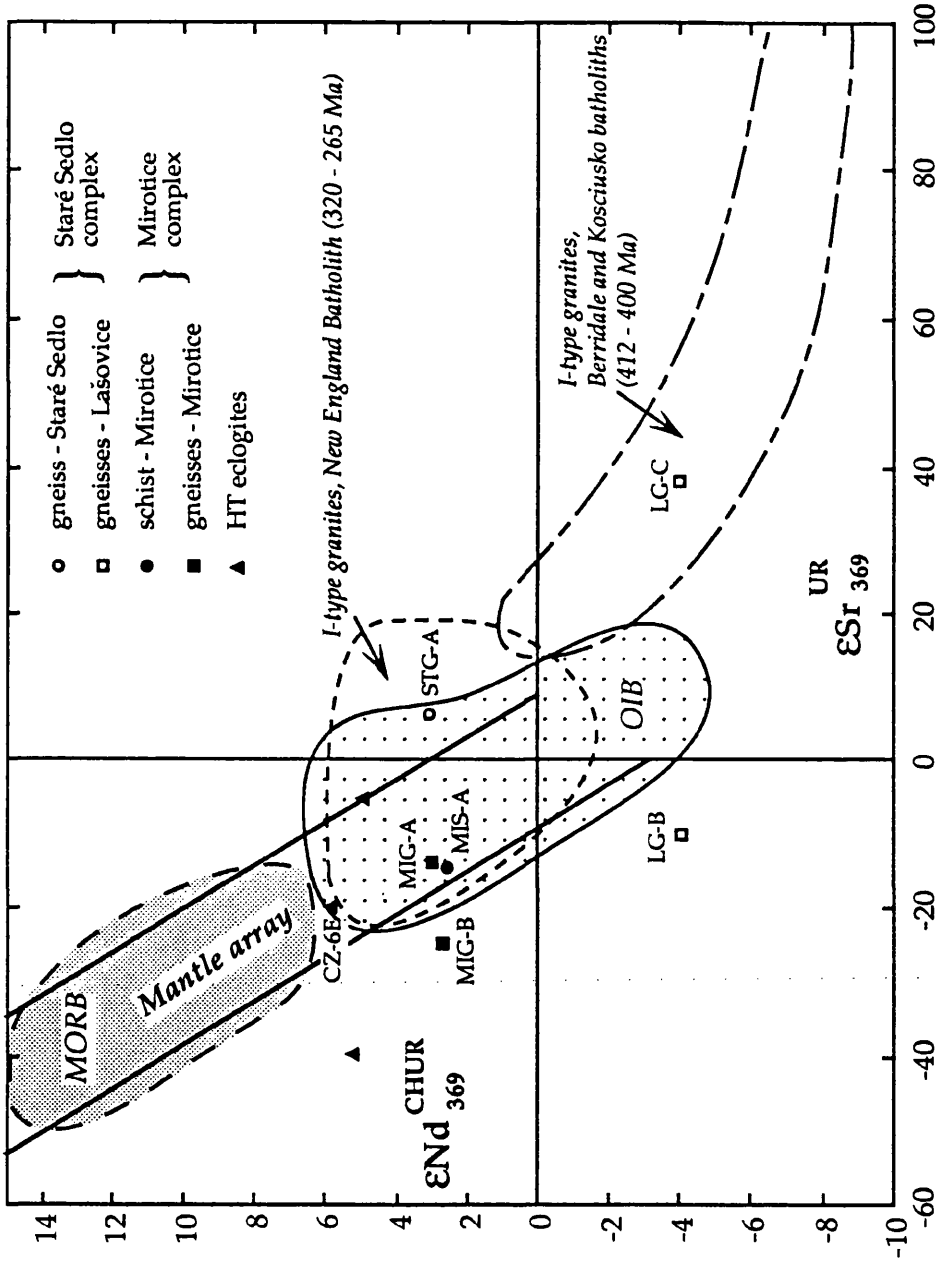

Fig.8.3

Sr and Nd isotopic compositions of gneisses from the Staré Sedlo and Mirotice complexes and schist from the Mirotice complex; the fields for mid ocean ridge basalts (MORB) and oceanic island basalts (OIB) are from *Faure (1986)*; the fields for New England, Berridale and Kosciusko batholiths are those of *McCulloch and Chappell (1982)*; composition of HT eclogites from the Kutná Hora crystalline complex are from *Beard et al. (1992)*.

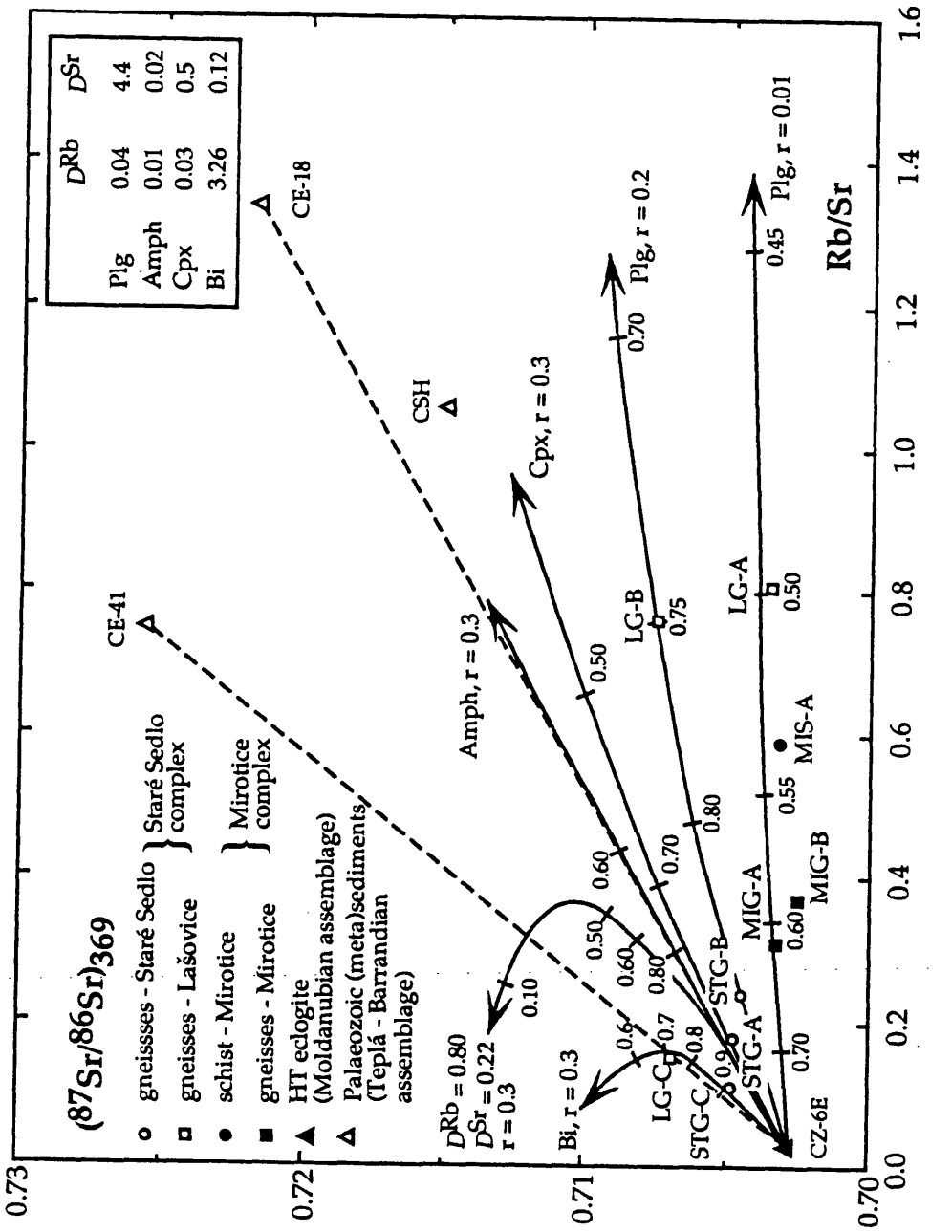

Fig.8.4

$^{87}Sr/^{86}Sr$ and Rb/Sr changes in magma affected by concurrent assimilation and fractional crystallization processes; solid lines correspond to a shift in magma composition at a given ratio of assimilation and fractionation rates (r); the labels correspond to relative mass of remaining magma F; dashed lines represent simple mixing of end-members; the mineral/melt distribution coefficients are from *Hanson (1978)* and *Cox et al. (1979)*.

9. SIGNIFICANCE FOR EASTERN HERCYNIDES

The evidence presented in Chapters 2 - 5 and especially that given in Chapters 6 - 8 forms the basis not only for determination of the petrogenesis and affiliations of rocks from the Staré Sedlo and Mirotice complexes within the Bohemian Massif, but it also has considerable significance in understanding the time span and processes operative during the Hercynian episode in central Europe particularly in relation to its early stages during mid - late Devonian times. In addition it means that re-interpretation is required in relation to some previously published assumptions on the ages and affiliations of the roof pendants of the Central Bohemian Pluton (e.g *Zelenka, 1929; Svoboda, 1966; Suk, 1973; Tonika et al., 1980; Mísař et al, 1983; Suk, 1984; Žežulková et al., 1985; Waldhausrová et al., 1986*). The new data, particularly that presented in Chapters 7 and 8, also shed light on the petrogenesis, source and mechanism of emplacement of at least some of the early intrusions making up the Central Bohemian Pluton during early Carboniferous times.

9.1 Petrogenesis and affiliations of the Staré Sedlo and Mirotice complexes

The data presented in Chapters 2 - 8 indicate that the protolith of gneisses within the Staré Sedlo and Mirotice complexes consisted of mantle-derived isotopically depleted tonalites - granodiorites that were products of an arc-type magmatic activity in mid - late Devonian times. Although no age constraints are available for the time of crystallization of the schists from the Mirotice complex, the general correspondence of Sr and Nd isotopic data for both schists and gneisses suggest the two rock units were derived from the same source, and possibly within a relatively short time span. Any correlation with other rock units of the Bohemian Massif must take into account both their mid - late Devonian crystallization age and their arc-related and Sr and Nd depleted composition.

Although the general geochemical signatures of most of the orthogneisses present within the Moldanubian zone in the Bohemian Massif are consistent with a grossly granitoid composition, there are features indicating that the products of a number of distinct phases of acidic magmatism are present (cf. *Fediuk, 1976; Vrána and Cháb, 1981; van Breemen et al., 1982; Zikmund, 1983; Němec and Páša, 1986; Liew and Hofmann, 1988; Klečka, 1989; Povondra, 1989; Souček et al., 1992*). None of the other

orthogneisses from the Moldanubian zone is known to have a isotopically depleted mantle-derived composition, but additional data is required. However *Wendt et al. (1992)* interpret 367 ± 8 and 362 ± 9 Ma (U - Pb, zircon) ages from granulites in the Blanský les Massif, southern Bohemia as giving a mid - late Devonian age of crystallization of their volcanic protolith(s). However more isotopic (Sr and Nd) evidence is clearly needed to show whether the protoliths of the granulites from the Blanský les Massif and those of the gneisses and schist from the Staré Sedlo and Mirotice complexes represent the products of the same tectonomagmatic regime.

There is a widespread evidence for mid - late Devonian tectonothermal activity within the Moldanubian zone in the Bohemian Massif. In the Münchberg gneiss complex, NE Bavaria, metamorphism at 370 ± 8 Ma has been recorded (Rb - Sr, mineral - whole-rock; *Söllner et al., 1981*, see also *Stosch and Lugmair, 1990*), while eclogitization of a tholeiitic protolith within the gneisses there at 380 (+14/-22) Ma has been reported (U - Pb zircon; *Gebauer and Grünenfelder, 1979*). A 380 Ma (U - Pb, monazite) age of a metamorphic overprint has been recorded in a paragneiss from the Erbendorf-Vohenstrauss zone (*Teufel, 1988*) while *Kröner et al. (1988)* interpret U - Pb zircon lower intercept ages of 367 (+18/-20) and 347 (+9/-10) Ma in metasedimentary Moldanubian assemblages of southern Bohemia and western Moravia, respectively, as indicative of Hercynian tectonothermal activity. In addition a widespread phase of eclogite facies rock formation (mostly interpreted as the age of metamorphism but also as the age of the protolith of the eclogite facies rocks) has been documented by Sm - Nd mineral - whole rock ages of 370 ± 15, 373 ± 7, 379 ± 9 and 377 ± 20 Ma in the Moldanubian zone in Moravia and Lower Austria (garnet pyroxenites) and in western and eastern Bohemia (eclogites) (*Carswell and Jamtweit, 1990; Brueckner et. al., 1991; Beard et al., 1991; Beard et al., 1992*). The K - Ar isotope data of *Kreuzer et al. (1989, 1992)* for the northwestern and western margins of the Bohemian Massif (Münchberg upper nappes, Erbendorf-Vohenstrauss Zone and Teplá - Domažlice Zone) could also indicate tectonothermal activity at ca 380 Ma. However, it is not clear whether the data presented represent cooling ages from amphibole facies metamorphism or a partial resetting of older K - Ar systems.

Correspondence in time of an extensive phase of eclogite rock formation and the crystallization of the protolith of the granitoid gneisses from the Staré Sedlo and Mirotice complexes in mid - late Devonian times, together with corresponding depleted Sr and Nd isotopic signatures of gneisses (and associated schists) and eclogites (cf. Chapter 8), suggests that these rocks could have originally been

derived from the same source. While the gneisses and schist underwent an extensive differentiation and the compositions of at least some of them are consistent with contamination of their parent magma with more differentiated crustal material (see Figs 8.3 and 8.4), the eclogites that have retained an ultrabasic - basic mantle-like composition are interpreted as having been derived from the upper mantle without any crustal history prior to their emplacement into the continental crust (*Beard et al., 1992*). Due to the lack of corresponding data, corresponding consanguinity cannot be proved for the granulites and the gneisses. However the spatial association of some granulites, eclogites and, or, peridotites even within a single outcrop (*Vrána, 1989; 1992* and the references therein), the occurrence within some granulites of the products of mantle magmatism (*Vrána, 1989*) and the temporal correspondence of at least some of the eclogites and granulites with the gneisses and schists of the Staré Sedlo and Mirotice complexes suggests that some of the granulites may have originally come from the same source as the eclogites, gneisses and schists. This is consistent with the petrological evidence (e.g. the orthopyroxene and plagioclase coronas around garnet in both the eclogites and granulites; *Vrána, 1992*) suggesting that some mafic granulites in southern Bohemia may have originated from a granulite facies recrystallization of eclogites. Evidence for the association of the gneisses and schists from the Staré Sedlo and Mirotice complexes with eclogites and peridotites of the Moldanubian zone is also supported by the occurrence of a small serpentinite body amongst the metasedimentary and metavolcanic rocks of the adjacent Mirovice islet (cf. Fig.1.1; *Svoboda, 1966*).

Subsequent to derivation, possibly from the same source, the gneisses and schists, the granulites and the eclogites show divergence in their history. While the mineral assemblages of the eclogites and granulites are consistent with a crystallization in the upper mantle and the lower crust, respectively, the parent magmas of the gneisses and schists were emplaced into the upper crust of the Moldanubian zone (into the Teplá - Barrandian assemblage; cf. *Mrázek, 1963*). Both the eclogites and the granulites subsequently were brought up to their present tectonic positions in the upper crust as a result of a SE-directed overthrusting during the Hercynian D3 phase at ca 340 - 330 Ma (*Vrána, 1979; van Breemen et al., 1982; Hopgood and Bowes, 1987*). In the case of the gneisses and schists of the Staré Sedlo and Mirotice complexes, this early Carboniferous tectonic activity resulted in upward movement from a level in the upper crust where ductile (mylonitic) deformation was operational through a crustal level where the

Rb - Sr system in biotite became closed to a crustal level where brittle fracturing took place (cf. Chapter 7).

As well as overall consanguinity amongst the eclogites and granulites from the Moldanubian zone of the Bohemian Massif, there is also heterogeneity which must be accounted for when correlating these rocks with the gneisses and schists from the Staré Sedlo and Mirotice complexes (cf. *Brueckner et al., 1991; Beard et al., 1992; Vrána, 1992*). However, additional data are needed not only to shed more light on these compositional variations and relationships, but also to elucidate any possible links with the minor intrusions of amphibolite and meta-aplite within the Staré Sedlo and Mirotice complexes. Also yet to be established are the spatial and temporal relations between the gneisses and schists of the Staré Sedlo and Mirotice complexes and the metavolcanic rocks present in other roof pendants of the Central Bohemian Pluton. However the evidence presented here does not suggest that either their protoliths or the strong foliation they exhibit were formed during late Proterozoic times as has been suggested previously (cf. *Waldhausrová, 1984* and the references therein). It seems much more likely that they can be linked with at least some of the metamorphosed acidic intrusive rocks present within other roof pendants of the Central Bohemian Pluton and that their deformation took place during the Hercynian episode (cf. *Rajlich, 1988*).

9.2 Staré Sedlo and Mirotice complexes - Central Bohemian Pluton relations

The occurrence of deformed granitoid rocks of the Staré Sedlo and Mirotice complexes within the roof pendants of the large and essentially undeformed Central Bohemian Pluton means that the possibility of them representing early and late products of the same magmatic phase requires assessment. In order to do so, the data for gneisses and schists are compared with some previously published results from the granitoids of the Central Bohemian Pluton (CBP; *Vejnar, 1973; 1974; Jakeš, 1977; van Breemen et al., 1982*) and with new isotopic data for granodiorite and aplite (Blatná type).

In literature, the petrogenesis of the calc-alkaline granitoid rocks which make up most of the CBP has often been interpreted on the basis of an Andean-type subduction and magma generation above a shallow-dipping subduction zone. However there are at least two different calc-alkaline trends for different rock suites of the CBP (Fig.9.1; cf. Par.1.1.2; *Vejnar, 1973*). Most of the granite - granodiorite, tonalite

and some of the rocks from the gabbro - diorite suites have a trend on an AFM diagram which shows a relative iron enrichment compared to the rocks of durbachite suite (Fig.9.1.). *Vejnar (1973)* interpreted the two trends as representing two separate magmatic phases, viz. (1) pre-Hercynian magmatism which had a shallow intrusive character and the magma contained a considerable proportion of tholeiitic component and (2) Hercynian magmatism with a large proportion of palingenetic magma where K-content dominates over Na-content. These conclusions are not based on any geochronological data or cross-cutting relations. In addition trace element data indicate that at least some of the high-potassic rocks contain a substantial proportion of a mantle-derived component and that the shift in composition between the two trends may be explained by variations in tectonic regimes (i.e. compression and extension; cf. *Bowes and Košler, 1993*). In contrast the composition of gneisses and schists from the Staré Sedlo and Mirotice complexes plot within a tightly constrained field on an AFM plot but with some of their AFM values corresponding to some of those of the granite - granodiorite, tonalite and some of those of the gabbro - diorite suites of the CBP.

While the trace element signatures of the gneisses and schists from the Staré Sedlo and Mirotice complexes indicate they have been derived in an arc-type regime (cf. Fig.4.15), a corresponding discrimination for granitoids of the CBP points to correspondence with both volcanic arc and syn-collision granites (*Melín, 1988*). However, like the Staré Sedlo and Mirotice gneisses and schist (cf. Fig.4.18), the LIL and HFS element composition of granitoids of the CBP suggests their derivation from an arc-type regime with at least some of them corresponding to typical calc-alkaline andesites from northern Chile (Fig.9.2). In addition, as demonstrated for the rocks of the Staré Sedlo and Mirotice complexes (cf. Chapter 4), the Rb/Cs ratio in granitoids from the CBP is also indicative of the operation of subduction process which resulted in the decoupling of alkali metals (Fig.9.3; cf. Fig.4.20).

As a means of assessing the origin of magma from which at least some granitoids of the Central Bohemian Pluton crystallized, Nd data has been obtained for the granodiorite and aplite of the Blatná type for which *van Breemen et al. (1982)* and *Bendl and Vokurka (1989)* have provided Sr isotopic data (Table 9.1) and for which an Rb - Sr isochron age (interpreted as the emplacement age of Blatná granodiorite) calculated from six whole-rock samples (2 granodiorites and 4 aplites) is 331 ± 4 Ma (*van Breemen et al., 1982*). The corresponding $^{87}Sr/^{86}Sr$ initial ratio of 0.7089 ± 2 is indicative of a large amount of crustal involvement, although it is lower than it might have been expected if the granodiorite had been derived

from gneisses of the Moldanubian assemblage. Accordingly models of mixed mantle - crustal origin (*van Breemen et al., 1982; Bendl and Vokurka, 1989*) and an origin by melting lower crustal rocks (*van Breemen et al., 1982*) have been proposed for this part of the Central Bohemian Pluton.

The Nd isotopic results also indicate a substantial crustal involvement in the parent magma of both the Blatná granodiorite and aplite with both plotting well into the Nd-enriched field on a εSr_T vs εNd_T diagram (Fig.9.4). The εSr_T and εNd_T values of +65 - +66.2 and -6.5 - -5.9, respectively, show that partial melting of gneisses of the Moldanubian assemblage alone could not have resulted in magma corresponding to either rock type (cf. *Gorokhov et al., 1979; van Breemen et al., 1982; Liew and Hofmann, 1988; Kröner et al., 1988*). However the lack of coupled Sr - Nd isotopic data from rocks of the Moldanubian assemblage, or from lower crustal rocks (e.g. granulites), does not allow any assessment on their source material.

The $T_{Nd(DM)}$ model ages for the Blatná granitoids are within the range of 1.37 - 1.42 Ga. However, based on the assumption that the composition(s) of their parent magma is consistent with a mixed mantle - crustal source, these model ages cannot be interpreted as being indicative of a crust-forming event. Rather they reflect the Nd isotopic compositions in sources from which their parent magma(s) were derived and the proportions in which they were mixed.

The marked crustal affinities of the Blatná granodiorite and aplite contrast with the mantle affinities of the gneisses and schists from the Staré Sedlo and Mirotice complexes (Fig.9.4, cf. Chapter 8). Although there are rocks amongst the gneisses of the Staré Sedlo complex whose Sr and Nd isotopic compositions are consistent with some crustal involvement, the combined evidence from all the geochemical data points to these rocks as being the products of concurrent fractional crystallization and wall-rock assimilation of parent magma originally corresponding to that of much of the gneiss (cf. Par.8.2.2). In addition, the large positive εSr_T and negative εNd_T values for the Blatná granodiorite and aplite are not consistent with them being derived from the same sources or by the same processes attributed to the rocks of the Staré Sedlo and Mirotice complexes, as this would involve an unrealistically large amount of crustal material having to be assimilated by a mantle-derived magma. In addition the large gap of ca 40 Ma between the emplacement of the protolith(s) of the Staré Sedlo and Mirotice gneisses (ca 369 Ma) and Blatná granodiorite (ca 331 Ma) suggest that the two plutonic suites are likely to represent products of two different magmatic phases. Accordingly, although the major and trace element

compositions of the gneisses and schists from the Staré Sedlo and Mirotice complexes and granite - granodiorite, tonalite and some of the rocks of the gabbro - diorite suites from the Central Bohemian Pluton indicate they both represent products of subduction-related processes, the contrasting Sr and Nd isotopic compositions and the time gap between their emplacement suggest they are not likely to be related to the same magmatic phase.

The differences in isotopic compositions between the gneisses and schists and the Blatná granodiorite may reflect both different source material of their parent magmas and, or, different mechanisms of magma separation, differentiation and emplacement. A model involving considerable crustal thickening between 369 and 331 Ma would be consistent with both the contrasting isotopic compositions of the gneiss - schist and the granodiorite - aplite and also the existence of a phase of granulite facies metamorphism at ca 340 Ma reported from the Moldanubian zone in the Bohemian Massif (*van Breemen et al., 1982; Aftalion et al., 1989; Wendt et al., 1992*). Alternatively, the contrasting isotopic signatures could reflect a major change in the speed of plate motion(s) and the subduction angle (see *Cross and Pilger, 1982*). Nevertheless, any model must account for the apparent scarcity of the products of mid - late Devonian magmatic activity, the very limited (or absence of) magmatic activity between 360 and 340 Ma and the large volume of Carboniferous granitoids in the Moldanubian zone.

The ca 340 - 330 Ma biotite cooling ages from gneisses of the Staré Sedlo complex are interpreted as indicating the end of metamorphism associated with ductile deformation of the protolith of the gneisses (for the discussion of a possible resetting of their Rb - Sr system see Chapter 7). Accordingly, as most of granitoids in the Central Bohemian Pluton do not show any effects of ductile deformation which is present in rocks of the roof pendants, the emplacement of most of the CBP granitoids must have taken place after the 340 - 330 Ma deformation (D3 phase of *Vrána, 1979; van Breemen, 1982*).

The disposition of the foliation in rocks of the Staré Sedlo and Mirotice complexes and elsewhere within the metasedimentary and metavolcanic roof pendants of the Central Bohemian Pluton is generally flat-lying in the SE and steeply disposed in the NW and is generally grossly parallel to the NE - NNE-trending margins of the elongate roof pendants (cf. Fig.1.1). In addition in the country rocks NW of the CBP there is a steeply-disposed planar fabric which in places is mylonitic and which represents ductile deformation due to simple shear along a NE- to NNE-trending sub-vertical lineament (*Rajlich, 1988;*

Rajlich et al., 1988). As there is a time overlap of the 340 - 330 Ma deformation and the 331 Ma emplacement of Blatná granodiorite, it likely that it was this sub-vertical lineament which controlled the emplacement of at least some, and possibly much, of the early Carboniferous granitoid masses of the composite CBP. The variations in disposition of the planar fabric from sub-horizontal to steeply dipping can be explained on the basis of ramping, a feature described as being typical for major listric thrust zones which generally have a staircase-like trajectory with long flats in ductile horizons and short ramps through the more competent units (*Elliott and Johnson, 1980*). Such a model also accounts for (1) some early parts of the CBP being foliated and even mylonitic (cf. *Vrána and Cháb, 1981; Palivcová and Franke, 1982*), (2) composite nature of the pluton in a NE-trending zone and (3) its overall tongue-shape (*Kettner, 1930b*) with most of its volume being due to steeply disposed ramps predominating over flats but with the tip of the tongue curving over towards the SE where the flats predominate over ramps (Fig.9.5a-d). The emplacement mechanism was likely to have been similar to that proposed by *Hutton et al. (1990)* for the intrusion of an early Proterozoic rapakivi granite into an extensional shear zone in southern Greenland.

9.3 Nature of plate activity in the eastern Hercynides in mid - late Devonian times

Most of the recent tectonic models of Hercynian orogen concentrate on analogies with an Andean-type of subduction regime, i.e. a low-angle subduction of young oceanic lithosphere characterized by rapid absolute upper plate motion or rapid convergence generally (for a comprehensive review see *Patočka, 1989*). However there is no agreement on the number of subduction zones, their spatial distribution, the spatial distribution of sutures and direction(s) and exact timing of subduction(s). The models centre aspects of the following three ideas.

1. The Hercynian orogen formed as the result of the closure of the Rheic (Central European, Prevariscian, Hercynian) Ocean due to a S-directed subduction of oceanic lithosphere followed by collision of the Northern Continent (Laurasia or Baltica and Laurentia) and the Southern Continent (Gondwana).

2. The Hercynian orogen formed as the result of combined collision of the Northern Continent with Armorica (i.e. microcontinent(s) distributed along the northern margin of Gondwana) and the collision of Gondwana with Armorica. The first was preceded by S-directed subduction of oceanic lithosphere (Rheic

Ocean) beneath Armorica while the second followed a N-directed subduction of the Theic (Southern) Ocean beneath Armorica. The apparent space and mechanical problems in places where these opposite-directed subduction zones are only several tenths kilometres apart (e.g. Black Forest) are explained by alternative (non-simultaneous) operation of the two subduction zones.

3. The Hercynian orogen resulted from an oblique collision of Laurasia and Gondwana followed by horizontal slip. This model accounts for structural and lithological discontinuities of the relics of the orogen as well as for the discontinuity of sutures and numerous WNW- and SSE-directed shear zones present within the orogen.

The explanation of the precise timing of phases of the Hercynian episode in various parts of the orogen is intimately related to an understanding the operative mechanisms. In the region of the Bohemian Massif (eastern Hercynides) most authors accept the 380 Ma age of eclogite formation in the Münchberg Massif (*Gebauer and Grünenfelder, 1979*) as marking the beginning of Hercynian tectonothermal activity there. Although there is no corresponding agreement on the timing of the final phases of the Hercynian episode in this part of the orogen, the cessation of the orogenic episode is probably indicated by ca 260 - 250 Ma cooling ages of late granitoids (cf. *Bergner et al., 1988* and the references therein). Accordingly the mid - late Devonian crystallization age of the protolith of the Staré Sedlo and Mirotice gneisses is consistent with representing an early phase of the Hercynian episode.

The scarcity of products of mid - late Devonian magmatic activity, the very limited (or absence of) magmatic activity between 360 and 340 Ma and the emplacement of large volume of granitoids at 330 - 300 Ma in the Moldanubian zone, together with the evidence for contrasting isotopic signatures of subduction-related mid - late Devonian and early Carboniferous granitoids (see above) suggests the possibility of a major change in the nature of subduction during this period. Some of the mid - late Devonian magmatic activity (e.g. in the French Massif Central; for review of Rb - Sr geochronological data see *Dornsiepen, 1978*) has been interpreted as resulting from a N- or NW-directed subduction of the Theic lithosphere under the southernmost part of Armorica prior to its collision with Laurasia (*Leeder, 1982*). This implies subduction beneath a relatively thin crust along the margin of Armorica resulting in the formation of various continent-based volcanic arcs including the Liguro - Moldanubian Cordillera (*Leeder, 1982*). Previous to the present work no products of a more easterly expression of such a volcanic arc(s) have been reported from the eastern part of Hercynides. However the mid - late Devonian

crystallization age of the Staré Sedlo and Mirotice gneisses and the geochemical and isotopic signatures suggesting their origin in a continent-based arc regime provide evidence for an extension of Liguro - Moldanubian Cordillera into the Moldanubian zone of the Bohemian Massif: the volcanic arc magmatism responsible for the Staré Sedlo and Mirotice rocks was probably close to the southern margin of Armorica prior to its collision with Laurasia. The voluminous masses of early Carboniferous granitoids within the Moldanubian zone are thus interpreted as having been emplaced into thickened continental crust after this continent - continent collision. Locally this is linked with the later phases of, or shortly after, the D3 deformation; *Vrána, 1979; van Breemen, 1982*). However it is not clear whether their origin(s) is related to the S- or N-directed subduction (cf. *van Breemen et al., 1982; Finger and Steyer, 1990; 1991*). More integrated structural and isotopic data are needed to shed light on this aspect of Hercynian evolution.

9.4 Suggestions for nomenclature

The present study indicates that the roof pendants of the Central Bohemian Pluton are characterized by considerable lithological variability. Accordingly it is proposed that the commonly used term "Islet zone" should be restricted to areas dominated by units of sedimentary and volcanosedimentary origin, i.e. in the way used by *Svoboda (1933)* and *Chlupáč (1986; 1989)*. For those rock associations dominated by lithologies of magmatic derivation, the term "complex" is suggested. Then the term "roof pendant" could be used in the descriptive sense of a downward projection into an igneous intrusion of the country rock in its roof (*Whyte, 1989*).

The evidence for mid - late Devonian primitive granitoid plutonism which is interpreted as resulting from a continent-based arc regime followed by ca 40 Ma period with only little magmatic activity before the emplacement of differentiated early Carboniferous granitoid masses suggests the two periods of granitoid plutonism means that it is essential to clearly indicate which phase of Hercynian granitoid plutonism is being referred to. Although they both fit within the previously defined period of Hercynian orogenic activity (ca 380 - 250 Ma), they have contrasting compositional signatures which are indicative of different tectonic regimes. Accordingly it is suggested that the time period should always be specified.

9.5 Conclusions

1. The temporal association of the gneisses from the Staré Sedlo and Mirotice complexes with some eclogites and granulites from the Moldanubian zone, the depleted Sr and Nd isotopic compositions of the gneisses, schists and eclogites and the spatial association of gneisses with schists in the Mirotice complex, and that of eclogites with granulites elsewhere in the Moldanubian zone, suggests that the gneisses, schists and at least some of the eclogites and granulites may represent products of the same mid - late Devonian magmatic activity.

2. Both the depleted Sr and Nd isotopic compositions of the gneisses and schists, which contrast with the crustal Nd and Sr isotopic signatures of granitoids from the Central Bohemian Pluton (Blatná granodiorite and aplite), and the ca 40 Ma time gap between their emplacement suggests that they represent products of two separate magmatic phases related to different tectonic regimes.

3. In a scheme of plate tectonic activity in Hercynian Europe, the gneisses and schists from the Staré Sedlo and Mirotice complexes within the Moldanubian zone of the Bohemian Massif are correlated with continent-based magmatic arc-related rocks of the Liguro - Moldanubian Cordillera located on the southern margin of Armorica.

Table 9.1

Whole-rock Rb - Sr and Sm - Nd data from Blatná granodiorite (RC-1971, 1972) and aplite (RC-1974) from the Central Bohemian Pluton.

Blanket 2σ errors for $^{87}Rb/^{86}Sr$ and $^{147}Sm/^{144}Nd$ are 0.7% and 0.1%, respectively; εSr and εNd are calculated at 331 Ma; Rb - Sr data are from *van Breemen et al. (1982; table 3)* and specimen nubers correspond to those of *van Breemen et al. (1982; p. 105).*

	Rb ppm	Sr ppm	$^{87}Rb/^{86}Sr$	$^{87}Sr/^{86}Sr \pm 2\sigma$	Sm ppm	Nd ppm	$^{147}Sm/^{144}Nd$	$^{143}Nd/^{144}Nd \pm 2\sigma$	ε_{Sr}^{331}	ε_{Nd}^{331}	T_{CHUR}^{Nd} Ga	T_{DM}^{Nd} Ga
RC-1971	190	352	1.562	0.71627±5	5.953	31.95	0.112619	0.512132±6	65.5	-6.3	0.92	1.37
RC-1972	196	331	1.711	0.71694±8	6.178	31.91	0.117029	0.512134±6	65.0	-6.5	0.96	1.42
RC-1974	210	104	5.89	0.73671±4	6.134	31.23	0.118718	0.512168±6	66.2	-5.9	0.92	1.39

The rock powders used used came from the same sample bottles as used by *van Breemen et al. (1982).* The Sm - Nd analytical procedure was the same as that for the gneisses and schists (cf. Chapter 8, Appendix 2).

The notations used in Chapter 9 correspond to those from Chapter 8.

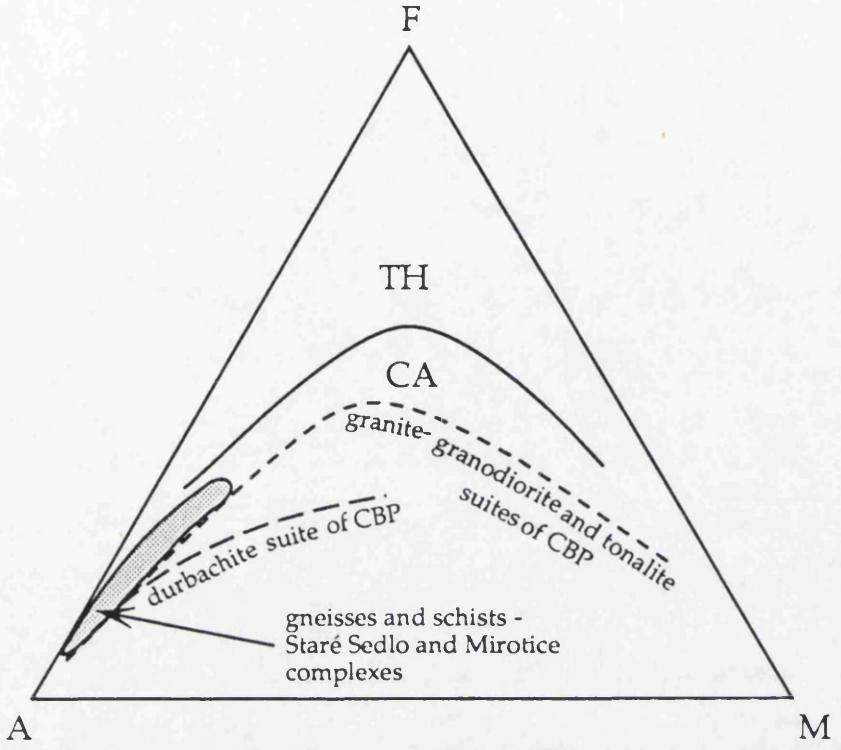

Fig.9.1

AFM plots for gneisses and schists from the Staré Sedlo and Mirotice complexes and trends for granitoids and the durbachite suite from the Central Bohemian Pluton (*Vejnar, 1973*); TH - tholeiitic field; CA - calc-alkaline field.

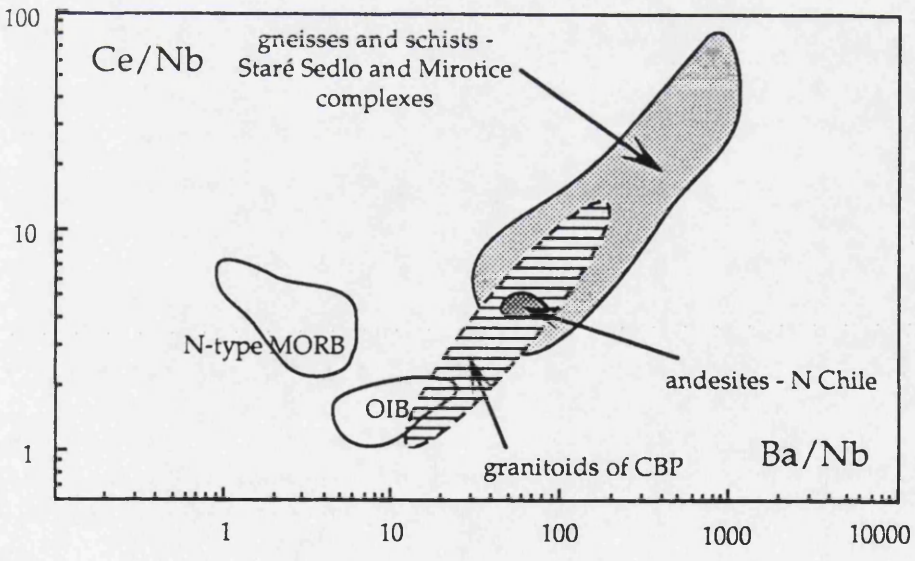

Fig.9.2

LIL vs HFS diagram for rocks from the Staré Sedlo and Mirotice complexes and granitoids and durbachites from the Central Bohemian Pluton; MORB - mid ocean ridge basalts; OIB - ocean island basalts; data from *Jakeš (1977), Bouška et al. (1984), Thorpe et al. (1984), Saunders et al. (1991).*

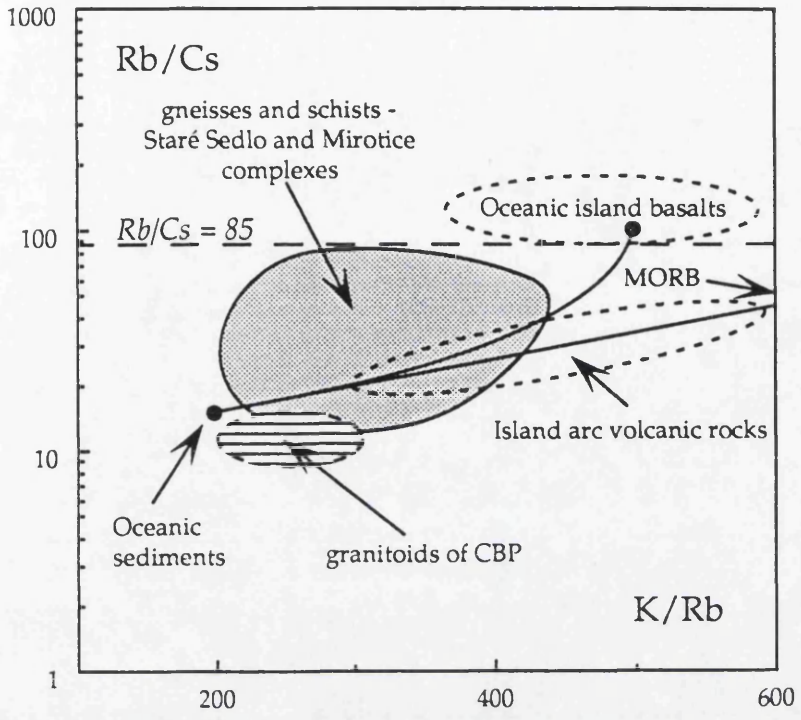

Fig.9.3 Rb/Cs vs K/Rb plots for gneisses and schists from the Staré Sedlo and Mirotice complexes and granitoids and durbachites from the Central Bohemian Pluton (CBP); solid lines represent mixing between an average composition of oceanic sediments, oceanic island basalts and mid ocean ridge basalts (MORB); data from *Jakeš (1977), Hart and Reid (1991)* and the references therein.

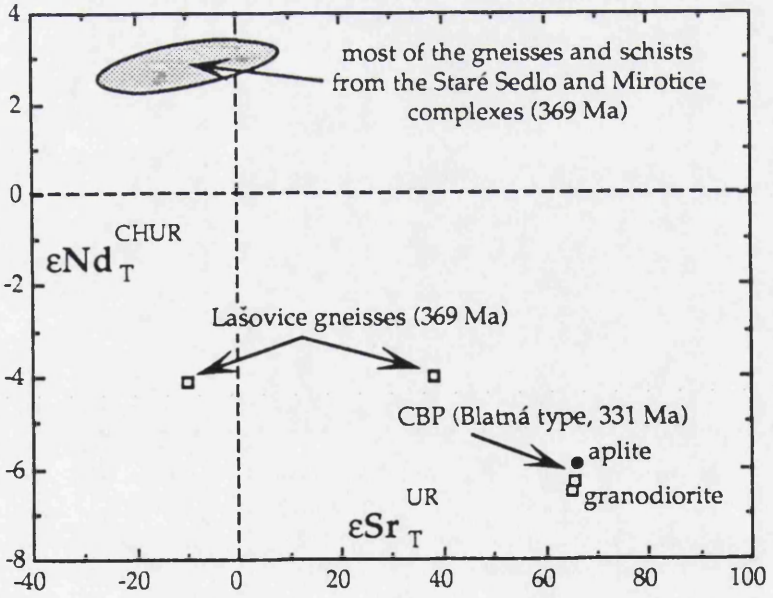

Fig.9.4 Plots of Sr and Nd isotopic compositions of gneisses and schists from the Staré Sedlo and Mirotice complexes (cf. Fig.8.3) and granodiorite and aplite from the Blatná intrusion of the Central Bohemian Pluton (CBP).

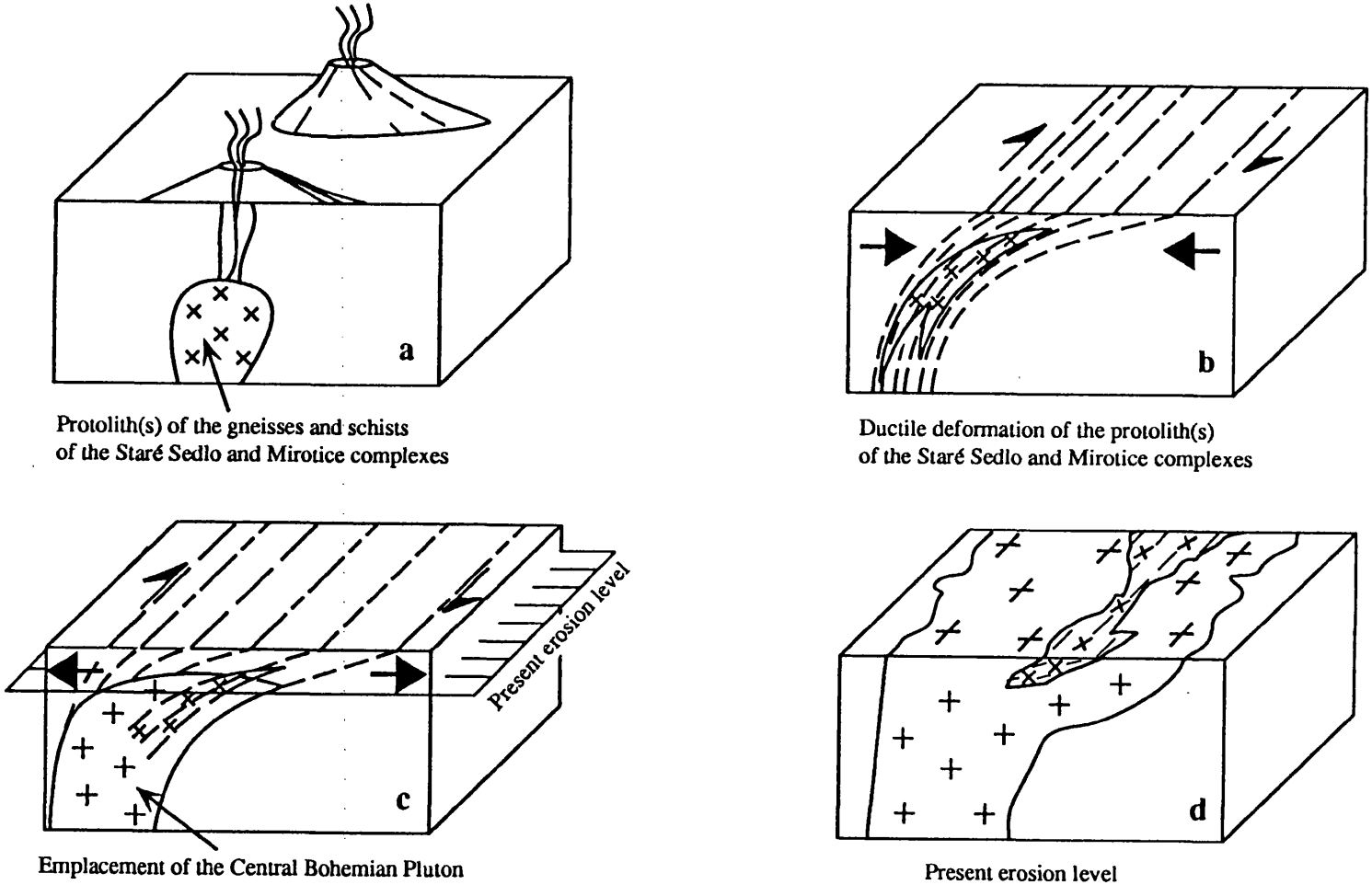

Fig.9.5

Evolution of Staré Sedlo and Mirotice complexes as roof pendants in the Central Bohemian Pluton; (a) mid - late Devonian arc-type plutonism - intrusion of tonalitic - granodioritic magma; (b) ductile deformation between mid - late Devonian plutonism and early Carboniferous plutonism; (c) early Carboniferous plutonism controlled by the pre-existing shear zone; (d) present state after erosion revealing the juxtaposition of the mid - late Devonian and early Carboniferous plutonic rocks; movement directions are from *Rajlich (1987)*.

10. SUMMARY OF RESULTS

The petrological, geochemical and isotopic evidence presented in this thesis gives an explanation for magmatic and metamorphic activity and sheds more light on least part of the Hercynian episode in the Moldanubian zone in the Bohemian Massif. It also shows that much work remains to be done in order to understand fully the precise timing of and mechanisms operative during different events which led to the present nature of the Hercynian orogen. This future work will need to take into account the following main conclusions of the present study.

1. Within the southern part of the Bohemian Massif there are metamorphic complexes (Staré Sedlo and Mirotice) with the gross form of the roof pendants of the late Hercynian granitoids of the Central Bohemian Pluton. They consist of strongly foliated mylonitic biotite- and amphibole-bearing gneisses associated with K-feldspar-bearing schists. These rocks are cut by minor intrusions of amphibolite and meta-aplite (cf. Chapters 1 and 2).

2. The petrographical, geochemical and isotopic data are consistent with the rocks of these complexes having igneous protoliths corresponding to tonalite - granodiorite and alkali feldspar granite (rhyolite) for the gneisses and schists, respectively (cf. Chapters 2, 4, 6 and 8).

3. Zircon U - Pb isotopic study indicates a crystallization age for the plutonic protolith of the Staré Sedlo and Mirotice gneisses in mid - late Devonian times (380 - 365 Ma; cf. Chapter 6).

4. Both the whole-rock chemical compositions and the depleted Sr and Nd isotopic signatures of the gneisses and schists suggest that their protoliths were derived from a depleted mantle source without a long crustal history before their crystallization. Their compositions are consistent with their derivation from a magmatic arc-type regime. However the composition of some of the gneisses indicates some contamination of their parent magma with crustal (sedimentary) material (cf. Chapters 4, 7 and 8).

5. The calculated $T_{Nd(DM)}$ model ages for the gneisses and schist cannot be related to any geological event. However, assuming that the composition of HT eclogites from the Moldanubian zone corresponds to that of mantle source of the Staré Sedlo and Mirotice gneisses and schists, their corresponding crystallization ages and depleted OIB-like isotopic compositions indicate the growth of continental crust within the Moldanubian zone in the Bohemian Massif in mid - late Devonian times (cf. Chapter 8).

6. The petrographical study of the gneisses, schists and amphibolites and the chemistry of their rock-forming minerals indicate that the origin of the foliation in rocks of the Staré Sedlo and Mirotice complexes resulted from ductile deformation and mylonitization. In parts there is the evidence for an early Carboniferous thermal overprint by the adjacent granitoids of the Central Bohemian Pluton (cf. Chapters 2, 3 and 5).

7. A mineral - whole-rock Rb - Sr isotopic study indicates that the ductile deformation took place at ca 340 - 330 Ma, shortly before the emplacement of the early Carboniferous granitoids of the Central Bohemian Pluton (cf. Chapter 7).

8. The ductile deformation of the protolith of gneisses had only a very limited effect on the U - Pb isotopic system in zircons. It resulted in a small loss of Pb due to the fracturing of zircons and leaching along the cracks (cf. Chapter 6).

9. The generally sub-horizontal disposition of the mylonitic - gneissic fabric in the Staré Sedlo complex is interpreted as being on a flat in a major listric thrust zone with a staircase-like trajectory. The emplacement and gross shape of the Central Bohemian Pluton are interpreted as having been controlled by a steeply-disposed ramp (or several ramps) through more competent units, with earlier intrusions of this composite body overlapping in time the later part of the phase of ductile deformation (cf. Chapters 7 and 9).

10. The overall temporal correspondence and spatial association of the gneisses and schists from the Staré Sedlo and Mirotice complexes with eclogites and granulites from the Moldanubian zone together with their isotopic compositions suggests that all these rocks represent products of the same tectonomagmatic regime. Subsequently there was divergence in their post-magmatic histories (cf. Chapter 9).

11. The age and chemical and isotopic signatures of the gneisses and schists from the Staré Sedlo and Mirotice complexes suggest that within the framework of a plate tectonic model for the Hercynian orogeny they can be correlated with products of an arc type magmatism on the southern margin of Armorica (Liguro - Moldanubian Cordillera; cf. Chapter 9).

11. REFERENCES

Aftalion M., Bowes D.R., Vrána S. (1989): Early Carboniferous U - Pb zircon age for garnetiferous, perpotassic granulites, Blanský les massif, Czechoslovakia.- N. Jb. Miner. Mh., **1989**, 145-152.

Allègre C.J., Albarède F., Grünenfelder M., Köppel V. (1974): $^{238}U/^{206}Pb$ - $^{235}U/^{207}Pb$ - $^{232}Th/^{208}Pb$ zircon geochronology in alpine and non-alpine environment.- Contrib. Mineral. Petrol., **43**, 163-194.

Andrusov D. (1932): 1:600 000 Geological map of Vltava region: Zvíkov to Orlík (in Czech).- Věst. St. geol. Úst. Čs. Rep., **8**, 1, 35-38.

Arndt N.T., Goldstein S.L. (1987): Use and abuse of crust-formation ages.- Geology, **15**, 893-895.

Arnold A., Scharbert H.G. (1973): Rb - Sr-Alterbestimmungen an Granuliten der südlichen Böhmischen Masse in Österreich.- Schweiz. Min. Petr. Mitt., **53**, 61-78.

Batchelor R.A., Bowden P. (1985): Petrogenetic interpretation of granitoid rock series using multicationic parameters.- Chem. Geol., **48**, 43-55.

Bea F. (1980): Geochemistry of biotites in an assimilation process: an approach to recognition of metamorphic biotites from magmatic occurence.- Krystalinikum, **15**, 103-124.

Beach A. (1973): The mineralogy of the high temperature shear zones at Scourie, NW Scotland.- J. Petrol., **14**, 231-248.

Beard B.L., Medaris L.G., Johnson C.M., Brueckner H.K., Mísař Z. (1992): Petrogenesis of Variscian high-temperature group A eclogites from the Moldanubian Zone of the Bohemian Massif, Czechoslovakia.- Contrib. Mineral. Petrol., **111**, 468-483.

Beard B.L., Medaris L.G., Johnson C.M., Mísař Z., Jelínek E. (1991): Nd and Sr isotope geochemistry of Moldanubian eclogites and garnet peridotites, Bohemian massif, Czechoslovakia.- Terra Abstracts, **6**, 4.

Bell T.H., Etheridge M.A. (1973): Microstructure of mylonites and their descriptive terminology.- Lithos, **6**, 337-348.

Bendl J., Vokurka K. (1989): Strontium isotope model of formation of Blatná granodiorite.- Geol. Carp., **40**, 655-664.

Bendl J., Vokurka K., Sundvoll B. (1993): Strontium and neodymium isotope study of Bohemian basalts.- Mineralogy and Petrology, **48**, 35-45.

Bergner R., Hofmann J., Dubanský A., Gunia T., Wojcziechowska I., Hofmann J., Köhler H., Povondra P., Scharbert S., Zoubek V. (1988): Isotopic ages obtained from Precambrian complexes in the Bohemian Massif.- In: Zoubek V. (ed.): Precambrian in younger fold belts, John Willey and Sons, Chichester, 305-325.

Bernard-Griffiths J., Peucat J.J., Sheppard S., Vidal P. (1985): Petrogenesis of Hercynian leucogranites from the southern Armorician Massif: contribution of REE and isotopic (Sr, Nd, Pb and O) geochemical data to the study of source rock characteristics and ages.- Earth Planet. Sci. Lett., **74**, 235-250.

Bhattacharya A., Mohanty L., Maji A., Sen S.K., Raith M. (1992): Non-ideal mixing in the phlogopite-annite binary: constraints from experimental data on Mg-Fe partitioning and a reformualtion of the biotite-garnet geothermometer.- Contrib. Mineral. Petrol., **111**, 87-93.

Blundy J.D., Holland T.J.B. (1990): Calcic amphibole equilibria and a new amphibole - plagioclase geothermometer.- Contrib. Mineral. Petrol., **104**, 208-224.

Blundy J.D., Holland T.J.B. (1992a): "Calcic amphibole equilibria and a new amphibole - plagioclase geothermometer": reply to the comments of Hammastrom and Zen, and Rutherford and Johnson.- Contrib. Mineral. Petrol., **111**, 269-272.

Blundy J.D., Holland T.J.B. (1992b): "Calcic amphibole equilibria and a new amphibole - plagioclase geothermometer" - reply to the comment of Poli and Schmidt.- Contrib. Mineral. Petrol., **111**, 278-282.

Boullier A.M. (1980): A preliminary study on the behaviour of brittle minerals in a ductile matrix: example of zircons and feldspars.- J. Struct. Geol., **2**, 211-217.

Bouška V., Jelínek E., Pačesová M., Řanda Z., Ulrych J. (1984): Rare earth elements and other trace elements in the rocks of the Central Bohemian Pluton.- Geol. Carp., **35**, 355-376.

Bouška V. (1968): On the original rock source of tectites.- Lithos, **1**, 102-112.

Bowes D.R. (1992): Age of tectonothermal activity in the southwestern part of the Scottish Caledonides and its significance in studies of Palaeozoic history of the Bohemian Massif.- In: Kukal Z. (ed.): Proceedings of the 1st International Conference on the Bohemian Massif, Czech Geological Survey, Prague, 33-35.

Bowes D.R., Aftalion M. (1991): U - Pb zircon isotopic evidence for early Ordovician and late Proterozoic units in the Mariánské Lazně complex, Central European Hercynides.- N. Jb. Miner. Mh., **1991**, 315-326.

Bowes D.R., Košler J. (1993): Geochemical comparison of the subvolcanic appinite suite of the British Caledonides and the durbachite suite of the Central European Hercynides: evidence for associated shoshonitic and granitic magmatism.- Mineralogy and Petrology, **48**, 47-63.

Boynton W.V. (1984): Cosmochemistry of the rare earth elements: meteorite studies.- In: Henderson P. (ed.): Rare earth element geochemistry, Elsevier, Amsterdam, 63-114.

Brodie K.H., Rutter E.H. (1985): On the relationship between deformation and metamorphism, with special reference to the behaviour of basic rocks.- In: Thompson A.B., Rubie D.C. (eds): Metamorphic reactions, kinetics, textures, and deformation, Springer Verlag, New York, 138-179.

Brown E.H. (1977): The crossite content of Ca-amphibole as a guide to pressure of metamorphism.- J. Petrol., **18**, 53-72.

Brown G.C. (1982): Calc-alkaline intrusive rocks, their diversity, evolution and relation to volcanic arcs.- In: Thorpe R.S. (ed.): Andesites, John Wiley & Sons, New York, 437-461.

Brown W.L., Parsons I. (1981): Towards a more practical two-feldspar geothermometer.- Contrib. Mineral. Petrol., **76**, 369-377.

Brueckner H.K., Medaris L.G., Bakun-Czubarov N. (1991): Nd and Sr age and isotope patterns from Variscian eclogites of the eastern Bohemian Massif.- N. Jb. Miner. Abh., **163**, 169-196.

Bryan W.B., Finger L.W., Chayes F. (1969): Estimating proportions in petrographic mixing equations by least squares approximation.- Science, **163**, 926-927.

Burkhard D.J.M. (1991): Temperature and redox path of biotite-bearing intrusives: a method of estimation applied to S- and I-type granites from Australia.- Earth Planet. Sci. Lett., **104**, 89-98.

Cambel B., Vilinovič V. (1987): Geochemistry and petrology of the granitoid rocks of the Malé Karpaty Mts.- Veda, Bratislava, 247pp.

Carswell D.A., Jamtweit B. (1990): Variscian Sm-Nd ages for the high-pressure metamorphism in the Moldanubian Zone of the Bohemian Massif, Lower Austria.- N. Jb. Miner. Abh., **162**, 69-78.

Cawthorn R.G. (1976): Some chemical controls on igneous amphibole compositions.- Geochim. Cosmochim. Acta, **40**, 1319-1328.

Chappell B.W., White A.J.R. (1974): Two contrasting granite types.- Pacif. Geol., **8**, 173-174.

Chappell B.W., White A.J.R. (1983): Granitoid types and their distribution in the Lachlan Fold Belt, southeastern Australia.- Geol. Soc. Amer. Mem., **159**, 21-34.

Chappell B.W., White A.J.R. (1992): I- and S-type granites in the Lachlan Fold Belt.- Trans. R. Soc. Edinburgh Earth Sci., **83**, 1-26.

Chlupáč I. (1981): Stratigraphy and facial evolution of metamorphosed Palaeozoic in the Sedlčany - Krásná Hora metamorphic islet (in Czech).- Věst. Ústř. úst. geol., **55**, 225-232.

Chlupáč I. (1986): Silurian in the Sedlčany - Krásná Hora metamorphic islet (in Czech).- Věst. Ústř. úst. geol., **61**, 1-10.

Chlupáč I. (1989): Stratigraphy of the Sedlčany - Krásná Hora metamorphic islet in Bohemia (Proterozoic? to Devonian).- Čas. Miner. Geol., **34**, 1-16.

Cimbalníková A., Palivcová M., Hejl V., Maštalka A. (1976): Biotite in tonalites and their basic xenolites (Teletín quarry, Central Bohemian pluton).- Acta Univ. Carol. Geol., **1976**, 1-20.

Cliff R.A. (1985): Isotopic dating in metamorphic belts.- J. Geol. Soc. London, **142**, 97-110.

Condie, K. (1973): Archean magmatism and crustal thickening.- Geol. Soc. Amer. Bull., **84**, 2981-2972.

Condie, K. (1981): Archean greenstone belts.- Elsevier, Amsterdam, 434pp.

Cox K.G., Bell J.D., Pankhurst R.J. (1979): The interpretation of igneous rocks.- Unwin Hyman, London, 450pp.

Cross T.A., Pilger R.H. (1982): Controls of subduction geometry, location of magmatic arcs, and tectonics of arc and back-arc regions.- Bull. Geol. Soc. Amer., **93**, 545-562.

Cullers R.L., Graf J.L. (1984): Rare earth elements in igneous rocks of the continental crust: intermediate and silic rocks.- In: Henderson P. (ed.): Rare earth element geochemistry, Elsevier, Amsterdam, 275-316.

Czamanske G.K., Ishihara S., Atkin S.A. (1981): Chemistry of rock-forming minerals of the Cretaceous - Paleocene batolith in southwestern Japan and implications for magma genesis.- J. Geophys. Res., **86**, B11, 10431-10469.

Davis G.A., Anderson J.L., Frost E.G., Schackelford T.J. (1980): Mylonitization and detachment faulting in the Whipple-Buckskin-Rawhide Mountain terrrane, southern California and western Arizona.- In: Crittenden M., Davis G.H., Coney P.J. (eds): Cordilleran metamorphic core complexes, Geol. Soc. Amer. Mem., **153**, 79-129.

Davis J.C. (1973): Statistics and data analysis in geology.- John Willey & Sons, New York, 568pp.

De Jongh W.K. (1973): X-ray fluorescence analysis aplying theoretical matrix corrections.- X-ray Spectrometry, **2**, 151-158.

De la Roche H., Letterier J., Grand Claude P., Marchal M. (1980): A classification of volcanic and plutonic rocks using R1-R2 diagrams and major element analyses - its relatioships with current nomenclature.- Chem. Geol., **29**, 183-210.

Deer W.A., Howie R.A., Zussman J. (1962): Rock-forming minerals, Vol.1.- Longmans, London, 77-112.

DePaolo D.J. (1981): Trace element and isotopic effects of combined wallrock assimilation and fractional crystallization.- Earth Planet. Sci. Lett., **53**, 189-202.

DePaolo D.J. (1988): Neodymium isotope geochemistry.- Springer Verlag, Berlin, 187pp.

Dornsiepen U.F. (1978): Rb - Sr whole rock ages within the European Hercynian. A review.- Krystalinikum, **14**, 39-49.

Dörr W., Fišera M., Franke W. (1992): Cadomian magmatic events in the Bohemian Massif - U - Pb data from felsic magmatic pebbles.- Styles of superposed Variscian nappe tectonics, 7th geological workshop abstracts, Kutná Hora, Czechoslovakia.

Drake M.J., Weill D.F. (1972): New rare earth element standards for electron microprobe analysis.- Chem. Geol., **10**, 179-181.

Dudek A., Jelínek E., Nekovařík C. (1988): Geochronological data from the Bohemian Massif (in Czech).- MS Charles University, Prague, 1-16.

Dunning G.R., Krogh T.E. (1985): Geochronology of ophiolites of the Newfoundland Appalachian.- Can. J. Earth Sci., **22**, 1659-1670.

El Bouseily A.M., El Sokkary A.A. (1975): The relatioship between Rb, Ba and Sr in granite rocks.- Chem. Geol., **16**, 207-219.

Ellenberger F., Tamain A.L.G. (1980): Hercynian Europe.- Episodes, **1980**, 22-27.

Elliott D., Johnson M.R.W. (1980): Structural evolution in the northern part of the Moine thrust belt, NW Scotland.- Trans. R. Soc. Edinburgh Earth Sci., **71**, 69-96.

Faure G. (1986): Principles of isotope geology.- John Wiley & Sons, 2nd ed., New York, 589pp.

Fediuk F. (1976): The Bechyně "orthogneiss": an anatectic type of Moldanubian orthogneissoids.- Acta Univ. Carol. Geol., **1976**, 187-207.

Ferry J.M., Spear F.S. (1978): Experimental calibration of the partitioning of Fe and Mg between biotite and garnet.- Contrib. Mineral. Petrol., **66**, 113-117.

Finger F., Steyer H.P. (1990): I-type granitoids as indicators of a late Paleozoic convergent ocean-continent margin along the southern flank of the Central European Variscian orogen.- Geology, **18**, 1207-1210.

Finger F., Steyer H.P. (1991): Comments and Replies on "I-type granitoids as indicators of a late Paleozoic convergent ocean-continent margin along the southern flank of the Central European Variscian orogen".- Geology, **19**, 1245-1246.

Foster M.D. (1960): Interpretation of the composition of trioctahedral micas.- U.S. Geol. Surv. Prof. Pap., **354B**, 11-49.

Ganguly J., Saxena S.K. (1984): Mixing properties of aluminosilicate garnets: constraints from natural and experimental data, and applications to geothermo-barometry.- Amer. Miner., **69**, 88-97.

Gebauer D., Grünenfelder M. (1979): U - Pb zircon and Rb - Sr dating of eclogites and their country rocks. Example: Münchberg gneiss massif, Northeast Bavaria.- Earth Planet. Sci. Lett., **42**, 35-44.

Ghose S. (1965): A scheme of cation distribution in the amphibole.- Min. Mag., **35**, 46-54.

Gilbert M.C., Helz R.T., Popp R.K., Spear F.S. (1982): Experimental studies of amphibole stability.- Reviews in mineralogy, **9B**, 229-354.

Giletti B.J. (1991): Rb and Sr diffusion in alkali feldspars, with implications for cooling histories of rocks.- Geochim. Cosmochim. Acta, **55**, 1331-1343.

Gorokhov I.M., Losert I., Varshavskaya E.S., Kutyavin E.P., Melnikov N.N., Cekulayev V.P. (1979): Rb - Sr geochronology of metamorphic rocks from eastern part of the Bohemian Massif (Železné hory Mts and adjacent Bohemian - Moravian Highlands).- In: Afanasjev T.D. (ed.): Opyt korelatsii magmaticheskikh porod Czechoslovakii i nekotorych rayonov SSSR (in Russian), Nauka, Moscow, 81-100.

Govindaraju K. (1989): Compilation of working values and sample description for 272 geostandards.- Geostand. Newslett., **13**, 1-113.

Grauch R.I. (1989): Rare earth elements in metamorphic rocks.- Reviews in mineralogy, **21**, 147-168.

Gregerová M., Suk M. (1991): Suggestions for nomenclature of metamorphic rocks (in Czech).- Gabriel, Prague, 186pp.

Gromet L.P., Silver L.T. (1983): Rare earth element distribution among minerals in a granodiorite and their petrogenetic implications.- Geochim. Cosmochim. Acta, **47**, 925-939.

Hackler R.T., Wood B.J. (1989): Experimental determination of Fe and Mg exchange between garnet and olivine and estimation of Fe-Mg garnet mixing properties.- Amer. Miner., **74**, 994-999.

Hammastrom J.M., Zen E-An. (1986): Aluminium in hornblende: an empirical igneous geobarometer.- Amer. Miner., **71**, 1297-1313.

Hammastrom J.M., Zen E-An. (1992): Discussion of Blundy and Holland's (1990) "Calcic amphibole equilibria and a new amphibole - plagioclase geothermometer.- Contrib. Mineral. Petrol., **111**, 264-268.

Hanson G.N. (1978): The application of trace elements to the igneous rocks of granitic composition.- Earth Planet. Sci. Lett., **38**, 26-43.

Harmon R.S., Barreiro B.A., Moorbath S., Hoefs J., Francis P.W., Thorpe R.S., Deruelle B., McHugh J., Viglino J.A. (1984): Regional O-, Sr- and Pb-isotope relationships in late Cenozoic calc-alkaline lavas of the Andean Cordillera.- J. Geol. Soc. London, **141**, 803-822.

Harrison T.M., Aleinikoff J.N., Compston W. (1987): Observations and controls on the occurrence of inherrited zircon in Concord-type granitoids, New Hampshire.- Geochim. Cosmochim. Acta, **51**, 2549-2558.

Hart S.R., Brooks C., Krogh T.E., Davis G.L., Nava L. (1970): Ancient and modern volcanic rocks: a trace element model.- Earth Planet. Sci. Lett., **10**, 17-28.

Hart S.R., Reid M.R. (1991): Rb/Cs fractionation: A link between granulite metamorphism and the S-process.- Geochim. Cosmochim. Acta, **55**, 2379-2383.

Harvey P.K., Atkin B.P. (1982): The estimation of mass absorption coefficients by Compton scattering: extensions to the use of RhKα Compton radiation and intensity ratios.- Amer. Mineral., **67**, 534-537.

Harvey P.K., Taylor D.M., Hendry R.D., Bancroft F. (1973): An accurate fusion method for the analysis of rocks and chemically related materials by x-ray fluorescence spectrometry.- X-ray Spectrometry, **2**, 33-34.

Haugerud R.A., van der Heyden P., Tabor R.W., Stacey J.S., Zartman R.E. (1991): Late Cretaceous and early Tertiary plutonism and deformation in the Skagit Gneiss Complex, North Cascade Range, Washington and British Columbia.- Geol. Soc. Amer. Bull., **103**, 1297-1307.

Hawkesworth C.J., Ellam R.M. (1989): Chemical fluxes and wedge replenishment rates along recent destructive plate margins.- Geology, **17**, 46-49.

Hawkesworth C.J., Kempton P.D., Rogers N.W., Ellam R.M., van Calsteren P.W. (1990): Continental mantle litosphere and shallow level enrichment processes in the Earth's mantle.- Earth Planet. Sci. Lett., **26**, 256-268.

Heier K.S. (1973): Geochemistry of granulite facies rocks and problems of their origin.- Phil. Trans. R. Soc. London, **A273**, 429-442.

Heier K.S., Billings G.K. (1978): Potassium.- In: Wedepohl K.H. (ed.): Handbook of Geochemistry, Springer Verlag, Berlin.

Hickey R.L.F., Frey F.A., Gerlach D.C. (1986): Multiple sources for basaltic arc rocks from the southern volcanic zone of the Andes (34-41^{o}S): trace element and isotopic evidence for contributions from subducted oceanic crust, mantle and continental crust.- J. Geophys. Res., **91**, 5963-5983.

Higgins M.W. (1971): Cataclastic rocks.- U.S. Geol. Surv. Prof. Pap., **687**, 1-97.

Hodges K.V., Spear F.S. (1982): Geothermometry, geobarometry and the Al_2SiO_5 triple point at Mt Moosilauke, New Hampshire.- Amer. Miner., **67**, 1118-1134.

Hoffman A.W., White W.M. (1983): Ba, Rb and Cs in the Earth's mantle.- Z. Naturforsch., **38a**, 256-266.

Holl P.K., von Drach V., Müller-Sohnius D., Köhler H. (1989): Caledonian ages in Variscian rocks: Rb - Sr and Sm - Nd isotopic variations in dioritic intrusives from the nortwestern Bohemian Massif, West Germany.- Tectonophysics, **157**, 179-194.

Hollister L.S., Grissom G.C., Peters E.K., Stowell H.H., Sisson V.B. (1987): Confirmation of the empirical correlation of Al in hornblende with pressure of solidification of calc-alkaline plutons.- Amer. Miner., **72**, 231-239.

Holub F. (1989): Durbachite.- In: Bowes D.R. (ed.): Encyclopedia of igneous and metamorphic petrology, Van Nostrand Reinhold, New York, 133-134.

Holub F., Žežulková V. (1978): Relative ages of intrusives of the Central Bohemian Pluton near Zvíkov.- Věst. Ústř. úst. geol., **53**, 289-297.

Hooker P.J., O'Nions R.K., Pankhurst R.J. (1975): Determination of rare-earth elements in USGS standard rocks by mixed-solvent ion exchange and mass-spectrometric isotope dilution.- Chem. Geol., **16**, 189-196.

Hopgood A.M. (1984): Structural evolution of Svecocarelian migmatites, southern Finland: a study of Proterozoic crustal development.- Trans. R. Soc. Edinburgh Earth Sci., **74** (for 1983), 229-264.

Hopgood A.M., Bowes D.R. (1987): Structural succession and tectonic history of the gneiss - amphibolite - granulite - mantle peridotite association near the eastern margin of the Moldanubian zone, Central European Hercynides.- Acta Univ. Carol. Geol., **1987**, 51-88.

Humphris S.E. (1984): The mobility of the rare earth elements in the crust.- In: Henderson P. (ed.): Rare earth element geochemistry, Elsevier, Amsterdam, 317-342.

Hutton D.H.W. (1988): Granite emplacement mechanisms and tectonic controls: inferences from deformation studies.- Trans. R. Soc. Edinburgh Earth Sci., **79**, 245-255.

Hutton D.H.W. (1992): Granite sheeted complexes: evidence for the dyking ascent mechanism.- Trans. R. Soc. Edinburgh Earth Sci., **83**, 377-382.

Hutton D.H.W., Dempster T.J., Brown P.E., Becker S.M. (1990): A new mechanism of granite emplacement: intrusion in active extensional shear zones.- Nature, **343**, 452-455.

Hutton D.H.W., Ingram G.M. (1992): The Great Tonalite Sill of southeastern Alaska and British Columbia: emplacement into an active contractional high angle reverse shear zone.- Trans. R. Soc. Edinburgh Earth Sci., **83**, 383-386.

Jacobsen S.B., Wasserburg G.J. (1980): Sm - Nd evolution of chondrites.- Earth Planet. Sci. Lett., **50**, 139-155.

Jaffey A.H., Flynn K.F., Glendenin L.E., Bentley W.C., Essing A.M. (1971): Precision measurement of half-lives and specific activities of ^{235}U and ^{238}U.- Phys. Rev. C**4**, 1889-1906.

Jäger E. (1979): Introduction to geochronology.- In: Jäger E., Hunziker J.C. (eds): Lectures in isotope geology, Springer Verlag, Berlin, pp 1-12.

Jakeš P. (1977): Geochemical characteristics of various rock types within the Central Bohemian Pluton (in Czech).- MS P117/1977, Czech Geological Survey, Prague, 1-16.

Jakeš P. (1984): Rare earth elements - myth and reality.- Mineralia Slov., **16**, 283-301.

Jakeš P., White A.J.R. (1972): Major and trace element abundances in volcanic rocks of orogenic areas.- Geol. Soc. Amer. Bull., **83**, 29-40.

Jarvis I. (1992): Sample preparation for ICP-MS.- In: Jarvis K.E., Gray A.L., Houk R.S. (eds): Handbook of inductively coupled plasma mass spectrometry, Blackie, Glasgow, 172-224.

Jarvis K.E. (1988): Inductively coupled plasma mass spectrometry: a new technique for the rapid or ultra-trace level determination of the rare-earth elements in geological materials.- Chem. Geol., **68**, 31-39.

Johnson M.C., Rutherford M.J. (1989): Experimental calibration of the aluminium-in-hornblende geobarometer with application to Long Valley caldera (California) volcanic rocks.- Geology, **17**, 837-841.

Jokély J. (1855): Geognostische Verhältnisse in einem Theile des mittleren Böhmen.- Jb. K. Kön. geol. Reichsanst., **6**, 305-404.

Kettner R. (1930a): The position of metamorphic islets within the Central Bohemian Granitic Massif (in Czech).- Sbor. Stát. Geol. Úst. Čs. rep., **9**, 301-332.

Kettner R. (1930b): Geology of the Central Bohemian Granitic Massif (in Czech).- Příroda, **23**, 431-437.

Klečka M. (1989): Petrological and structural investigation of the Stráž type orthogneisses in Moldanubicum (in Czech).- Zpr. geol. výzk., **1987**, 68-70.

Knowles C.R. (1987): A basic program to recast garnet end-members.- Comp. Geosci., **13**, 655-658.

Kodym O. (1956): Geological mapping in the Blatná and Strakonice regions: a report (in Czech).- Zpr. geol. výzk., **1955**, 88-89.

Kodym O. ed. (1963): Geological map of CSSR 1:200 000 M-33-XXI Tábor: Comments (in Czech).- Czech Geological Survey, Prague.

Kodym O., Suk M. (1958): Geology and petrography of Blatná and Strakonice regions (in Czech).- Geol. Práce, Zpr. **50**, Bratislava.

Köhler, A., Raaz, F. (1951): Über eine neue berechnung und graphische Darstellung von Gesteinanalysen.- N. Jb. Miner. Mh., **1951**, 247-263.

Košler J. (1988): Geochemistry of the Central Bohemian Islet Zone.- Thesis, MS Charles University, Prague, 108pp.

Košler J., Aftalion M., Bowes D.R. (1993): Mid - late Devonian plutonic activity in the Bohemian Massif: U - Pb zircon isotopic evidence from the Staré Sedlo and Mirotice gneiss complexes, Czechoslovakia.- N. Jb. Miner. Mh., **1993**, in press.

Košler J., Rogers G., Bowes D.R. (1993): Rb - Sr isotopic evidence for early Carboniferous ductile deformation in the Hercynides of the southern part of the Bohemian Massif, Czech Republic.- MS submitted for publication.

Kreuzer H., Seidel E., Schussler U., Okrusch M., Lenz K.L., Raschka H. (1989): K - Ar geochronology of different tectonic units at the northwestern margin of the Bohemian Massif.- Tectonophysics, **157**, 149-178.

Kreuzer H., Vejnar Z., Schussler U., Okrusch M., Seidel E. (1992): K - Ar dating in the Teplá - Domazlice zone at the western margin of the Bohemian Massif.- In: Kukal Z. (ed.): Proceedings of the 1st International Conference on the Bohemian Massif, Czech Geological Survey, Prague, 168-175.

Krogh T.E. (1973): A low contamination method for hydrothermal decomposition of zircon and extraction of U and Pb for isotopic age determinations.- Geochim. Cosmochim. Acta, **37**, 485-494.

Kröner A., Wendt I., Liew T.C., Compston W., Todt W., Fiala J., Vaňková V., Vaněk J. (1988): U - Pb zircon and Sm - Nd model ages of high-grade Moldanubian metasediments, Bohemian Massif, Czechoslovakia.- Contrib. Mineral. Petrol., **99**, 257-266.

Kullerud L. (1991): On the calculation of isochrons.- Chem. Geol., **87**, 115-124.

Laird J., Abee A.L. (1981): Pressure, temperature and time indicators in mafic schist: their applications to reconstructing the polymetamorphic history of Vermont.- Amer. J. Sci., **281**, 127-175.

Lang M. (1990): Distribution of Or-component in plagioclase of some orthogneisses and migmatites of the Bohemian Massif.- Acta Univ. Carol. Geol., **1990**, 1-8.

Lang M., Cimbalníková A., Kašpar P., Palivcová M., Pivec E., Ulrych J. (1978): Rocks of the Teletín quarries: petrology of the intrusive contact of tonalite near Teletín.- Studie ČSAV, 3, Academia, Prague, 110pp.

Le Maitre R.W. (1989): A classification of igneous rocks and glossary of terms.- Blackwell, Oxford, 193pp.

Leake B.E. (1965): The relationship between composition of calciferous amphibole and grade of metamorphism.- In: Pitcher W.S., Flinn G.W. (eds): Controls of metamorphism, Oliver & Boyd, Edinburgh, 299-318.

Leake B.E. (1971): On aluminous and edenitic hornblende.- Min. Mag., **38**, 389-407.

Leake B.E. (1978): Nomenclature of amphiboles.- Min. Mag., **42**, 533-563.

Leake B.E., Hendry G.L., Kemp A., Plant A.G., Harvey P.K., Wilson J.R., Coats J.S., Aucott J.W., Lünel T., Howarth R.J. (1969): The chemical analysis of rock powders by automatic x-ray fluorescence.- Chem. Geol., **5**, 7-86.

Leeder M.R. (1982): Upper Palaeozoic basins of the British Isles - Caledonide inheritance versus Hercynian plate margin processes.- J. Geol. Soc. London, **139**, 479-491.

Liew T.C., Finger F., Höck V. (1989): The Moldanubian granitoid plutons of Austria: Chemical and isotopic studies bearing on their environmental setting.- Chem. Geol., **76**, 41-55.

Liew T.C., Hofmann A.W. (1988): Precambrian crustal components, plutonic associations, plate-environment of the Hercynian Fold Belt of central Europe: Indications from Nd and Sr isotopic study.- Contrib. Mineral. Petrol., **98**, 129-138.

Lloyd G.E. (1987): Atomic number and crystallographic contrast images with the SEM: a review of backscattered electron techniques.- Min. Mag., **51**, 3-19.

Lyons P.C.(1976): IUGS classification of igneous rocks: A critique.- Geology, **4**, 425-426.

Macintyre R.M., Bowes D.R., Hamidullah S., Onstott T.C. (1992): K - Ar and Ar - Ar isotopic study of amphiboles from meta-ophiolite complexes, eastern Bohemian Massif.- In: Kukal Z. (ed.): Proceedings of the 1st International Conference on the Bohemian Massif, Czech Geological Survey, Prague, 195-199.

Matějka D. (1980): Geochemistry of Proterozoic rocks near Svojšín and Neveklov (in Czech).- Thesis, MS Charles University, Prague, 68pp.

McCulloch M.T., Chappell B.W. (1982): Nd isotopic characteristics of S- and I-type granites.- Earth Planett. Sci. Lett., **58**, 51-64.

McCulloch M.T., Wasserburg G.J. (1978): Sm - Nd and Rb - Sr chronology of continental crust formation.- Science, **200**, 1003-1011.

Melín M. (1988): Geochemistry and petrology of Blatná and Červená granodiorites in the Horažďovice region (in Czech).- Thesis, MS Charles University, Prague, 48 pp.

Michard A., Gurriet P., Soudant M., Albarède F. (1985): Nd isotopes in French Phanerozoic shales: external vs internal aspects of crustal evolution.- Geochim. Cosmichim. Acta, **49**, 601-610.

Mielke P., Winkler H.G.F. (1979): Eine bessere Berechnung der Mesonorm für granitische Gesteine.- N. Jb. Miner. Mh., **1979**, 471-480.

Minařík L., Cimbálníková A., Ulrych J. (1988): Coexisting amphibole-biotite pairs in durbachitic rocks of the Central Bohemian Pluton.- Acta Univ. Carol. Geol., **1988**, 259-287.

Mísař Z. ed. (1983): Gelogy of CSSR I. Bohemian Massif (in Czech).- SPN, Prague, 333pp.

Mrázek P. (1963): New geological data from the Sedlčany - Krásná Hora metamorphic islet (in Czech).- Zpr. geol. výzk., **1963**, 25-27.

Mueller R.F. (1972): Stability of biotite: a discussion.- Amer. Miner., **57**, 300-316.

Němec D., Páša J. (1986): Regionally metamorphosed greisens of the Moldanubicum.- Mineral. Deposita, **21**, 12-21.

O'Brien P.J., Röhr C., Okrusch M., Patzak M. (1992): Eclogite facies relics and a multistage breakdown in metabasites of the KTB pilot hole, NE Bavaria: implications for the Variscian tectonometamorphic evolution of the NW Bohemian Massif.- Contrib. Mineral. Petrol., **112**, 261-278.

Palivcová M. (1984): Basic series of an andinotype batholitic association in the variscian Central Bohemian Pluton.- Geol. Carp., **35**, 39-60.

Palivcová M., Franke W. (1982): Shear zones in granitoids as a structural control of the development of leucodioritic bodies (Central Bohemian Pluton).- Krystalinikum, **16**, 755-786.

Park A.F., Bowes D.R., Halden N.M., Koistinen T.J. (1984): Tectonic evolution at an early Proterozoic contionental margin: the Svecocarelides of eastern Finland.- J. Geodynamics, **1**, 359-386.

Patchett J., Kouvo O. (1986): Origin of continental crust of 1.9 - 1.76 Ga age: Nd isotopes and U - Pb zircon ages in the Svecocarelian terrain of South Finland.- Contrib. Mineral. Petrol., **92**, 1-12.

Paterson B.A., Rogers G., Stephens W.E. (1992): Evidence for inherited Sm-Nd isotopes in granitoid rocks.- Contrib. Mineral. Petrol., **111**, 378-390.

Paterson B.A., Stephens W.E., Herd D.A. (1989): Zoning in granitoid accessory minerals as revealed by backscattered electron imagery.- Min. Mag., **53**, 55-61.

Paterson B.A., Stephens W.E., Rogers G., Williams I.S., Hinton R.W., Herd D.A. (1992): The nature of zircon inheritance in two granite plutons.- Trans. R. Soc. Edinburgh Earth Sci., **83**, 459-471.

Paterson S.R., Vernon R.H., Tobisch O.T. (1989): A review of criteria for identification of magmatic and tectonic foliations in granitoids.- J. Struct. Geol., **11**, 349-363.

Patočka F. (1989): The European Hercynides in the plate tectonics theory (in Czech).- Rozpr. ČSAV, ř MPV, **99**, 4, 7-103.

Peacock M.A. (1931): Classification of igneous rock series.- J. Geol., **39**, 54-67.

Pearce J.A., Harris N.B.W., Tindle A.G. (1984): Trace element discrimination diagrams for the tectonic interpretation of granitic rocks.- J. Petrol., **25**, 956-983.

Perchuk L.L. (1970): Mineral equilibria of rock-forming minerals (in Russian).- Nauka, Moscow, 390pp.

Peucat J.J., Jegouzo P., Vidal P., Bernard-Griffiths J. (1988): Continental crust formation seen through the Sr and Nd isotope systematics of S-type granites in the Hercynian Belt of western France.- Earth Planet. Sci. Lett., **88**, 60-68.

Pidgeon R.T. (1992): Recrystallization of oscillatory zoned zircon: some geochronological and petrological implications.- Contrib. Mineral. Petrol., **110**, 463-472.

Pin C., Duthou J.L. (1990): Sources of Hercynian granitoids from the French Massif Central: Inferences from Nd isotopes and consequences for crustal evolution.- Chem. Geol., **83**, 281-296.

Poli S., Schmidt M.W. (1992): A comment on "Calcic amphibole equilibria and a new amphibole - plagioclase geothermometer" by J.D. Blundy and T.J.B. Holland (Contrib Mineral Petrol (1990) 104: 208-224).- Contrib. Mineral. Petrol., **111**, 273-282.

Poubová M. (1971): Optical and chemical characteristics of some hornblendes from the Central Bohemian Pluton.- Krystalinikum, **7**, 119-134.

Poubová M. (1974): Composition of amphiboles and rock type subdivisions in the Central Bohemian Pluton.- Krystalinikum, **10**, 149-169.

Povondra P. (1989): Geochemistry of micas from pegmatites and other rocks of the Bechyně orthogneissoid.- Acta Univ. Carol. Geol., **1989**, 127-138.

Powell R. (1984): Inversion of the assimilation and fractional crystallization (AFC) equations: Characterization of contaminants from isotope and trace element relationships in volcanic suites.- J. Geol. Soc. London, **141**, 447-452.

Pratt J.P. (1894): On the determination of ferrous iron in silicates.- Amer. J. Sci., **48**, 149-151.

Price J.G. (1985): Ideal site mixing in solid solutions, with an application to two-feldspar geothermometry.- Amer. Miner., **70**, 696-701.

Pupin J.P. (1980): Zircon and granite petrology.- Contrib. Mineral. Petrol., **73**, 207-220.

Putnis A., Fernandez-Diaz L., Prieto M. (1992): Experimentally produced oscillatory zoning in the $(Ba,Sr)SO_4$ solid solution.- Nature, **358**, 743-745.

Rajlich P. (1987): Variszische duktile Tektonik im Böhmische massif.- Geol. Rundch., **76**, 755-786.

Rajlich P. (1988): Tectonics of the NW border of the Central Bohemian Pluton and the Variscian transpression of the Bohemicum block structure.- Sbor. Geol. Věd G, **43**, 9-81.

Rajlich P., Schulmann K., Synek J. (1988): Strain analysis on conglomerates from the Central Bohemian Shear Zone.- Krystalinikum, **19**, 119-134.

Ramsay C.R. (1973): Controls of biotite zone mineral chemistry in Archaean meta-sediments near Yellowknitw, Northwest Territories, Canada.- J. Petrol., **14**, 467-488.

Rickwood P.C. (1968): On recasting analyses of garnet into end-member molecules.- Contrib. Mineral. Petrol., **18**, 175-198.

Riley J.P. (1958): Simultaneous determination of water and carbon dioxide in rocks and minerals.- Analyst, **83**, 42-49.

Robinson D., Leake B.E. (1975): Sedimentary and igneous trends on AFM diagrams.- Geol. Mag., **112**, 305-307.

Robinson P., Spear F.S., Schumacher J.C., Laird J., Klein C., Evans B.W., Doolan B.L. (1982): Phase relations of metamorphic amphiboles: natural occurence and theory.- Reviews in mineralogy, **9B**, 1-228.

Rogers G., Hawkesworth C.J. (1989): A geochemical traverse across the North Chilean Andes: evidence for crust generation from the mantle wedge.- Earth Planet. Sci. Lett., **91**, 271-285.

Romans P.A., Brown L.L., White J.C. (1975): An electron microprobe study of yttrium, rare earth and phosphorus distribution in zoned and ordinary zircon.- Amer. Miner., **60**, 475-480.

Rutherford M.J. (1973): The phase relations of aluminous iron biotites in the system $KAlSi_3O_8$ - $KAlSiO_4$ - Al_2O_3 - Fe - O - H.- J. Petrol., **14**, 159-180.

Rutherford M.J., Johnson M.C. (1992): Comment on Blundy and Holland's (1990) "Calcic amphibole equilibria and a new amphibole - plagioclase geothermometer".- Contrib. Mineral. Petrol., **111**, 266-268.

Saunders A.D., Norry M.J., Tarney J. (1988): Origin of MORB and chemically depleted mantle reservoirs: trace element constraints.- J. Petrol., Spec. Issue, 415-455.

Saunders A.D., Norry M.J., Tarney J. (1991): Fluid influence on the trace element compositions of subduction zone magmas.- Phil. Trans. R. Soc. London, **A335**, 377-392.

Scharbert S. (1987a): Rb - Sr Untersuchungen granitoider gesteine des Moldanubikums in Österreich.- Mitt. Öster. Min. Ges., **132**, 21-347.

Scharbert S. (1987b): Rb - Sr analysen des Tonalits und Granits von der Lokalität Křižanovice (Železné hory).- Čas. Miner. Geol., **32**, 411-412.

Scharbert S., Batík P. (1980): The age of the Thaya (Dyje) pluton.- Verh. Geol. Bundesanst, **3**, 325-381.

Scharbert S., Veselá M. (1990): Rb - Sr systematics of intrusive rocks from the Moldanubicum around Jihlava.- In: Minaříková D., Lobitzer H. (eds): Thirty years of geological cooperation between Austria and Czechoslovakia, Czech Geological Survey, Prague, 262-272.

Seyfert C.K. (1987): Mylonitic rocks.- In: Seyfert C.K. (ed.): The encyclopedia of structural geology and plate tectonics, Van Nostrand Reinhold, New York, 440-459.

Shand S.J. (1927): Eruptive rocks.- Murby, London, 360pp.

Shido F., Miyashiro A. (1959): Hornblendes of basic metamorphic rocks.- J. Fac. Sci. Tokyo Univ. II, **12**, 85-102.

Smith J.V., Brown L.W. (1988): Feldspar minerals 1, crystal structures, physical, chemical and microtextural properties.- Springer Verlag, Berlin, 828 pp.

Söllner F., Köhler H., Mühler-Sohnius D. (1981): Rb - Sr dating of rocks from the Münchberg Gneiss Massif (MM), NE Bavaria (Germany)-part 2, mineral dating (in German).- N. Jb. Miner. Abh., **142**, 178-198.

Souček J., Jelínek E., Bowes D.R. (1992): Geochemistry of gneisses of the eastern margin of the Bohemian Massif.- In: Kukal Z. (ed.): Proceedings of the 1st International Conference on the Bohemian Massif, Czech Geological Survey, Prague, 269-285.

Spear K.S., Kimball K.L. (1984): Recamp - a fortran IV program for estimating Fe3+ contents in amphiboles.- Comp. Geosci., **10**, 317-325.

Steiger R.H., Jäger E. (1977): Subcommission on geochronology: convention on the use of decay constants in geo- and cosmochronology.- Earth Planet. Sci. Lett., **36**, 359-362.

Štelcl J. (1960): Petrography of Culm conglomerates of the southern part of Drahanská vysočina.- Folia Fac. Sci. Nat. Univ. Brno, I/1.

Štorch P., Waldhausrová J., Žežulková V. (1984): Early Palaeozoic (Rožmitál facies) in the Mirovice metamorphic islet (in Czech).- Věst. Ústř. úst. geol., **59**, 105-107.

Stosch H.G., Lugmair G.W. (1990): Geochemistry and evolution of MORB-type eclogites from the Münchberg Massif, southern Germany.- Earth Planet. Sci. Lett., **99**, 230-249.

Streckeisen A., Le Maitre R.W. (1979): A chemical approximation to the modal QAPF classification of igneous rocks.- N. Jb. Miner. Abh., **136**, 169-206.

Suk M. (1973): Reconstruction of the mantle of the Central Bohemian Pluton.- Čas. Miner. Geol., **18**, 345-364.

Suk M. ed. (1984): Geological history of the territory of the Czech Socialist Republic.- Geological Survey, Prague, 396pp.

Svoboda J. (1933): Sedlčany - Krásná Hora metamorphic islet (in Czech).- Arch. přírod. výzk. Čech, **18**, 1-62.

Svoboda J. (1966): Regional geology of Czechoslovakia. Part I: The Bohemian Massif.- Czech Geological Survey, Prague, 5-668.

Taylor S.R., McLennan S.M. (1985): The continental crust, its composition and evolution.- Blackwell, Oxford, 323pp.

Teufel S. (1988): Vergleichende U - Pb- and Rb - Sr-Altersbestimmungen an Gesteinen des Übergangsbereiches Saxothuringikum/Moldanubikum, NE Bayern.- Göttinger Arbeiten zur Geologie und Paläontologie, **35**, 3-87.

Thirwall M.F. (1982): A triple-filament method for rapid and precise analysis of rare-earth elements by isotope dilution.- Chem. Geol., **35**, 155-166.

Thomas W.M., Ernst W.G. (1990): The aluminium of hornblende in calc-alkaline granitic rocks: a mineralogic barometer calibrated experimentally to 12 kbars.- In: Spencer R.J., Chou I-Ming (eds): Fluid-mineral interactions: a tribute to H.P. Eugster.- Geochem. Soc. Spec. Publ. **2**, Pergamon Press, Oxford, 59-63.

Thompson M., Walsh J.N. (1989): Handbook of inductively coupled plasma spectrometry.- Blackie, London, 316pp.

Thorpe R.S., Francis P.W., O'Callaghan L. (1984): Relative roles of source composition, fractional crystallization and crustal contamination in the petrogenesis of Andean volcanic rocks.- Phil. Trans. R. Soc. London, **A310**, 675-692.

Tonika J. ed. (1980): 1:25000 geological map of ČSSR 22-144 Blatná: Comments (in Czech).- Czech Geological Survey, Prague, 56pp.

Turpin L., Cuney M., Friedrich M., Bouchez J.L., Aubertin M. (1990): Meta-igneous origin of Hercynian peraluminous granites in N.W. French Massif Central: implications for crustal history reconstructions.- Contrib. Mineral. Petrol., **104**, 163-172.

Urban K. (1932): A contribution to the petrography of Zvíkov and Orlík areas (in Czech).- Sbor. Geol. Úst. Čs. rep., **9**, 109-187.

Valley J.W., O'Neil J.R. (1981): $^{13}C/^{12}C$ exchange between calcite and graphite: a possible thermometer in Grenwille marbles.- Geochim. Cosmochim. Acta, **45**, 411-419.

van Blanckenburg F. (1992): Combined high-precision chronometry and geochemical tracing using accessory minerals: applied to the Central-Alpine Bergell intrusion (Central Europe).- Chem. Geol., **100**, 19-40.

van Breemen O., Bowes D.R., Aftalion M., Żelaźniewicz A. (1988): Devonian tectonothermal activity in the Sowie Góry gneissic block, Sudetes, southwestern Poland: evidence from Rb - Sr and U - Pb isotopic studies.- Ann. Soc. Geol. Polon., **58**, 3-19.

van Breemen, O., Aftalion, M., Bowes, D.R., Dudek, A., Mísař, Z., Povondra, P., Vrána, S. (1982): Geochronological studies of the Bohemian massif, Czechoslovakia, and their significance in the evolution of Central Europe.- Trans. R. Soc. Edinburgh Earth Sci., **73**, 89-108.

Vejnar Z. (1973): Petrochemistry of the Central Bohemian Pluton.- Geochemistry, Geochemical methods and data 2, Geological Survey, Prague, 155pp.

Vejnar Z. (1974): Trace elements in rocks of the Central Bohemian Pluton.- Věst. Ústř. úst. geol., **49**, 159-165.

Vidal P., Auvray B., Charlot R., Fediuk F., Hameurt J., Waldhausrová J. (1975): Radiometric age of volcanics of the Cambrian Křivoklát - Rokycany complex (Bohemian Massif).- Geol. Rundsch., **64**, 536-570.

Vinokurov V.M., Gaingullina N.M., Evgrafova L.A., Nizamutdinov N.M., Suslina A.N. (1971): Zr^{4+}-Y^{3+} isomorphism in zircon and associated charge compensation.- Soviet Physics Crystallography, **16**, 262-265.

Vlašímský P. (1986): A contribution to the discussion on Carboniferous arkoses and the depth of denudation of Variscian plutons.- Čas. Miner. Geol., **31**, 429-433.

Vokurka K., Kober B. (1992): Heterogeneity of the Earth's mantle below the Bohemian Massif.- In: Kukal Z. (ed.): Proceedings of the 1st International Conference on the Bohemian Massif, Czech Geological Survey, Prague, 327-330.

Vrána S. (1979): Polyphase shear folding and thrusting in the Moldanubicum of Southern Bohemia.- Věst. Ústř. úst. geol., **54**, 75-86.

Vrána S. (1989): Perpotassic granulites from southern Bohemia - a new rock type derived from partial melting of crustal rocks under upper mantle conditions.- Contrib. Mineral. Petrol., **103**, 510-522.

Vrána S. (1992): The Moldanubian zone in southern Bohemia: polyphase evolution of imbricated crustal and upper mantle segments.- In: Kukal Z. (ed.): Proceedings of the 1st International Conference on the Bohemian Massif, Czech Geological Survey, Prague, 331-336.

Vrána S., Cháb J. (1981): Metatonalite - metaconglomerate relation: the problem of the upper Proterozoic sequence and its basement in the NE part of the Central Bohemian Pluton.- Sbor. Geol. Věd G, **35**, 145-187.

Wada H., Suzuki K. (1983): Carbon isotope thermometry calibrated by dolomite-calcite solvus temperatures.- Geochim. Cosmochim. Acta, **47**, 697-706.

Waldhausrová J. (1984): Proterozoic volcanites and intrusive rocks of the Jílové zone in Central Bohemia.- Krystalinikum, **17**, 77-97.

Waldhausrová J. ed. (1986): 1:25000 geological map of ČSSR 22-232 Kostelec nad Vltavou: Comments (in Czech).- Czech Geological Survey, Prague, 62pp.

Watson E.B., Harrison T.M. (1983): Zircon saturation revisited: temperature and composition effects in a variety of crustal magma types.- Earth Planet. Sci. Lett., **64**, 295-304.

Wayne D.M., Sinha K.A. (1988): Physical response of zircons to deformation.- Contrib. Mineral. Petrol., **98**, 109-121.

Wayne D.M., Sinha K.A. (1992): Stability of zircon U - Pb systematics in a greenschist-grade mylonite from the Rockfish Valley Fault Zone, Central Virginia, USA.- J. Geol., **100**, 593-603.

Wendt J.I., Kröner A., Todt W., Fiala J., Rajlich P., Liew T.C., Vaněk J. (1992): U - Pb zircon ages and Nd whole-rock systematics for Moldanubian rocks of the Bohemian Massif, Czechoslovakia.- In: Kukal Z. (ed.): Proceedings of the 1st International Conference on the Bohemian Massif, Czech Geological Survey, Prague, 346.

Wenk E. (1970): Distribution of Al between coexisting micas in metamorphic rocks from the Central Alps.- Contrib. Mineral. Petrol., **26**, 50-61.

Whyte F. (1989): Intrusion.- In: Bowes D.R. (ed.): The encyclopedia of igneous and metamorphic petrology, New York, Van Nostrand Reinhold, 252-253.

Wilson M. (1989): Igneous Petrogenesis.- Unwin Hyman, London, 466pp.

Wise D.U., Dunn D.E., Engelder J.T., Geiser P.A., Hatcher R.D., Kish S.A., Odom A.L., Schamel S. (1984): Fault-related rocks: Suggestions for terminology.- Geology, **12**, 391-394.

Wones D.R., Eugster H.P. (1965): Stability of biotite: experiment, theory and application.- Amer. Miner., **50**, 1228-1272.

York D. (1969): Least square fitting of a straight line with correlated errors.- Earth Planet. Sci. Lett., **5**, 320-324.

Zelenka L. (1929): Contributions to the tectonics of the southern and southeastern Bohemia (in Czech).- Věst. Stát. Geol. Úst. Čs. rep., **5**, 218-240.

Zemann J. (1966): Kristallchemie.- W. de Gruyter and Co., Berlin, 144pp.

Zen E-an, Hammastrom J.M. (1984): Magmatic epidote and its petrological significance.- Geology, **12**, 515-518.

Žežulková V. ed. (1985): 1:25000 geological map of ČSSR 22-233 Mirotice: Comments (in Czech).- Czech Geological Survey, Prague, 62pp.

Zikmund J. (1983): Relict granites and the genesis of the Blaník type orthogneiss (Bohemian Massif).- Čas. Miner. Geol., **28**, 81-87.

Zoubek V. ed. (1988): Precambrian in younger fold belts.- John Willey and Sons, Chichester, 867 pp.

APPENDIX I

Sample locations

Samples are located on ungrided 1:25000 topographical map of Czech Geographical and Cartographical Survey.

Sample	Rock type	Map no.	Locality
		Gneisses - Staré Sedlo	
STG-1	Biotite - plagioclase mylonite gneiss	22-232;	0.6 km SE of Chrást, Žebrákovský potok gorge
STG-2	Biotite - plagioclase mylonite gneiss	22-232;	0.6 km SSE of Chrást, Žebrákovský potok gorge
STG-3	Biotite - plagioclase mylonite gneiss	22-232;	0.4 km NNE of Kostelec n.Vlt., 0.1 km S of rd.19
STG-4	Amphibole - biotite mylonite gneiss	22-232;	1.5 km WNW of Kostelec n.Vlt., old quarry
STG-5	Amphibole - biotite mylonite gneiss	22-232;	1.5 km SW of Kostelec n.Vlt., Doubrava
STG-6	Amphibole - biotite mylonite gneiss	22-232;	1.7 km WSW of Kostelec n.Vlt., roadcut
STG-7	Biotite mylonite gneiss	22-232;	3.2 km N of Zbonín, Vltava River valley, Husárna
STG-8	Biotite mylonite gneiss	22-232;	1.0 km ESE of Orlík n.Vlt., Vltava River valley
STG-9	Biotite mylonite gneiss	22-232;	0.8 km E of Orlík n. Vlt., Vltava River valley
STG-10	Amphibole - biotite mylonite gneiss	22-232;	1.3 km SE of Orlík n.Vlt., Vltava River valley
STG-11	Amphibole - biotite mylonite gneiss	22-232;	3.0 km S of Orlík n.Vlt., Vltava River valley, Peklo
STG-12	Amphibole - biotite mylonite gneiss	22-232;	2.0 km NW of Zbonín, 1.5 km W of Ochoz
STG-13	Plagioclase meta-aplite	22-232;	2.0 km NE of Kostelec n.Vlt., Strašná
STG-14	Amphibole - biotite gneiss	22-232;	1.7 km WSW of Kostelec n.Vlt., roadcut
STG-15	Biotite mylonite gneiss	22-232;	0.6 km SW of Kostelec n.Vlt., old quarry
STG-16	Biotite - amphibole mylonite gneiss	22-232;	3.0 km S of Orlík n.Vlt., Vltava River valley, Peklo
STG-17	Biotite mylonite gneiss	22-232;	3.3 km NWN of Zbonín, Vltava River valley, Luh
STG-18	Biotite - amphibole mylonite gneiss	22-232;	3.0 km S of Orlík n.Vlt., Vltava River valley, Peklo
STG-19	Biotite mylonite gneiss	22-232;	2.4 km SW of Kostelec n.Vlt., Zelený les gorge
STG-20	Biotite - amphibole mylonite gneiss	22-232;	2.4 km SW of Kostelec n.Vlt., Zelený les gorge
STG-21	Biotite mylonite gneiss	22-232;	2.4 km SW of Kostelec n.Vlt., Zelený les gorge
STG-22	Biotite mylonite gneiss	22-232;	2.4 km SE of Kostelec n.Vlt., Vltava River valley
STG-23	Amphibole - biotite mylonite gneiss	22-232;	2.4 km SW of Kostelec n.Vlt., Zelený les gorge
STG-24	Amphibole - biotite mylonite gneiss	22-232;	1.9 km SW of Kostelec n.Vlt., Na Pískách
STG-25	Amphibole - biotite mylonite gneiss	22-232;	1.9 km SW of Kostelec n.Vlt., Na Pískách
STG-26	Biotite mylonite gneiss	22-232;	1.7 km WSW of Kostelec n.Vlt., roadcut
STG-27	Biotite mylonite gneiss	22-232;	1.2 km NNE of Orlík n.Vlt., Vltava River valley
STG-28	Biotite mylonite gneiss	22-232;	1.2 km NE of Orlík n.Vlt., Vltava River valley
		Gneisses - Lašovice	
LG-1	Biotite mylonite gneiss	22-214;	0.2 km NNW of Lašovice, quarry
LG-2	Biotite mylonite gneiss	22-214;	0.2 km NNW of Lašovice, quarry
LG-3	Biotite mylonite gneiss	22-214;	0.2 km NNW of Lašovice, quarry
LG-4	Plagioclase mylonite gneiss	22-214;	0.2 km NNW of Lašovice, quarry
LG-5	Biotite mylonite gneiss	22-214;	0.2 km NNW of Lašovice, quarry
LG-6	Biotite - plagioclase mylonite gneiss	22-214;	0.2 km NNW of Lašovice, quarry
LG-7	Biotite - plagioclase mylonite gneiss	22-214;	0.2 km NNW of Lašovice, quarry
LG-8	Biotite mylonite gneiss	22-214;	0.2 km NNW of Lašovice, quarry
LG-9	Biotite mylonite gneiss	22-214;	0.2 km NNW of Lašovice, quarry
LG-10	Biotite - plagioclase mylonite gneiss	22-214;	0.2 km NNW of Lašovice, quarry

		Amphibolites - Staré Sedlo	
STA-1	Amphibolite	22-232;	3.0 km S of Orlík n.Vlt., Vltava River valley, Peklo
STA-2	Amphibolite	22-232;	0.6 km SW of Kostelec n.Vlt., old quarry
STA-3	Amphibolite	22-232;	2.4 km SW of Kostelec n.Vlt., Zelený les gorge
STA-4	Amphibolite	22-232;	2.4 km SW of Kostelec n.Vlt., Zelený les gorge
STA-5	Amphibolite	22-232;	1.7 km WSW of Kostelec n.Vlt., roadcut
STA-6	Amphibolite	22-232;	1.7 km WSW of Kostelec n.Vlt., roadcut
		Meta-aplites - Staré Sedlo	
STM-1	Amphibole - biotite meta-aplite	22-232;	1.7 km WSW of Kostelec n.Vlt., roadcut
STM-2	Biotite - plagioclase meta-aplite	22-232;	1.7 km WSW of Kostelec n.Vlt., roadcut
STM-3	Biotite meta-aplite	22-232;	2.0 km SW of Chrást, Vltava River valley
		Gneisses - Mirotice	
MIG-1	Biotite mylonite gneiss	22-231;	0.8 km SSW of Lety, 0.4 km N of Pazderna
MIG-2	Biotite mylonite gneiss	22-231;	0.5 km S of Lety, Homole, old small quarry
MIG-3	Biotite mylonite gneiss	22-231;	1.7 km SW of Pohoří, old quarry
MIG-4	Biotite - plagioclase mylonite gneiss	22-142;	0.8 km SSE of Svobodka, 1.0 km NE of Kožlí
MIG-5	Amphibole - biotite mylonite gneiss	22-231;	0.7 km E of Chrást, 0.5 km NNE of U Brožáka
MIG-6	Amphibole - biotite mylonite gneiss	22-231;	0.4 km E of Výšice, 0.1 km N of U Brožáka
MIG-7	Biotite - plagioclase mylonite gneiss	22-233;	0.6 km N of Neradov, 0.9 km S of Boudy, roadcut
MIG-8	Amphibole - biotite mylonite gneiss	22-231;	1.3 km NW of Boudy, 1.0 km S of U Nováků
MIG-9	Amphibole - biotite mylonite gneiss	22-231;	0.4 km WNW of Boudy, 0.3 km SE of Velký Kosatín
MIG-10	Amphibole - biotite mylonite gneiss	22-144;	1.0 km SWS of Škvořetice, 0.2 km ESE of Hradiště
MIG-11	Garnet - biotite mylonite gneiss	22-144;	0.4 km SE of Hněvkov, 0.3 km E of Chocholka, old quarry
MIG-12	Biotite mylonite gneiss	22-144;	1.6 km NE of Laciná, Kostrata
MIG-13	Biotite mylonite gneiss	22-144;	0.8 km NE of Buzičky, 0.9 km SE of Václavov, old quarry
MIG-14	Biotite mylonite gneiss	22-144;	0.7 km ESE of Václavov, Lomnice River valley
MIG-15	Biotite mylonite gneiss	22-144;	0.8 km E of Václavov, Lomnice River valley
MIG-16	Amphibole - biotite mylonite gneiss	22-144;	1.0 km SE of Buzičky, 1.8 km WNW of Neradov
MIG-17	Garnet - biotite mylonite gneiss	22-144;	0.6 km SSE of Buzičky, Zbuzy
MIG-18	Garnet - biotite mylonite gneiss	22-144;	0.9 km SSE of Buzičky, 0.6 km NE of Pohodnice
MIG-19	Amphibole - biotite mylonite gneiss	22-144;	0.6 km NW of Míreč, Lomnice River valley
MIG-20	Biotite mylonite gneiss	22-144;	0.2 km N of Pacelice, Křesovec
MIG-21	Biotite mylonite gneiss	22-144;	0.7 km NW of Míreč, Lomnice River valley
MIG-22	Amphibole - biotite mylonite gneiss	22-233;	0.4 km NNW of Lučkovice, 0.8 km S of U Brožáka
MIG-23	Biotite mylonite gneiss	22-231;	1.0 km NNW of Boudy, Hrad
MIG-24	Amphibole - biotite mylonite gneiss	22-213;	0.5 km SE of Dobrá Voda, 0.3 km N of Strážiště
MIG-25	Biotite mylonite gneiss	22-213;	0.5 km W of Dobrá Voda, 1.1 km SE of Bor, old quarry
MIG-26	Biotite - plagioclase mylonite gneiss	22-233;	1.0 km S of Mirotice, 0.8 km NNE of Radobytce, roadcut
MIG-27	Amphibole - biotite mylonite gneiss	22-142;	1.0 km SE of Hudčice, Stráž, old quarry
MIG-28	Biotite - amphibole mylonite gneiss	22-142;	1.9 km E of Hudčice, Hradec
MIG-29	Biotite - plagioclase mylonite gneiss	22-142;	1.8 km E of Hudčice, 0.1 km W of Hradec

MIG-30	Biotite mylonite gneiss	22-144;	0.4 km SE of Hněvkov, 0.3 km E of Chocholka, old quarry
MIG-31	Amphibole - biotite mylonite gneiss	22-144;	0.7 km NW of Míreč, Lomnice River valley
MIG-32	Amphibole - biotite mylonite gneiss	22-231;	0.7 km E of Chrást, 0.5 km NNE of U Brožáka
	Schists - Mirotice		
MIS-1	K-feldspar - biotite blastomylonite	22-233;	0.3 km NE of Mirotice, Neradov, old quarry
MIS-2	K-feldspar - biotite mylonite schists	22-233;	0.3 km NE of Mirotice, Neradov, old quarry
MIS-3	K-feldspar - biotite blastomylonite	22-231;	2.0 km SW of Rakovice, 0.5 km ESE of U Nováků
MIS-4	K-feldspar - biotite blastomylonite	22-231;	0.4 km WNW of Boudy, 0.3 km SE of Velký Kosatín
MIS-5	K-feldspar - biotite mylonite schist	22-144;	2.6 km NW of Mužetice, 0.3 km SE of Škvořetice
MIS-6	K-feldspar - biotite mylonite schist	22-144;	2.2 km WSW of Lom, 0.9 km E of Škvořetice, old quarry
MIS-7	K-feldspar - biotite mylonite schist	22-144;	1.5 km SW of Sedlice, 0.4 km W of Křídlí
MIS-8	K-feldspar - biotite mylonite schist	22-144;	1.0 km N of Lom, 0.5 km NE of Neradov, old quarry
MIS-9	K-feldspar - biotite mylonite schist	22-144;	1.0 km NE of Škvořetice, Pahorek
MIS-10	K-feldspar - biotite blastomylonite	22-231;	2.0 km SW of Rakovice, 0.5 km ESE of U Nováků
MIS-11	K-feldspar - biotite mylonite schist	22-144;	2.2 km WSW of Lom, 0.9 km E of Škvořetice, old quarry
	Samples for Rb - Sr and Sm - Nd isotopic study		
STG-A	Amphibole - biotite mylonite gneiss	22-232;	1.7 km WSW of Kostelec n.Vlt., roadcut
STG-B	Amphibole - biotite mylonite gneiss	22-232;	0.6 km SW of Kostelec n.Vlt., old quarry
STG-C	Amphibole - biotite mylonite gneiss	22-232;	1.5 km WNW of Kostelec n.Vlt., old quarry
LG-A	Biotite mylonite gneiss	22-214;	0.2 km NNW of Lašovice, quarry
LG-B	Biotite mylonite gneiss	22-214;	0.2 km NNW of Lašovice, quarry
LG-C	Biotite mylonite gneiss	22-214;	0.2 km NNW of Lašovice, quarry
MIG-A	Amphibole - biotite mylonite gneiss	22-144;	0.7 km NW of Míreč, Lomnice River valley
MIG-B	Amphibole - biotite mylonite gneiss	22-231;	0.7 km E of Chrást, 0.5 km NNE of U Brožáka
MIS-A	K-feldspar biotite blastomylonite	22-231;	2.0 km SW of Rakovice, 0.5 km ESE of U Nováků
RC-1971	Biotite granodiorite	22-144;	2.0 km NW of Blatná, Řečice quarry
RC-1972	Biotite granodiorite	22-144;	2.0 km NW of Blatná, Řečice quarry
RC-1974	aplite	22-144;	2.0 km NW of Blatná, Řečice quarry
	Samples for U - Pb zircon isotopic study		
RC-2274	Amphibole - biotite mylonite gneiss	22-232;	0.6 km SW of Kostelec n.Vlt., old quarry
RC-2284	Amphibole - biotite mylonite gneiss	22-231;	0.7 km E of Chrást, 0.5 km NNE of U Brožáka

APPENDIX II

Sampling and laboratory techniques

Sampling and sample preparation

The paucity of outcrops limited the collection of samples for whole-rock chemical analysis to 90; 9 samples were also collected for Rb - Sr and Sm - Nd isotopic analysis and 2 samples were collected for U - Pb zircon study. The size of samples was sufficient to satisfy both the analytical methods and the reproducibility of analytical data. Accordingly ca 6 kg samples were taken for whole-rock chemical analysis, 40 - 50 kg of rock were used for Rb - Sr and Sm - Nd study and 10 kg samples were taken for U - Pb zircon study. For the whole-rock chemical analysis the 250 mesh rock powders were prepared using a standard jaw crusher followed by grinding in agate mortar. Similar procedure was used for sample preparation for Rb - Sr and Sm - Nd isotopic study although in order to obtain homogeneous material for analysis, the samples were carefully mixed in a large plastic barrel.

Separation of minerals for isotope analysis

After crushing the rock at least to the mineral grain-size, the minerals were separated as follows.

Biotite was separated by a combination of grinding and sieving in a stream of water. This procedure was repeated several times in order to obtain a pure biotite fraction. Periodic checks of purity were carried out using both an optical microscope and XRD techniques.

Plagioclase was isolated from the rock using a Frantz isodynamic magnetic separator followed by a repeated separation in tetra-bromethane with density adjusted to 2.55. In order to separate plagioclase porphyroclasts from the matrix, only the fraction 100 - 250 μm was used. Periodic checks of purity were carried out using XRD technique.

Zircon grains were separated from the rock using a Wilfley shaking table followed by separation of the heavy fraction in tetra-bromethane. The most magnetic fraction was then removed using magnet and a Frantz isodynamic separator at current of 0.5 A and side tilt 15^{o}. The separate was then boiled for few minutes in dilute HCl (to remove Fe-oxides) and the magnetic separation was repeated at 1.25 A and 10^{o}. The heavy fraction isolated in di-iodomethane was then boiled for few minutes in 1 : 1 HNO_3 to dissolve sulphides (if present). The least magnetic fraction of zircon was obtained by a step magnetic separation at

constant current of 1.75 A and side tilts of 8^{o}, 5^{o}, 3^{o} and 2^{o}. The zircon separate was then split by sieving into several size fractions.

Electron microprobe and backscattered electron study of rock-forming minerals

Electron microprobe analyses of the main rock-forming minerals were carried out on diamond-polished and carbon-coated thin sections using a Cambridge Microscan 5 instrument (EDS mode) at the University of Glasgow. In order to produce spot analyses a focused beam of 20 kV and 30 nA was used. A cobalt metal target was used as a drift monitor and the current response was normalized against natural wollastonite, jadeite and K-feldspar standards. Contents of Si, Ti, Al, Fe, Mn, Mg, Ca, Na and K were calculated from integrals of their Kα peaks collected for 100 s. ZAF corrections for atomic number (Z), x-ray absorption (A) and secondary fluorescence (F) were employed using a built-in computer program (Link Analytical). Mineral formulae were calculated by stochiometry on the basis of assumed number of oxygen (F, Cl, OH, ...) atoms in a unit cell.

Zircon spot analyses were obtained from diamond-polished and carbon-coated zircon separates mounted in epoxy resin using a focused beam of 20 kV and 50 nA on a JEOL JCXA-733 electron microprobe (WDS mode) at the University of St Andrews. The method closely followed that of *Paterson et al. (1992)*. The samples were analyzed for Si ($K\alpha_1$), Zr ($L\alpha_1$) and Hf ($M\alpha_1$) against a natural zircon standard and for U ($M\alpha_1$), REE ($L\alpha_1$) and Y ($L\alpha_1$) against UO_2 and REE-doped glass standards of *Drake and Weill (1972)*, respectively. Count times of 100 s were used for both peaks of elements in standards and samples and corresponding backgrounds. ZAF corrections were also employed.

The backscattered electron study of zircon grains was carried out on the same samples using a Cambridge Stereoscan 360 electron microscope at the University of Glasgow fitted with 4 quadrant BSE detector (Si N-type) following the principles of BSE imagery given in *Lloyd (1987)*. A beam of 20 kV and probe current of 6 - 12 nA (varying for individual grains) were used.

XRF technique for major and trace element rock analysis

Major and trace elements in 250 mesh rock powders were analyzed using a Phillips PW 1450/20 automatic sequential x-ray spectrometer at the University of Glasgow with Cr and Mo tube targets, respectively. Fused glass discs prepared according to the method of *Harvey et al. (1973)* were used for determination of major elements and pressed powder pellets (*Leake et al., 1969; Harvey and Atkin, 1982*) for trace elements. Glass discs were made up of 0.375 g of rock powder and 2.000 g of Johnson Mattey lithium tetraborate spectroflux. For pressed pellets six parts of rock powder and one part of binder (organic resin) were used. Nb was determined from pressed powder pellets and analyzed using a Cr-target tube. The external calibration was carried out and periodic checks of accuracy were made using University of Glasgow laboratory standards, the composition of which was previously determined by XRF analysis against several international geological reference materials and by wet chemistry analysis (for major elements). In order to correct for remaining absorption - enhancement effects, the influence factors (*de Jongh, 1973*) were employed in the major element analysis while the correction for absorption using the intensity of incoherently scattered Compton peak were used in the trace element analysis. The approximate detection limits (in ppm and wt% for trace and major elements, respectively) were calculated as the average detection limits for each Glasgow standard and were as follows.

Rb	2	Y	1	Ni	5	Nb	7	MnO	0.01
Sr	2	Th	12	Cr	2	SiO_2	0.09	MgO	0.17
Ba	12	Zr	3	Cu	4	TiO_2	0.02	CaO	0.01
La	4	Ga	2	Pb	12	Al_2O_3	0.09	Na_2O	0.16
Ce	3	Co	3	Zn	2	Fe_2O_3	0.05	K_2O	0.01
								P_2O_5	0.02

Ferrous iron determination

Ferrous iron in rock powders and biotite separates was determined using the method of *Pratt (1894)*. To prevent any negative error in the analysis due to a possible sample oxidation, 250 mesh rock powders

ground in acetone were used for the whole-rock FeO determination. Aproximately 0.5 g of sample in a Pt crucible was carefully dissolved in a 40% HNO_3 - 50% H_2SO_4 mixture on the hotplate at 160 ^oC for 15 minutes and analyzed for FeO content using titration by potassium dichromate with indication to sodium diphenylamine. Based on the repeated analysis of Glasgow laboratory standards, the estimated precision of FeO determination is 0.1 wt%.

Water and carbon dioxide determination

Water and carbon dioxide were determined gravimetrically from 250 mesh rock powder using the method of *Riley (1958)*. Approximately 0.5 g of sample was weighed into previously ignited alumina boat and heated for 30 minutes at 1100 ^oC in a combustion tube. Both water and carbon dioxide released from the rock were removed by a flow of dry nitrogen and present sulphur was reduced on a hot copper spiral. Water and carbon dioxide were then captured in absorption tubes filled with anhydrous magnesium perchlorate and soda asbestos with a small amount of magnesium perchlorate, respectively. Their contents were determined gravimetrically after thermal equilibration of absorption tubes in desicator. The estimated precisions based upon several analyses of Glasgow laboratory standards are 0.2 and 0.4 wt% for water and carbon dioxide, respectively.

ICP-MS technique for REE and Cs determination

The decomposition procedure of the whole-rock samples was similar to that suggested by *Thompson and Walsh (1989)* using exclusively Aristar grade chemicals. Approximately 0.250 g of 250 mesh rock powder was weighed into a PTFE beaker and a mixture of 4 ml of 70% HNO_3 + 1 ml of 70% $HCLO_4$ + 10 ml of 48% HF was added. The beaker was then heated on the hotplate on the following scheme: covered with a PTFE lid for 3 hours at 120 ^oC, uncovered for 3 hours at 160 ^oC and uncovered for 10 hours at 210 ^oC. Dry salts in a PTFE beaker were then dissolved in 5% HNO_3 and heated on the hotplate at 50 ^oC for 30 minutes. Precipitated hydroxides and hydro-oxides of Fe^{2+} were dissolved by adding few drops of concentrated H_2O_2 and the solution was diluted to 100 ml and transferred to polyethylene flasks.

The dilution factor of final solution was 408. For the REE, Cs and Ta analysis a VG Plasma Quad-I ICP-MS instrument at the SURRC with the following operating conditions was used:

Plasma power	1,300 W
Generator	27 MHz
Auxiliary gas flow	0.6 l min^{-1}
Nebuliser gas flow	0.79 l min^{-1}
Nebuliser	Meinhart
Spray chamber	VG
Sample uptake rate	0.65 ml min^{-1}

The external standards were made up by diluting Johnson Mattey specpure REE and Cs solutions. ^{104}Ru, ^{187}Re and ^{115}In were used as internal standards. The periodic checks of accuracy made against international geological reference materials yielded satisfatory results. In fact the REE recovery from an open digestion of a GSP-1 granodiorite (international reference material) was approximately 80%. XRD study has shown zircon being present in an insoluble residue and therefore contributing to the negative error. However as the estimated zircon content in GSP-1 granodiorite (based on its Zr-content of 530 ppm; *Govindaraju, 1989*) is approximately four times the average of the zircon content in studied rocks or even more, the estimated negative error does not exceed 5 %. As zircon concentrates preferentially heavy REE, its incomplete dissolution would result in only a slight rotation of the REE spectra which does not affect the geological interpretations. The limits of quantitation (in $\mu g\ g^{-1}$) for an open digestion and dilution factor of 500 (*Jarvis, 1988; Jarvis, 1992*) are as follows:

La	0.125	Sm	0.25	Dy	0.20	Yb	0.10
Ce	0.17	Eu	0.10	Ho	0.05	Lu	0.10
Pr	0.15	Gd	0.15	Er	0.10	Cs	0.25
Nd	0.35	Tb	0.05	Tm	0.02		

Data treatment

All data below the stated detection limits were discarded and are referred to as "b.d.l." or "- - -". For Nb also some of the data close to the detection limit were used as this has no influence upon the geochemical characterization of the studied rocks (cf. Chapter 4). The statistical parameters used in Chapters 3 and 4 were calculated using Microsoft Excel for Apple Macintosh version 4.0. The formulae used for calculations are listed in corresponding manuals. The value of the geometrical average (G) for any particular element or oxide and a number of samples n was calculated as n-th root from the product of concentrations.

Analytical procedures for Rb, Sr, Sm and Nd isotope chemistry and mass spectrometry

Samples were dissolved in PFA teflon screw-top beakers (Savillex) using 10ml of 40% HF and 1ml of 14M HNO_3 on a hotplate at 150 ^{o}C overnight. The beakers were removed, cooled, and then the solution was dried down under lamps. The residue was then dissolved in 3 ml of 14M HNO_3 overnight on a hotplate, and dried down as before. The residue was then dissolved in 2 ml of 6M HCl on a hotplate for 2 hours. For Sm and Nd isotope dilution analysis the 6M HCl solution was aliquoted and one part spiked with ^{145}Nd and ^{149}Sm spike solutions. For Rb and Sr isotope dilution analysis samples were spiked with ^{87}Rb and ^{84}Sr spikes at the same stage. Samples were heated for 5 mins on the hotplate at 150 ^{o}C to equlibrate with the spike solutions, then dried down and the final solution were taken up in 2 ml of 2.5M HCl.

Rb, Sr and the REE were separated using standard cation exchange chromatography techniques. The samples were transferred to a centrifuge tube and any residue was centrifuged off. The solutions were then loaded onto a preconditioned cation exchange column containing 10 ml of Bio-Rad AG50W x 8, 200-400 mesh resin. The samples were washed in with 2 * 1 ml of 2.5M HCl and eluted with 21 ml of 2.5M HCl. The Rb fraction was then collected with a further 5 ml of 2.5M HCl and evaporated to dryness. 20 ml of 2.5M HCl were then eluted. The Sr fraction was collected with a further 10 ml of 2.5M HCl and evaporated to dryness. Sr blanks were less than 5ng.

Separation of REE followed a modified three-stage procedure described in *Hooker et al. (1975)* and *Thirlwall (1982)*. Samples were loaded onto a preconditioned first set of anion exchange columns containing cca 5 ml of Bio-Rad AG1 x 8, 200-400 mesh resin and washed in with 2 * 1 ml of 90/10 acetic - nitric mixture (AN) solution (90/10 mixture of concentrated CH_3COOH and 5M HNO_3). Unwanted cations were eluted with a further 50 ml of 90/10 AN solution and the REE fractions were collected with 15 ml of 0.05M HNO_3. Sm and Nd isolation from the bulk REE fractions was performed in similar anion exchange columns (second set) with a water jacket temperature control adjusted to 25 ^oC. Samples were loaded onto preconditioned columns and washed in with 2 * 1 ml of OC (orange cocktail) solution (3000/668/204/128 mixture of CH_3OH, water, concentrated CH_3COOH and 14M HNO_3). 65 ml of OC solution were eluted and Sm fraction was collected in 10 ml of YC (yellow cocktail) solution (3000/732/204/128 mixture of CH_3OH, water, concentrated CH_3COOH and 14M HNO_3). 10 ml of YC solution were eluted and Nd fraction was collected in 40 ml of YC solution. A third set of anion exchange columns (similar to the first one) was used for final Ba clean-up of Nd fractions. Samples were washed in onto preconditioned resin with 2 * 1 ml of 90/10 AN solution. Then 15 ml of 90/10 AN solution were eluted and pure Nd fractions were collected in 10 ml of 0.05M HNO_3.

All Sr samples were run on a VG 54E thermal ionisation mass spectrometer. Rb samples were run on a VG MM30 and NdIR, NdID and Sm samples on a VG Sector 54-30 thermal ionization mass spectrometers at the SURRC.

Sr

Sr samples were dissolved in 1µl 1M H_3PO_4 and were loaded onto a single outgassed Ta filament. A small current was passed through the filament to dry the samples. The current was then increased slowly until the H_3PO_4 fumed off and the filament glowed dull red. Sr beams were managed to give an intensity of 0.15V ^{86}Sr. Peak intensities were corrected for zero, dynamic memory and Rb interference (if necessary). The $^{87}Sr/^{86}Sr$ ratios were corrected for mass fractionation using $^{86}Sr/^{88}Sr = 0.1194$. Replicate analyses of NBS 987 Sr standard gave $^{87}Sr/^{86}Sr = 0.71028 \pm 3$ (2σ): all data given here are reported relative to NBS 987 $^{87}Sr/^{86}Sr = 0.71022$.

Rb

Rb samples were dissolved in 1µl double distilled H_2O and loaded onto one side filament of an outgassed triple Ta filament assembly. The samples were dried carefully, taking care not to let the loads bubble up on the filament. Rb beams were run with a current of 3 A through the centre filament and up to 1 A on the side filaments.

Sm - Nd

NdIR, NdID and Sm samples were dissolved in 1 µl H_2O and loaded onto Ta side filaments of a triple (Ta - Re - Ta) filament assembly. The samples were dried carefully at 0.5 A. NdIR beams were managed to give a ^{144} Nd peak intensity of 1V, and data acquisition was made using a 5 collector multi-dynamic routine, correcting the 144 peak for Sm interference as neccessary. The $^{143}Nd/^{144}Nd$ ratio was corrected for mass fractionation using $^{146}Nd/^{144}Nd$ - 0.7219. Replicate analyses of a JM standard gave $^{143}Nd/^{144}Nd = 0.511500 \pm 12$ (2σ). NdID beams were managed to give a ^{143}Nd peak intensity of 0.05V. For Sm runs a ^{147}Sm peak intensity of 0.05V was maintained. For both Sm and NdID samples data were collected in static mode, with inter-Farraday gains being calibrated on a daily basis.

U and Pb zircon isotope analysis

The digestion of the hand-picked zircon size fractions and the analytical techniques used for U and Pb isolation followed closely those of *Krogh (1973)*. Zircons were washed twice in 6M HNO_3 in an ultrasonic basin and decanted with water. Dried samples were weighed into PTFE capsules, then 4 ml of 48% HF and few drops of concentrated HNO_3 were added. PTFE capsules were assembled into stainless steel bombs and heated in the oven at 220 ^{o}C for five full days. After cooling down to the room temperature, the capsules were opened and samples dried on the hotplate at 150 ^{o}C and then in closed capsules dissolved again in 5-10 ml of 3M HCl on the hotplate at 120 ^{o}C for 4 days. The samples were aliquoted and one part was spiked with ^{208}Pb and ^{235}U mixed spike. Spike and samples were mixed and equilibrated in ultrasonic basin and on the hotplate (150 ^{o}C for 24 hours), then dried down and taken up with 2 ml of 3M HCl. Columns were made of shrinkable teflon tubing (cca 7 mm in diameter): these were thorougly washed with 6M HNO3 and water before the addition of cca 5 ml of DOWEX AG50W x

8, 200-400 mesh resin. Samples were loaded onto preconditioned cation exchange columns and unwanted cations were eluted with 2/3 column volume (cv) 3M HCl. Pb was collected in 1 cv 6M HCl and U was washed out using 2/3 cv of water. Samples were dried down and then, using few drops of concentrated HNO_3, converted to nitrates.

Both U and Pb samples were run on a VG MM30 thermal ionization mass spectrometer at the Isotope Geology Unit, SURRC. U was loaded in cca 1% HNO_3 onto specpure Ta_2O_5 in 15% H_3PO_4 on a W-single filament and left to dry down. Pb was loaded in 15% H_3PO_4 onto silica gel on a single Re filament and slowly heated until the white smoke died out. The measured Pb isotopic ratios were corrected for common Pb using the Pb composition of the nitric acid ($^{206}Pb/^{204}Pb$ = 17.640, $^{207}Pb/^{204}Pb$ = 15.582 and $^{208}Pb/^{204}Pb$ = 37.664), which was considered to be the main contaminant. During this study the NBS standards SRM 983 and U 500, respectively, gave the following results: $^{207}Pb/^{206}Pb$ = 0.071205 ± 32 (2σ), $^{208}Pb/^{206}Pb$ = 0.013643 ± 19 (2σ), $^{206}Pb/^{204}Pb$ = 2758 ± 14 (2σ) and $^{238}U/^{235}U$ = 0.99975 ± 25 (2σ).

APPENDIX III

Chemical analyses and mineral formulae of rock-forming minerals

Mineral formulae are calculated from electron microprobe data (wt%) using procedures described in Chapter 3; Plg = plagioclase, KF = potassium feldspar, Bi = biotite, Amph = amphibole, Gt = garnet, C = core, R = rim, for other symbols see Chapter 3.

	STG-1 Plg-1	STG-1 Plg-2	STG-1 Plg-3	STG-1 Plg-4	STG-1 Plg-5	STG-2 Plg-1C	STG-2 Plg-1R	STG-2 Plg-2C	STG-2 Plg-2R	STG-2 Plg-3	STG-3 Plg-1	STG-3 Plg-2	STG-3 Plg-3
SiO2	62.72	65.45	63.28	63.18	63.95	62.29	63.42	61.40	64.54	63.31	61.73	60.17	60.07
TiO2	0.02	0.05	0.02	0.04	0.04	0.06	0.05	0.05	0.00	0.04	0.08	0.07	0.02
Al2O3	22.82	21.25	23.07	22.73	22.71	23.29	23.31	24.32	22.28	22.81	23.81	24.80	25.05
FeO(tot.)	0.00	0.00	0.01	0.06	0.04	0.09	0.04	0.05	0.06	0.02	0.05	0.18	0.12
MnO	0.00	0.05	0.01	0.02	0.01	0.02	0.00	0.00	0.00	0.04	0.08	0.07	0.03
MgO	0.00	0.00	0.00	0.00	0.00	0.00	0.01	0.15	0.07	0.00	0.00	0.00	0.00
CaO	3.78	2.26	4.13	3.81	3.69	4.57	3.97	5.45	2.89	3.56	5.38	6.44	5.80
Na2O	8.78	10.24	9.51	9.37	9.63	9.11	9.83	8.92	10.43	9.65	9.14	8.45	8.01
K2O	0.18	0.28	0.17	1.12	0.76	0.28	0.22	0.22	0.23	0.23	0.25	0.18	0.56
Total	98.30	99.58	100.20	100.33	100.83	99.71	100.85	100.56	100.50	99.66	100.52	100.36	99.66
Si	11.24	11.56	11.18	11.20	11.25	11.08	11.14	10.87	11.35	11.23	10.94	10.71	10.74
Ti	0.00	0.01	0.00	0.01	0.01	0.01	0.01	0.01	0.00	0.01	0.01	0.01	0.00
Al	4.82	4.43	4.80	4.75	4.71	4.88	4.83	5.07	4.62	4.77	4.97	5.21	5.28
Fe	0.00	0.00	0.00	0.01	0.01	0.01	0.01	0.01	0.01	0.00	0.01	0.03	0.02
Mn	0.00	0.01	0.00	0.00	0.00	0.00	0.00	0.00	0.00	0.01	0.01	0.01	0.00
Mg	0.00	0.00	0.00	0.00	0.00	0.00	0.00	0.04	0.02	0.00	0.00	0.00	0.00
Ca	0.73	0.43	0.78	0.72	0.70	0.87	0.75	1.03	0.54	0.68	1.02	1.23	1.11
Na	3.05	3.51	3.26	3.22	3.28	3.14	3.35	3.06	3.56	3.32	3.14	2.92	2.78
K	0.04	0.06	0.04	0.25	0.17	0.06	0.05	0.05	0.05	0.05	0.06	0.04	0.13
Ab	79.84	87.75	79.90	76.85	79.04	77.15	80.72	73.91	85.78	81.98	74.41	69.69	69.15
An	19.11	10.75	19.12	17.18	16.87	21.38	18.07	24.88	13.01	16.79	24.17	29.36	27.61
Or	1.05	1.50	0.98	5.97	4.10	1.47	1.20	1.21	1.20	1.23	1.42	0.95	3.23

	STG-3 Plg-4	STG-3 Plg-5	STG-3 Plg-6	STG-3 Plg-7	STG-3 Plg-8	STG-3 Plg-9	STG-4 Plg-1	STG-4 Plg-2	STG-4 Plg-3	STG-4 Plg-4	STG-4 Plg-5	STG-4 Plg-6	STG-4 Plg-7C
SiO2	60.26	60.81	60.30	60.91	60.31	60.46	59.57	60.30	59.49	60.58	61.02	61.35	57.99
TiO2	0.00	0.06	0.00	0.08	0.00	0.04	0.03	0.04	0.03	0.00	0.10	0.00	0.00
Al2O3	24.79	24.89	25.25	24.20	24.60	25.03	24.92	24.68	23.73	24.31	24.42	24.15	26.01
FeO(tot.)	0.00	0.08	0.45	0.03	0.09	0.12	0.00	0.02	0.06	0.11	0.22	0.00	0.14
MnO	0.01	0.00	0.00	0.00	0.08	0.00	0.02	0.07	0.06	0.00	0.00	0.05	0.04
MgO	0.09	0.14	0.02	0.00	0.05	0.03	0.03	0.12	0.03	0.03	0.00	0.09	0.00
CaO	6.46	6.34	5.34	5.66	6.28	6.61	6.75	6.45	7.08	5.89	6.01	5.49	7.88
Na2O	8.30	8.66	8.24	8.54	8.11	8.12	7.74	7.99	8.33	8.45	8.12	8.16	7.15
K2O	0.24	0.13	0.38	0.14	0.25	0.24	0.26	0.20	0.19	0.10	0.26	1.00	0.17
Total	100.15	101.11	99.98	99.56	99.77	100.65	99.32	99.87	99.00	99.47	100.15	100.29	99.38
Si	10.74	10.74	10.74	10.88	10.78	10.72	10.70	10.76	10.76	10.84	10.85	10.91	10.45
Ti	0.00	0.01	0.00	0.01	0.00	0.01	0.00	0.01	0.00	0.00	0.01	0.00	0.00
Al	5.21	5.18	5.30	5.09	5.18	5.23	5.27	5.19	5.06	5.13	5.12	5.06	5.52
Fe	0.00	0.01	0.07	0.00	0.01	0.02	0.00	0.00	0.01	0.02	0.03	0.00	0.02
Mn	0.00	0.00	0.00	0.00	0.01	0.00	0.00	0.01	0.01	0.00	0.00	0.01	0.01
Mg	0.02	0.04	0.01	0.00	0.01	0.01	0.01	0.03	0.01	0.01	0.00	0.02	0.00
Ca	1.23	1.20	1.02	1.08	1.20	1.26	1.30	1.23	1.37	1.13	1.14	1.05	1.52
Na	2.87	2.96	2.85	2.96	2.81	2.79	2.69	2.76	2.92	2.93	2.80	2.81	2.50
K	0.05	0.03	0.09	0.03	0.06	0.05	0.06	0.05	0.04	0.02	0.06	0.23	0.04
Ab	69.16	70.64	71.97	72.73	69.04	68.05	66.42	68.32	67.44	71.81	70.00	68.70	61.58
An	29.64	28.64	25.76	26.54	29.48	30.73	32.10	30.45	31.64	27.70	28.50	25.67	37.44
Or	1.20	0.72	2.27	0.74	1.47	1.22	1.48	1.24	0.92	0.49	1.50	5.62	0.99

	STG-4 Plg-7R	STG-4 Plg-8	STG-4 Plg-9	STG-5 Plg-1C	STG-5 Plg-1R	STG-5 Plg-2C	STG-5 Plg-2R	STG-5 Plg-3	STG-5 Plg-4	STG-5 Plg-5	STG-5 Plg-6	STG-5 Plg-7C	STG-5 Plg-7R
SiO2	58.72	62.41	60.90	59.33	60.36	58.53	61.04	60.61	61.01	59.57	61.06	60.32	60.93
TiO2	0.00	0.01	0.00	0.03	0.00	0.00	0.01	0.05	0.00	0.01	0.00	0.04	0.00
Al2O3	25.59	23.72	24.55	25.03	24.19	25.49	24.03	23.85	23.80	24.67	23.84	24.09	24.02
FeO(tot.)	0.07	0.02	0.09	0.05	0.14	0.09	0.10	0.07	0.01	0.08	0.10	0.08	0.08
MnO	0.10	0.05	0.02	0.00	0.00	0.01	0.06	0.00	0.00	0.03	0.00	0.02	0.01
MgO	0.12	0.05	0.11	0.00	0.00	0.06	0.04	0.01	0.08	0.00	0.04	0.00	0.01
CaO	7.63	5.18	5.76	6.53	5.89	7.31	5.78	5.42	5.35	6.72	5.45	6.10	5.75
Na2O	7.61	8.64	8.34	7.93	8.00	7.02	8.30	7.98	8.53	7.32	7.98	8.33	8.02
K2O	0.23	0.10	0.23	0.17	0.19	0.29	0.16	0.18	0.11	0.31	0.14	0.17	0.27
Total	100.07	100.18	100.00	99.07	98.77	98.80	99.52	98.17	98.89	98.71	98.61	99.15	99.09
Si	10.51	11.04	10.83	10.68	10.86	10.57	10.91	10.95	10.95	10.75	10.97	10.84	10.92
Ti	0.00	0.00	0.00	0.00	0.00	0.00	0.00	0.01	0.00	0.00	0.00	0.01	0.00
Al	5.40	4.95	5.15	5.31	5.13	5.43	5.06	5.08	5.03	5.25	5.05	5.10	5.07
Fe	0.01	0.00	0.01	0.01	0.02	0.01	0.01	0.01	0.00	0.01	0.02	0.01	0.01
Mn	0.02	0.01	0.00	0.00	0.00	0.00	0.01	0.00	0.00	0.00	0.00	0.00	0.00
Mg	0.03	0.01	0.03	0.00	0.00	0.02	0.01	0.00	0.02	0.00	0.01	0.00	0.00
Ca	1.46	0.98	1.10	1.26	1.14	1.42	1.11	1.05	1.03	1.30	1.05	1.17	1.10
Na	2.64	2.96	2.88	2.77	2.79	2.46	2.88	2.79	2.97	2.56	2.78	2.90	2.79
K	0.05	0.02	0.05	0.04	0.04	0.07	0.04	0.04	0.03	0.07	0.03	0.04	0.06
Ab	63.61	74.75	71.46	68.06	70.28	62.28	71.46	71.91	73.70	65.14	72.02	70.56	70.63
An	35.18	24.75	27.30	30.96	28.72	35.95	27.54	27.06	25.56	33.08	27.20	28.47	27.85
Or	1.20	0.51	1.24	0.98	1.01	1.77	0.99	1.03	0.74	1.78	0.78	0.97	1.52

	STG-5 Plg-8	STG-5 Plg-9	STG-5 Plg-10	STG-5 Plg-11	STG-5 Plg-12	STG-5 Plg-13	STG-5 Plg-14	STG-5 Plg-15	STG-10 Plg-1	STG-10 Plg-2C	STG-10 Plg-2R	STG-10 Plg-3	STG-10 Plg-4
SiO2	58.76	58.96	59.74	60.20	60.68	60.54	60.30	67.93	59.57	58.08	61.11	60.07	59.80
TiO2	0.06	0.00	0.00	0.01	0.00	0.03	0.00	0.00	0.00	0.02	0.04	0.01	0.06
Al2O3	25.81	25.37	24.56	24.43	24.42	24.64	24.74	19.35	24.98	26.01	24.41	24.59	24.83
FeO(tot.)	0.28	0.14	0.06	0.12	0.18	0.04	0.13	0.03	0.19	0.14	0.06	0.16	0.21
MnO	0.07	0.00	0.03	0.00	0.00	0.03	0.00	0.05	0.00	0.00	0.00	0.00	0.01
MgO	0.20	0.02	0.01	0.00	0.04	0.00	0.00	0.03	0.02	0.00	0.07	0.00	0.06
CaO	3.96	7.29	6.54	6.03	5.86	6.17	6.25	4.95	6.80	8.05	5.98	6.39	5.28
Na2O	7.14	7.43	7.74	7.78	7.57	7.82	7.93	6.75	7.76	7.27	8.57	8.11	7.37
K2O	2.05	0.24	0.29	0.28	0.35	0.29	0.30	0.14	0.21	0.16	0.15	0.16	1.50
Total	98.33	99.45	98.97	98.85	99.10	99.56	99.65	99.23	99.53	99.73	100.39	99.49	99.12
Si	10.66	10.59	10.76	10.83	10.87	10.82	10.78	11.94	10.68	10.44	10.84	10.76	10.77
Ti	0.01	0.00	0.00	0.00	0.00	0.00	0.00	0.00	0.00	0.00	0.01	0.00	0.01
Al	5.52	5.37	5.21	5.18	5.16	5.19	5.21	4.01	5.28	5.51	5.10	5.19	5.27
Fe	0.04	0.02	0.01	0.02	0.03	0.01	0.02	0.00	0.03	0.02	0.01	0.02	0.03
Mn	0.01	0.00	0.00	0.00	0.00	0.00	0.00	0.01	0.00	0.00	0.00	0.00	0.00
Mg	0.05	0.01	0.00	0.00	0.01	0.00	0.00	0.01	0.01	0.00	0.02	0.00	0.02
Ca	0.77	1.40	1.26	1.16	1.13	1.18	1.20	0.93	1.31	1.55	1.14	1.23	1.02
Na	2.51	2.59	2.70	2.71	2.63	2.71	2.75	2.30	2.70	2.53	2.95	2.82	2.57
K	0.47	0.06	0.07	0.06	0.08	0.07	0.07	0.03	0.05	0.04	0.03	0.04	0.34
Ab	66.93	63.95	67.00	68.96	68.49	68.43	68.41	70.55	66.50	61.41	71.60	68.95	65.39
An	20.53	34.57	31.27	29.52	29.43	29.80	29.85	28.53	32.27	37.62	27.67	30.07	25.95
Or	12.53	1.48	1.74	1.53	2.08	1.77	1.74	0.92	1.23	0.97	0.73	0.98	8.65

	STG-10 Plg-5	STG-10 Plg-6	STG-10 Plg-7	STG-10 Plg-8	STG-10 Plg-9	STG-11 Plg-1	STG-11 Plg-2	STG-11 Plg-3	STG-11 Plg-4	STG-11 Plg-5	STG-11 Plg-6	STG-11 Plg-7	STG-11 Plg-8
SiO2	60.73	60.55	60.87	60.01	60.71	59.51	58.97	60.19	59.74	59.90	59.88	59.90	60.02
TiO2	0.05	0.00	0.00	0.11	0.05	0.00	0.06	0.01	0.00	0.04	0.04	0.04	0.09
Al2O3	24.10	24.27	24.19	24.31	24.09	24.72	24.65	24.81	24.62	24.54	24.78	24.88	24.87
FeO(tot.)	0.15	0.22	0.13	0.06	0.12	0.14	0.16	0.16	0.11	0.12	0.07	0.14	0.26
MnO	0.02	0.00	0.00	0.04	0.00	0.00	0.03	0.00	0.00	0.00	0.09	0.05	0.00
MgO	0.00	0.06	0.00	0.05	0.00	0.00	0.00	0.09	0.00	0.08	0.00	0.00	0.02
CaO	5.92	6.11	6.04	5.89	5.79	6.43	6.95	6.48	6.41	6.52	6.54	6.61	6.64
Na2O	8.13	8.25	8.17	7.91	8.23	7.73	7.54	7.83	7.82	8.03	8.05	7.83	7.84
K2O	0.29	0.24	0.42	0.51	0.33	0.22	0.32	0.34	0.13	0.22	0.24	0.29	0.32
Total	99.39	99.70	99.82	98.89	99.32	98.75	98.68	99.91	98.83	99.45	99.69	99.74	100.06
Si	10.88	10.83	10.86	10.81	10.88	10.74	10.68	10.74	10.76	10.75	10.72	10.72	10.71
Ti	0.01	0.00	0.00	0.01	0.01	0.00	0.01	0.00	0.00	0.01	0.01	0.01	0.01
Al	5.09	5.11	5.09	5.16	5.09	5.26	5.26	5.22	5.23	5.19	5.23	5.25	5.23
Fe	0.02	0.03	0.02	0.01	0.02	0.02	0.02	0.02	0.02	0.02	0.01	0.02	0.04
Mn	0.00	0.00	0.00	0.01	0.00	0.00	0.00	0.00	0.00	0.00	0.01	0.01	0.00
Mg	0.00	0.02	0.00	0.01	0.00	0.00	0.00	0.02	0.00	0.02	0.00	0.00	0.01
Ca	1.14	1.17	1.16	1.14	1.11	1.24	1.35	1.24	1.24	1.25	1.25	1.27	1.27
Na	2.82	2.86	2.83	2.76	2.86	2.70	2.65	2.71	2.73	2.79	2.79	2.72	2.71
K	0.07	0.05	0.10	0.12	0.08	0.05	0.07	0.08	0.03	0.05	0.05	0.07	0.07
Ab	69.98	70.10	69.19	68.66	70.62	67.67	65.11	67.25	68.25	68.22	68.22	67.00	66.91
An	28.29	28.68	28.36	28.36	27.41	31.08	33.17	30.77	31.00	30.56	30.56	31.28	31.36
Or	1.74	1.23	2.44	2.99	1.98	1.25	1.72	1.99	0.75	1.22	1.22	1.72	1.73

	STG-11 Plg-9C	STG-11 Plg-9R	STG-11 Plg-10	STG-11 Plg-11	STG-11 Plg-12	STG-11 Plg-13	STG-11 Plg-14C	STG-11 Plg-14R	STG-11 Plg-15	STG-11 Plg-16	STG-11 Plg-17	STG-11 Plg-18	STG-11 Plg-19
SiO2	59.77	60.44	60.63	60.48	61.00	60.67	57.29	60.22	60.34	60.17	59.54	59.32	57.78
TiO2	0.00	0.08	0.00	0.00	0.08	0.00	0.00	0.00	0.05	0.06	0.00	0.00	0.03
Al2O3	24.86	24.41	24.17	24.07	24.23	23.64	26.51	23.81	23.93	23.90	24.97	25.10	25.51
FeO(tot.)	0.06	0.12	0.22	0.08	0.28	0.14	0.05	0.05	0.02	0.10	0.11	0.11	0.13
MnO	0.00	0.00	0.01	0.00	0.00	0.00	0.06	0.00	0.00	0.00	0.00	0.00	0.04
MgO	0.00	0.00	0.09	0.00	0.04	0.00	0.14	0.00	0.00	0.00	0.00	0.00	0.00
CaO	6.47	6.10	5.75	5.78	5.92	5.62	8.44	5.96	5.73	5.71	6.65	7.06	7.66
Na2O	7.28	7.94	8.11	8.20	8.15	8.43	6.61	8.03	8.33	8.24	7.89	7.39	7.17
K2O	0.30	0.27	0.35	0.31	0.26	0.35	0.23	0.29	0.18	0.03	0.20	0.20	0.28
Total	98.74	99.36	99.33	98.92	99.96	98.85	99.33	98.36	98.58	98.21	99.36	99.18	98.60
Si	10.76	10.83	10.87	10.88	10.86	10.93	10.34	10.89	10.88	10.88	10.69	10.67	10.49
Ti	0.00	0.01	0.00	0.00	0.01	0.00	0.00	0.00	0.01	0.01	0.00	0.00	0.00
Al	5.28	5.15	5.11	5.10	5.09	5.02	5.64	5.08	5.09	5.10	5.28	5.32	5.46
Fe	0.01	0.02	0.03	0.01	0.04	0.02	0.01	0.01	0.00	0.02	0.02	0.02	0.02
Mn	0.00	0.00	0.00	0.00	0.00	0.00	0.01	0.00	0.00	0.00	0.00	0.00	0.01
Mg	0.00	0.00	0.02	0.00	0.01	0.00	0.04	0.00	0.00	0.00	0.00	0.00	0.00
Ca	1.25	1.17	1.10	1.11	1.13	1.08	1.63	1.15	1.11	1.11	1.28	1.36	1.49
Na	2.54	2.76	2.82	2.86	2.81	2.94	2.31	2.82	2.91	2.89	2.75	2.58	2.53
K	0.07	0.06	0.08	0.07	0.06	0.08	0.05	0.07	0.04	0.01	0.05	0.05	0.06
Ab	65.80	69.17	70.50	70.79	70.25	71.71	57.89	69.80	71.67	72.19	67.46	64.69	61.88
An	32.38	29.32	27.50	27.48	28.25	26.34	40.85	28.47	27.34	27.64	31.42	34.15	36.53
Or	1.81	1.50	2.00	1.73	1.50	1.95	1.25	1.73	0.99	0.17	1.13	1.15	1.59

	STG-11 Plg-20	STG-11 Plg-21	STG-11 Plg-22	STG-11 Plg-23	STG-11 Plg-24	STG-11 Plg-25	STG-11 Plg-26	STG-11 Plg-27	STG-11 Plg-28	STG-11 Plg-29	STG-11 Plg-30	STG-11 Plg-31	STG-11 Plg-32
SiO2	58.39	57.83	58.47	58.45	58.84	58.14	59.39	59.75	59.14	59.21	59.46	59.63	60.18
TiO2	0.00	0.00	0.00	0.00	0.05	0.00	0.00	0.03	0.00	0.00	0.02	0.03	0.00
Al2O3	25.80	26.25	25.65	25.51	25.61	25.68	25.22	24.43	24.63	25.38	25.37	24.87	24.69
FeO(tot.)	0.11	0.08	0.17	0.12	0.10	0.09	0.09	0.10	0.19	0.13	0.13	0.09	0.19
MnO	0.00	0.00	0.00	0.00	0.00	0.10	0.00	0.00	0.00	0.00	0.01	0.05	0.04
MgO	0.00	0.05	0.00	0.00	0.03	0.05	0.11	0.10	0.19	0.03	0.09	0.06	0.02
CaO	7.79	8.19	7.61	7.87	7.33	7.69	6.97	6.37	6.03	7.09	7.16	6.81	6.13
Na2O	7.16	6.58	7.07	7.07	7.61	7.33	7.56	8.02	7.56	7.73	7.46	7.71	8.21
K2O	0.31	0.23	0.22	0.10	0.18	0.18	0.23	0.07	0.35	0.17	0.26	0.29	0.15
Total	99.56	99.21	99.19	99.12	99.75	99.26	99.57	98.87	98.09	99.74	99.96	99.54	99.61
Si	10.50	10.42	10.54	10.54	10.55	10.49	10.64	10.76	10.74	10.61	10.62	10.69	10.77
Ti	0.00	0.00	0.00	0.00	0.01	0.00	0.00	0.00	0.00	0.00	0.00	0.00	0.00
Al	5.47	5.58	5.45	5.42	5.41	5.46	5.33	5.19	5.27	5.36	5.34	5.26	5.21
Fe	0.02	0.01	0.03	0.02	0.01	0.01	0.01	0.02	0.03	0.02	0.02	0.01	0.03
Mn	0.00	0.00	0.00	0.00	0.00	0.02	0.00	0.00	0.00	0.00	0.00	0.01	0.01
Mg	0.00	0.01	0.00	0.00	0.01	0.01	0.03	0.03	0.05	0.01	0.02	0.02	0.01
Ca	1.50	1.58	1.47	1.52	1.41	1.49	1.34	1.23	1.17	1.36	1.37	1.31	1.18
Na	2.50	2.30	2.47	2.47	2.65	2.56	2.63	2.80	2.66	2.68	2.58	2.68	2.85
K	0.07	0.05	0.05	0.02	0.04	0.04	0.05	0.02	0.08	0.04	0.06	0.07	0.03
Ab	61.36	58.45	61.91	61.56	64.61	62.66	65.38	69.22	67.97	65.73	64.38	66.10	70.19
An	36.89	40.20	36.82	37.87	34.39	36.33	33.31	30.38	29.96	33.32	34.15	32.26	28.96
Or	1.75	1.34	1.27	0.57	1.01	1.01	1.31	0.40	2.07	0.95	1.48	1.64	0.84

	STG-12 Plg-1C	STG-12 Plg-1R	STG-12 Plg-2	STG-12 Plg-3C	STG-12 Plg-3R	STG-12 Plg-4C	STG-12 Plg-4R	STG-12 Plg-5C	STG-12 Plg-5R	STG-12 Plg-6C	STG-12 Plg-6R	STG-12 Plg-7	STG-12 Plg-8
SiO2	57.73	62.17	59.96	59.31	58.81	59.20	59.42	60.26	60.78	59.83	60.55	62.47	63.02
TiO2	0.00	0.06	0.05	0.01	0.04	0.01	0.00	0.00	0.00	0.00	0.01	0.01	0.00
Al2O3	26.42	23.12	25.11	24.93	25.44	25.68	24.90	25.17	24.25	24.54	23.93	23.23	22.83
FeO(tot.)	0.06	0.08	0.05	0.00	0.04	0.12	0.05	0.05	0.09	0.08	0.00	0.00	0.01
MnO	0.00	0.00	0.00	0.09	0.03	0.00	0.00	0.09	0.09	0.00	0.05	0.05	0.00
MgO	0.00	0.12	0.07	0.06	0.00	0.10	0.00	0.07	0.05	0.04	0.00	0.00	0.01
CaO	8.54	4.57	6.69	6.67	7.28	7.62	7.03	6.59	5.84	6.38	5.76	4.71	4.29
Na2O	6.83	9.06	7.86	7.86	7.43	7.36	7.84	7.96	8.12	7.86	8.16	8.83	9.19
K2O	0.20	0.20	0.21	0.29	0.23	0.25	0.18	0.23	0.24	0.32	0.25	0.40	0.21
Total	99.78	99.38	100.00	99.22	99.30	100.34	99.42	100.42	99.46	99.05	98.71	99.70	99.56
Si	10.37	11.09	10.69	10.67	10.58	10.55	10.67	10.70	10.87	10.77	10.90	11.11	11.20
Ti	0.00	0.01	0.01	0.00	0.01	0.00	0.00	0.00	0.00	0.00	0.00	0.00	0.00
Al	5.59	4.86	5.28	5.29	5.39	5.40	5.27	5.27	5.11	5.20	5.08	4.87	4.78
Fe	0.01	0.01	0.01	0.00	0.01	0.02	0.01	0.01	0.01	0.01	0.00	0.00	0.00
Mn	0.00	0.00	0.00	0.01	0.00	0.00	0.00	0.01	0.01	0.00	0.01	0.01	0.00
Mg	0.00	0.03	0.02	0.02	0.00	0.03	0.00	0.02	0.01	0.01	0.00	0.00	0.00
Ca	1.64	0.87	1.28	1.29	1.40	1.46	1.35	1.25	1.12	1.23	1.11	0.90	0.82
Na	2.38	3.13	2.72	2.74	2.59	2.54	2.73	2.74	2.82	2.74	2.85	3.04	3.17
K	0.05	0.05	0.05	0.07	0.05	0.06	0.04	0.05	0.05	0.07	0.06	0.09	0.05
Ab	58.48	77.28	67.16	66.83	64.11	62.56	66.26	67.82	70.68	67.82	70.90	75.43	78.47
An	40.29	21.48	31.60	31.46	34.65	35.96	32.77	30.94	28.07	30.45	27.61	22.33	20.30
Or	1.23	1.23	1.23	1.71	1.24	1.48	0.97	1.24	1.25	1.73	1.49	2.23	1.24

	LG-B Plg-1	LG-B Plg-2	LG-B Plg-3	LG-B Plg-4	LG-B Plg-5	LG-C Plg-1	LG-C Plg-2	LG-C Plg-3	LG-C Plg-4	MIG-2 Plg-1C	MIG-2 Plg-1R	MIG-2 Plg-2C	MIG-2 Plg-2R
SiO2	57.15	55.75	58.63	56.08	56.89	60.93	59.73	58.10	61.86	65.03	64.17	64.17	64.39
TiO2	0.00	0.00	0.00	0.02	0.02	0.02	0.00	0.03	0.08	0.00	0.00	0.00	0.00
Al2O3	25.98	27.22	25.45	26.90	26.22	23.75	24.74	25.51	22.87	22.68	23.05	22.68	22.49
FeO(tot.)	0.10	0.01	0.09	0.14	0.00	0.01	0.05	0.06	0.00	0.00	0.00	0.00	0.13
MnO	0.02	0.00	0.01	0.00	0.01	0.01	0.02	0.00	0.06	0.00	0.00	0.00	0.00
MgO	0.01	0.12	0.00	0.01	0.00	0.00	0.06	0.17	0.08	0.00	0.17	0.17	0.00
CaO	8.00	9.45	7.49	8.90	8.43	5.65	6.14	7.22	4.24	3.08	3.92	3.50	3.22
Na2O	6.71	6.30	7.07	6.18	6.49	8.09	8.23	7.32	9.27	9.57	9.97	9.57	9.30
K2O	0.22	0.15	0.26	0.18	0.11	0.23	0.19	0.20	0.22	0.24	0.24	0.48	0.72
Total	98.19	99.00	99.00	98.41	98.17	98.69	99.16	98.61	98.68	100.59	101.52	100.56	100.24
Si	10.42	10.13	10.58	10.22	10.37	10.96	10.74	10.53	11.11	11.38	11.20	11.28	11.35
Ti	0.00	0.00	0.00	0.00	0.00	0.00	0.00	0.00	0.01	0.00	0.00	0.00	0.00
Al	5.58	5.83	5.41	5.78	5.63	5.03	5.24	5.45	4.84	4.68	4.74	4.70	4.67
Fe	0.02	0.00	0.01	0.02	0.00	0.00	0.01	0.01	0.00	0.00	0.00	0.00	0.02
Mn	0.00	0.00	0.00	0.00	0.00	0.00	0.00	0.00	0.01	0.00	0.00	0.00	0.00
Mg	0.00	0.03	0.00	0.00	0.00	0.00	0.02	0.05	0.02	0.00	0.04	0.04	0.00
Ca	1.56	1.84	1.45	1.74	1.65	1.09	1.18	1.40	0.82	0.58	0.73	0.66	0.61
Na	2.37	2.22	2.47	2.18	2.29	2.82	2.87	2.57	3.23	3.25	3.37	3.26	3.18
K	0.05	0.03	0.06	0.04	0.03	0.05	0.04	0.05	0.05	0.05	0.05	0.11	0.16
Ab	59.55	54.28	62.06	55.05	57.84	71.21	70.17	63.93	78.78	83.76	81.20	80.89	80.51
An	39.20	44.99	36.43	43.94	41.52	27.53	28.85	34.83	20.00	14.95	17.59	16.38	15.44
Or	1.26	0.73	1.51	1.01	0.65	1.26	0.98	1.24	1.22	1.29	1.20	2.73	4.05

	MIG-2 Plg-3C	MIG-2 plg-3R	MIG-2 Plg-4	MIG-5 Plg-1C	MIG-5 Plg-1R	MIG-5 Plg-2	MIG-5 Plg-3	MIG-5 Plg-4C	MIG-5 Plg-4R	MIG-6 Plg-1C	MIG-6 Plg-1R	MIG-6 Plg-2	MIG-6 Plg-3
SiO2	63.53	64.39	63.74	57.54	60.53	60.53	61.60	58.82	61.60	59.89	63.10	59.04	59.47
TiO2	0.00	0.00	0.00	0.00	0.00	0.00	0.00	0.00	0.00	0.00	0.17	0.00	0.00
Al2O3	22.49	22.49	22.49	26.83	24.75	24.57	24.00	25.70	24.00	25.89	23.05	26.46	26.08
FeO(tot.)	0.13	0.00	0.00	0.13	0.13	0.00	0.13	0.13	0.13	0.00	0.13	0.00	0.13
MnO	0.00	0.00	0.00	0.00	0.00	0.00	0.00	0.00	0.00	0.00	0.00	0.00	0.00
MgO	0.00	0.17	0.00	0.17	0.17	0.17	0.17	0.00	0.33	0.17	0.17	0.17	0.17
CaO	3.64	3.22	3.36	8.26	5.74	5.74	5.32	6.44	5.32	7.14	3.92	7.70	7.28
Na2O	9.30	9.70	9.84	6.47	8.36	8.22	8.90	7.28	8.90	7.68	9.84	7.14	7.55
K2O	0.24	0.60	0.36	0.12	0.12	0.00	0.12	0.48	0.12	0.12	0.12	0.24	0.12
Total	99.32	100.56	99.79	99.51	99.80	99.22	100.23	98.85	100.40	100.89	100.49	100.74	100.78
Si	11.29	11.32	11.29	10.34	10.79	10.83	10.93	10.61	10.91	10.59	11.13	10.47	10.54
Ti	0.00	0.00	0.00	0.00	0.00	0.00	0.00	0.00	0.00	0.00	0.02	0.00	0.00
Al	4.71	4.66	4.70	5.68	5.20	5.18	5.02	5.46	5.01	5.40	4.79	5.53	5.45
Fe	0.02	0.00	0.00	0.02	0.02	0.00	0.02	0.02	0.02	0.00	0.02	0.00	0.02
Mn	0.00	0.00	0.00	0.00	0.00	0.00	0.00	0.00	0.00	0.00	0.00	0.00	0.00
Mg	0.00	0.04	0.00	0.05	0.05	0.05	0.04	0.00	0.09	0.04	0.04	0.04	0.04
Ca	0.69	0.61	0.64	1.59	1.10	1.10	1.01	1.24	1.01	1.35	0.74	1.46	1.38
Na	3.21	3.31	3.38	2.25	2.89	2.85	3.06	2.55	3.06	2.63	3.37	2.46	2.59
K	0.05	0.13	0.08	0.03	0.03	0.00	0.03	0.11	0.03	0.03	0.03	0.05	0.03
Ab	81.27	81.73	82.44	58.14	71.89	72.15	74.63	65.38	74.63	65.59	81.40	61.96	64.75
An	17.47	15.06	15.61	41.09	27.36	27.85	24.63	31.79	24.63	33.67	17.87	36.78	34.50
Or	1.27	3.21	1.95	0.78	0.75	0.00	0.73	2.82	0.73	0.75	0.72	1.26	0.75

	MIG-6 Plg-4	MIG-6 Plg-5	MIG-10 Plg-1C	MIG-10 Plg-1R	MIG-10 Plg-2C	MIG-10 Plg-2R	MIG-10 Plg-3	MIG-10 Plg-4	MIG-10 Plg-5	MIG-11 Plg-1	MIG-11 Plg-2	MIG-11 Plg-3	MIG-11 Plg-4C
SiO2	57.75	59.47	63.10	61.60	63.53	61.39	62.25	58.82	57.54	63.74	64.81	63.96	63.53
TiO2	0.00	0.00	0.00	0.00	0.00	0.00	0.00	0.00	0.00	0.00	0.00	0.00	0.00
Al2O3	26.27	26.08	23.43	24.19	23.62	24.19	23.24	26.27	26.27	23.43	22.86	23.05	23.62
FeO(tot.)	0.00	0.00	0.13	0.00	0.13	0.00	0.00	0.13	0.00	0.00	0.00	0.00	0.00
MnO	0.00	0.13	0.00	0.00	0.00	0.00	0.00	0.00	0.00	0.00	0.00	0.13	0.00
MgO	0.00	0.17	0.17	0.17	0.17	0.00	0.00	0.17	0.00	0.17	0.00	0.17	0.00
CaO	7.84	7.42	4.20	5.18	4.20	5.32	4.20	7.42	8.12	4.20	3.50	3.64	4.34
Na2O	7.28	7.55	9.70	8.63	9.30	8.63	9.17	7.55	6.47	9.44	9.97	9.57	9.30
K2O	0.12	0.12	0.12	0.12	0.24	0.12	0.24	0.12	0.12	0.24	0.12	0.24	0.24
Total	99.25	100.92	100.85	99.88	101.18	99.64	99.09	100.47	98.51	101.21	101.27	100.75	101.03
Si	10.41	10.53	11.10	10.94	11.12	10.93	11.12	10.47	10.43	11.15	11.30	11.22	11.13
Ti	0.00	0.00	0.00	0.00	0.00	0.00	0.00	0.00	0.00	0.00	0.00	0.00	0.00
Al	5.58	5.44	4.86	5.06	4.87	5.08	4.89	5.51	5.61	4.83	4.70	4.77	4.88
Fe	0.00	0.00	0.02	0.00	0.02	0.00	0.00	0.02	0.00	0.00	0.00	0.00	0.00
Mn	0.00	0.02	0.00	0.00	0.00	0.00	0.00	0.00	0.00	0.00	0.00	0.02	0.00
Mg	0.00	0.04	0.04	0.04	0.04	0.00	0.00	0.05	0.00	0.04	0.00	0.04	0.00
Ca	1.51	1.41	0.79	0.99	0.79	1.02	0.80	1.42	1.58	0.79	0.65	0.68	0.81
Na	2.55	2.59	3.31	2.97	3.16	2.98	3.18	2.61	2.27	3.20	3.37	3.26	3.16
K	0.03	0.03	0.03	0.03	0.05	0.03	0.05	0.03	0.03	0.05	0.03	0.05	0.05
Ab	62.35	64.27	80.15	74.44	79.00	73.95	78.91	64.29	58.51	79.21	83.21	81.70	78.61
An	36.92	34.99	19.13	24.81	19.75	25.31	19.85	34.98	40.72	19.55	16.05	17.04	20.15
Or	0.73	0.74	0.73	0.75	1.25	0.74	1.24	0.74	0.77	1.24	0.74	1.25	1.24

	MIG-11 Plg-4R	MIG-20 Plg-1C	MIG-20 Plg-1R	MIG-20 Plg-2	MIG-20 Plg-3C	MIG-20 Plg-3R	MIG-20 Plg-4C	MIG-20 Plg-4R	MIG-22 Plg-1C	MIG-22 Plg-1R	MIG-22 Plg-2	MIG-22 Plg-3C	MIG-22 Plg-3R
SiO2	64.39	65.45	65.88	65.67	63.96	66.52	65.24	65.45	64.39	61.60	59.25	58.82	58.61
TiO2	0.00	0.00	0.00	0.00	0.00	0.00	0.00	0.00	0.00	0.00	0.00	0.00	0.00
Al2O3	23.24	22.49	22.30	22.11	23.43	22.30	23.05	22.86	22.49	24.38	26.08	26.46	26.27
FeO(tot.)	0.00	0.13	0.13	0.00	0.00	0.13	0.13	0.00	0.00	0.00	0.00	0.13	0.13
MnO	0.00	0.00	0.00	0.00	0.00	0.00	0.00	0.13	0.00	0.00	0.00	0.00	0.00
MgO	0.00	0.17	0.00	0.00	0.00	0.17	0.17	0.00	0.17	0.00	0.17	0.17	0.00
CaO	3.78	2.80	2.80	2.52	4.20	2.52	3.64	3.22	3.22	5.46	7.28	7.84	7.84
Na2O	9.70	10.11	10.38	10.11	9.44	10.78	9.97	10.11	9.97	8.63	7.68	7.28	7.28
K2O	0.12	0.12	0.12	0.12	0.12	0.12	0.24	0.12	0.12	0.12	0.12	0.24	0.12
Total	101.23	101.26	101.61	100.53	101.14	102.54	102.44	101.90	100.35	100.18	100.57	100.93	100.24
Si	11.23	11.39	11.43	11.48	11.18	11.44	11.27	11.34	11.32	10.91	10.52	10.43	10.46
Ti	0.00	0.00	0.00	0.00	0.00	0.00	0.00	0.00	0.00	0.00	0.00	0.00	0.00
Al	4.78	4.61	4.56	4.56	4.83	4.52	4.69	4.67	4.66	5.09	5.46	5.53	5.53
Fe	0.00	0.02	0.02	0.00	0.00	0.02	0.02	0.00	0.00	0.00	0.00	0.02	0.02
Mn	0.00	0.00	0.00	0.00	0.00	0.00	0.00	0.02	0.00	0.00	0.00	0.00	0.00
Mg	0.00	0.04	0.00	0.00	0.00	0.04	0.04	0.00	0.04	0.00	0.05	0.04	0.00
Ca	0.71	0.52	0.52	0.47	0.79	0.46	0.67	0.60	0.61	1.04	1.39	1.49	1.50
Na	3.28	3.41	3.49	3.43	3.20	3.60	3.34	3.40	3.40	2.97	2.64	2.50	2.52
K	0.03	0.03	0.03	0.03	0.03	0.03	0.05	0.03	0.03	0.03	0.03	0.05	0.03
Ab	81.59	86.11	86.39	87.28	79.60	88.02	82.27	84.37	84.16	73.51	65.02	61.88	62.22
An	17.66	13.13	12.87	11.96	19.65	11.25	16.50	14.89	15.10	25.74	34.24	36.88	37.04
Or	0.75	0.76	0.74	0.76	0.75	0.73	1.23	0.74	0.74	0.74	0.74	1.24	0.74

	MIG-22 Plg-4	MIG-24 Plg-1	MIG-24 Plg-2	MIG-24 Plg-3C	MIG-24 Plg-3R	MIG-24 Plg-4	MIG-24 Plg-5	MIG-29 Plg-1	MIG-29 Plg-2	MIG-29 Plg-3	MIG-29 Plg-4	MIG-30 Plg-1	MIG-30 Plg-2
SiO2	59.89	59.68	61.39	61.39	61.18	62.25	59.89	62.25	62.03	61.60	61.60	62.46	62.25
TiO2	0.00	0.00	0.00	0.00	0.00	0.00	0.00	0.00	0.00	0.00	0.17	0.00	0.00
Al2O3	25.70	25.89	24.75	24.19	24.57	23.62	25.51	23.62	24.00	24.19	24.38	24.57	24.57
FeO(tot.)	0.00	0.13	0.13	0.00	0.13	0.00	0.00	0.13	0.13	0.13	0.26	0.00	0.13
MnO	0.00	0.00	0.00	0.00	0.00	0.00	0.00	0.00	0.00	0.00	0.00	0.00	0.00
MgO	0.17	0.17	0.00	0.17	0.00	0.00	0.00	0.00	0.17	0.00	0.00	0.00	0.00
CaO	7.00	7.00	5.74	5.32	5.60	4.76	6.72	4.62	4.90	5.32	5.74	5.46	5.46
Na2O	7.68	7.55	8.22	8.63	8.49	8.90	7.68	9.03	8.76	8.36	8.09	9.17	8.63
K2O	0.24	0.12	0.12	0.00	0.12	0.12	0.12	0.24	0.12	0.24	0.24	0.24	0.24
Total	100.68	100.53	100.35	99.69	100.08	99.64	99.92	99.88	100.10	99.84	100.47	101.89	101.26
Si	10.61	10.59	10.86	10.92	10.86	11.06	10.67	11.05	10.99	10.95	10.90	10.91	10.92
Ti	0.00	0.00	0.00	0.00	0.00	0.00	0.00	0.00	0.00	0.00	0.02	0.00	0.00
Al	5.37	5.41	5.16	5.07	5.14	4.95	5.36	4.94	5.01	5.07	5.08	5.06	5.08
Fe	0.00	0.02	0.02	0.00	0.02	0.00	0.00	0.02	0.02	0.02	0.04	0.00	0.02
Mn	0.00	0.00	0.00	0.00	0.00	0.00	0.00	0.00	0.00	0.00	0.00	0.00	0.00
Mg	0.04	0.04	0.00	0.05	0.00	0.00	0.00	0.00	0.04	0.00	0.00	0.00	0.00
Ca	1.33	1.33	1.09	1.01	1.07	0.91	1.28	0.88	0.93	1.01	1.09	1.02	1.03
Na	2.64	2.60	2.82	2.98	2.92	3.07	2.65	3.11	3.01	2.88	2.77	3.10	2.94
K	0.05	0.03	0.03	0.00	0.03	0.03	0.03	0.05	0.03	0.05	0.05	0.05	0.05
Ab	65.67	65.66	71.57	74.69	72.64	76.56	66.92	76.98	75.82	73.10	70.84	74.34	73.13
An	33.08	33.59	27.66	25.31	26.62	22.69	32.32	21.78	23.43	25.63	27.88	24.46	25.62
Or	1.24	0.76	0.76	0.00	0.75	0.75	0.76	1.24	0.76	1.27	1.28	1.20	1.24

	MIG-30 Plg-3	MIG-30 Plg-4	MIG-31 Plg-1C	MIG-31 Plg-1R	MIG-31 Plg-2	MIG-31 Plg-3	MIG-31 Plg-4	MIG-31 Plg-5	MIS-6 Plg-1	MIS-6 Plg-2	MIS-7 Plg-1C	MIS-7 Plg-1R	MIS-7 Plg-2C
SiO2	62.67	62.46	59.04	62.46	58.61	62.46	59.68	62.67	67.17	67.59	61.60	63.74	63.96
TiO2	0.00	0.00	0.17	0.00	0.00	0.00	0.00	0.00	0.00	0.17	0.00	0.00	0.00
Al2O3	24.57	24.94	26.64	24.00	26.64	23.24	26.08	24.00	20.98	21.16	24.19	23.05	22.86
FeO(tot.)	0.00	0.00	0.00	0.13	0.13	0.13	0.13	0.00	0.13	0.00	0.00	0.13	0.00
MnO	0.00	0.00	0.00	0.00	0.00	0.00	0.00	0.00	0.00	0.00	0.00	0.00	0.00
MgO	0.17	0.00	0.00	0.17	0.00	0.00	0.17	0.00	0.00	0.17	0.00	0.00	0.17
CaO	5.04	5.46	7.70	4.90	8.26	4.34	7.42	4.90	1.12	1.12	5.32	3.78	3.64
Na2O	8.76	8.76	7.41	9.17	7.14	7.68	7.68	8.90	11.19	11.19	8.49	9.84	9.57
K2O	0.24	0.24	0.12	0.12	0.12	1.93	0.12	0.12	0.12	0.12	0.24	0.12	0.36
Total	101.44	101.86	101.08	100.94	100.90	99.78	101.27	100.59	100.70	101.52	99.84	100.66	100.56
Si	10.95	10.89	10.44	10.99	10.40	11.14	10.53	11.04	11.70	11.68	10.95	11.21	11.25
Ti	0.00	0.00	0.02	0.00	0.00	0.00	0.00	0.00	0.00	0.02	0.00	0.00	0.00
Al	5.06	5.13	5.55	4.98	5.57	4.88	5.43	4.98	4.31	4.31	5.07	4.78	4.74
Fe	0.00	0.00	0.00	0.02	0.02	0.02	0.02	0.00	0.02	0.00	0.00	0.02	0.00
Mn	0.00	0.00	0.00	0.00	0.00	0.00	0.00	0.00	0.00	0.00	0.00	0.00	0.00
Mg	0.04	0.00	0.00	0.04	0.00	0.00	0.04	0.00	0.00	0.04	0.00	0.00	0.04
Ca	0.94	1.02	1.46	0.92	1.57	0.83	1.40	0.92	0.21	0.21	1.01	0.71	0.69
Na	2.97	2.96	2.54	3.13	2.46	2.66	2.63	3.04	3.78	3.75	2.93	3.35	3.26
K	0.05	0.05	0.03	0.03	0.03	0.44	0.03	0.03	0.03	0.03	0.05	0.03	0.08
Ab	75.00	73.45	63.03	76.72	60.59	67.68	64.78	76.19	94.03	93.98	73.43	81.91	80.89
An	23.74	25.31	36.23	22.55	38.67	21.12	34.48	23.06	5.22	5.26	25.31	17.36	17.12
Or	1.26	1.24	0.74	0.74	0.74	11.20	0.74	0.75	0.75	0.75	1.25	0.73	1.99

	MIS-7 Plg-2R	MIS-10 Plg-1	MIS-10 Plg-2	MIS-10 Plg-3	MIS-10 Plg-4C	MIS-10 Plg-4R	STA-1 Plg-1	STA-1 Plg-2	STA-1 Plg-3	STA-1 Plg-4	STA-1 Plg-5	STA-1 Plg-6	STA-1 Plg-7
SiO2	62.89	64.17	64.39	63.96	64.39	63.53	59.57	59.90	60.41	60.22	60.35	59.95	60.05
TiO2	0.00	0.00	0.00	0.00	0.00	0.00	0.00	0.04	0.00	0.00	0.05	0.01	0.00
Al2O3	23.05	22.49	22.68	22.86	22.49	23.05	24.92	24.91	24.82	24.78	24.83	24.97	24.55
FeO(tot.)	0.00	0.00	0.00	0.00	0.13	0.00	0.13	0.10	0.23	0.13	0.22	0.12	0.25
MnO	0.00	0.00	0.00	0.00	0.00	0.00	0.02	0.00	0.00	0.00	0.00	0.00	0.04
MgO	0.00	0.00	0.17	0.17	0.00	0.00	0.13	0.00	0.00	0.00	0.00	0.08	0.04
CaO	4.06	3.64	3.36	3.78	2.94	3.78	6.74	6.64	6.34	6.24	6.25	6.48	6.32
Na2O	9.30	9.57	9.84	9.84	9.97	9.44	7.72	7.75	7.76	8.13	8.30	8.36	8.04
K2O	0.24	0.12	0.12	0.12	0.12	0.12	0.27	0.31	0.30	0.11	0.21	0.12	0.20
Total	99.54	99.99	100.54	100.73	100.03	99.92	99.50	99.65	99.86	99.61	100.21	100.09	99.49
Si	11.18	11.32	11.30	11.23	11.35	11.23	10.69	10.72	10.78	10.77	10.74	10.69	10.77
Ti	0.00	0.00	0.00	0.00	0.00	0.00	0.00	0.01	0.00	0.00	0.01	0.00	0.00
Al	4.83	4.68	4.69	4.73	4.67	4.80	5.27	5.25	5.22	5.22	5.21	5.25	5.19
Fe	0.00	0.00	0.00	0.00	0.02	0.00	0.02	0.01	0.03	0.02	0.03	0.02	0.04
Mn	0.00	0.00	0.00	0.00	0.00	0.00	0.00	0.00	0.00	0.00	0.00	0.00	0.01
Mg	0.00	0.00	0.04	0.04	0.00	0.00	0.03	0.00	0.00	0.00	0.00	0.02	0.01
Ca	0.77	0.69	0.63	0.71	0.56	0.72	1.30	1.27	1.21	1.20	1.19	1.24	1.21
Na	3.20	3.27	3.35	3.35	3.41	3.23	2.69	2.69	2.68	2.82	2.87	2.89	2.79
K	0.05	0.03	0.03	0.03	0.03	0.03	0.06	0.07	0.07	0.03	0.05	0.03	0.05
Ab	79.60	81.95	83.54	81.91	85.25	81.16	66.42	66.75	67.68	69.63	69.83	69.47	68.89
An	19.15	17.29	15.71	17.36	14.00	18.09	32.10	31.51	30.56	29.63	28.95	29.81	29.88
Or	1.24	0.75	0.75	0.73	0.75	0.75	1.48	1.74	1.77	0.74	1.22	0.72	1.23

	STG-1 KF-1	STG-1 KF-2	STG-1 KF-3	STG-1 KF-4	STG-2 KF-1	STG-2 KF-2C	STG-2 KF-2R	STG-2 KF-3C	STG-2 KF-3R	STG-2 KF-4	STG-2 KF-5	STG-3 KF-1	STG-3 KF-2
SiO2	64.98	64.00	64.41	64.51	64.24	64.36	64.38	64.26	64.46	64.19	63.78	64.17	64.60
TiO2	0.06	0.16	0.01	0.02	0.00	0.04	0.02	0.06	0.04	0.16	0.06	0.27	0.20
Al2O3	19.31	18.23	18.64	19.03	18.23	18.67	18.88	18.31	19.03	18.87	18.42	18.60	18.40
FeO(tot.)	0.07	0.00	0.01	0.00	0.00	0.08	0.02	0.08	0.08	0.04	0.00	0.09	0.10
MnO	0.00	0.04	0.08	0.00	0.00	0.02	0.00	0.02	0.04	0.01	0.09	0.05	0.00
MgO	0.00	0.00	0.10	0.17	0.00	0.08	0.00	0.00	0.05	0.12	0.07	0.08	0.08
CaO	0.71	0.00	0.02	0.62	0.16	0.00	0.00	0.01	0.09	0.09	0.04	0.02	0.04
Na2O	4.01	0.79	1.33	2.05	0.97	0.33	1.27	0.67	1.34	1.35	0.47	0.67	0.80
K2O	10.25	15.27	14.88	12.91	15.30	15.91	14.66	15.48	14.83	14.82	15.66	15.31	15.63
Total	99.39	98.49	99.48	99.31	98.90	99.49	99.23	98.89	99.96	99.65	98.59	99.26	99.85
Si	11.85	11.98	11.93	11.88	11.98	11.94	11.92	11.98	11.88	11.87	11.94	11.92	11.95
Ti	0.01	0.02	0.00	0.00	0.00	0.01	0.00	0.01	0.01	0.02	0.01	0.04	0.03
Al	4.15	4.02	4.07	4.13	4.01	4.08	4.12	4.02	4.13	4.11	4.07	4.07	4.01
Fe	0.01	0.00	0.00	0.00	0.00	0.01	0.00	0.01	0.01	0.01	0.00	0.01	0.02
Mn	0.00	0.01	0.01	0.00	0.00	0.00	0.00	0.00	0.01	0.00	0.01	0.01	0.00
Mg	0.00	0.00	0.03	0.05	0.00	0.02	0.00	0.00	0.01	0.03	0.02	0.02	0.02
Ca	0.14	0.00	0.00	0.12	0.03	0.00	0.00	0.00	0.02	0.02	0.01	0.00	0.01
Na	1.42	0.29	0.48	0.73	0.35	0.12	0.46	0.24	0.48	0.48	0.17	0.24	0.29
K	2.39	3.65	3.52	3.03	3.64	3.77	3.46	3.68	3.49	3.50	3.74	3.63	3.69

	STG-3 KF-3	STG-3 KF-4	STG-3 KF-5	STG-4 KF-1	STG-4 KF-2	STG-4 KF-3	STG-5 KF-1	STG-5 KF-2	STG-5 KF-3	STG-10 KF-1	STG-10 KF-2	STG-10 KF-3	MIG-2 KF-1
SiO2	64.20	64.33	63.60	63.83	63.38	64.16	64.02	64.40	64.21	64.50	63.85	63.84	63.74
TiO2	0.21	0.27	0.41	0.24	0.27	0.24	0.25	0.19	0.22	0.24	0.33	0.28	0.33
Al2O3	18.45	18.55	18.46	18.25	18.40	18.40	18.38	18.30	18.50	18.70	18.53	18.30	18.71
FeO(tot.)	0.12	0.11	0.01	0.10	0.05	0.19	0.09	0.08	0.00	0.07	0.05	0.07	0.00
MnO	0.03	0.10	0.00	0.00	0.14	0.09	0.05	0.00	0.04	0.00	0.00	0.04	0.00
MgO	0.06	0.08	0.00	0.03	0.14	0.05	0.02	0.01	0.00	0.14	0.11	0.00	0.00
CaO	0.01	0.05	0.02	0.12	0.17	0.00	0.00	0.03	0.01	0.02	0.14	0.03	0.14
Na2O	0.97	0.86	1.08	0.79	0.70	0.95	0.80	0.99	1.08	0.66	1.15	0.84	1.08
K2O	15.42	15.19	14.86	15.38	15.23	15.12	15.12	14.73	14.78	15.40	14.58	15.13	15.06
Total	99.47	99.54	98.44	98.74	98.48	99.20	98.73	98.73	98.84	99.73	98.74	98.53	99.06
Si	11.92	11.92	11.90	11.94	11.89	11.93	11.95	11.99	11.95	11.92	11.90	11.94	11.87
Ti	0.03	0.04	0.06	0.03	0.04	0.03	0.04	0.03	0.03	0.03	0.05	0.04	0.05
Al	4.04	4.05	4.07	4.02	4.07	4.03	4.04	4.02	4.06	4.07	4.07	4.04	4.11
Fe	0.02	0.02	0.00	0.02	0.01	0.03	0.01	0.01	0.00	0.01	0.01	0.01	0.00
Mn	0.00	0.02	0.00	0.00	0.02	0.01	0.01	0.00	0.01	0.00	0.00	0.01	0.00
Mg	0.02	0.02	0.00	0.01	0.04	0.01	0.01	0.00	0.00	0.04	0.03	0.00	0.00
Ca	0.00	0.01	0.00	0.02	0.03	0.00	0.00	0.01	0.00	0.00	0.03	0.01	0.03
Na	0.35	0.31	0.39	0.29	0.25	0.34	0.29	0.36	0.39	0.24	0.42	0.30	0.39
K	3.65	3.59	3.55	3.67	3.64	3.59	3.60	3.50	3.51	3.63	3.47	3.61	3.58

	MIG-2 KF-2	MIG-2 KF-3	MIG-5 KF-1	MIG-5 KF-2	MIG-5 KF-3	MIG-6 KF-1	MIG-6 KF-2C	MIG-6 KF-2R	MIG-6 KF-3	MIG-10 KF-1C	MIG-10 KF-1R	MIG-10 KF-2C	MIG-10 KF-2R
SiO2	63.74	64.17	64.17	63.74	64.17	64.39	64.60	64.39	63.10	64.17	64.17	63.74	64.17
TiO2	0.33	0.33	0.17	0.17	0.17	0.17	0.17	0.17	0.17	0.17	0.17	0.17	0.17
Al2O3	18.90	19.09	18.52	18.71	18.52	18.71	18.71	18.71	18.33	18.52	18.90	19.46	18.90
FeO(tot.)	0.13	0.00	0.13	0.00	0.00	0.00	0.13	0.00	0.00	0.00	0.00	0.00	0.00
MnO	0.00	0.00	0.00	0.00	0.00	0.13	0.13	0.00	0.13	0.00	0.00	0.00	0.13
MgO	0.17	0.00	0.00	0.17	0.00	0.00	0.00	0.00	0.00	0.00	0.17	0.17	0.00
CaO	0.28	0.42	0.14	0.00	0.00	0.00	0.00	0.00	0.00	0.00	0.42	1.12	0.00
Na2O	0.67	1.89	0.54	0.54	1.21	0.54	0.40	0.67	0.54	0.81	1.48	2.56	0.40
K2O	15.30	13.37	15.78	15.78	14.94	15.78	16.02	15.90	15.90	15.06	14.34	12.41	15.90
Total	99.52	99.27	99.45	99.11	99.01	99.72	100.16	99.84	98.17	98.73	99.65	99.63	99.67
Si	11.83	11.84	11.93	11.88	11.94	11.92	11.92	11.92	11.90	11.96	11.85	11.72	11.89
Ti	0.05	0.05	0.02	0.02	0.02	0.02	0.02	0.02	0.02	0.02	0.02	0.02	0.02
Al	4.13	4.15	4.06	4.11	4.06	4.08	4.07	4.08	4.08	4.07	4.11	4.22	4.13
Fe	0.02	0.00	0.02	0.00	0.00	0.00	0.02	0.00	0.00	0.00	0.00	0.00	0.00
Mn	0.00	0.00	0.00	0.00	0.00	0.02	0.02	0.00	0.02	0.00	0.00	0.00	0.02
Mg	0.05	0.00	0.00	0.05	0.00	0.00	0.00	0.00	0.00	0.00	0.05	0.05	0.00
Ca	0.06	0.08	0.03	0.00	0.00	0.00	0.00	0.00	0.00	0.00	0.08	0.22	0.00
Na	0.24	0.68	0.19	0.20	0.44	0.19	0.14	0.24	0.20	0.29	0.53	0.91	0.14
K	3.62	3.15	3.74	3.75	3.55	3.73	3.77	3.75	3.83	3.58	3.38	2.91	3.76

	MIG-10 KF-3	MIG-11 KF-1	MIG-11 KF-2C	MIG-11 KF-2R	MIG-20 KF-1	MIG-20 KF-2	MIG-20 KF-3	MIG-22 KF-1	MIG-22 KF-2	MIG-24 KF-1	MIG-29 KF-2	MIG-29 KF-3	MIG-29 KF-4C
SiO2	64.17	65.03	65.03	64.81	64.60	65.67	65.24	64.17	64.17	63.96	64.81	65.03	64.60
TiO2	0.17	0.17	0.17	0.17	0.17	0.17	0.17	0.33	0.17	0.33	0.17	0.17	0.17
Al2O3	18.52	18.90	18.90	19.27	18.52	19.27	18.90	18.71	19.09	18.90	18.90	18.52	18.90
FeO(tot.)	0.00	0.00	0.00	0.00	0.00	0.00	0.00	0.13	0.13	0.13	0.00	0.00	0.13
MnO	0.00	0.13	0.00	0.00	0.00	0.00	0.00	0.00	0.00	0.00	0.00	0.00	0.00
MgO	0.00	0.00	0.17	0.00	0.00	0.00	0.00	0.00	0.00	0.17	0.17	0.00	0.17
CaO	0.00	0.00	0.00	0.00	0.00	0.00	0.00	0.00	0.28	0.00	0.00	0.00	0.00
Na2O	0.81	1.21	1.48	1.21	0.54	1.35	0.40	0.94	0.81	0.67	1.21	0.81	0.94
K2O	15.06	15.30	14.70	15.06	16.14	15.18	16.50	15.18	15.18	15.54	14.94	15.78	15.66
Total	98.73	100.74	100.45	100.52	99.97	101.64	101.21	99.46	99.83	99.70	100.20	100.31	100.57
Si	11.96	11.91	11.90	11.87	11.95	11.90	11.93	11.90	11.85	11.85	11.90	11.97	11.87
Ti	0.02	0.02	0.02	0.02	0.02	0.02	0.02	0.05	0.02	0.05	0.02	0.02	0.02
Al	4.07	4.08	4.08	4.16	4.04	4.11	4.07	4.09	4.16	4.13	4.09	4.02	4.09
Fe	0.00	0.00	0.00	0.00	0.00	0.00	0.00	0.02	0.02	0.02	0.00	0.00	0.02
Mn	0.00	0.02	0.00	0.00	0.00	0.00	0.00	0.00	0.00	0.00	0.00	0.00	0.00
Mg	0.00	0.00	0.05	0.00	0.00	0.00	0.00	0.00	0.00	0.05	0.05	0.00	0.05
Ca	0.00	0.00	0.00	0.00	0.00	0.00	0.00	0.00	0.06	0.00	0.00	0.00	0.00
Na	0.29	0.43	0.53	0.43	0.19	0.47	0.14	0.34	0.29	0.24	0.43	0.29	0.33
K	3.58	3.57	3.43	3.52	3.81	3.51	3.85	3.59	3.58	3.67	3.50	3.70	3.67

	MIG-29 KF-4R	MIG-30 KF-1	MIG-30 KF-2	MIG-30 KF-3	MIG-31 KF-1	MIG-31 KF-2	MIG-31 KF-3	MIG-31 KF-4C	MIG-31 KF-4R	MIS-6 KF-1	MIS-6 KF-2	MIS-6 KF-3	MIS-7 KF-1
SiO2	64.60	64.81	65.24	65.24	64.39	63.96	64.17	64.60	62.46	63.96	64.17	63.96	63.32
TiO2	0.33	0.17	0.17	0.33	0.33	0.17	0.17	0.17	0.00	0.33	0.17	0.33	0.67
Al2O3	18.71	19.09	19.09	19.46	18.90	18.52	18.90	19.09	23.81	18.71	18.52	18.71	18.71
FeO(tot.)	0.13	0.00	0.00	0.00	0.00	0.00	0.00	0.13	0.00	0.00	0.13	0.00	0.00
MnO	0.00	0.00	0.00	0.00	0.00	0.00	0.00	0.00	0.00	0.00	0.00	0.00	0.00
MgO	0.00	0.00	0.00	0.00	0.00	0.00	0.00	0.00	0.17	0.00	0.00	0.00	0.00
CaO	0.00	0.14	0.00	0.00	0.00	0.00	0.00	0.14	4.62	0.00	0.00	0.00	0.00
Na2O	0.54	1.08	1.21	1.35	0.81	1.48	0.67	0.67	8.90	0.54	0.54	0.81	1.35
K2O	15.66	14.94	15.06	14.94	15.78	14.82	15.90	15.42	0.48	15.66	15.66	15.54	14.09
Total	99.97	100.23	100.77	101.32	100.21	98.95	99.81	100.22	100.44	99.20	99.19	99.35	98.14
Si	11.92	11.89	11.91	11.85	11.87	11.91	11.88	11.88	11.03	11.90	11.94	11.89	11.85
Ti	0.05	0.02	0.02	0.05	0.05	0.02	0.02	0.02	0.00	0.05	0.02	0.05	0.09
Al	4.07	4.13	4.11	4.17	4.11	4.07	4.13	4.14	4.96	4.10	4.06	4.10	4.13
Fe	0.02	0.00	0.00	0.00	0.00	0.00	0.00	0.02	0.00	0.00	0.02	0.00	0.00
Mn	0.00	0.00	0.00	0.00	0.00	0.00	0.00	0.00	0.00	0.00	0.00	0.00	0.00
Mg	0.00	0.00	0.00	0.00	0.00	0.00	0.00	0.00	0.04	0.00	0.00	0.00	0.00
Ca	0.00	0.03	0.00	0.00	0.00	0.00	0.00	0.03	0.87	0.00	0.00	0.00	0.00
Na	0.19	0.38	0.43	0.48	0.29	0.53	0.24	0.24	3.05	0.19	0.19	0.29	0.49
K	3.69	3.50	3.51	3.46	3.71	3.52	3.76	3.62	0.11	3.72	3.72	3.68	3.36

	MIS-7 KF-2C	MIS-7 KF-2R	MIS-7 KF-3	MIS-7 KF-4	MIS-10 KF-1	MIS-10 KF-2	MIS-10 KF-3
SiO2	63.32	63.96	64.17	64.17	64.17	63.53	63.96
TiO2	0.67	0.17	0.33	0.33	0.17	0.17	0.17
Al2O3	18.52	18.52	18.71	18.71	18.71	18.71	18.71
FeO(tot.)	0.00	0.00	0.13	0.00	0.00	0.00	0.00
MnO	0.00	0.00	0.00	0.00	0.00	0.00	0.00
MgO	0.00	0.17	0.00	0.17	0.17	0.00	0.00
CaO	0.00	0.00	0.00	0.00	0.00	0.00	0.00
Na2O	1.08	0.81	1.08	1.21	0.94	0.94	0.67
K2O	14.70	15.30	14.58	15.06	15.42	14.94	15.66
Total	98.29	98.93	99.00	99.65	99.58	98.29	99.17
Si	11.86	11.92	11.91	11.87	11.89	11.90	11.91
Ti	0.09	0.02	0.05	0.05	0.02	0.02	0.02
Al	4.09	4.07	4.09	4.08	4.09	4.13	4.11
Fe	0.00	0.00	0.02	0.00	0.00	0.00	0.00
Mn	0.00	0.00	0.00	0.00	0.00	0.00	0.00
Mg	0.00	0.05	0.00	0.05	0.05	0.00	0.00
Ca	0.00	0.00	0.00	0.00	0.00	0.00	0.00
Na	0.39	0.29	0.39	0.43	0.34	0.34	0.24
K	3.51	3.64	3.45	3.55	3.65	3.57	3.72

	STG-2 Bi-1	STG-2 Bi-2	STG-2 Bi-3	STG-2 Bi-4	STG-2 Bi-5	STG-2 Bi-6	STG-3 Bi-1	STG-3 Bi-2	STG-4 Bi-1	STG-4 Bi-2	STG-4 Bi-3	STG-4 Bi-4	STG-4 Bi-5
SiO2	35.65	35.72	35.90	35.55	35.81	36.07	36.06	35.38	36.16	35.92	35.57	36.02	35.80
TiO2	3.14	2.28	3.91	2.26	2.29	2.83	3.14	3.17	2.60	2.44	2.72	2.75	2.53
Al2O3	18.63	19.51	17.84	19.72	19.67	18.57	14.60	14.55	14.30	14.12	14.22	14.38	14.32
Fe2O3	6.10	5.56	5.90	5.50	5.73	5.83	7.81	7.99	7.73	7.66	7.93	7.84	7.81
FeO	11.66	10.64	11.27	10.52	10.96	11.15	14.94	15.28	14.79	14.65	15.16	15.00	14.94
MnO	0.32	0.39	0.38	0.35	0.38	0.45	0.80	0.82	0.72	0.79	0.80	0.85	0.81
MgO	10.55	11.49	10.98	11.52	11.74	11.37	8.73	8.91	9.87	10.73	9.65	9.93	10.01
CaO	0.06	0.00	0.00	0.00	0.00	0.00	0.09	0.09	0.06	0.06	0.03	0.02	0.10
Na2O	0.34	0.30	0.22	0.22	0.24	0.31	0.00	0.00	0.02	0.05	0.25	0.23	0.06
K2O	9.39	9.47	9.52	9.56	9.56	9.54	8.98	9.06	9.35	9.32	9.16	9.18	9.15
Total	95.23	94.80	95.33	94.65	95.81	95.54	94.37	94.45	94.83	94.98	94.69	95.42	94.75
Si	5.30	5.30	5.33	5.28	5.27	5.33	5.53	5.45	5.53	5.48	5.47	5.48	5.48
Ti	0.35	0.25	0.44	0.25	0.25	0.32	0.36	0.37	0.30	0.28	0.31	0.32	0.29
Al(tot.)	3.27	3.41	3.12	3.45	3.41	3.24	2.64	2.64	2.58	2.54	2.58	2.58	2.59
Al(iv)	2.70	2.70	2.67	2.72	2.74	2.67	2.47	2.55	2.48	2.52	2.54	2.52	2.52
Al(vi)	0.57	0.71	0.45	0.73	0.67	0.57	0.17	0.09	0.10	0.03	0.04	0.06	0.07
Fe3	0.68	0.62	0.66	0.62	0.63	0.65	0.90	0.93	0.89	0.88	0.92	0.90	0.90
Fe2	1.45	1.32	1.40	1.31	1.35	1.38	1.92	1.97	1.89	1.87	1.95	1.91	1.91
Mn	0.04	0.05	0.05	0.04	0.05	0.06	0.10	0.11	0.09	0.10	0.10	0.11	0.11
Mg	2.34	2.54	2.43	2.55	2.57	2.50	2.00	2.04	2.25	2.44	2.21	2.25	2.29
Ca	0.01	0.00	0.00	0.00	0.00	0.00	0.02	0.02	0.01	0.01	0.01	0.00	0.02
Na	0.10	0.09	0.06	0.06	0.07	0.09	0.00	0.00	0.01	0.02	0.07	0.07	0.02
K	1.78	1.79	1.80	1.81	1.79	1.80	1.76	1.78	1.82	1.82	1.80	1.78	1.79

	STG-4 Bi-6	STG-5 Bi-1	STG-11 Bi-1	STG-11 Bi-2	STG-11 Bi-3	STG-11 Bi-4	STG-11 Bi-5	STG-11 Bi-6	STG-11 Bi-7	STG-11 Bi-8	STG-11 Bi-9	STG-11 Bi-10	LG-B Bi-1
SiO2	36.30	35.80	36.77	36.57	36.67	36.13	36.22	36.43	36.53	36.40	36.72	36.87	35.43
TiO2	2.58	3.01	2.99	2.88	2.67	2.77	2.90	2.87	2.48	3.10	2.60	2.89	2.50
Al2O3	14.51	14.08	14.40	14.24	14.50	14.24	14.57	14.62	14.40	14.39	14.31	14.20	15.37
Fe2O3	7.72	7.42	6.60	6.71	6.66	6.70	6.65	6.74	6.75	6.42	6.60	6.77	2.69
FeO	14.76	14.18	12.61	12.82	12.73	12.82	12.71	12.89	12.91	12.27	12.63	12.95	19.60
MnO	0.67	1.41	0.56	0.50	0.58	0.51	0.43	0.60	0.69	0.82	0.72	0.63	0.46
MgO	10.40	10.43	12.02	12.31	12.08	12.49	12.24	12.20	11.72	11.83	12.29	12.12	10.55
CaO	0.00	0.00	0.11	0.00	0.07	0.01	0.12	0.07	0.06	0.05	0.07	0.09	0.08
Na2O	0.00	0.19	0.36	0.31	0.23	0.32	0.19	0.15	0.04	0.25	0.10	0.34	0.23
K2O	9.35	9.38	9.48	9.07	9.38	8.97	8.95	9.32	9.13	9.28	9.28	9.48	8.98
Total	95.52	95.16	95.24	94.74	94.90	94.29	94.31	95.22	94.04	94.16	94.66	95.67	95.62
Si	5.50	5.46	5.53	5.52	5.53	5.48	5.48	5.48	5.56	5.53	5.55	5.53	5.44
Ti	0.29	0.35	0.34	0.33	0.30	0.32	0.33	0.33	0.28	0.35	0.30	0.33	0.29
Al(tot.)	2.59	2.53	2.55	2.53	2.58	2.55	2.60	2.59	2.58	2.58	2.55	2.51	2.78
Al(iv)	2.50	2.54	2.47	2.48	2.47	2.52	2.52	2.52	2.44	2.48	2.46	2.47	2.56
Al(vi)	0.09	0.00	0.08	0.05	0.11	0.03	0.08	0.07	0.14	0.10	0.09	0.04	0.22
Fe3	0.88	0.85	0.75	0.76	0.76	0.77	0.76	0.76	0.77	0.73	0.75	0.76	0.31
Fe2	1.87	1.81	1.59	1.62	1.61	1.63	1.61	1.62	1.64	1.56	1.60	1.62	2.52
Mn	0.09	0.18	0.07	0.06	0.07	0.07	0.06	0.08	0.09	0.11	0.09	0.08	0.06
Mg	2.35	2.37	2.69	2.77	2.71	2.83	2.76	2.74	2.66	2.68	2.77	2.71	2.41
Ca	0.00	0.00	0.02	0.00	0.01	0.00	0.02	0.01	0.01	0.01	0.01	0.01	0.01
Na	0.00	0.06	0.11	0.09	0.07	0.09	0.06	0.04	0.01	0.07	0.03	0.10	0.07
K	1.81	1.83	1.82	1.75	1.80	1.74	1.73	1.79	1.77	1.80	1.79	1.81	1.76

	LG-B Bi-2	LG-B Bi-3	LG-C Bi-1	LG-C Bi-2	MIG-2 Bi-1	MIG-2 Bi-2	MIG-2 Bi-3	MIG-2 Bi-4	MIG-2 Bi-5	MIG-2 Bi-6	MIG-5 Bi-1	MIG-5 Bi-2	MIG-5 Bi-3
SiO2	35.22	35.32	36.19	36.34	34.87	34.87	34.87	35.08	34.65	34.65	36.58	36.58	36.58
TiO2	3.09	3.31	3.67	3.59	2.84	4.00	3.17	3.34	3.50	3.50	1.83	2.17	1.83
Al2O3	15.20	15.26	16.25	16.25	15.50	15.31	15.68	15.12	15.68	15.68	15.50	14.74	15.50
Fe2O3	2.69	2.69	2.09	2.10	8.15	8.62	8.49	8.66	8.66	8.49	6.13	6.26	6.22
FeO	19.59	19.61	15.24	15.32	17.11	18.10	17.83	18.19	18.19	17.83	12.88	13.15	13.06
MnO	0.49	0.47	0.28	0.34	0.39	0.52	0.52	0.65	0.52	0.52	1.29	1.03	1.29
MgO	9.65	9.62	11.56	11.34	8.29	7.46	7.96	7.96	7.63	7.79	12.27	11.77	12.27
CaO	0.02	0.04	0.06	0.02	0.00	0.00	0.14	0.00	0.00	0.00	0.00	0.00	0.00
Na2O	0.10	0.19	0.24	0.16	0.40	0.40	0.27	0.27	0.13	0.00	0.40	0.27	0.27
K2O	9.40	9.47	9.42	9.57	9.28	9.16	8.91	9.04	9.16	9.16	9.64	9.40	9.52
Total	95.18	95.71	94.79	94.82	96.01	97.58	96.99	97.45	97.26	96.77	95.91	94.74	95.91
Si	5.45	5.43	5.47	5.50	5.33	5.27	5.29	5.31	5.26	5.27	5.48	5.54	5.48
Ti	0.36	0.38	0.42	0.41	0.33	0.46	0.36	0.38	0.40	0.40	0.21	0.25	0.21
Al(tot.)	2.77	2.77	2.90	2.90	2.79	2.73	2.80	2.70	2.80	2.81	2.74	2.63	2.74
Al(iv)	2.56	2.57	2.53	2.50	2.67	2.73	2.71	2.69	2.75	2.73	2.52	2.46	2.52
Al(vi)	0.22	0.20	0.37	0.39	0.12	0.00	0.09	0.01	0.06	0.08	0.21	0.18	0.21
Fe3	0.31	0.31	0.24	0.24	0.94	0.98	0.97	0.99	0.99	0.97	0.69	0.71	0.70
Fe2	2.53	2.52	1.93	1.94	2.19	2.29	2.26	2.30	2.31	2.27	1.61	1.67	1.63
Mn	0.06	0.06	0.04	0.04	0.05	0.07	0.07	0.08	0.07	0.07	0.16	0.13	0.16
Mg	2.22	2.21	2.61	2.56	1.89	1.68	1.80	1.80	1.72	1.77	2.74	2.66	2.74
Ca	0.00	0.01	0.01	0.00	0.00	0.00	0.02	0.00	0.00	0.00	0.00	0.00	0.00
Na	0.03	0.06	0.07	0.05	0.12	0.12	0.08	0.08	0.04	0.00	0.12	0.08	0.08
K	1.85	1.86	1.82	1.85	1.81	1.77	1.72	1.75	1.77	1.78	1.84	1.82	1.82

	MIG-5 Bi-4	MIG-6 Bi-1	MIG-6 Bi-2	MIG-6 Bi-3	MIG-6 Bi-4	MIG-10 Bi-1	MIG-10 Bi-2	MIG-11 Bi-1	MIG-11 Bi-2	MIG-11 Bi-3	MIG-11 Bi-4	MIG-11 Bi-5	MIG-11 Bi-6
SiO2	36.58	36.58	36.58	35.94	36.36	37.01	36.79	34.65	34.87	34.65	34.65	34.44	35.29
TiO2	1.67	2.50	2.00	2.17	2.17	1.83	1.67	4.50	4.50	3.50	4.34	4.00	3.67
Al2O3	15.50	15.12	15.12	14.74	14.74	14.93	15.68	17.20	17.20	17.95	17.57	17.57	17.57
Fe2O3	6.13	6.35	6.09	6.30	6.05	6.30	6.26	8.45	8.45	8.28	8.53	8.15	8.53
FeO	12.88	13.33	12.79	13.24	12.70	13.24	13.15	17.74	17.74	17.38	17.92	17.11	17.92
MnO	1.16	1.03	1.03	1.03	1.16	1.16	1.16	0.77	0.77	0.77	0.65	0.77	0.65
MgO	12.27	12.10	11.94	11.94	12.60	11.11	11.11	5.80	5.64	5.80	5.64	5.47	5.80
CaO	0.00	0.00	0.00	0.00	0.00	0.28	0.14	0.00	0.00	0.14	0.00	0.00	0.00
Na2O	0.27	0.13	0.13	0.27	0.13	0.13	0.13	0.00	0.27	0.27	0.27	0.00	0.27
K2O	9.64	9.28	9.40	9.16	9.28	9.04	9.28	9.64	9.40	9.16	9.64	9.52	9.52
Total	95.49	95.78	94.47	94.16	94.58	94.40	94.74	97.90	97.99	97.07	98.36	96.21	98.37
Si	5.50	5.48	5.54	5.48	5.51	5.61	5.56	5.21	5.23	5.23	5.19	5.25	5.27
Ti	0.19	0.28	0.23	0.25	0.25	0.21	0.19	0.51	0.51	0.40	0.49	0.46	0.41
Al(tot.)	2.75	2.67	2.70	2.65	2.63	2.67	2.79	3.05	3.04	3.19	3.10	3.16	3.09
Al(iv)	2.51	2.52	2.46	2.52	2.50	2.39	2.44	2.79	2.77	2.77	2.81	2.75	2.73
Al(vi)	0.24	0.15	0.24	0.14	0.14	0.28	0.35	0.26	0.28	0.43	0.29	0.41	0.36
Fe3	0.69	0.72	0.69	0.72	0.69	0.72	0.71	0.96	0.95	0.94	0.96	0.94	0.96
Fe2	1.62	1.67	1.62	1.69	1.61	1.68	1.66	2.23	2.23	2.19	2.25	2.18	2.24
Mn	0.15	0.13	0.13	0.13	0.15	0.15	0.15	0.10	0.10	0.10	0.08	0.10	0.08
Mg	2.75	2.70	2.70	2.72	2.84	2.51	2.50	1.30	1.26	1.31	1.26	1.24	1.29
Ca	0.00	0.00	0.00	0.00	0.00	0.05	0.02	0.00	0.00	0.02	0.00	0.00	0.00
Na	0.08	0.04	0.04	0.08	0.04	0.04	0.04	0.00	0.08	0.08	0.08	0.00	0.08
K	1.85	1.77	1.82	1.78	1.79	1.75	1.79	1.85	1.80	1.76	1.84	1.85	1.81

	MIG-11 Bi-7	MIG-11 Bi-8	MIG-22 Bi-1	MIG-22 Bi-2	MIG-22 Bi-3	MIG-22 Bi-4	MIG-22 Bi-5	MIG-24 Bi-1	MIG-24 Bi-2	MIG-24 Bi-3	MIG-24 Bi-4	MIG-29 Bi-1	MIG-29 Bi-2
SiO2	34.87	35.08	36.79	36.79	37.01	37.01	37.01	34.65	34.87	35.08	35.08	37.22	37.43
TiO2	4.17	3.50	2.00	2.34	2.17	2.34	2.17	2.67	3.00	4.17	4.34	3.67	3.17
Al2O3	17.57	17.57	15.50	15.68	14.93	15.12	15.50	16.25	15.87	15.50	15.31	14.74	14.74
Fe2O3	8.41	8.41	6.39	6.30	6.26	6.43	6.30	8.66	8.53	8.66	8.71	6.60	6.99
FeO	17.65	17.65	13.42	13.24	13.15	13.51	13.24	18.19	17.92	18.19	18.28	13.87	14.68
MnO	0.77	0.52	0.90	1.03	0.90	1.03	1.03	0.65	0.52	0.65	0.52	0.65	0.52
MgO	5.97	5.80	12.10	12.10	12.44	11.94	12.27	7.63	7.30	6.47	6.63	10.78	10.78
CaO	0.00	0.00	0.14	0.00	0.14	0.14	0.00	0.00	0.00	0.00	0.00	0.00	0.00
Na2O	0.27	0.13	0.27	0.13	0.27	0.27	0.27	0.00	0.00	0.40	0.13	0.13	0.40
K2O	9.52	9.40	9.40	9.52	8.79	9.52	9.64	8.79	9.52	9.40	8.91	9.76	9.64
Total	98.36	97.22	96.27	96.50	95.43	96.67	96.80	96.63	96.68	97.66	97.04	96.76	97.65
Si	5.21	5.29	5.48	5.46	5.54	5.50	5.49	5.27	5.32	5.31	5.32	5.53	5.53
Ti	0.47	0.40	0.22	0.26	0.24	0.26	0.24	0.31	0.34	0.47	0.50	0.41	0.35
Al(tot.)	3.10	3.12	2.72	2.75	2.63	2.65	2.71	2.92	2.85	2.77	2.74	2.58	2.57
Al(iv)	2.79	2.71	2.52	2.54	2.46	2.50	2.52	2.73	2.69	2.69	2.68	2.47	2.47
Al(vi)	0.31	0.41	0.21	0.21	0.17	0.15	0.19	0.19	0.17	0.07	0.06	0.11	0.10
Fe3	0.95	0.95	0.72	0.71	0.71	0.72	0.70	0.99	0.98	0.99	0.99	0.74	0.78
Fe2	2.21	2.23	1.67	1.64	1.65	1.68	1.64	2.32	2.28	2.30	2.32	1.72	1.81
Mn	0.10	0.07	0.11	0.13	0.11	0.13	0.13	0.08	0.07	0.08	0.07	0.08	0.07
Mg	1.33	1.30	2.69	2.68	2.77	2.65	2.71	1.73	1.66	1.46	1.50	2.39	2.37
Ca	0.00	0.00	0.02	0.00	0.02	0.02	0.00	0.00	0.00	0.00	0.00	0.00	0.00
Na	0.08	0.04	0.08	0.04	0.08	0.08	0.08	0.00	0.00	0.12	0.04	0.04	0.12
K	1.82	1.81	1.79	1.80	1.68	1.81	1.82	1.71	1.85	1.81	1.73	1.85	1.82

	MIG-29 Bi-3	MIG-29 Bi-4	MIG-30 Bi-1	MIG-30 Bi-2	MIG-30 Bi-3	MIG-30 Bi-4	MIG-30 Bi-5	MIG-31 Bi-1	MIG-31 Bi-2	MIG-31 Bi-3	MIG-31 Bi-4	MIG-31 Bi-5	MIG-31 Bi-6
SiO2	36.79	37.22	35.08	35.29	35.94	35.08	35.08	36.15	36.36	35.51	36.36	36.36	36.58
TiO2	2.50	4.00	3.84	3.84	4.00	3.50	3.67	2.00	2.50	1.83	2.17	2.17	2.17
Al2O3	15.12	15.12	18.33	18.33	18.52	18.14	18.14	15.87	14.74	15.31	15.12	15.31	15.31
Fe2O3	6.86	6.90	7.16	7.46	7.29	7.38	7.38	6.69	6.56	7.03	6.78	6.78	6.65
FeO	14.41	14.50	15.04	15.67	15.31	15.49	15.49	14.05	13.78	14.77	14.23	14.23	13.96
MnO	0.52	0.52	0.26	0.26	0.26	0.26	0.26	1.16	1.16	1.16	1.16	1.16	1.16
MgO	10.94	10.61	7.30	7.46	6.96	7.63	7.46	11.44	11.28	11.28	11.44	11.28	11.61
CaO	0.00	0.00	0.00	0.00	0.14	0.14	0.00	0.00	0.00	0.00	0.14	0.00	0.00
Na2O	0.27	0.13	0.13	0.00	0.13	0.27	0.13	0.27	0.13	0.27	0.27	0.13	0.13
K2O	9.52	9.76	9.52	9.76	9.64	9.76	9.64	9.04	9.16	8.19	9.40	9.28	9.52
Total	96.24	98.07	95.94	97.33	97.46	96.91	96.51	96.00	95.01	94.65	96.39	96.02	96.42
Si	5.51	5.47	5.28	5.25	5.32	5.25	5.26	5.42	5.51	5.41	5.45	5.46	5.47
Ti	0.28	0.44	0.43	0.43	0.45	0.39	0.41	0.23	0.29	0.21	0.25	0.25	0.24
Al(tot.)	2.67	2.62	3.25	3.22	3.23	3.20	3.21	2.81	2.63	2.75	2.67	2.71	2.70
Al(iv)	2.49	2.53	2.73	2.75	2.68	2.75	2.74	2.58	2.49	2.59	2.55	2.54	2.53
Al(vi)	0.18	0.09	0.52	0.47	0.55	0.45	0.47	0.23	0.14	0.16	0.13	0.17	0.17
Fe3	0.77	0.76	0.81	0.84	0.81	0.83	0.83	0.76	0.75	0.81	0.77	0.77	0.75
Fe2	1.80	1.78	1.89	1.95	1.89	1.94	1.94	1.76	1.75	1.88	1.79	1.79	1.75
Mn	0.07	0.07	0.03	0.03	0.03	0.03	0.03	0.15	0.15	0.15	0.15	0.15	0.15
Mg	2.44	2.32	1.64	1.65	1.54	1.70	1.67	2.56	2.55	2.56	2.56	2.53	2.59
Ca	0.00	0.00	0.00	0.00	0.02	0.02	0.00	0.00	0.00	0.00	0.02	0.00	0.00
Na	0.08	0.04	0.04	0.00	0.04	0.08	0.04	0.08	0.04	0.08	0.08	0.04	0.04
K	1.82	1.83	1.83	1.85	1.82	1.86	1.85	1.73	1.77	1.59	1.80	1.78	1.82

	MIS-7 Bi-1	MIS-7 Bi-2	MIS-7 Bi-3	MIS-7 Bi-4	MIS-7 Bi-5	MIS-10 Bi-1	MIS-10 Bi-2	MIS-10 Bi-3	MIS-10 Bi-4	STA-1 Bi-1
SiO2	35.72	35.29	35.08	35.29	34.87	35.51	35.29	36.15	35.29	37.14
TiO2	3.34	3.67	3.34	3.67	3.17	2.50	2.50	2.17	2.34	3.39
Al2O3	16.44	16.44	16.82	16.44	16.25	16.82	17.01	17.57	17.20	14.49
Fe2O3	7.63	7.16	7.25	7.42	7.33	7.33	7.25	7.03	7.29	6.38
FeO	16.03	15.04	15.22	15.58	15.40	15.40	15.22	14.77	15.31	12.21
MnO	0.77	0.77	0.65	0.65	0.65	0.90	0.90	0.90	0.90	0.52
MgO	7.63	8.62	8.29	8.29	7.96	8.95	8.79	8.62	8.95	11.99
CaO	0.00	0.00	0.00	0.00	0.14	0.00	0.00	0.00	0.14	0.00
Na2O	0.00	0.27	0.27	0.27	0.13	0.13	0.13	0.27	0.13	0.29
K2O	9.40	9.52	9.64	9.52	9.40	9.64	9.40	8.07	9.52	9.50
Total	96.20	96.06	95.83	96.39	94.57	96.45	95.76	94.85	96.34	95.27
Si	5.40	5.33	5.32	5.32	5.36	5.35	5.34	5.45	5.32	5.56
Ti	0.38	0.42	0.38	0.42	0.37	0.28	0.29	0.25	0.27	0.38
Al(tot.)	2.93	2.93	3.01	2.92	2.95	2.99	3.04	3.12	3.06	2.56
Al(iv)	2.60	2.67	2.68	2.68	2.64	2.65	2.66	2.55	2.68	2.44
Al(vi)	0.33	0.26	0.32	0.25	0.31	0.34	0.38	0.57	0.37	0.11
Fe3	0.87	0.81	0.83	0.84	0.85	0.83	0.83	0.80	0.83	0.72
Fe2	2.03	1.90	1.93	1.97	1.98	1.94	1.93	1.86	1.93	1.53
Mn	0.10	0.10	0.08	0.08	0.09	0.12	0.12	0.12	0.12	0.07
Mg	1.72	1.94	1.87	1.86	1.82	2.01	1.98	1.94	2.01	2.67
Ca	0.00	0.00	0.00	0.00	0.02	0.00	0.00	0.00	0.02	0.00
Na	0.00	0.08	0.08	0.08	0.04	0.04	0.04	0.08	0.04	0.08
K	1.81	1.83	1.86	1.83	1.84	1.85	1.82	1.55	1.83	1.81

	STG-4 Amph-1	STG-4 Amph-2	STG-4 Amph-3	STG-4 Amph-4	STG-4 Amph-5	STG-4 Amph-6	STG-4 Amph-7	STG-5 Amph-1	STG-5 Amph-2	STG-5 Amph-3	STG-10 Amph-1C	STG-10 Amph-1R	STG-10 Amph-2
SiO2	45.73	44.17	46.98	44.31	48.85	49.86	45.02	44.79	45.21	44.76	43.91	44.16	44.00
TiO2	0.77	1.01	0.71	0.93	0.49	0.46	0.87	0.68	0.76	0.72	0.89	1.25	1.01
Al2O3	7.26	8.34	6.71	8.15	4.73	4.67	7.84	7.63	7.38	7.77	9.17	8.13	8.11
FeO(tot.)	18.70	19.51	17.84	19.60	16.57	16.60	18.82	17.78	18.26	18.60	18.96	19.42	19.93
MnO	1.42	1.37	1.40	1.33	1.34	1.34	1.27	1.90	1.81	1.80	1.58	1.86	1.87
MgO	9.89	9.48	10.74	9.01	12.20	12.30	10.36	10.25	9.98	9.77	9.85	9.00	8.78
CaO	11.43	11.22	11.34	11.40	11.84	11.69	11.49	11.31	11.13	11.22	11.32	10.94	11.19
Na2O	1.09	1.15	1.06	1.33	0.85	0.63	1.33	1.39	1.23	1.24	1.57	1.34	1.04
K2O	0.77	0.89	0.64	0.90	0.37	0.39	0.79	0.72	0.76	0.81	0.92	0.91	0.80
Total	97.06	97.14	97.42	96.96	97.24	97.94	97.79	96.45	96.52	96.69	98.17	97.01	96.73
Si	6.91	6.69	7.02	6.76	7.25	7.32	6.75	6.80	6.87	6.80	6.58	6.73	6.72
Al(iv)	1.09	1.31	0.98	1.24	0.75	0.68	1.25	1.20	1.13	1.20	1.42	1.27	1.28
Al(vi)	0.21	0.18	0.21	0.23	0.08	0.13	0.14	0.17	0.19	0.19	0.20	0.19	0.18
AlT	1.29	1.49	1.18	1.47	0.83	0.81	1.39	1.37	1.32	1.39	1.62	1.46	1.46
Ti	0.09	0.12	0.08	0.11	0.05	0.05	0.10	0.08	0.09	0.08	0.10	0.14	0.12
Fe3	0.40	0.58	0.38	0.37	0.38	0.37	0.54	0.49	0.46	0.51	0.57	0.44	0.59
Fe2	1.97	1.89	1.85	2.14	1.68	1.67	1.82	1.77	1.86	1.86	1.80	2.03	1.96
Mg	2.23	2.14	2.39	2.05	2.70	2.69	2.32	2.32	2.26	2.21	2.20	2.05	2.00
Mn	0.18	0.18	0.18	0.17	0.17	0.17	0.16	0.24	0.23	0.23	0.20	0.24	0.24
Ca	1.85	1.82	1.82	1.86	1.88	1.84	1.85	1.84	1.81	1.83	1.82	1.79	1.83
NaM4	0.08	0.10	0.10	0.07	0.06	0.09	0.08	0.09	0.10	0.09	0.10	0.11	0.09
NaA	0.24	0.24	0.21	0.32	0.18	0.09	0.30	0.32	0.26	0.27	0.36	0.28	0.22
NaT	0.32	0.34	0.31	0.39	0.24	0.18	0.39	0.41	0.36	0.37	0.46	0.40	0.31
K	0.15	0.17	0.12	0.18	0.07	0.07	0.15	0.14	0.15	0.16	0.18	0.18	0.16

	STG-10 Amph-3	STG-10 Amph-4	STG-10 Amph-5	STG-11 Amph-1	STG-11 Amph-2	STG-11 Amph-3	STG-11 Amph-4	STG-11 Amph-5	STG-11 Amph-6	STG-11 Amph-7	STG-11 Amph-8	STG-11 Amph-9	STG-11 Amph-10
SiO2	44.02	43.65	43.84	47.59	48.67	45.37	47.42	45.33	48.07	48.31	44.71	45.05	45.84
TiO2	0.98	1.09	0.69	0.58	0.65	1.17	0.79	1.05	0.65	0.65	0.94	1.00	1.07
Al2O3	7.99	8.53	8.42	6.47	5.86	7.95	6.86	7.67	6.66	6.18	8.45	7.81	7.46
FeO(tot.)	20.83	20.35	21.22	15.13	14.39	16.81	15.71	16.91	15.18	15.30	17.62	16.85	16.74
MnO	2.02	1.86	1.71	0.94	0.84	0.93	0.83	1.00	0.90	1.08	1.10	1.02	1.24
MgO	8.42	8.41	7.74	12.91	13.56	11.31	12.33	11.46	13.02	12.98	10.53	11.23	11.57
CaO	10.93	10.96	11.11	11.73	12.13	11.76	11.94	11.73	11.95	11.78	11.67	11.52	11.72
Na2O	1.25	1.38	1.13	1.04	0.81	1.33	1.04	1.24	1.15	1.09	1.37	1.18	1.45
K2O	0.75	0.89	0.81	0.58	0.49	0.81	0.58	0.76	0.57	0.54	0.99	0.82	0.80
Total	97.19	97.12	96.67	96.97	97.40	97.44	97.50	97.15	98.15	97.91	97.38	96.48	97.89
Si	6.72	6.67	6.74	7.04	7.13	6.78	7.01	6.78	7.03	7.08	6.73	6.79	6.82
Al(iv)	1.28	1.33	1.26	0.96	0.87	1.22	0.99	1.22	0.97	0.92	1.27	1.21	1.18
Al(vi)	0.15	0.21	0.27	0.17	0.14	0.18	0.20	0.14	0.18	0.15	0.23	0.18	0.13
AlT	1.44	1.54	1.53	1.13	1.01	1.40	1.20	1.35	1.15	1.07	1.50	1.39	1.31
Ti	0.11	0.13	0.08	0.06	0.07	0.13	0.09	0.12	0.07	0.07	0.11	0.11	0.12
Fe3	0.62	0.50	0.51	0.41	0.36	0.36	0.32	0.46	0.35	0.37	0.37	0.46	0.37
Fe2	2.04	2.10	2.22	1.46	1.40	1.75	1.62	1.65	1.51	1.50	1.85	1.67	1.71
Mg	1.91	1.92	1.77	2.85	2.96	2.52	2.72	2.56	2.84	2.84	2.36	2.52	2.57
Mn	0.26	0.24	0.22	0.12	0.10	0.12	0.10	0.13	0.11	0.13	0.14	0.13	0.16
Ca	1.79	1.80	1.83	1.86	1.90	1.88	1.89	1.88	1.87	1.85	1.88	1.86	1.87
NaM4	0.11	0.11	0.09	0.08	0.05	0.06	0.06	0.06	0.07	0.08	0.06	0.08	0.07
NaA	0.26	0.30	0.25	0.22	0.18	0.32	0.24	0.30	0.26	0.23	0.34	0.27	0.35
NaT	0.37	0.41	0.34	0.30	0.23	0.39	0.30	0.36	0.33	0.31	0.40	0.34	0.42
K	0.15	0.17	0.16	0.11	0.09	0.15	0.11	0.15	0.11	0.10	0.19	0.16	0.15

	STG-11 Amph-11	STG-11 Amph-12	STG-11 Amph-13	STG-11 Amph-14C	STG-11 Amph-14R	STG-11 Amph-15C	STG-11 Amph-15R	STG-13 Amph-1	STG-13 Amph-2	STG-13 Amph-3	STG-13 Amph-4	STG-13 Amph-5	STG-13 Amph-6
SiO2	45.89	44.91	46.19	45.43	45.58	46.53	45.07	51.99	52.74	52.26	52.70	51.82	51.69
TiO2	0.86	1.03	1.07	1.11	0.77	1.05	1.05	0.41	0.41	0.34	0.28	0.31	0.62
Al2O3	7.11	7.73	7.44	7.45	7.94	6.78	7.95	2.65	2.25	2.55	2.30	2.95	2.94
FeO(tot.)	16.73	17.40	16.73	16.67	17.13	16.53	16.74	14.06	13.88	14.03	13.99	14.10	15.80
MnO	1.10	1.23	0.98	1.27	1.27	1.24	1.08	0.24	0.30	0.27	0.29	0.29	0.32
MgO	11.58	10.95	11.53	11.25	11.05	11.58	11.12	14.91	14.59	14.79	14.57	14.25	13.95
CaO	11.65	11.45	11.61	11.69	11.62	11.56	11.58	11.91	12.10	11.80	12.18	12.53	11.83
Na2O	1.43	1.38	1.02	0.99	1.32	1.51	1.06	0.54	0.65	0.49	0.27	0.36	0.68
K2O	0.72	0.86	0.75	0.80	0.78	0.66	0.79	0.23	0.23	0.21	0.13	0.27	0.23
Total	97.07	96.94	97.32	96.66	97.46	97.44	96.44	96.94	97.15	96.74	96.71	96.88	98.06
Si	6.88	6.77	6.88	6.83	6.81	6.95	6.79	7.58	7.69	7.63	7.70	7.59	7.53
Al(iv)	1.12	1.23	1.12	1.17	1.19	1.05	1.21	0.42	0.31	0.37	0.30	0.41	0.47
Al(vi)	0.14	0.14	0.18	0.15	0.21	0.15	0.20	0.04	0.08	0.07	0.10	0.10	0.03
AlT	1.26	1.37	1.31	1.32	1.40	1.19	1.41	0.46	0.39	0.44	0.40	0.51	0.50
Ti	0.10	0.12	0.12	0.13	0.09	0.12	0.12	0.05	0.05	0.04	0.03	0.03	0.07
Fe3	0.37	0.45	0.42	0.45	0.42	0.26	0.45	0.24	0.08	0.19	0.11	0.11	0.19
Fe2	1.73	1.75	1.66	1.64	1.73	1.81	1.65	1.48	1.61	1.52	1.60	1.61	1.73
Mg	2.59	2.46	2.56	2.52	2.46	2.58	2.50	3.24	3.17	3.22	3.17	3.11	3.03
Mn	0.14	0.16	0.12	0.16	0.16	0.16	0.14	0.03	0.04	0.03	0.04	0.04	0.04
Ca	1.87	1.85	1.85	1.88	1.86	1.85	1.87	1.86	1.89	1.85	1.91	1.97	1.85
NaM4	0.07	0.08	0.08	0.06	0.07	0.08	0.07	0.07	0.09	0.08	0.04	0.02	0.06
NaA	0.35	0.32	0.22	0.23	0.31	0.36	0.24	0.08	0.10	0.06	0.04	0.09	0.13
NaT	0.42	0.40	0.29	0.29	0.38	0.44	0.31	0.15	0.18	0.14	0.08	0.10	0.19
K	0.14	0.17	0.14	0.15	0.15	0.13	0.15	0.04	0.04	0.04	0.02	0.05	0.04

	STG-13 Amph-7	MIG-5 Amph-1	MIG-5 Amph-2	MIG-5 Amph-3	MIG-5 Amph-4	MIG-5 Amph-5	MIG-6 Amph-1	MIG-6 Amph-2	MIG-6 Amph-3	MIG-6 Amph-4	MIG-10 Amph-1C	MIG-10 Amph-1R	MIG-10 Amph-2
SiO2	51.85	45.13	44.92	45.35	46.20	44.71	45.13	47.06	45.78	46.84	43.21	43.42	44.06
TiO2	0.47	0.50	0.67	0.83	0.50	0.83	0.83	0.50	0.67	0.67	0.50	0.67	0.50
Al2O3	2.77	8.13	7.75	7.75	7.56	8.69	7.94	6.99	6.99	7.18	9.07	9.26	8.50
FeO(tot.)	14.31	17.63	17.37	16.85	16.85	18.14	17.50	16.60	16.47	16.98	18.91	19.17	18.53
MnO	0.25	1.68	1.68	1.68	1.81	1.68	1.68	1.68	1.68	1.81	1.81	1.81	1.94
MgO	14.80	10.78	10.94	11.44	11.94	10.78	10.78	12.10	11.77	11.94	10.11	9.45	9.95
CaO	11.74	11.61	11.47	11.33	11.33	11.47	11.47	11.33	11.19	11.61	11.47	11.33	11.33
Na2O	0.82	1.08	1.21	1.48	1.48	1.48	1.48	1.35	1.35	0.94	1.35	1.62	1.35
K2O	0.19	0.60	0.72	0.72	0.72	0.84	0.84	0.60	0.60	0.60	0.84	0.84	0.84
Total	97.20	97.14	96.73	97.43	98.39	98.62	97.65	98.21	96.50	98.57	97.27	97.57	97.00
Si	7.56	6.75	6.76	6.77	6.81	6.63	6.76	6.93	6.87	6.86	6.51	6.56	6.67
Al(iv)	0.44	1.25	1.24	1.23	1.19	1.37	1.24	1.07	1.13	1.14	1.49	1.44	1.33
Al(vi)	0.04	0.19	0.14	0.13	0.12	0.15	0.17	0.14	0.11	0.10	0.13	0.22	0.18
AlT	0.48	1.43	1.38	1.36	1.31	1.52	1.40	1.21	1.24	1.24	1.61	1.65	1.52
Ti	0.05	0.06	0.08	0.09	0.06	0.09	0.09	0.06	0.08	0.07	0.06	0.08	0.06
Fe3	0.21	0.67	0.62	0.55	0.63	0.64	0.46	0.56	0.58	0.71	0.85	0.61	0.65
Fe2	1.54	1.54	1.57	1.56	1.44	1.60	1.73	1.49	1.48	1.37	1.53	1.82	1.69
Mg	3.22	2.40	2.45	2.54	2.62	2.38	2.41	2.65	2.63	2.61	2.27	2.13	2.24
Mn	0.03	0.21	0.21	0.21	0.23	0.21	0.21	0.21	0.21	0.22	0.23	0.23	0.25
Ca	1.83	1.86	1.85	1.81	1.79	1.82	1.84	1.79	1.80	1.82	1.85	1.84	1.84
NaM4	0.09	0.07	0.08	0.10	0.11	0.10	0.08	0.11	0.11	0.10	0.08	0.09	0.09
NaA	0.15	0.24	0.27	0.33	0.31	0.33	0.35	0.27	0.29	0.17	0.32	0.39	0.31
NaT	0.23	0.31	0.35	0.43	0.42	0.43	0.43	0.39	0.39	0.27	0.39	0.47	0.40
K	0.04	0.11	0.14	0.14	0.14	0.16	0.16	0.11	0.11	0.11	0.16	0.16	0.16

	MIG-10 Amph-3	MIG-10 Amph-4	MIG-22 Amph-1	MIG-22 Amph-2	MIG-22 Amph-3	MIG-22 Amph-4	MIG-24 Amph-1	MIG-24 Amph-2	MIG-24 Amph-3	MIG-24 Amph-4	STA-1 Amph-1	STA-1 Amph-2	STA-1 Amph-3
SiO2	43.64	42.57	45.78	45.13	45.13	45.35	43.42	41.28	43.21	40.86	46.19	45.11	45.71
TiO2	0.67	0.67	1.17	1.33	1.33	1.50	0.83	1.17	0.67	1.17	0.94	1.00	1.07
Al2O3	9.07	9.64	7.75	7.94	8.13	7.56	9.45	10.39	9.07	11.34	7.75	7.84	7.67
FeO(tot.)	18.91	19.30	17.50	17.50	17.75	17.24	24.44	24.83	24.57	25.09	16.47	16.60	16.59
MnO	1.68	1.81	1.68	1.68	1.55	1.68	1.16	1.03	1.16	1.03	0.82	0.82	0.69
MgO	9.78	9.62	11.11	11.44	10.78	11.11	6.80	5.80	6.47	5.64	11.74	11.45	11.57
CaO	11.47	11.47	11.47	11.33	11.19	11.33	11.05	11.19	11.05	11.19	11.70	11.92	11.85
Na2O	1.62	1.48	1.48	1.48	1.35	1.35	1.48	1.35	1.35	1.35	1.18	0.93	1.43
K2O	0.84	0.96	0.84	0.84	0.96	0.84	0.84	1.08	0.84	1.20	0.74	0.76	0.75
Total	97.68	97.52	98.78	98.67	98.17	97.96	99.47	98.12	98.39	98.87	97.53	96.43	97.33
Si	6.58	6.43	6.77	6.67	6.72	6.76	6.56	6.37	6.61	6.26	6.86	6.78	6.83
Al(iv)	1.42	1.57	1.23	1.33	1.28	1.24	1.44	1.63	1.39	1.74	1.14	1.22	1.17
Al(vi)	0.19	0.15	0.13	0.06	0.15	0.09	0.24	0.26	0.24	0.31	0.21	0.17	0.19
AlT	1.61	1.72	1.35	1.38	1.43	1.33	1.68	1.89	1.64	2.05	1.36	1.39	1.35
Ti	0.08	0.08	0.13	0.15	0.15	0.17	0.09	0.14	0.08	0.13	0.11	0.11	0.12
Fe3	0.59	0.80	0.45	0.60	0.49	0.47	0.65	0.64	0.63	0.71	0.39	0.49	0.29
Fe2	1.79	1.64	1.72	1.56	1.73	1.68	2.44	2.56	2.51	2.51	1.66	1.59	1.79
Mg	2.20	2.17	2.45	2.52	2.39	2.47	1.53	1.33	1.47	1.29	2.60	2.56	2.58
Mn	0.21	0.23	0.21	0.21	0.20	0.21	0.15	0.13	0.15	0.13	0.10	0.10	0.09
Ca	1.85	1.86	1.82	1.79	1.79	1.81	1.79	1.85	1.81	1.84	1.86	1.92	1.90
NaM4	0.08	0.08	0.10	0.11	0.11	0.10	0.11	0.08	0.10	0.09	0.07	0.04	0.05
NaA	0.40	0.36	0.33	0.32	0.28	0.29	0.32	0.32	0.30	0.31	0.27	0.23	0.36
NaT	0.47	0.43	0.42	0.42	0.39	0.39	0.43	0.40	0.40	0.40	0.34	0.27	0.41
K	0.16	0.19	0.16	0.16	0.18	0.16	0.16	0.21	0.16	0.23	0.14	0.15	0.14

	STA-1 Amph-4	STA-1 Amph-5	STA-1 Amph-6
SiO2	45.39	48.81	43.93
TiO2	1.13	0.73	0.85
Al2O3	7.47	5.53	8.89
FeO(tot.)	16.66	15.07	17.44
MnO	0.89	0.79	0.84
MgO	11.81	13.44	11.02
CaO	11.82	12.14	11.70
Na2O	1.19	1.11	1.49
K2O	0.70	0.47	0.94
Total	97.06	98.09	97.10
Si	6.78	7.14	6.61
Al(iv)	1.22	0.86	1.39
Al(vi)	0.10	0.09	0.19
AlT	1.32	0.95	1.58
Ti	0.13	0.08	0.10
Fe3	0.50	0.31	0.52
Fe2	1.58	1.54	1.67
Mg	2.63	2.93	2.47
Mn	0.11	0.10	0.11
Ca	1.89	1.90	1.89
NaM4	0.06	0.05	0.06
NaA	0.29	0.26	0.37
NaT	0.34	0.31	0.43
K	0.13	0.09	0.18

	MIG-11 Gt-1C	MIG-11 Gt-1R	MIG-11 Gt-2	MIG-11 Gt-3C	MIG-11 Gt-3R	MIG-11 Gt-4
SiO2	37.01	37.01	37.01	36.79	37.22	37.01
TiO2	0.00	0.17	0.00	0.00	0.00	0.17
Al2O3	21.16	20.98	21.35	21.35	21.16	21.35
FeO(tot.)	25.73	25.86	25.99	25.99	25.99	26.24
MnO	15.62	15.49	15.36	15.24	15.49	15.36
MgO	1.16	1.16	1.33	1.33	1.33	1.33
CaO	1.82	1.82	1.54	1.68	1.68	1.68
Na2O	0.00	0.00	0.00	0.13	0.00	0.00
K2O	0.00	0.00	0.00	0.00	0.00	0.00
Total	102.50	102.49	102.58	102.51	102.87	103.14
Si	2.95	2.95	2.95	2.93	2.95	2.93
Ti	0.00	0.00	0.00	0.00	0.00	0.00
Al	1.98	1.97	2.00	2.01	1.98	1.99
Fe3	0.09	0.10	0.09	0.09	0.09	0.10
Fe2	1.63	1.64	1.64	1.65	1.64	1.65
Mn	1.05	1.05	1.04	1.03	1.04	1.03
Mg	0.14	0.14	0.16	0.16	0.16	0.16
Ca	0.16	0.16	0.13	0.14	0.14	0.14

APPENDIX IV

Major and trace element rock compositions

Major elements and normative values (*Mielke and Winkler, 1979*) are in wt %, trace elements are in ppm; b.d.l. = below detection limit.

	STG-1	STG-2	STG-3	STG-4	STG-5	STG-6	STG-7	STG-8	STG-9	STG-10	STG-11	STG-12	STG-13	STG-14	STG-15	STG-16	STG-17	STG-18
SiO2	74.90	74.81	74.45	69.87	71.22	73.46	73.46	71.80	73.63	70.96	71.21	75.28	75.96	71.93	69.41	71.07	71.73	71.54
TiO2	0.19	0.23	0.20	0.30	0.24	0.20	0.26	0.25	0.22	0.27	0.26	0.15	0.28	0.30	0.29	0.24	0.26	0.27
Al2O3	13.37	14.11	13.87	15.42	15.81	14.25	15.22	15.53	14.60	15.32	14.67	13.73	14.23	14.30	16.63	14.89	15.12	15.50
Fe2O3	0.75	0.60	0.90	0.95	1.16	0.98	0.91	1.22	1.35	1.33	1.35	0.48	0.18	1.60	0.85	1.14	1.41	1.31
FeO	0.24	0.82	0.57	1.81	1.37	0.99	1.43	1.22	1.01	1.26	1.20	0.40	0.50	1.45	1.49	1.21	1.31	1.47
MnO	0.00	0.01	0.03	0.09	0.09	0.05	0.01	0.06	0.07	0.11	0.05	0.00	0.03	0.13	0.12	0.09	0.09	0.10
MgO	0.02	0.49	0.25	0.97	0.84	0.63	0.96	0.87	0.67	0.77	0.83	0.34	0.46	0.98	0.96	0.72	0.76	0.81
CaO	0.93	1.51	2.19	3.35	2.65	2.09	2.83	1.48	1.42	2.73	2.87	1.04	3.87	2.28	4.39	2.28	1.42	3.22
Na2O	3.82	4.67	4.12	4.75	4.73	3.70	4.78	3.59	3.99	3.96	3.81	3.16	5.08	3.53	4.10	3.82	3.86	3.91
K2O	4.20	3.35	2.82	2.26	2.88	4.85	1.40	3.34	3.46	2.81	3.25	6.12	0.18	3.45	2.03	3.33	3.77	3.59
P2O5	0.04	0.11	0.05	0.12	0.11	0.09	0.08	0.09	0.07	0.11	0.09	0.10	0.10	0.12	0.11	0.08	0.09	0.11
H2O+	0.25	0.35	0.80	0.59	0.59	0.50	0.82	0.46	0.51	0.65	0.28	0.21	0.34	0.67	0.80	0.71	1.11	0.49
CO2	0.15	0.08	0.24	0.24	0.27	0.26	0.24	0.17	0.19	0.24	0.18	0.13	0.27	0.17	0.11	0.17	0.27	0.12
Total	98.84	101.12	100.46	100.70	101.95	102.02	102.40	100.06	101.18	100.50	100.03	101.13	101.46	100.89	101.27	99.73	101.19	102.43
KF	24.36	17.82	15.72	9.44	13.74	26.60	4.59	16.65	18.17	13.68	16.32	35.06	1.15	16.85	8.04	16.87	19.39	18.45
Ab	32.36	39.55	34.90	40.23	40.06	31.34	40.49	30.41	33.80	33.54	32.27	26.77	43.03	29.90	34.73	32.36	32.69	33.12
An	3.41	6.27	9.02	13.74	10.72	7.73	12.00	5.68	5.39	11.31	12.51	3.68	14.02	9.45	20.36	9.71	4.75	13.73
Qz	35.11	32.10	35.78	27.19	28.03	29.69	35.10	35.66	34.83	32.27	31.19	31.86	37.50	34.09	28.99	31.89	32.77	28.51
Ap	0.09	0.26	0.12	0.28	0.26	0.21	0.19	0.21	0.17	0.26	0.21	0.24	0.24	0.28	0.26	0.19	0.21	0.26
Mag	0.00	0.87	1.31	1.38	1.68	1.42	1.32	1.77	1.96	1.93	1.96	0.70	0.26	2.32	1.23	1.65	2.04	1.90
Hem	0.75	0.00	0.00	0.00	0.00	0.00	0.00	0.00	0.00	0.00	0.00	0.00	0.00	0.00	0.00	0.00	0.00	0.00
Ilm	0.18	0.22	0.19	0.28	0.23	0.19	0.25	0.24	0.21	0.26	0.25	0.14	0.27	0.28	0.28	0.23	0.25	0.26
Bl	0.76	3.17	1.46	6.38	5.28	3.27	5.93	4.90	3.58	4.67	4.56	1.71	-0.21	5.62	6.42	4.51	4.61	4.44
Amph	0.00	0.00	0.00	0.93	0.00	0.65	0.00	0.00	0.00	0.00	0.00	0.00	4.37	0.00	0.00	0.00	0.00	1.22
Calc	0.41	0.22	0.65	0.65	0.73	0.71	0.65	0.46	0.52	0.65	0.49	0.35	0.73	0.46	0.30	0.46	0.73	0.33
Cord	1.28	0.49	0.72	0.00	0.96	0.00	1.42	3.91	2.30	1.60	0.28	0.55	0.00	1.28	0.20	1.43	2.94	0.00
Residue	0.22	0.22	0.74	0.32	0.38	0.35	0.58	0.26	0.36	0.46	0.09	0.13	0.25	0.44	0.54	0.53	0.92	0.28
Total	98.93	101.18	100.60	100.83	102.08	102.17	102.51	100.16	101.28	100.63	100.13	101.20	101.60	100.99	101.34	99.83	101.32	102.49
Q'	0.37	0.34	0.37	0.30	0.30	0.31	0.38	0.40	0.38	0.36	0.34	0.33	0.39	0.38	0.31	0.35	0.37	0.30
ANOR	12.27	26.02	36.46	59.28	43.84	22.51	72.36	25.44	22.87	45.25	43.40	9.51	92.42	35.93	71.70	36.54	19.68	42.67
Rb	132	125	61	47	93	90	63	101	83	68	81	159	b.d.l.	107	53	85	131	137
Sr	300	315	370	453	486	384	503	341	339	390	408	205	441	405	293	426	456	499
Ba	803	697	1251	790	813	804	519	888	969	739	849	1003	264	788	1837	825	1265	1037
La	25	22	25	34	40	35	30	27	27	31	31	11	20	31	35	31	24	27
Ce	58	47	55	73	65	59	60	52	45	69	59	31	50	68	76	62	59	59
Y	20	11	14	23	19	17	17	14	17	22	18	6	29	20	23	17	13	12
Th	14	b.d.l.	14	b.d.l.	b.d.l.	12	b.d.l.	12	12	12	b.d.l.	b.d.l.	12	b.d.l.	b.d.l.	b.d.l.	b.d.l.	14
Zr	97	114	106	124	109	196	130	182	126	130	116	77	170	140	80	118	97	115
Ga	12	12	12	14	13	15	14	15	13	13	13	12	13	12	12	12	13	14
Co	8	b.d.l.	3	3	3	3	7	3	6	b.d.l.	4	4	3	4	b.d.l.	b.d.l.	3	6
Ni	b.d.l.	8	b.d.l.	6	b.d.l.	b.d.l.	b.d.l.	b.d.l.	b.d.l.	b.d.l.	b.d.l.	b.d.l.	5	b.d.l.	b.d.l.	b.d.l.	b.d.l.	b.d.l.
Cr	30	24	32	21	14	19	20	2	9	13	14	18	5	47	9	25	20	23
Cu	b.d.l.	b.d.l.	b.d.l.	b.d.l.	b.d.l.	b.d.l.	18	12	b.d.l.	9	b.d.l.	b.d.l.	b.d.l.	8	b.d.l.	b.d.l.	8	b.d.l.
Pb	15	27	b.d.l.	b.d.l.	b.d.l.	14	b.d.l.	b.d.l.	b.d.l.	b.d.l.	b.d.l.	41	b.d.l.	b.d.l.	b.d.l.	12	b.d.l.	33
Zn	14	14	15	29	104	19	16	15	25	93	18	11	7	25	31	17	20	25
Nb	8	3	4	3	2	4	5	b.d.l.	5	2	0	2	5	6	2	1	2	4

	STG-19	STG-20	STG-21	STG-22	STG-23	STG-24	STG-25	STG-26	STG-27	STG-28	LG-1	LG-2	LG-3	LG-4	LG-5	LG-6	LG-7	LG-8
SiO2	71.97	78.78	70.13	70.40	70.42	71.51	69.82	66.66	72.69	73.22	73.22	73.21	78.20	81.52	73.46	76.38	78.97	72.54
TiO2	0.28	0.11	0.26	0.25	0.28	0.26	0.26	0.30	0.30	0.29	0.32	0.31	0.13	0.12	0.28	0.13	0.12	0.32
Al2O3	15.34	11.86	14.76	15.13	14.70	15.33	15.13	15.95	13.79	13.51	14.88	14.67	12.94	12.06	14.55	13.02	12.73	14.62
Fe2O3	0.73	0.10	0.56	1.01	1.21	1.09	0.89	1.20	1.52	0.91	0.52	0.45	0.24	0.54	0.60	0.33	0.23	0.53
FeO	1.71	0.44	2.04	1.33	1.51	1.37	1.75	2.17	1.39	1.10	2.30	2.77	1.03	1.39	2.46	1.65	1.32	2.58
MnO	0.08	0.02	0.09	0.08	0.07	0.09	0.08	0.09	0.09	0.05	0.03	0.10	0.05	0.04	0.07	0.08	0.02	0.08
MgO	0.64	0.00	0.75	0.60	0.70	0.80	0.54	0.90	0.50	0.44	0.71	1.04	0.36	0.27	0.61	0.94	0.21	0.75
CaO	2.59	1.48	1.89	1.76	2.81	2.10	2.77	2.13	2.44	1.55	1.44	1.75	0.80	0.55	2.28	2.63	0.94	1.83
Na2O	4.11	4.28	3.81	3.95	3.81	4.21	4.03	3.55	4.46	3.67	4.82	4.55	2.33	1.56	3.65	2.73	3.34	3.21
K2O	2.70	1.01	2.93	3.75	3.18	3.85	3.33	4.31	2.65	4.09	2.20	1.91	4.46	2.62	2.82	2.55	3.04	3.62
P2O5	0.11	0.01	0.10	0.08	0.10	0.10	0.10	0.13	0.07	0.08	0.09	0.08	0.02	0.03	0.06	0.01	0.02	0.07
H2O+	0.62	0.33	0.63	0.65	0.48	0.85	1.32	1.08	0.41	1.04	1.35	1.18	0.44	0.36	0.33	0.36	0.52	0.23
CO2	0.26	0.19	0.15	0.21	0.21	0.15	0.23	0.28	0.21	0.23	0.13	0.24	0.35	0.23	0.02	0.16	0.20	0.17
Total	101.11	98.60	98.08	99.19	99.47	101.69	100.22	98.74	100.50	100.16	101.98	102.23	101.34	101.26	101.16	100.94	101.64	100.53
KF	12.44	5.37	13.02	19.41	15.69	19.51	16.44	21.01	14.09	22.04	8.48	5.28	24.20	13.26	12.19	10.79	15.82	16.36
Ab	34.81	36.25	32.27	33.46	32.27	35.66	34.13	30.07	37.78	31.08	40.83	38.54	19.74	13.21	30.92	23.12	28.29	27.19
An	10.49	6.08	7.77	6.88	11.96	8.82	11.64	7.95	9.16	5.72	5.73	6.64	1.63	1.08	10.79	11.97	3.27	7.55
Qz	33.18	47.38	33.38	30.08	30.91	28.46	28.59	26.06	31.74	33.73	34.27	36.55	46.85	61.94	36.76	45.56	46.48	36.74
Ap	0.26	0.02	0.24	0.19	0.24	0.24	0.24	0.31	0.17	0.19	0.21	0.19	0.05	0.07	0.14	0.02	0.05	0.17
Mag	1.06	0.15	0.81	1.46	1.75	1.58	1.29	1.74	2.20	1.32	0.75	0.65	0.35	0.78	0.87	0.48	0.33	0.77
Hem	0.00	0.00	0.00	0.00	0.00	0.00	0.00	0.00	0.00	0.00	0.00	0.00	0.00	0.00	0.00	0.00	0.00	0.00
Ilm	0.27	0.10	0.25	0.24	0.27	0.25	0.25	0.28	0.28	0.28	0.30	0.29	0.12	0.11	0.27	0.12	0.11	0.30
Bl	5.86	1.06	7.21	4.50	5.06	5.23	5.42	7.38	2.51	3.47	7.63	10.12	3.63	3.82	7.65	7.08	3.74	8.54
Amph	0.00	0.00	0.00	0.00	0.00	0.00	0.00	0.00	1.84	0.00	0.00	0.00	0.00	0.00	0.00	0.00	0.00	0.00
Calc	0.71	0.52	0.41	0.57	0.57	0.41	0.63	0.76	0.57	0.63	0.35	0.65	0.95	0.63	0.05	0.44	0.54	0.46
Cord	1.79	1.48	2.46	2.04	0.59	0.99	0.61	2.52	0.00	0.94	2.45	2.66	3.68	6.26	1.52	1.37	2.74	2.64
Residue	0.39	0.29	0.35	0.47	0.28	0.64	1.11	0.79	0.27	0.90	1.06	0.80	0.30	0.22	0.04	0.09	0.38	-0.09
Total	101.26	98.70	98.17	99.29	99.57	101.78	100.35	98.88	100.62	100.28	102.07	102.37	101.51	101.39	101.20	101.04	101.75	100.63
Q'	0.36	0.50	0.39	0.33	0.34	0.31	0.31	0.31	0.34	0.36	0.38	0.42	0.51	0.69	0.41	0.50	0.50	0.42
ANOR	45.75	53.09	37.39	26.18	43.26	31.12	41.44	27.45	39.39	20.59	40.34	55.74	6.32	7.54	46.96	52.59	17.14	31.57
Rb	116	19	129	116	81	157	81	145	49	105	58	66	96	66	83	87	67	93
Sr	385	434	495	377	428	424	413	478	278	320	119	133	69	39	126	81	67	122
Ba	658	241	1013	923	788	841	727	2114	684	1206	508	420	391	340	397	632	422	575
La	32	22	31	29	34	30	29	48	19	24	14	18	17	17	20	18	13	13
Ce	69	54	66	54	69	66	62	96	53	56	37	36	37	37	34	43	35	36
Y	18	16	15	15	19	13	19	19	29	17	25	22	16	16	20	24	14	20
Th	b.d.l.	15	b.d.l.	b.d.l.	b.d.l.	b.d.l.	b.d.l.	39	b.d.l.	b.d.l.	b.d.l.	b.d.l.	b.d.l.	b.d.l.	b.d.l.	b.d.l.	b.d.l.	b.d.l.
Zr	126	109	104	105	126	118	129	158	143	135	156	140	156	148	138	136	153	147
Ga	15	9	13	12	13	11	14	15	13	12	15	13	12	13	14	12	10	14
Co	5	b.d.l.	7	4	7	3	4	6	5	3	8	b.d.l.	5	b.d.l.	5	4	4	3
Ni	b.d.l.	b.d.l.	b.d.l.	b.d.l.	5	b.d.l.	b.d.l.	6	b.d.l.	b.d.l.	5	b.d.l.	b.d.l.	b.d.l.	6	b.d.l.	b.d.l.	5
Cr	40	28	19	31	23	38	19	42	20	22	25	28	19	44	39	12	19	21
Cu	b.d.l.	b.d.l.	11	45	b.d.l.	b.d.l.	8	13	b.d.l.	11	b.d.l.	b.d.l.	b.d.l.	b.d.l.	6	b.d.l.	b.d.l.	b.d.l.
Pb	18	b.d.l.	16	b.d.l.	b.d.l.	b.d.l.	b.d.l.	20	b.d.l.	29	20	20	36	b.d.l.	22	17	29	27
Zn	28	6	27	18	26	28	25	22	19	19	52	50	25	17	37	22	13	41
Nb	4	7	4	2	6	0	6	8	6	6	3	5	4	1	3	5	5	5

	LG-9	LG-10	MIG-1	MIG-2	MIG-3	MIG-4	MIG-5	MIG-6	MIG-7	MIG-8	MIG-9	MIG-10	MIG-11	MIG-12	MIG-13	MIG-14	MIG-15	MIG-16
SiO2	74.29	77.72	70.28	69.66	71.67	75.49	68.65	68.21	73.17	70.80	69.76	71.96	74.47	72.21	76.48	76.35	75.37	68.22
TiO2	0.33	0.13	0.20	0.29	0.22	0.16	0.25	0.26	0.15	0.24	0.25	0.23	0.17	0.19	0.17	0.19	0.16	0.27
Al2O3	14.04	13.01	14.57	14.38	14.55	11.91	15.22	15.10	13.25	15.02	14.64	14.30	12.98	12.97	13.01	12.88	13.06	15.13
Fe2O3	0.56	0.27	1.07	0.74	1.12	1.17	1.23	1.35	0.74	1.43	1.57	1.34	0.42	1.06	0.63	0.81	0.75	1.16
FeO	2.16	1.25	1.44	2.58	0.52	0.24	1.15	1.12	0.32	1.00	0.88	0.72	0.68	0.40	0.36	0.52	0.40	1.44
MnO	0.06	0.03	0.05	0.08	0.04	0.05	0.11	0.09	0.02	0.10	0.09	0.08	0.03	0.05	0.05	0.08	0.07	0.12
MgO	0.47	0.20	0.41	0.94	0.54	0.75	0.94	1.12	0.53	0.56	0.38	0.63	0.31	0.35	0.00	0.42	0.01	0.96
CaO	1.77	0.58	1.80	2.81	1.96	1.04	2.92	2.54	1.22	2.64	2.61	2.36	1.14	1.39	0.96	1.15	1.14	1.89
Na2O	3.26	2.68	3.90	3.86	3.55	3.38	3.78	3.67	3.01	3.12	3.81	3.23	2.59	4.34	3.47	3.03	3.02	3.57
K2O	3.29	4.27	2.54	2.27	3.02	3.90	3.11	3.39	3.77	2.76	3.29	3.32	4.07	3.75	3.87	3.74	3.95	3.34
P2O5	0.06	0.02	0.04	0.07	0.07	0.04	0.08	0.09	0.03	0.08	0.11	0.06	0.02	0.04	0.03	0.03	0.03	0.09
H2O+	0.75	0.27	2.25	1.36	1.61	1.37	1.08	0.87	1.21	1.17	1.49	0.98	1.13	1.45	0.29	1.01	0.89	1.93
CO2	0.31	0.06	0.32	0.19	0.79	0.18	0.09	0.08	0.09	0.16	0.13	0.09	0.11	0.22	0.04	0.02	0.11	0.14
Total	101.33	100.45	98.87	99.23	99.66	99.68	98.61	97.89	97.51	99.08	99.01	99.30	98.12	98.42	99.36	100.23	98.96	98.26
KF	15.63	23.21	12.65	8.08	16.41	20.86	15.16	16.53	20.97	14.30	18.09	17.78	22.57	21.26	22.61	20.72	23.06	16.04
Ab	27.61	22.70	33.03	32.69	30.07	28.63	32.02	31.08	25.49	26.43	32.27	27.36	21.94	36.76	29.39	25.66	25.58	30.24
An	6.43	2.37	6.65	12.28	4.29	3.76	13.39	11.51	5.29	11.56	11.41	10.75	4.83	4.35	4.31	5.38	4.77	7.90
Qz	39.94	44.75	34.98	33.20	37.59	39.26	28.96	28.90	38.93	37.08	30.06	35.81	41.72	30.03	39.60	42.07	40.61	31.24
Ap	0.14	0.05	0.09	0.17	0.17	0.09	0.19	0.21	0.07	0.19	0.26	0.14	0.05	0.09	0.07	0.07	0.07	0.21
Mag	0.81	0.39	1.55	1.07	1.62	0.00	1.78	1.96	1.07	2.07	2.28	1.94	0.61	0.00	0.91	1.17	1.09	1.68
Hem	0.00	0.00	0.00	0.00	0.00	1.17	0.00	0.00	0.00	0.00	0.00	0.00	0.00	1.06	0.00	0.00	0.00	0.00
Ilm	0.31	0.12	0.19	0.28	0.21	0.15	0.24	0.25	0.14	0.23	0.24	0.22	0.16	0.18	0.16	0.18	0.15	0.26
Bl	6.51	3.52	3.94	8.95	2.14	3.38	5.08	5.47	1.95	3.17	2.10	2.79	2.42	1.42	0.41	2.13	0.46	5.95
Amph	0.00	0.00	0.00	0.00	0.00	0.00	0.00	0.00	0.00	0.00	0.00	0.00	0.00	1.40	0.00	0.00	0.00	0.00
Calc	0.84	0.16	0.87	0.52	2.15	0.49	0.24	0.22	0.24	0.44	0.35	0.24	0.30	0.60	0.11	0.05	0.30	0.38
Cord	2.75	3.11	2.95	1.05	3.86	0.74	0.71	1.16	2.27	2.65	0.61	1.44	2.54	0.00	1.52	1.87	2.06	2.73
Residue	0.51	0.14	2.10	1.02	1.51	1.23	0.87	0.64	1.12	1.04	1.40	0.86	1.03	1.36	0.27	0.92	0.87	1.69
Total	101.49	100.52	99.01	99.32	100.02	99.76	98.65	97.93	97.55	99.15	99.07	99.34	98.17	98.52	99.38	100.24	99.01	98.32
Q'	0.45	0.48	0.40	0.38	0.43	0.42	0.32	0.33	0.43	0.41	0.33	0.39	0.46	0.32	0.41	0.45	0.43	0.37
ANOR	29.15	9.26	34.45	60.31	20.71	15.28	46.90	41.04	20.14	44.72	38.68	37.66	17.63	16.99	16.02	20.61	17.13	33.01
Rb	83	92	52	50	72	118	91	97	88	73	92	97	131	99	107	112	114	104
Sr	110	66	149	188	325	174	369	334	268	383	362	315	189	228	173	188	192	377
Ba	426	431	592	613	1198	855	824	759	1139	887	803	880	908	969	880	882	924	812
La	12	15	21	18	29	37	33	43	29	37	36	36	30	27	24	26	29	32
Ce	31	37	36	33	48	49	54	63	45	54	67	63	44	40	45	39	47	59
Y	23	16	23	25	14	15	18	15	9	19	20	17	13	13	15	14	13	19
Th	b.d.l.	b.d.l.	7	b.d.l.	14	13	13	b.d.l.	12	12	12	12	12	14	13	13	12	12
Zr	244	161	113	142	164	127	173	164	145	182	176	158	136	148	123	144	133	203
Ga	14	10	15	14	13	12	15	14	11	14	13	13	11	12	12	13	11	15
Co	6	6	3	4	b.d.l.	b.d.l.	4	3	b.d.l.	b.d.l.	3	b.d.l.	b.d.l.	b.d.l.	3	b.d.l.	b.d.l.	3
Ni	b.d.l.	b.d.l.	b.d.l.	b.d.l.	b.d.l.	b.d.l.	b.d.l.	b.d.l.	b.d.l.	b.d.l.	6	b.d.l.	b.d.l.	b.d.l.	5	b.d.l.	b.d.l.	5
Cr	20	21	10	12	5	24	12	55	88	38	45	6	8	11	b.d.l.	6	26	19
Cu	b.d.l.	b.d.l.	16	5	b.d.l.	b.d.l.	b.d.l.	8	11	10	19	b.d.l.	b.d.l.	b.d.l.	b.d.l.	b.d.l.	b.d.l.	8
Pb	26	46	b.d.l.	b.d.l.	b.d.l.	15	b.d.l.	b.d.l.	b.d.l.	b.d.l.	b.d.l.	15	19	14	13	b.d.l.	b.d.l.	b.d.l.
Zn	40	14	22	35	8	5	24	28	3	25	27	27	12	11	10	12	12	34
Nb	10	3	11	2	2	2	13	9	6	9	1	4	7	4	6	6	4	10

	MIG-17	MIG-18	MIG-19	MIG-20	MIG-21	MIG-22	MIG-23	MIG-24	MIG-25	MIG-26	MIG-27	MIG-28	MIG-29	MIG-30	MIG-31	MIG-32	MIS-1	MIS-2
SiO2	73.00	73.11	68.68	73.99	74.71	68.54	72.49	70.88	73.40	73.63	71.70	72.75	73.90	70.10	69.84	70.54	75.58	73.02
TiO2	0.18	0.16	0.27	0.15	0.19	0.28	0.17	0.21	0.19	0.19	0.17	0.19	0.17	0.39	0.32	0.29	0.21	0.11
Al2O3	13.55	13.28	14.74	15.95	13.31	15.01	13.33	14.38	13.58	12.33	13.65	13.63	13.60	14.52	14.44	13.70	12.16	13.46
Fe2O3	0.69	0.77	1.52	0.82	0.97	1.26	0.94	0.73	1.59	0.93	1.20	0.50	0.57	1.02	1.49	1.42	0.44	0.32
FeO	0.44	0.40	1.32	0.32	0.24	1.28	0.40	1.83	1.00	0.29	0.68	0.71	0.44	1.40	1.52	1.20	1.04	0.24
MnO	0.07	0.08	0.10	0.04	0.05	0.09	0.11	0.06	0.01	0.02	0.03	0.03	0.03	0.02	0.12	0.10	0.05	0.02
MgO	0.37	0.53	0.88	0.00	1.01	1.02	0.44	0.76	0.53	0.82	0.59	0.20	0.32	0.60	1.24	0.80	0.99	0.77
CaO	1.13	1.11	2.84	1.08	0.77	2.74	1.42	2.65	2.16	0.84	2.01	3.36	2.35	1.67	2.62	2.55	2.06	1.18
Na2O	3.65	3.58	3.52	2.26	4.12	3.83	3.32	2.91	3.83	2.93	4.18	3.74	3.77	5.23	3.59	2.94	3.12	2.84
K2O	3.88	3.79	2.92	3.80	1.44	3.09	4.22	2.12	1.00	4.83	2.44	2.37	2.02	4.20	3.06	3.11	1.79	5.55
P2O5	0.04	0.02	0.09	0.02	0.03	0.09	0.10	0.04	0.03	0.02	0.05	0.03	0.02	0.14	0.10	0.10	0.03	0.05
H2O+	1.62	1.47	1.72	1.29	1.24	1.27	0.78	1.32	1.56	1.66	1.07	1.36	0.72	1.23	0.26	1.11	1.02	1.12
CO2	0.21	0.13	0.24	0.13	0.10	0.11	0.17	0.03	0.12	0.11	0.09	0.06	0.06	0.05	0.09	0.06	0.06	0.10
Total	98.83	98.43	98.84	99.85	98.18	98.61	97.89	97.92	99.00	98.60	97.86	98.93	97.97	100.57	98.69	97.92	98.55	98.78
KF	21.72	20.91	14.13	21.91	5.70	14.72	23.72	8.65	4.20	26.15	12.75	16.40	10.83	26.45	13.80	15.52	7.03	30.82
Ab	30.92	30.32	29.81	19.14	34.90	32.44	28.12	24.65	32.44	24.82	35.40	31.68	31.93	44.30	30.41	24.90	26.43	24.05
An	4.02	4.56	11.99	4.41	2.99	12.31	5.32	12.69	9.76	3.34	9.08	10.65	11.15	0.34	11.77	11.62	9.64	4.90
Qz	35.16	35.79	31.84	44.38	43.93	29.10	34.71	40.35	43.07	36.64	34.11	33.18	39.41	18.35	32.15	36.51	46.41	33.12
Ap	0.09	0.05	0.21	0.05	0.07	0.21	0.24	0.09	0.07	0.05	0.12	0.07	0.05	0.33	0.24	0.24	0.07	0.12
Mag	1.00	1.12	2.20	0.00	0.00	1.83	1.36	1.06	2.31	0.00	1.74	0.73	0.83	1.48	2.16	2.06	0.64	0.46
Hem	0.00	0.00	0.00	0.82	0.97	0.00	0.00	0.00	0.00	0.93	0.00	0.00	0.00	0.00	0.00	0.00	0.00	0.00
Ilm	0.17	0.15	0.26	0.14	0.18	0.27	0.16	0.20	0.18	0.18	0.16	0.18	0.16	0.37	0.30	0.28	0.20	0.10
Bl	1.87	2.25	4.96	0.95	4.30	5.61	1.84	6.46	2.65	3.69	2.55	-4.13	1.72	-2.84	6.79	4.52	5.67	3.00
Amph	0.00	0.00	0.00	0.00	0.00	0.00	0.00	0.00	0.00	0.00	0.00	8.71	0.00	10.57	0.00	0.00	0.00	0.00
Calc	0.57	0.35	0.65	0.35	0.27	0.30	0.46	0.08	0.33	0.30	0.24	0.16	0.16	0.14	0.24	0.16	0.16	0.27
Cord	1.86	1.61	1.38	6.50	3.86	0.84	1.34	2.63	2.60	1.05	0.79	0.00	1.11	0.00	0.89	1.23	1.54	0.98
Residue	1.54	1.37	1.51	1.25	1.06	1.04	0.70	1.07	1.45	1.50	0.96	1.34	0.65	1.12	-0.02	0.92	0.79	0.99
Total	98.92	98.49	98.95	99.91	98.22	98.66	97.97	97.93	99.05	98.65	97.90	98.96	98.00	100.60	98.73	97.95	98.58	98.82
Q'	0.38	0.39	0.36	0.49	0.50	0.33	0.38	0.47	0.48	0.40	0.37	0.36	0.42	0.21	0.36	0.41	0.52	0.36
ANOR	15.62	17.88	45.90	16.75	34.41	45.54	18.31	59.49	69.92	11.33	41.59	39.37	50.73	1.27	46.04	42.81	57.84	13.71
Rb	110	106	90	110	63	99	107	64	44	140	67	61	54	219	92	96	50	122
Sr	198	198	382	202	108	353	229	161	168	158	118	127	74	173	310	295	88	245
Ba	913	909	729	902	247	843	1062	736	689	2340	782	502	433	957	792	711	412	1036
La	30	31	37	32	38	33	31	20	10	24	21	26	28	48	32	29	14	18
Ce	43	44	62	50	55	58	60	28	13	39	45	43	43	102	60	58	14	29
Y	15	14	22	16	14	17	19	18	19	9	30	28	28	31	20	17	17	5
Th	12	b.d.l.	12	14	15	b.d.l.	13	b.d.l.	7	19	8	13	9	26	b.d.l.	b.d.l.	8	21
Zr	126	130	185	130	133	192	129	119	116	126	102	119	98	237	186	172	90	102
Ga	12	12	14	11	10	14	11	14	13	10	16	15	15	18	13	13	12	9
Co	b.d.l.	b.d.l.	b.d.l.	b.d.l.	b.d.l.	b.d.l.	b.d.l.	7	b.d.l.	b.d.l.	b.d.l.	b.d.l.	b.d.l.	b.d.l.	b.d.l.	b.d.l.	b.d.l.	b.d.l.
Ni	b.d.l.	b.d.l.	b.d.l.	b.d.l.	b.d.l.	b.d.l.	b.d.l.	6	b.d.l.	5	b.d.l.	b.d.l.	b.d.l.	9	b.d.l.	b.d.l.	5	b.d.l.
Cr	17	41	11	11	33	6	22	24	20	52	9	24	10	14	17	47	19	33
Cu	5	b.d.l.	6	b.d.l.	b.d.l.	b.d.l.	b.d.l.	b.d.l.	5	12	b.d.l.	b.d.l.	b.d.l.	b.d.l.	37	b.d.l.	9	b.d.l.
Pb	16	14	b.d.l.	15	b.d.l.	b.d.l.	b.d.l.	20	b.d.l.	56	13	b.d.l.	b.d.l.	20	18	b.d.l.	27	49
Zn	13	26	24	9	15	28	5	37	7	99	22	6	8	47	77	27	41	4
Nb	6	4	5	6	5	5	8	7	4	4	11	11	10	9	8	6	8	1

	MIS-3	MIS-4	MIS-5	MIS-6	MIS-7	MIS-8	MIS-9	MIS-10	MIS-11	STA-1	STA-2	STA-3	STA-4	STA-5	STA-6	STM-1	STM-2	STM-3
SiO2	74.49	74.48	75.40	73.50	72.67	73.52	76.54	75.67	74.87	47.08	47.81	53.63	49.59	55.38	48.65	71.82	74.18	70.69
TiO2	0.17	0.17	0.26	0.18	0.18	0.20	0.17	0.17	0.39	0.97	0.88	0.62	0.69	0.91	1.01	0.26	0.28	0.25
Al2O3	13.40	13.27	13.26	13.18	13.54	12.55	12.21	12.99	12.44	18.87	16.38	18.09	19.53	11.91	17.50	15.07	16.02	15.35
Fe2O3	0.80	0.96	0.98	1.04	0.59	0.83	1.14	0.73	0.94	3.73	3.53	3.19	2.00	1.38	2.83	1.39	0.43	0.33
FeO	0.36	0.40	0.64	0.16	0.68	0.24	0.16	0.50	0.12	7.32	7.10	5.25	6.66	4.69	6.71	1.23	1.07	0.72
MnO	0.06	0.04	0.02	0.07	0.05	0.00	0.00	0.05	0.03	0.20	0.25	0.19	0.24	0.14	0.18	0.09	0.04	0.03
MgO	0.18	0.28	0.68	0.47	0.63	0.78	0.06	0.42	0.87	7.25	6.63	3.24	4.20	8.97	4.84	0.68	0.78	0.46
CaO	1.08	1.07	0.49	0.52	1.41	0.76	0.42	1.04	0.53	11.17	11.19	6.83	9.07	5.17	9.20	2.86	1.06	0.63
Na2O	3.17	3.61	4.06	3.46	3.23	3.77	4.15	3.22	3.43	2.29	2.69	3.93	2.93	1.52	3.18	4.07	3.56	4.80
K2O	3.86	4.07	3.37	4.09	3.82	4.01	3.45	3.79	4.00	1.72	1.56	2.21	1.92	5.11	2.03	3.22	4.50	5.13
P2O5	0.03	0.04	0.04	0.01	0.03	0.02	0.02	0.02	0.02	0.20	0.25	0.33	0.27	0.98	0.30	0.10	0.16	0.16
H2O+	1.07	1.22	1.28	0.81	1.04	1.20	0.89	0.67	1.50	1.58	1.92	1.43	1.64	2.79	1.45	0.29	0.65	0.77
CO2	0.09	0.16	0.16	0.11	0.03	0.17	0.07	0.23	0.22	0.19	0.14	0.18	0.17	0.21	0.24	0.23	0.19	0.32
Total	98.76	99.77	100.64	97.60	97.90	98.05	99.28	99.50	99.36	102.55	100.32	99.10	98.89	99.13	98.11	101.30	102.92	99.61
KF	22.22	23.30	17.92	22.69	20.42	21.48	19.95	21.05	21.22	7.75	19.31	7.32	3.82	13.34	12.62	16.42	23.46	28.34
Ab	26.85	30.58	34.39	29.31	27.36	31.93	35.15	27.27	29.05	19.40	22.78	33.29	24.82	12.87	26.93	34.47	30.15	40.66
An	4.59	4.04	1.16	1.82	6.61	2.57	1.51	3.58	1.11	19.33	3.00	19.73	26.74	3.29	12.75	12.08	3.01	0.06
Qz	39.27	36.14	38.36	36.91	36.39	35.11	38.52	40.87	39.11	-6.60	-12.94	5.54	1.95	14.48	-5.40	30.59	34.93	23.08
Ap	0.07	0.09	0.09	0.02	0.07	0.05	0.05	0.05	0.05	0.47	0.59	0.78	0.64	2.31	0.71	0.24	0.38	0.38
Mag	1.16	1.39	1.42	0.00	0.86	0.00	0.00	1.06	0.00	5.41	5.12	4.63	2.90	2.00	4.10	2.02	0.62	0.48
Hem	0.00	0.00	0.00	1.04	0.00	0.83	1.14	0.00	0.94	0.00	0.00	0.00	0.00	0.00	0.00	0.00	0.00	0.00
Ilm	0.16	0.16	0.25	0.17	0.17	0.19	0.16	0.16	0.37	0.92	0.84	0.59	0.66	0.86	0.96	0.25	0.27	0.24
Bi	0.88	1.10	3.04	2.29	3.39	3.39	0.70	2.09	3.62	2.87	-17.65	8.98	11.84	25.99	-1.94	4.17	5.05	3.18
Amph	0.00	0.00	0.00	0.00	0.00	0.00	0.00	0.00	0.00	52.26	78.04	17.16	24.52	22.34	46.31	0.00	0.00	0.00
Calc	0.24	0.44	0.44	0.30	0.08	0.46	0.19	0.63	0.60	0.52	0.38	0.49	0.46	0.57	0.65	0.63	0.52	0.87
Cord	2.32	1.44	2.50	2.39	1.66	1.06	1.08	2.27	2.05	0.00	0.00	0.00	0.00	0.00	0.00	0.44	4.18	1.87
Residue	1.03	1.17	1.15	0.71	0.90	1.06	0.86	0.58	1.34	0.36	0.98	0.71	0.66	1.20	0.55	0.12	0.44	0.64
Total	98.80	99.84	100.71	97.65	97.91	98.13	99.31	99.60	99.46	102.69	100.44	99.21	99.00	99.27	98.26	101.41	103.01	99.78
Q'	0.42	0.38	0.42	0.41	0.40	0.39	0.40	0.44	0.43	-0.17	-0.40	0.08	0.03	0.33	-0.12	0.33	0.38	0.25
ANOR	17.13	14.77	6.08	7.43	24.45	10.68	7.04	14.53	4.98	71.38	13.43	72.95	87.50	19.78	50.27	42.39	11.38	0.21
Rb	117	81	65	128	137	88	115	110	143	48	35	90	107	227	61	125	201	225
Sr	195	307	136	92	182	147	89	185	91	612	624	650	689	283	649	372	208	206
Ba	904	1144	1809	1788	1695	2090	1691	915	1646	1021	1263	1171	634	2385	1437	1345	705	579
La	27	33	28	23	19	24	11	28	20	21	28	25	16	31	27	23	17	29
Ce	43	51	49	34	31	41	13	41	21	42	53	55	37	53	48	49	49	77
Y	13	17	25	14	8	11	12	13	8	25	28	22	21	22	26	10	7	6
Th	b.d.l.	13	18	20	19	23	20	b.d.l.	b.d.l.	b.d.l.	b.d.l.	b.d.l.	b.d.l.	55	12	31	b.d.l.	20
Zr	130	166	150	98	116	119	102	124	110	45	54	96	84	199	58	88	136	154
Ga	13	12	12	10	12	10	10	11	11	17	17	17	18	14	16	14	18	26
Co	b.d.l.	b.d.l.	b.d.l.	b.d.l.	b.d.l.	b.d.l.	b.d.l.	b.d.l.	b.d.l.	23	18	10	16	32	20	6	4	b.d.l.
Ni	b.d.l.	b.d.l.	b.d.l.	b.d.l.	b.d.l.	6	b.d.l.	b.d.l.	b.d.l.	13	28	7	10	100	20	7	5	5
Cr	6	4	10	7	23	12	22	30	b.d.l.	79	185	30	39	717	83	23	24	17
Cu	b.d.l.	b.d.l.	b.d.l.	b.d.l.	10	b.d.l.	b.d.l.	b.d.l.	b.d.l.	6	10	12	13	11	68	4	b.d.l.	10
Pb	14	b.d.l.	15	19	21	18	15	b.d.l.	14	b.d.l.	b.d.l.	15	b.d.l.	44	b.d.l.	18	54	30
Zn	11	12	13	17	15	8	15	11	7	70	86	82	88	73	55	23	14	12
Nb	6	8	5	7	8	8	12	9	7	3	1	4	6	14	3	6	5	11

	STG-11	STG-14	STG-15	STG-18	STG-21	LG-2	LG-7	LG-8	LG-9	MIG-10	MIG-11	MIG-20	MIG-24	MIG-29
La	31.59	33.63	34.01	27.61	30.05	19.66	18.29	18.68	15.83	32.91	34.98	30.21	19.52	24.19
Ce	64.08	62.69	65.58	50.93	52.89	39.30	33.79	36.87	31.55	63.48	63.01	53.96	36.71	47.41
Pr	6.32	6.03	6.22	4.56	5.19	4.27	3.41	4.03	3.49	5.88	5.98	5.67	3.79	5.45
Nd	21.22	25.28	25.18	17.93	20.74	19.62	14.19	18.68	15.59	18.40	18.34	17.84	12.78	19.10
Sm	3.56	4.35	3.98	2.95	3.37	3.35	2.30	3.18	3.19	2.90	2.74	2.67	2.38	3.71
Eu	1.12	1.05	1.22	0.81	0.98	0.80	0.56	0.82	0.77	0.83	0.77	0.74	0.66	0.75
Gd	4.10	4.01	3.91	2.69	3.33	3.21	1.95	2.75	2.75	2.84	2.52	2.43	2.41	3.86
Tb	0.43	0.48	0.45	0.31	0.34	0.30	0.21	0.30	0.29	0.32	0.27	0.26	0.30	0.57
Dy	2.42	2.72	2.54	1.67	1.87	1.38	1.06	1.47	1.50	2.05	1.42	1.41	1.83	3.54
Ho	0.44	0.50	0.45	0.29	0.33	0.21	0.19	0.22	0.25	0.35	0.22	0.26	0.33	0.69
Er	1.51	1.73	1.54	0.94	1.16	0.60	0.61	0.71	0.86	1.13	0.62	0.84	1.02	2.07
Tm	0.24	0.27	0.24	0.15	0.16	0.08	0.09	0.10	0.12	0.18	0.09	0.12	0.14	0.31
Yb	1.52	2.04	1.79	1.07	1.28	0.65	0.75	0.77	1.03	1.22	0.62	0.95	1.06	2.04
Lu	0.23	0.28	0.26	0.16	0.19	0.09	0.12	0.12	0.16	0.19	0.10	0.15	0.16	0.32
Eu/Eu*	0.89	0.76	0.93	0.87	0.82	0.73	0.79	0.83	0.77	0.87	0.88	0.87	0.83	0.60
Cs	1.80	6.40	9.50	4.90	11.60	4.20	7.40	4.50	4.40	1.80	4.70	2.20	1.70	0.80

	MIG-31	MIG-32	MIS-1	MIS-2	MIS-5	MIS-7	MIS-9	MIS-10	MIS-11	STA-1	STA-2	STA-3	STA-4	STA-6
La	33.03	31.62	17.69	19.10	27.21	18.98	9.38	32.17	18.27	22.23	23.85	22.34	16.82	24.37
Ce	67.54	66.48	31.62	30.90	49.55	41.36	17.63	58.04	29.42	46.86	51.73	48.91	36.02	48.97
Pr	6.56	6.23	3.57	3.03	5.56	3.00	1.69	5.85	2.97	5.82	5.95	5.64	4.44	6.04
Nd	21.53	20.46	12.60	9.41	18.57	9.31	5.11	18.03	8.67	23.48	28.88	26.16	21.99	29.42
Sm	3.66	3.50	2.36	1.54	3.57	1.67	1.04	2.72	1.48	4.91	6.18	5.38	4.39	5.87
Eu	1.15	1.08	0.61	0.72	0.81	0.72	0.46	0.73	0.62	1.51	1.60	1.41	1.26	1.66
Gd	3.61	3.58	1.89	1.40	3.00	1.45	0.95	2.43	1.08	5.39	5.59	4.65	4.14	5.67
Tb	0.46	0.46	0.20	0.16	0.33	0.16	0.14	0.28	0.15	0.62	0.63	0.52	0.49	0.63
Dy	2.72	2.68	1.00	0.94	1.85	0.96	0.99	1.41	1.03	3.56	3.47	2.88	2.73	3.62
Ho	0.52	0.51	0.14	0.16	0.30	0.18	0.21	0.22	0.20	0.62	0.61	0.49	0.49	0.60
Er	1.59	1.54	0.40	0.47	0.94	0.58	0.78	0.63	0.69	1.95	1.90	1.55	1.56	1.93
Tm	0.25	0.24	0.05	0.07	0.15	0.09	0.13	0.09	0.12	0.25	0.26	0.22	0.21	0.26
Yb	1.68	1.68	0.35	0.50	1.07	0.65	1.00	0.71	0.96	1.66	1.79	1.70	1.57	1.87
Lu	0.27	0.27	0.06	0.07	0.17	0.10	0.18	0.12	0.16	0.24	0.24	0.21	0.22	0.24
Eu/Eu*	0.96	0.92	0.86	1.47	0.74	1.38	1.39	0.85	1.43	0.89	0.88	0.84	0.89	0.87
Cs	1.40	1.60	3.60	4.10	1.30	6.50	1.70	1.60	0.90	7.30	12.40	5.80	11.00	7.20

APPENDIX V

Sample descriptions

STG-1 Biotite - plagioclase mylonite gneiss

The rock is intensely deformed, shows planar fabric and consists of matrix (70%, grain size 0.05 - 0.1 mm) and porphyroclasts (30%, grain size 1 - 2 mm). Minerals present in the matrix are quartz (40%), plagioclase (35%), K-feldspar (20%), biotite (1%), apatite (<0.5%), zircon (<0.5%), muscovite (<0.5%), opaque iron ore (<0.5%); minerals present as porphyroclasts are plagioclase (65%) and K-feldspar (35%). Ca 20% of feldspars are retrogressed to sericite and clay minerals.

STG-2 Biotite - plagioclase mylonite gneiss

The rock is weakly deformed, shows weak planar fabric and consists of matrix (60%, grain size 0.03 - 0.15 mm) and porphyroclasts (40%, grain size 1 - 1.5 mm). Minerals present in the matrix are quartz (35%), plagioclase (35%), K-feldspar (20%), biotite (5%), muscovite (1%), apatite (<0.5%), zircon (<0.5%); minerals present as porphyroclasts are plagioclase (65%) and K-feldspar (35%). Ca 10% of feldspars are retrogressed to sericite and clay minerals, ca 5% of biotite is retrogressed to chlorite.

STG-3 Biotite - plagioclase mylonite gneiss

The rock shows medium intensity deformation and a weak planar fabric, it consists of matrix (60%, grain size 0.03 - 0.15 mm) and porphyroclasts (40%, grain size 1 - 2 mm). Minerals present in the matrix are quartz (35%), plagioclase (40%), K-feldspar (15%), biotite (2%), opaque iron ore (1%), apatite (<0.5%); minerals present as porphyroclasts are quartz (50%), plagioclase (30%) and K-feldspar (20%). Ca 10% of feldspars are retrogressed to sericite and clay minerals, ca 5% of biotite is retrogressed to chlorite, ca 5% of iron ore is retrogressed to iron hydro-oxides.

STG-4 Amphibole - biotite mylonite gneiss

The rock is intensely deformed, shows strong planar fabric and consists of matrix (85%, grain size 0.01 - 0.1 mm) and porphyroclasts (15%, grain size 0.8 - 2 mm). Minerals present in the matrix are plagioclase (45%), quartz (30%), K-feldspar (10%), biotite (7%), amphibole (3%), opaque iron ore (1%), titanite (<0.5%), zircon (<0.5%); minerals present as porphyroclasts are plagioclase (50%), quartz (35%) and K-feldspar (15%). Ca 5% of feldspars are retrogressed to sericite and clay minerals, ca 1% of biotite is retrogressed to chlorite, ca 1% of iron ore is retrogressed to iron hydro-oxides.

STG-5 Amphibole - biotite mylonite gneiss

The rock is strongly deformed, shows strong planar fabric and consists of matrix (80%, grain size 0.01 - 0.15 mm) and porphyroclasts (20%, grain size 1 - 3 mm). Minerals present in the matrix are plagioclase (50%), quartz (30%), K-feldspar (10%), biotite (4%), amphibole (2%), opaque iron ore (1%), apatite (<0.5%), allanite (<0.5%); minerals present as porphyroclasts are plagioclase (80%) and K-feldspar (20%). Ca 10% of feldspars are retrogressed to sericite and clay minerals, ca 3% of biotite is retrogressed to chlorite, ca 1% of iron ore is retrogressed to iron hydro-oxides.

STG-6 Amphibole - biotite mylonite gneiss

The rock shows medium intensity deformation and planar fabric and consists of matrix (90%, grain size 0.01 - 0.15 mm) and porphyroclasts (10%, grain size 1 - 1.5 mm). Minerals present in the matrix are plagioclase (40%), quartz (30%), K-feldspar (20%), biotite (4%), amphibole (2%), opaque iron ore (1%), apatite (<0.5%), zircon (<0.5%); minerals present as porphyroclasts are plagioclase (70%) and K-feldspar (30%). Ca 5% of feldspars are retrogressed to sericite and clay minerals, ca 5% of biotite is retrogressed to chlorite.

STG-7 Biotite mylonite gneiss

The rock is strongly deformed, shows strong planar mylonitic fabric and consists of matrix (80%, grain size 0.01 - 0.1 mm) and porphyroclasts (20%, grain size 1 - 3 mm). Minerals present in the matrix are plagioclase (50%), quartz (30%), K-feldspar (10%), biotite (5%), opaque iron ore (1%), epidote (1%), apatite (<0.5%), zircon (<0.5%); minerals present as porphyroclasts are plagioclase (60%), quartz (30%) and K-feldspar (10%). Ca 20% of feldspars are retrogressed to sericite and clay minerals, ca 5% of biotite is retrogressed to chlorite, ca 1% of iron ore is retrogressed to iron hydro-oxides.

STG-8 Biotite mylonite gneiss

The rock shows medium intensity deformation and planar fabric and consists of matrix (80%, grain size 0.02 - 0.3 mm) and porphyroclasts (20%, grain size 1 - 3 mm). Minerals present in the matrix are plagioclase (35%), quartz (35%), K-feldspar (15%), biotite (10%), opaque iron ore (1%), apatite (<0.5%); minerals present as porphyroclasts are plagioclase (60%) and K-feldspar (40%). Ca 10% of feldspars are retrogressed to sericite and clay minerals, ca 5% of biotite is retrogressed to chlorite, ca 1% of iron ore is retrogressed to iron hydro-oxides.

STG-9 Biotite mylonite gneiss

The rock is strongly deformed, shows strong planar fabric and consists of matrix (70%, grain size 0.01 - 0.15 mm) and porphyroclasts (30%, grain size 0.8 - 1 mm). Minerals present in the matrix are plagioclase (40%), quartz (35%), K-feldspar (20%), biotite (5%), opaque iron ore (2%), apatite (<0.5%), zircon (<0.5%); minerals present as porphyroclasts are plagioclase (60%) and K-feldspar (40%). Ca 25% of feldspars are retrogressed to sericite and clay minerals, ca 10% of biotite is retrogressed to chlorite.

STG-10 Amphibole - biotite mylonite gneiss

The rock shows medium intensity deformation and planar fabric and consists of matrix (70%, grain size 0.01 - 0.2 mm) and porphyroclasts (30%, grain size 1 - 3 mm). Minerals present in the matrix are plagioclase (40%), quartz (30%), K-feldspar (10%), biotite (10%), amphibole (3%), opaque iron ore (1%), apatite (<0.5%); minerals present as porphyroclasts are plagioclase (80%) and K-feldspar (20%). Ca 5% of feldspars are retrogressed to sericite and clay minerals, ca 3% of biotite is retrogressed to chlorite.

STG-11 Amphibole - biotite mylonite gneiss

The rock is intensely deformed, shows strong planar fabric and consists of matrix (70%, grain size 0.1 - 0.2 mm) and porphyroclasts (30%, grain size 1 - 3 mm). Minerals present in the matrix are plagioclase (45%), quartz (30%), K-feldspar (10%), biotite (8%), amphibole (3%), opaque iron ore (1%), titanite (1%), apatite (<0.5%), zircon (<0.5%); minerals present as porphyroclasts are plagioclase (80%), quartz (10%) and K-feldspar (10%). Ca 5% of feldspars are retrogressed to sericite and clay minerals, ca 3% of biotite is retrogressed to chlorite.

STG-12 Biotite mylonite gneiss

The rock shows weak deformation and weakly expressed planar fabric and consists of matrix (90%, grain size 0.1 - 0.2 mm) and porphyroclasts (10%, grain size 0.8 - 1 mm). Minerals present in the matrix are plagioclase (35%), quartz (35%), K-feldspar (20%), biotite (5%), opaque iron ore (1%), zircon (<0.5%), allanite (<0.5%); minerals present as porphyroclasts are plagioclase (80%) and K-feldspar (20%). Ca 10% of feldspars are retrogressed to sericite and clay minerals, ca 10% of biotite is retrogressed to chlorite, ca 5% of ore mineral is retrogressed to iron hydro-oxides.

STG-13 Plagioclase mylonite gneiss

The rock shows weak deformation and granoblastic fabric and consists of matrix (90%, grain size 0.01 - 0.2 mm) and porphyroclasts (10%, grain size 1 - 2 mm). Minerals present in the matrix are plagioclase (50%), quartz (40%), K-feldspar (5%), amphibole (3%), titanite (1%), apatite (<0.5%); minerals present as porphyroclasts are plagioclase (90%) and K-feldspar (10%). Ca 5% of feldspars are retrogressed to sericite and clay minerals.

STG-14 Amphibole - biotite gneiss

The rock shows medium intensity deformation and planar fabric and consists of matrix (70%, grain size 0.1 - 0.2 mm) and porphyroclasts (30%, grain size 1 - 3 mm). Minerals present in the matrix are plagioclase (35%), quartz (35%), K-feldspar (15%), biotite (10%), amphibole (3%), opaque iron ore (1%), titanite (<0.5%), apatite (<0.5%); minerals present as porphyroclasts are plagioclase (70%) and K-feldspar (30%). Ca 10% of feldspars are retrogressed to sericite and clay minerals, ca 5% of biotite is retrogressed to chlorite, ca 1% of ore mineral is retrogressed to iron hydro-oxides.

STG-15 Biotite mylonite gneiss

The rock shows medium intensity deformation and planar fabric and consists of matrix (70%, grain size 0.05 - 0.2 mm) and porphyroclasts (30%, grain size 1 - 2 mm). Minerals present in the matrix are plagioclase (50%), quartz (30%), K-feldspar (10%), biotite (5%), opaque iron ore (1%), apatite (<0.5%), zircon (<0.5%); minerals present as porphyroclasts are plagioclase (90%) and K-feldspar (10%). Ca 10% of feldspar porphyroclasts are retrogressed to sericite and clay minerals, ca 5% of biotite is retrogressed to chlorite.

STG-16 Biotite - amphibole mylonite gneiss

The rock shows medium intensity deformation and planar fabric and consists of matrix (80%, grain size 0.1 - 0.2 mm) and porphyroclasts (20%, grain size 1 - 2 mm). Minerals present in the matrix are plagioclase (40%), quartz (35%), K-feldspar (15%), biotite (5%), amphibole (3%), opaque iron ore (<0.5%), apatite (<0.5%), allanite (<0.5%); minerals present as porphyroclasts are plagioclase (70%) and K-feldspar (20%), quartz (10%). Ca 5% of feldspars are retrogressed to sericite and clay minerals, ca 3% of biotite is retrogressed to chlorite.

STG-17 Biotite mylonite gneiss

The rock shows weak deformation and weakly expressed planar fabric and consists of matrix (80%, grain size 0.05 - 0.2 mm) and porphyroclasts (20%, grain size 1.5 - 2 mm). Minerals present in the matrix are plagioclase (40%), quartz (30%), K-feldspar (20%), biotite (5%), opaque iron ore (1%), epidote (1%), apatite (<0.5%); minerals present as porphyroclasts are plagioclase (60%) and K-feldspar (40%). Ca 10% of feldspars are retrogressed to sericite and clay minerals, ca 10% of biotite is retrogressed to chlorite.

STG-18 Biotite - amphibole mylonite gneiss

The rock shows medium intensity deformation and granoblastic fabric and consists of matrix (90%, grain size 0.1 - 0.2 mm) and porphyroclasts (10%, grain size 1 - 2 mm). Minerals present in the matrix are plagioclase (45%), quartz (30%), K-feldspar (15%), amphibole (5%), biotite (3%), opaque iron ore (1%), titanite (1%), apatite (<0.5%); minerals present as porphyroclasts are plagioclase (80%) and K-feldspar (20%). Ca 1% of feldspars are retrogressed to sericite and clay minerals.

STG-19 Biotite mylonite gneiss

The rock shows medium intensity deformation and planar fabric and consists of matrix (70%, grain size 0.1 - 0.3 mm) and porphyroclasts (30%, grain size 1 - 3 mm). Minerals present in the matrix are plagioclase (40%), quartz (30%), K-feldspar (10%), biotite (15%), apatite (<0.5%), Zircon (<0.5%); minerals present as porphyroclasts are plagioclase (80%) and K-feldspar (20%). Ca 5% of feldspars are retrogressed to sericite and clay minerals, ca 1% of biotite is retrogressed to chlorite.

STG-20 Biotite mylonite gneiss

The rock shows weak deformation and weakly expressed planar fabric and consists of matrix (90%, grain size 0.01 - 0.1 mm) and porphyroclasts (10%, grain size 0.8 - 1 mm). Minerals present in the matrix are quartz (45%), plagioclase (40%), K-feldspar (10%), biotite (2%), opaque iron ore (1%), apatite (<0.5%); minerals present as porphyroclasts are quartz (60%), plagioclase (30%) and K-feldspar (10%). Ca 5% of feldspars are retrogressed to sericite and clay minerals.

STG-21 Biotite mylonite gneiss

The rock shows medium intensity deformation and planar fabric and consists of matrix (70%, grain size 0.1 - 0.2 mm) and porphyroclasts (30%, grain size 1 - 3 mm). Minerals present in the matrix are

plagioclase (45%), quartz (35%), K-feldspar (10%), biotite (5%), opaque iron ore (1%), titanite (<0.5%), apatite (<0.5%); minerals present as porphyroclasts are plagioclase (80%) and K-feldspar (20%). Ca 15% of feldspars are retrogressed to sericite and clay minerals, ca 40% of biotite is retrogressed to chlorite.

STG-22 Biotite mylonite gneiss

The rock shows medium intensity deformation and planar fabric and consists of matrix (70%, grain size 0.1 - 0.2 mm) and porphyroclasts (30%, grain size 1.5 - 2 mm). Minerals present in the matrix are plagioclase (40%), quartz (30%), K-feldspar (20%), biotite (8%), opaque iron ore (<0.5%), titanite (<0.5%), apatite (<0.5%); minerals present as porphyroclasts are plagioclase (70%) and K-feldspar (30%). Ca 10% of feldspars are retrogressed to sericite and clay minerals, ca 10% of biotite is retrogressed to chlorite.

STG-23 Amphibole - biotite mylonite gneiss

The rock shows strong deformation and planar fabric and consists of matrix (80%, grain size 0.01 - 0.1 mm) and porphyroclasts (30%, grain size 1 - 2 mm). Minerals present in the matrix are plagioclase (40%), quartz (30%), K-feldspar (15%), biotite (5%), amphibole (3%), opaque iron ore (1%), titanite (1%), apatite (<0.5%); minerals present as porphyroclasts are plagioclase (90%) and K-feldspar (10%). Ca 5% of feldspars are retrogressed to sericite and clay minerals.

STG-24 Amphibole - biotite mylonite gneiss

The rock shows medium intensity deformation and planar fabric and consists of matrix (70%, grain size 0.2 - 0.25 mm) and porphyroclasts (30%, grain size 1 - 2.5 mm). Minerals present in the matrix are plagioclase (40%), quartz (30%), K-feldspar (15%), biotite (10%), amphibole (2%), opaque iron ore (1%), apatite (<0.5%), zircon (<0.5%); minerals present as porphyroclasts are plagioclase (85%) and K-feldspar (15%). Ca 10% of feldspars are retrogressed to sericite and clay minerals, ca 5% of biotite is retrogressed to chlorite, ca 1% of ore mineral is retrogressed to iron hydro-oxides.

STG-25 Amphibole - biotite mylonite gneiss

The rock shows weak deformation and weakly expressed planar fabric and consists of matrix (90%, grain size 0.1 - 0.2 mm) and porphyroclasts (10%, grain size 1 - 2 mm). Minerals present in the matrix are plagioclase (45%), quartz (30%), K-feldspar (15%), biotite (4%), amphibole (4%), opaque iron ore (1%), apatite (<0.5%), zircon (<0.5%); minerals present as porphyroclasts are plagioclase (80%) and K-feldspar (20%). Ca 5% of feldspars are retrogressed to sericite and clay minerals, ca 10% of ore mineral is retrogressed to iron hydro-oxides.

STG-26 Biotite mylonite gneiss

The rock shows weak deformation and weakly expressed planar fabric and consists of matrix (70%, grain size 0.01 - 0.1 mm) and porphyroclasts (30%, grain size 0.5 - 1.5 mm). Minerals present in the matrix are plagioclase (40%), quartz (30%), K-feldspar (20%), biotite (5%), opaque iron ore (1%), titanite

(<0.5%), apatite (<0.5%); minerals present as porphyroclasts are plagioclase (65%) and K-feldspar (35%). Ca 20% of feldspars are retrogressed to sericite and clay minerals, ca 10% of biotite is retrogressed to chlorite, ca 10% of ore mineral is retrogressed to iron hydro-oxides.

STG-27 Biotite mylonite gneiss

The rock shows weak deformation and weakly expressed planar fabric and consists of matrix (80%, grain size 0.01 - 0.1 mm) and porphyroclasts (20%, grain size 0.8 - 1 mm). Minerals present in the matrix are plagioclase (45%), quartz (35%), K-feldspar (15%), biotite (3%), opaque iron ore (1%), titanite (<0.5%), allanite (<0.5%), apatite (<0.5%); minerals present as porphyroclasts are plagioclase (70%) and K-feldspar (30%). Ca 10% of feldspars are retrogressed to sericite and clay minerals, ca 10% of biotite is retrogressed to chlorite.

STG-28 Biotite mylonite gneiss

The rock shows strong deformation and planar fabric and consists of matrix (70%, grain size 0.01 - 0.2 mm) and porphyroclasts (30%, grain size 0.5 - 1.5 mm). Minerals present in the matrix are plagioclase (35%), quartz (35%), K-feldspar (20%), biotite (6%), opaque iron ore (1%), epidote (1%), apatite (<0.5%); minerals present as porphyroclasts are plagioclase (65%) and K-feldspar (35%). Ca 15% of feldspars are retrogressed to sericite and clay minerals, ca 5% of biotite is retrogressed to chlorite.

LG-1 Biotite mylonite gneiss

The rock shows medium intensity deformation and granoblastic fabric and consists of matrix (90%, grain size 0.01 - 0.3 mm) and porphyroclasts (10%, grain size 1 - 1.5 mm). Minerals present in the matrix are plagioclase (45%), quartz (35%), K-feldspar (10%), biotite (6%), muscovite (1%), opaque iron ore (1%), titanite (<0.5%), apatite (<0.5%); minerals present as porphyroclasts are plagioclase (60%) and K-feldspar (40%). Less than 1% of feldspars are retrogressed to sericite and clay minerals.

LG-2 Biotite mylonite gneiss

The rock shows medium intensity deformation and granoblastic fabric and consists of matrix (90%, grain size 0.05 - 0.3 mm) and porphyroclasts (10%, grain size 1.5 - 2 mm). Minerals present in the matrix are plagioclase (45%), quartz (35%), K-feldspar (5%), biotite (10%), muscovite (1%), opaque iron ore (1%), titanite (<0.5%), apatite (<0.5%); minerals present as porphyroclasts are plagioclase (60%) and K-feldspar (40%). Ca 5% of feldspars are retrogressed to sericite and clay minerals.

LG-3 Biotite mylonite gneiss

The rock shows strong deformation and planar fabric and consists of fine-grained matrix (80%, grain size 0.01 - 0.1 mm) and quartz ribbons (20%, grain size 1 - 1.5 mm). Minerals present in the matrix are plagioclase (35%), quartz (35%), K-feldspar (25%), muscovite (2%), biotite (1%), epidote (1%), opaque iron ore (<0.5%). Ca 5% of feldspars are retrogressed to sericite and clay minerals.

LG-4 Plagioclase mylonite gneiss

The rock shows medium intensity deformation and granoblastic fabric and consists of matrix (90%, grain size 0.01 - 0.3 mm) and quartz porphyroclasts (10%, grain size 0.8 - 1.5 mm). Minerals present in the matrix are quartz (60%), plagioclase (15%), K-feldspar (15%), muscovite (2%), biotite (1%), opaque iron ore (<0.5%), apatite (<0.5%). Less than 1% of feldspars are retrogressed to sericite and clay minerals.

LG-5 Biotite mylonite gneiss

The rock shows strong deformation and weakly expressed planar fabric and consists of matrix (80%, grain size 0.01 - 0.3 mm) and porphyroclasts (20%, grain size 1 - 2 mm). Minerals present in the matrix are plagioclase (40%), quartz (35%), K-feldspar (10%), biotite (10%), opaque iron ore (1.5%), zircon (<0.5%), apatite (<0.5%); minerals present as porphyroclasts are plagioclase (60%), quartz (30%) and K-feldspar (10%). Ca 5% of feldspars are retrogressed to sericite and clay minerals.

LG-6 Biotite - plagioclase mylonite gneiss

The rock shows strong deformation and planar fabric and consists of matrix (90%, grain size 0.01 - 0.05 mm) and porphyroclasts (10%, grain size 1 - 1.5 mm). Minerals present in the matrix are plagioclase (45%), quartz (35%), K-feldspar (15%), biotite (3%), muscovite (<0.5%), opaque iron ore (<0.5%), zircon (<0.5%); minerals present as porphyroclasts are quartz (90%) and plagioclase (10%). Less than 1% of feldspars are retrogressed to sericite and clay minerals.

LG-7 Biotite - plagioclase mylonite gneiss

The rock shows strong deformation and planar fabric and consists of matrix (70%, grain size 0.01 - 0.3 mm) and quartz ribbons (30%, grain size 1.5 - 3 mm). Minerals present in the matrix are plagioclase (45%), quartz (30%), K-feldspar (20%), biotite (2%), muscovite (1%), opaque iron ore (1%), zircon (<0.5%). Ca 2% of feldspars are retrogressed to sericite and clay minerals.

LG-8 Biotite mylonite gneiss

The rock shows medium intensity deformation and weakly expressed planar fabric and consists of matrix (70%, grain size 0.01 - 0.2 mm) and porphyroclasts (30%, grain size 1 - 2 mm). Minerals present in the matrix are plagioclase (35%), quartz (35%), K-feldspar (15%), biotite (10%), muscovite (2%), opaque iron ore (1%), zircon (<0.5%), apatite (<0.5%); minerals present as porphyroclasts are plagioclase (40%), quartz (30%) and K-feldspar (30%). Ca 10% of feldspars are retrogressed to sericite and clay minerals.

LG-9 Biotite mylonite gneiss

The rock shows medium intensity deformation and planar fabric and consists of matrix (70%, grain size 0.01 - 0.2 mm) and porphyroclasts (30%, grain size 1 - 2 mm). Minerals present in the matrix are quartz (40%), plagioclase (35%), K-feldspar (10%), biotite (10%), muscovite (2%), opaque iron ore (1%), zircon (<0.5%), apatite (<0.5%); minerals present as porphyroclasts are plagioclase (40%), quartz (40%) and K-feldspar (20%). Ca 10% of feldspars are retrogressed to sericite and clay minerals.

LG-10 Biotite - plagioclase mylonite gneiss

The rock shows medium intensity deformation and granoblastic fabric and consists of matrix (90%, grain size 0.01 - 0.05 mm) and porphyroclasts (10%, grain size 0.8 - 1.5 mm). Minerals present in the matrix are quartz (45%), plagioclase (25%), K-feldspar (25%), biotite (3%), muscovite (1%), opaque iron ore (<0.5%); minerals present as porphyroclasts are quartz (60%) and plagioclase (40%). Ca 2% of feldspars are retrogressed to sericite and clay minerals.

STA-1 Amphibolite

The rock shows medium intensity deformation and weakly expressed planar fabric and consists of matrix (90%, grain size 0.01 - 0.2 mm) and porphyroclasts (10%, grain size 0.6 - 1.2 mm). Minerals present in the matrix are amphibole (45%), plagioclase (45%), quartz (5%), biotite (2%), epidote (1%), opaque iron ore (2%), titanite (<0.5%); minerals present as porphyroclasts are plagioclase (80%) and amphibole (20%). Ca 30% of feldspar is retrogressed to sericite and clay minerals.

STA-2 Amphibolite

The rock shows medium intensity deformation and planar fabric and consists of matrix (80%, grain size 0.01 - 0.1 mm) and porphyroclasts (20%, grain size 0.8 - 1 mm). Minerals present in the matrix are amphibole (50%), plagioclase (40%), quartz (5%), biotite (2%), titanite (1%), opaque iron ore (2%), zircon (<0.5%); minerals present as porphyroclasts are amphibole (70%) and plagioclase (30%). Ca 30% of feldspar is retrogressed to sericite and clay minerals.

STA-3 Amphibolite

The rock shows medium intensity deformation and planar fabric and consists of matrix (80%, grain size 0.01 - 0.1 mm) and porphyroclasts (20%, grain size 0.5 - 2 mm). Minerals present in the matrix are amphibole (30%), plagioclase (45%), quartz (10%), K-feldspar (5%), biotite (5%), titanite (2%), opaque iron ore (2%), apatite (<0.5%); minerals present as porphyroclasts are amphibole (80%) and plagioclase (20%). Ca 5% of feldspars are retrogressed to sericite and clay minerals.

STA-4 Amphibolite

The rock shows weak deformation and weakly expressed planar fabric and consists of matrix (60%, grain size 0.01 - 0.3 mm) and porphyroclasts (40%, grain size 0.8 - 3 mm). Minerals present in the matrix are plagioclase (45%), amphibole (35%), quartz (15%), biotite (2%), titanite (1%), opaque iron ore (1%), zircon (<0.5%); minerals present as porphyroclasts are plagioclase (70%) and amphibole (30%). Ca 40% of feldspar porphyroclasts are retrogressed to sericite and clay minerals, ca 30% of biotite is retrogressed to chlorite.

STA-5 Amphibolite

The rock shows weak deformation and weakly expressed planar to granoblastic fabric and consists of matrix (95%, grain size 0.01 - 0.5 mm) and porphyroclasts (5%, grain size 0.8 - 1 mm). Minerals present in the matrix are plagioclase (50%), amphibole (30%), biotite (15%), quartz (1%), opaque iron ore (2%), apatite (<0.5%); minerals present as porphyroclasts are plagioclase (70%) and amphibole (30%). Ca 40% of feldspar is retrogressed to sericite and clay minerals, ca 40% of biotite is retrogressed to chlorite.

STA-6 Amphibolite

The rock shows medium intensity deformation and planar fabric and consists of amphibole (50%), plagioclase (40%), quartz (5%), biotite (1%), titanite (1%), opaque iron ore (2%), zircon (<0.5%); grain size is 0.01 - 0.5 mm. Ca 5% of feldspar is retrogressed to sericite and clay minerals.

STM-1 Amphibole - biotite meta-aplite

The rock shows medium intensity deformation and weakly expressed planar fabric and consists of matrix (90%, grain size 0.01 - 0.1 mm) and porphyroclasts (10%, grain size 0.8 - 1.5 mm). Minerals present in the matrix are plagioclase (45%), quartz (30%), K-feldspar (15%), biotite (5%), amphibole (3%), opaque iron ore (<0.5%), titanite (<0.5%), apatite (<0.5%); minerals present as porphyroclasts are plagioclase (65%), quartz (20%) and K-feldspar (15%). Ca 5% of feldspars are retrogressed to sericite and clay minerals.

STM-2 Biotite - plagioclase meta-aplite

The rock shows weak deformation and weakly expressed planar to granoblastic fabric and consists of matrix (80%, grain size 0.05 - 0.2 mm) and porphyroclasts (20%, grain size 1 - 2 mm). Minerals present in the matrix are plagioclase (35%), quartz (35%), K-feldspar (20%), biotite (6%), opaque iron ore (<0.5%), apatite (<0.5%), zircon (<0.5%); minerals present as porphyroclasts are plagioclase (40%), K-feldspar (40%) and quartz (20%). Ca 10% of feldspars are retrogressed to sericite and clay minerals, ca 5% of biotite is retrogressed to chlorite.

STM-3 Biotite meta-aplite

The rock shows intense deformation and weakly expressed planar fabric and consists of matrix (80%, grain size 0.01 - 0.3 mm) and porphyroclasts (20%, grain size 0.8 - 1.5 mm). Minerals present in the matrix are plagioclase (40%), K-feldspar (30%), quartz (25%), biotite (2%), opaque iron ore (<0.5%), apatite (<0.5%); minerals present as porphyroclasts are plagioclase (60%) and K-feldspar (40%). Ca 20% of feldspars are retrogressed to sericite and clay minerals, ca 10% of biotite is retrogressed to chlorite.

MIG-1 Biotite mylonite gneiss

The rock is intensely deformed, shows medium intensity planar fabric and consists of matrix (70%, grain size 0.01 - 0.2 mm) and porphyroclasts (30%, grain size 1 - 2.5 mm). Minerals present in the matrix are plagioclase (40%), quartz (35%), K-feldspar (15%), biotite (8%), opaque iron ore (1%), apatite (<0.5%),

zircon (<0.5%); minerals present as porphyroclasts are plagioclase (50%), quartz (40 and K-feldspar (10%). Ca 10% of feldspars are retrogressed to sericite and clay minerals, ca 10% of ore mineral is retrogressed to iron hydro-oxides.

MIG-2 Biotite mylonite gneiss

The rock is intensely deformed, shows strong planar fabric and consists of matrix (90%, grain size 0.01 - 0.2 mm) and porphyroclasts (10%, grain size 1 - 1.5 mm). Minerals present in the matrix are plagioclase (45%), quartz (30%), K-feldspar (10%), biotite (5%), opaque iron ore (1%), apatite (<0.5%); minerals present as porphyroclasts are plagioclase (50%) and quartz (50%). Ca 15% of feldspars are retrogressed to sericite and clay minerals, ca 10% of biotite is retrogressed to chlorite.

MIG-3 Biotite mylonite gneiss

The rock is intensely deformed, shows strong planar fabric and consists of matrix (60%, grain size 0.05 - 0.2 mm) and porphyroclasts (40%, grain size 1 - 3 mm). Minerals present in the matrix are quartz (45%), plagioclase (30%), K-feldspar (10%), biotite (5%), opaque iron ore (1%), apatite (<0.5%), titanite (<0.5%), muscovite (<0.5%); minerals present as porphyroclasts are plagioclase (70%), K-feldspar (20%) and quartz (50%). Ca 15% of feldspars are retrogressed to sericite and clay minerals, ca 10% of biotite is retrogressed to chlorite, ca 20% of ore mineral is retrogressed to iron hydro-oxides.

MIG-4 Biotite - plagioclase mylonite gneiss

The rock shows medium intensity deformation and planar fabric and consists of matrix (70%, grain size 0.01 - 0.2 mm) and porphyroclasts (30%, grain size 1 - 3 mm). Minerals present in the matrix are quartz (45%), plagioclase (35%), K-feldspar (15%), biotite (3%), opaque iron ore (1%), epidote (<0.5%), apatite (<0.5%), muscovite (<0.5%); minerals present as porphyroclasts are plagioclase (40%), K-feldspar (40%) and quartz (20%). Ca 30% of feldspars are retrogressed to sericite and clay minerals, ca 10% of biotite is retrogressed to chlorite.

MIG-5 Amphibole - biotite mylonite gneiss

The rock is intensely deformed, shows medium intensity planar fabric and consists of matrix (60%, grain size 0.05 - 0.2 mm) and porphyroclasts (40%, grain size 1.5 - 3 mm). Minerals present in the matrix are quartz (40%), plagioclase (35%), K-feldspar (15%), biotite (5%), amphibole (3%), opaque iron ore (<0.5%), apatite (<0.5%), titanite (<0.5%); minerals present as porphyroclasts are plagioclase (60%) and K-feldspar (40%). Ca 15% of feldspars are retrogressed to sericite and clay minerals, ca 1% of biotite is retrogressed to chlorite.

MIG-6 Amphibole - biotite mylonite gneiss

The rock is intensely deformed, shows medium intensity planar fabric and consists of matrix (60%, grain size 0.05 - 0.2 mm) and porphyroclasts (40%, grain size 1.5 - 3 mm). Minerals present in the matrix are quartz (50%), plagioclase (30%), K-feldspar (10%), biotite (5%), amphibole (2%), opaque iron ore (1%),

apatite (<0.5%), zircon (<0.5%), titanite (<0.5%), allanite (<0.5%); minerals present as porphyroclasts are plagioclase (70%) and K-feldspar (30%). Ca 10% of feldspars are retrogressed to sericite and clay minerals, ca 5% of biotite is retrogressed to chlorite.

MIG-7 Biotite - plagioclase mylonite gneiss

The rock is intensely deformed, shows strong planar fabric and consists of matrix (90%, grain size 0.01 - 0.2 mm) and porphyroclasts (10%, grain size 0.7 - 1.5 mm). Minerals present in the matrix are quartz (40%), plagioclase (30%), K-feldspar (20%), biotite (2%), opaque iron ore (<0.5%), apatite (<0.5%), muscovite (<0.5%); minerals present as porphyroclasts are plagioclase (70%) and K-feldspar (20%). Ca 20% of feldspars are retrogressed to sericite and clay minerals, ca 10% of biotite is retrogressed to chlorite.

MIG-8 Amphibole - biotite mylonite gneiss

The rock is intensely deformed, shows weak planar fabric and consists of matrix (70%, grain size 0.05 - 0.2 mm) and porphyroclasts (30%, grain size 1 - 3 mm). Minerals present in the matrix are quartz (45%), plagioclase (30%), K-feldspar (20%), biotite (3%), amphibole (1%), opaque iron ore (<0.5%), apatite (<0.5%), titanite (<0.5%), allanite (<0.5%); minerals present as porphyroclasts are plagioclase (80%) and K-feldspar (20%). Ca 20% of feldspars are retrogressed to sericite and clay minerals, ca 10% of biotite is retrogressed to chlorite.

MIG-9 Amphibole - biotite mylonite gneiss

The rock is intensely deformed, shows medium intensity planar fabric and consists of matrix (70%, grain size 0.05 - 0.2 mm) and porphyroclasts (30%, grain size 1 - 3 mm). Minerals present in the matrix are quartz (40%), plagioclase (30%), K-feldspar (20%), biotite (5%), amphibole (3%), opaque iron ore (1%), apatite (<0.5%), titanite (<0.5%), zircon (<0.5%); minerals present as porphyroclasts are plagioclase (80%) and K-feldspar (20%). Ca 10% of feldspars are retrogressed to sericite and clay minerals.

MIG-10 Amphibole - biotite mylonite gneiss

The rock is intensely deformed, shows strong planar fabric and consists of matrix (60%, grain size 0.03 - 0.2 mm) and porphyroclasts (40%, grain size 1.5 - 3 mm). Minerals present in the matrix are plagioclase (35%), quartz (35%), K-feldspar (20%), biotite (3%), amphibole (1%), opaque iron ore (1.5%), zircon (<0.5%), titanite (<0.5%), allanite (<0.5%), epidote (<0.5%); minerals present as porphyroclasts are plagioclase (60%) and K-feldspar (40%). Ca 15% of feldspars are retrogressed to sericite and clay minerals, ca 5% of biotite is retrogressed to chlorite.

MIG-11 Garnet - biotite mylonite gneiss

The rock shows medium intensity deformation, weak planar to granoblastic fabric and consists of matrix (95%, grain size 0.05 - 1 mm) and porphyroclasts (5%, plagioclase, grain size 1.5 - 2 mm). Minerals present in the matrix are quartz (40%), plagioclase (30%), K-feldspar (20%), biotite (5%), garnet (2%),

opaque iron ore (<0.5%), zircon (<0.5%), titanite (<0.5%); minerals present as porphyroclasts are plagioclase (60%) and K-feldspar (40%). Ca 15% of feldspars are retrogressed to sericite and clay minerals.

MIG-12 Biotite mylonite gneiss

The rock is intensely deformed, shows weak planar fabric and consists of matrix (80%, grain size 0.01 - 0.2 mm) and porphyroclasts (20%, grain size 1 - 2 mm). Minerals present in the matrix are plagioclase (40%), quartz (30%), K-feldspar (20%), biotite (4%), opaque iron ore (1%), muscovite (<0.5%), epidote (<0.5%); minerals present as porphyroclasts are plagioclase (80%) and K-feldspar (20%). Ca 25% of feldspars are retrogressed to sericite and clay minerals, ca 10% of biotite is retrogressed to chlorite, ca 10% of ore mineral is retrogressed to iron hydro-oxides.

MIG-13 Biotite mylonite gneiss

The rock shows medium intensity deformation and weak planar fabric and consists of matrix (80%, grain size 0.03 - 0.2 mm) and porphyroclasts (20%, grain size 1 - 1.5 mm). Minerals present in the matrix are quartz (40%), plagioclase (35%), K-feldspar (20%), biotite (3%), opaque iron ore (<0.5%), muscovite (<0.5%); minerals present as porphyroclasts are plagioclase (60%) and K-feldspar (40%). Ca 30% of feldspars are retrogressed to sericite and clay minerals, ca 20% of biotite is retrogressed to chlorite.

MIG-14 Biotite mylonite gneiss

The rock is intensely deformed, shows medium intensity planar fabric and consists of matrix (60%, grain size 0.01 - 0.2 mm) and porphyroclasts (40%, grain size 1 - 2.5 mm). Minerals present in the matrix are quartz (40%), plagioclase (35%), K-feldspar (20%), biotite (3%), opaque iron ore (1%), muscovite (<0.5%), allanite (<0.5%), epidote (<0.5%); minerals present as porphyroclasts are plagioclase (75%) and K-feldspar (25%). Ca 25% of feldspars are retrogressed to sericite and clay minerals, ca 25% of biotite is retrogressed to chlorite.

MIG-15 Biotite mylonite gneiss

The rock is intensely deformed, shows medium intensity planar fabric and consists of matrix (70%, grain size 0.01 - 0.3 mm) and porphyroclasts (30%, grain size 1.5 - 2.5 mm). Minerals present in the matrix are quartz (40%), plagioclase (35%), K-feldspar (20%), biotite (3%), opaque iron ore (1%), muscovite (<0.5%), epidote (<0.5%); minerals present as porphyroclasts are plagioclase (60%) and K-feldspar (40%). Ca 15% of feldspars are retrogressed to sericite and clay minerals, ca 15% of biotite is retrogressed to chlorite, ca 10% of ore mineral is retrogressed to iron hydro-oxides.

MIG-16 Amphibole - biotite mylonite gneiss

The rock is intensely deformed, shows medium intensity planar fabric and consists of matrix (70%, grain size 0.01 - 0.3 mm) and porphyroclasts (30%, grain size 1 - 2.5 mm). Minerals present in the matrix are quartz (45%), plagioclase (35%), K-feldspar (15%), biotite (3%), amphibole (1%), opaque iron ore (<0.5%), titanite (<0.5%), epidote (<0.5%); minerals present as porphyroclasts are plagioclase (90%) and

K-feldspar (10%). Ca 25% of feldspars are retrogressed to sericite and clay minerals, ca 25% of biotite is retrogressed to chlorite.

MIG-17 Garnet - biotite mylonite gneiss

The rock shows medium intensity deformation, weak planar to granoblastic fabric and consists of matrix (95%, grain size 0.05 - 0.5 mm) and porphyroclasts (5%, grain size 1.5 - 2 mm). Minerals present in the matrix are quartz (65%), plagioclase (20%), K-feldspar (10%), biotite (2%), garnet (1%), opaque iron ore (1%), titanite (<0.5%), muscovite (<0.5%); minerals present as porphyroclasts are plagioclase (70%) and K-feldspar (30%). Ca 10% of feldspars are retrogressed to sericite and clay minerals.

MIG-18 Garnet - biotite mylonite gneiss

The rock shows medium intensity deformation, weak planar fabric and consists of matrix (95%, grain size 0.05 - 0.5 mm) and porphyroclasts (5%, grain size 1 - 1.5 mm). Minerals present in the matrix are quartz (45%), plagioclase (30%), K-feldspar (20%), biotite (3%), garnet (1%), opaque iron ore (<0.5%), allanite (<0.5%), titanite (<0.5%); minerals present as porphyroclasts are plagioclase (70%) and K-feldspar (30%). Ca 15% of feldspars are retrogressed to sericite and clay minerals, ca 15% of biotite is retrogressed to chlorite.

MIG-19 Amphibole - biotite mylonite gneiss

The rock is intensely deformed, shows medium intensity planar fabric and consists of matrix (55%, grain size 0.01 - 0.5 mm) and porphyroclasts (45%, grain size 1.5 - 3 mm). Minerals present in the matrix are quartz (50%), plagioclase (25%), K-feldspar (10%), biotite (10%), amphibole (2%), opaque iron ore (1%), titanite (<0.5%), allanite (<0.5%), zircon (<0.5%), apatite (<0.5%), epidote (<0.5%); minerals present as porphyroclasts are plagioclase (80%) and K-feldspar (20%). Ca 25% of feldspars are retrogressed to sericite and clay minerals, ca 10% of biotite is retrogressed to chlorite.

MIG-20 Biotite mylonite gneiss

The rock is intensely deformed, shows medium intensity planar fabric and consists of matrix (90%, grain size 0.01 - 0.5 mm) and porphyroclasts (10%, grain size 1 - 2 mm). Minerals present in the matrix are quartz (50%), plagioclase (35%), K-feldspar (10%), biotite (2%), opaque iron ore (<0.5%), titanite (<0.5%), muscovite (<0.5%); minerals present as porphyroclasts are plagioclase (90%) and K-feldspar (10%). Ca 15% of feldspars are retrogressed to sericite and clay minerals, ca 10% of biotite is retrogressed to chlorite.

MIG-21 Biotite mylonite gneiss

The rock is intensely deformed, shows strong planar fabric and consists of matrix (95%, grain size 0.01 - 0.08 mm) and porphyroclasts (5%, grain size 0.8 - 1 mm). Minerals present in the matrix are quartz (45%), plagioclase (35%), K-feldspar (10%), biotite (5%), muscovite (1%), opaque iron ore (1%), zircon (<0.5%), epidote (<0.5%); minerals present as porphyroclasts are plagioclase (80%), quartz (10%) and K-

feldspar (10%). Ca 25% of feldspars are retrogressed to sericite and clay minerals, ca 10% of biotite is retrogressed to chlorite.

MIG-22 Amphibole - biotite mylonite gneiss

The rock shows medium intensity deformation and weakly expressed planar fabric and consists of matrix (70%, grain size 0.05 - 0.5 mm) and porphyroclasts (30%, grain size 1.5 - 3 mm). Minerals present in the matrix are quartz (45%), plagioclase (30%), K-feldspar (10%), biotite (7%), amphibole (2%), opaque iron ore (1%), titanite (<0.5%), allanite (<0.5%), zircon (<0.5%), apatite (<0.5%); minerals present as porphyroclasts are plagioclase (80%) and K-feldspar (20%). Ca 5% of feldspars are retrogressed to sericite and clay minerals, ca 5% of biotite is retrogressed to chlorite.

MIG-23 Biotite mylonite gneiss

The rock shows medium intensity deformation and planar fabric and consists of matrix (80%, grain size 0.01 - 0.2 mm) and porphyroclasts (20%, grain size 1 - 1.5 mm). Minerals present in the matrix are quartz (40%), plagioclase (35%), K-feldspar (20%), biotite (10%), opaque iron ore (1%), titanite (<0.5%), zircon (<0.5%), apatite (<0.5%); minerals present as porphyroclasts are plagioclase (75%) and K-feldspar (25%). Ca 15% of feldspars are retrogressed to sericite and clay minerals, ca 1% of biotite is retrogressed to chlorite.

MIG-24 Amphibole - biotite mylonite gneiss

The rock is intensely deformed and recrystallized, it shows medium intensity planar fabric and consists of matrix (90%, grain size 0.01 - 0.5 mm) and porphyroclasts (10%, grain size 0.8 - 1 mm). Minerals present in the matrix are quartz (60%), plagioclase (25%), K-feldspar (5%), biotite (5%), amphibole (4%), opaque iron ore (<0.5%), zircon (<0.5%), titanite (<0.5%); minerals present as porphyroclasts are plagioclase (90%) and quartz (10%). Ca 5% of feldspars are retrogressed to sericite and clay minerals.

MIG-25 Biotite mylonite gneiss

The rock is intensely deformed, shows strong planar fabric and consists of matrix (95%, grain size 0.01 - 0.5 mm) and porphyroclasts (5%, grain size 0.8 - 1 mm). Minerals present in the matrix are quartz (55%), plagioclase (35%), K-feldspar (5%), biotite (5%), opaque iron ore (1%), zircon (<0.5%), apatite (<0.5%); minerals present as porphyroclasts are plagioclase (95%) and K-feldspar (5%). Ca 5% of feldspars are retrogressed to sericite and clay minerals, ca 10% of ore mineral is retrogressed to iron hydro-oxides.

MIG-26 Biotite - plagioclase mylonite gneiss

The rock shows medium intensity deformation and weak planar to granoblastic fabric and consists of matrix (85%, grain size 0.01 - 0.5 mm) and porphyroclasts (15%, grain size 1 - 2 mm). Minerals present in the matrix are quartz (40%), plagioclase (35%), K-feldspar (20%), biotite (1%), opaque iron ore

(<0.5%); minerals present as porphyroclasts are quartz (80%) and plagioclase (20%). Ca 10% of feldspars are retrogressed to sericite and clay minerals, ca 10% of biotite is retrogressed to chlorite.

MIG-27 Amphibole - biotite mylonite gneiss

The rock is intensely recrystallized, shows weak planar to granoblastic fabric and consists of matrix (90%, grain size 0.05 - 0.8 mm) and porphyroclasts (10%, quartz, grain size 2 - 3 mm). Minerals present in the matrix are quartz (50%), plagioclase (35%), K-feldspar (10%), biotite (3%), opaque iron ore (1%), titanite (<0.5%), zircon (<0.5%), apatite (<0.5%). Ca 1% of feldspars are retrogressed to sericite and clay minerals.

MIG-28 Biotite - amphibole mylonite gneiss

The rock is intensely recrystallized, shows weak planar to granoblastic fabric and consists of matrix (95%, grain size 0.01 - 0.5 mm) and porphyroclasts (5%, grain size 1 - 1.5 mm). Minerals present in the matrix are quartz (65%), plagioclase (20%), K-feldspar (5%), amphibole (5%), biotite (1%), opaque iron ore (<0.5%), allanite (<0.5%), epidote (<0.5%); minerals present as porphyroclasts are quartz (90%) and plagioclase (10%). Ca 15% of feldspars are retrogressed to sericite and clay minerals.

MIG-29 Biotite - plagioclase mylonite gneiss

The rock is intensely recrystallized, shows weak planar to granoblastic fabric and consists of matrix (90%, grain size 0.01 - 0.5 mm) and porphyroclasts (10%, grain size 1.5 - 3 mm). Minerals present in the matrix are quartz (45%), plagioclase (40%), K-feldspar (10%), biotite (2%), opaque iron ore (1%), titanite (<0.5%), apatite (<0.5%); minerals present as porphyroclasts are quartz (80%) and plagioclase (20%). Ca 15% of feldspars are retrogressed to sericite and clay minerals, ca 10% of biotite is retrogressed to chlorite.

MIG-30 Biotite mylonite gneiss

The rock is intensely deformed and shows medium intensity planar fabric. The grain size is within the range of 0.02 - 1 mm. Minerals present are plagioclase (45%), K-feldspar (20%), quartz (20%), biotite (10%), opaque iron ore (<0.5%), titanite (<0.5%), zircon (<0.5%), apatite (<0.5%). Ca 10% of feldspars are retrogressed to sericite and clay minerals.

MIG-31 Amphibole - biotite mylonite gneiss

The rock is intensely deformed, shows medium intensity planar fabric and consists of matrix (60%, grain size 0.01 - 0.3 mm) and porphyroclasts (40%, grain size 1.5 - 3 mm). Minerals present in the matrix are quartz (50%), plagioclase (35%), K-feldspar (8%), biotite (3%), amphibole (2%), opaque iron ore (1%), titanite (<0.5%), allanite (<0.5%), zircon (<0.5%), apatite (<0.5%); minerals present as porphyroclasts are plagioclase (80%) and K-feldspar (20%). Ca 10% of feldspars are retrogressed to sericite and clay minerals, ca 1% of biotite is retrogressed to chlorite.

MIG-32 Amphibole - biotite mylonite gneiss

The rock is intensely deformed, shows medium intensity planar fabric and consists of matrix (60%, grain size 0.05 - 0.2 mm) and porphyroclasts (40%, grain size 1.5 - 3 mm). Minerals present in the matrix are quartz (50%), plagioclase (30%), K-feldspar (10%), biotite (5%), amphibole (2%), opaque iron ore (1%), apatite (<0.5%), zircon (<0.5%), titanite (<0.5%), allanite (<0.5%); minerals present as porphyroclasts are plagioclase (70%) and K-feldspar (30%). Ca 10% of feldspars are retrogressed to sericite and clay minerals, ca 5% of biotite is retrogressed to chlorite.

MIS-1 K-feldspar biotite blastomylonite

The rock is intensely recrystallized and shows strong planar fabric. The grain size varies within the range of 0.01 - 0.5 mm. It consists of quartz (45%), K-feldspar (30%), plagioclase (15%), biotite (3%), opaque iron ore (1%), zircon (<0.5%). Ca 15% of feldspars are retrogressed to sericite and clay minerals, ca 5% of biotite is retrogressed to chlorite.

MIS-2 K-feldspar biotite mylonite schists

The rock is intensely recrystallized, shows strong planar fabric and consists of matrix (90%, grain size 0.05 - 0.2 mm) and porphyroclasts (10%, grain size 1.5 - 3 mm). Minerals present in the matrix are quartz (35%), plagioclase (30%), K-feldspar (30%), biotite (2%), opaque iron ore (<0.5%), zircon (<0.5%), muscovite (<0.5%); minerals present as porphyroclasts are K-feldspar (60%) and quartz (40%). Ca 10% of feldspars are retrogressed to sericite and clay minerals, ca 10% of biotite is retrogressed to chlorite.

MIS-3 K-feldspar biotite blastomylonite

The rock is intensely recrystallized, shows weak planar fabric and consists of matrix (90%, grain size 0.02 - 0.3 mm) and porphyroclasts (10%, grain size 1.5 - 2.5 mm). Minerals present in the matrix are quartz (40%), plagioclase (30%), K-feldspar (25%), biotite (2%), opaque iron ore (1%), zircon (<0.5%); minerals present as porphyroclasts are K-feldspar (80%) and quartz (20%). Ca 5% of feldspars are retrogressed to sericite and clay minerals, ca 5% of biotite is retrogressed to chlorite, ca 10% of ore mineral is retrogressed to iron hydro-oxides.

MIS-4 K-feldspar biotite blastomylonite

The rock is intensely recrystallized, shows strong planar fabric and consists of matrix (95%, grain size 0.01 - 0.08 mm) and porphyroclasts (5%, grain size 0.5 - 0.8 mm). Minerals present in the matrix are quartz (35%), plagioclase (30%), K-feldspar (30%), biotite (3%), opaque iron ore (1%), zircon (<0.5%); minerals present as porphyroclasts are K-feldspar (90%) and quartz (10%). Ca 25% of feldspars are retrogressed to sericite and clay minerals, ca 25% of biotite is retrogressed to chlorite.

MIS-5 K-feldspar biotite mylonite schist

The rock is intensely recrystallized, shows strong planar fabric and consists of matrix (80%, grain size 0.05 - 0.1 mm) and porphyroclasts (20%, grain size 1.5 - 2.5 mm). Minerals present in the matrix are quartz (40%), plagioclase (30%), K-feldspar (25%), biotite (2%), muscovite (2%), opaque iron ore (<0.5%), zircon (<0.5%); minerals present as porphyroclasts are K-feldspar (90%) and quartz (10%). Ca 10% of feldspars are retrogressed to sericite and clay minerals some of which are recrystallized to muscovite (0.5 mm in size), ca 10% of biotite is retrogressed to chlorite.

MIS-6 K-feldspar biotite mylonite schist

The rock is intensely recrystallized, shows strong planar fabric and consists of matrix (80%, grain size 0.01 - 0.05 mm) and porphyroclasts (20%, grain size 1.5 - 2 mm). Minerals present in the matrix are quartz (35%), plagioclase (30%), K-feldspar (30%), biotite (4%), opaque iron ore (<0.5%), zircon (<0.5%); minerals present as porphyroclasts are quartz (60%), K-feldspar (30%) and plagioclase (10%). Ca 10% of feldspars are retrogressed to sericite and clay minerals.

MIS-7 K-feldspar biotite mylonite schist

The rock shows weak deformation and weak planar fabric and consists of matrix (60%, grain size 0.01 - 0.3 mm) and porphyroclasts (40%, grain size 1.5 - 5 mm but some K-feldspar porphyroclasts are up to 1.3 cm in size). Minerals present in the matrix are quartz (45%), plagioclase (20%), K-feldspar (20%), biotite (10%), opaque iron ore (1%), zircon (<0.5%), apatite (<0.5%); minerals present as porphyroclasts are K-feldspar (80%) and plagioclase (20%). Ca 2% of feldspars are retrogressed to sericite and clay minerals. The coarse-grained parts of the rock represent less deformed equivalent of K-feldspar biotite blastomylonite

MIS-8 K-feldspar biotite mylonite schist

The rock is intensely recrystallized, shows strong planar fabric and consists of matrix (90%, grain size 0.01 - 0.05 mm) and porphyroclasts (10%, grain size 1.5 - 2 mm). Minerals present in the matrix are quartz (35%), plagioclase (35%), K-feldspar (25%), biotite (2%), opaque iron ore (<0.5%), zircon (<0.5%); minerals present as porphyroclasts are quartz (50%) and K-feldspar (50%). Ca 30% of feldspars are retrogressed to sericite and clay minerals, ca 10% of biotite is retrogressed to chlorite.

MIS-9 K-feldspar biotite mylonite schist

The rock is intensely recrystallized, shows strong planar fabric and consists of matrix (80%, grain size 0.01 - 0.03 mm) and porphyroclasts (20%, grain size 1 - 2 mm). Minerals present in the matrix are quartz (40%), plagioclase (30%), K-feldspar (25%), biotite (3%), muscovite (1%), opaque iron ore (1%), apatite (<0.5%), zircon (<0.5%); minerals present as porphyroclasts are K-feldspar (50%), quartz (30%) and plagioclase (20%). Ca 40% of feldspars are retrogressed to sericite and clay minerals.

MIS-10 K-feldspar biotite blastomylonite

The rock is intensely recrystallized, shows weak planar fabric and consists of matrix (85%, grain size 0.02 - 0.3 mm) and porphyroclasts (15%, grain size 1 - 2.5 mm). Minerals present in the matrix are quartz (40%), plagioclase (30%), K-feldspar (25%), biotite (2%), opaque iron ore (1%), zircon (<0.5%); minerals present as porphyroclasts are K-feldspar (80%) and quartz (20%). Ca 3% of feldspars are retrogressed to sericite and clay minerals, ca 2% of biotite is retrogressed to chlorite, ca 5% of ore mineral is retrogressed to iron hydro-oxides.

MIS-11 K-feldspar biotite mylonite schist

The rock is intensely recrystallized, shows strong planar fabric and consists of matrix (85%, grain size 0.01 - 0.05 mm) and porphyroclasts (15%, grain size 1.5 - 2 mm). Minerals present in the matrix are quartz (35%), plagioclase (30%), K-feldspar (30%), biotite (4%), opaque iron ore (<0.5%), zircon (<0.5%); minerals present as porphyroclasts are quartz (60%), K-feldspar (30%) and plagioclase (10%). Ca 10% of feldspars are retrogressed to sericite and clay minerals.

STG-A Amphibole - biotite mylonite gneiss

The rock shows medium intensity deformation and planar fabric and consists of matrix (80%, grain size 0.01 - 0.15 mm) and porphyroclasts (20%, grain size 1 - 1.5 mm). Minerals present in the matrix are plagioclase (40%), quartz (30%), K-feldspar (20%), biotite (4%), amphibole (2%), opaque iron ore (1%), apatite (<0.5%), zircon (<0.5%); minerals present as porphyroclasts are plagioclase (70%) and K-feldspar (30%). Ca 10% of feldspars are retrogressed to sericite and clay minerals, ca 2% of biotite is retrogressed to chlorite.

STG-B Amphibole - biotite mylonite gneiss

The rock shows medium intensity deformation and planar fabric and consists of matrix (70%, grain size 0.05 - 0.2 mm) and porphyroclasts (30%, grain size 1 - 2 mm). Minerals present in the matrix are plagioclase (50%), quartz (30%), K-feldspar (10%), biotite (5%), amphibole (3%), opaque iron ore (1%), apatite (<0.5%), zircon (<0.5%), allanite (<0.5%); minerals present as porphyroclasts are plagioclase (90%) and K-feldspar (10%). Ca 10% of feldspar porphyroclasts are retrogressed to sericite and clay minerals, ca 5% of biotite is retrogressed to chlorite.

STG-C Amphibole - biotite mylonite gneiss

The rock is intensely deformed, shows medium intensity planar fabric and consists of matrix (85%, grain size 0.01 - 0.1 mm) and porphyroclasts (15%, grain size 0.8 - 2 mm). Minerals present in the matrix are plagioclase (45%), quartz (30%), K-feldspar (10%), biotite (7%), amphibole (3%), opaque iron ore (1%), epidote (1%), titanite (<0.5%), zircon (<0.5%), allanite (<0.5%); minerals present as porphyroclasts are plagioclase (50%), quartz (35%) and K-feldspar (15%). Ca 10% of feldspars are retrogressed to sericite and clay minerals, ca 4% of biotite is retrogressed to chlorite, ca 1% of iron ore is retrogressed to iron hydro-oxides.

LG-A Biotite mylonite gneiss

The rock is intensely deformed and recrystallized, shows weak planar to granoblastic fabric and consists of matrix (95%, grain size 0.01 - 0.4 mm) and porphyroclasts (5%, grain size 1 - 2 mm). Minerals present in the matrix are plagioclase (40%), quartz (35%), K-feldspar (15%), muscovite (3%), biotite (1%), opaque iron ore (1%), titanite (<0.5%), zircon (<0.5%); minerals present as porphyroclasts are quartz (70%) and plagioclase (30%). Ca 20% of feldspars are retrogressed to sericite and clay minerals some of which are recrystallized to muscovite, ca 1% of biotite is retrogressed to chlorite, ca 1% of iron ore is retrogressed to iron hydro-oxides.

LG-B Biotite mylonite gneiss

The rock is intensely deformed, shows strong planar fabric and consists of matrix (85%, grain size 0.01 - 0.2 mm) and porphyroclasts (15%, grain size 0.8 - 2 mm). Minerals present in the matrix are plagioclase (40%), quartz (40%), K-feldspar (10%), biotite (7%), opaque iron ore (1%), apatite (<0.5%), zircon (<0.5%); minerals present as porphyroclasts are quartz (60%) and plagioclase (40%). Ca 5% of feldspars are retrogressed to sericite and clay minerals.

LG-C Biotite mylonite gneiss

The rock is intensely deformed and recrystallized, shows weak planar to granoblastic fabric. The grain size varies within the range of 0.01 - 2 mm. Minerals present are plagioclase (45%), quartz (40%), K-feldspar (10%), biotite (3%), opaque iron ore (1%), titanite (<0.5%), apatite (<0.5%). Ca 10% of feldspars are retrogressed to sericite and clay minerals, ca 1% of biotite is retrogressed to chlorite.

MIG-A Amphibole - biotite mylonite gneiss

The rock is intensely deformed, shows medium intensity planar fabric and consists of matrix (60%, grain size 0.01 - 0.3 mm) and porphyroclasts (40%, grain size 1.5 - 3 mm). Minerals present in the matrix are quartz (50%), plagioclase (35%), K-feldspar (8%), biotite (3%), amphibole (2%), opaque iron ore (1%), titanite (<0.5%), allanite (<0.5%), zircon (<0.5%), apatite (<0.5%); minerals present as porphyroclasts are plagioclase (80%) and K-feldspar (20%). Ca 10% of feldspars are retrogressed to sericite and clay minerals, ca 1% of biotite is retrogressed to chlorite.

MIG-B Amphibole - biotite mylonite gneiss

The rock is intensely deformed, shows medium intensity planar fabric and consists of matrix (60%, grain size 0.05 - 0.2 mm) and porphyroclasts (40%, grain size 1.5 - 3 mm). Minerals present in the matrix are quartz (50%), plagioclase (30%), K-feldspar (10%), biotite (5%), amphibole (2%), opaque iron ore (1%), apatite (<0.5%), zircon (<0.5%), titanite (<0.5%), allanite (<0.5%); minerals present as porphyroclasts are plagioclase (70%) and K-feldspar (30%). Ca 10% of feldspars are retrogressed to sericite and clay minerals, ca 5% of biotite is retrogressed to chlorite.

MIS-A K-feldspar biotite blastomylonite

The rock is intensely recrystallized, shows weak planar fabric and consists of matrix (85%, grain size 0.02 - 0.3 mm) and porphyroclasts (15%, grain size 1 - 2.5 mm). Minerals present in the matrix are quartz (40%), plagioclase (30%), K-feldspar (25%), biotite (2%), opaque iron ore (1%), zircon (<0.5%); minerals present as porphyroclasts are K-feldspar (80%) and quartz (20%). Ca 3% of feldspars are retrogressed to sericite and clay minerals, ca 2% of biotite is retrogressed to chlorite, ca 5% of ore mineral is retrogressed to iron hydro-oxides.

RC-2274 Amphibole - biotite mylonite gneiss

The rock shows medium intensity deformation and planar fabric and consists of matrix (70%, grain size 0.05 - 0.2 mm) and porphyroclasts (30%, grain size 1 - 3 mm). Minerals present in the matrix are plagioclase (50%), quartz (30%), K-feldspar (10%), biotite (5%), amphibole (4%), opaque iron ore (<0.5%), apatite (<0.5%), zircon (<0.5%); minerals present as porphyroclasts are plagioclase (90%) and K-feldspar (10%). Ca 15% of feldspar porphyroclasts are retrogressed to sericite and clay minerals, ca 10% of biotite is retrogressed to chlorite.

RC-2284 Amphibole - biotite mylonite gneiss

The rock is intensely deformed, shows medium intensity planar fabric and consists of matrix (60%, grain size 0.05 - 0.2 mm) and porphyroclasts (40%, grain size 1.5 - 3 mm). Minerals present in the matrix are quartz (50%), plagioclase (30%), K-feldspar (10%), biotite (5%), amphibole (2%), opaque iron ore (1%), apatite (<0.5%), zircon (<0.5%), titanite (<0.5%), allanite (<0.5%); minerals present as porphyroclasts are plagioclase (70%) and K-feldspar (30%). Ca 10% of feldspars are retrogressed to sericite and clay minerals, ca 5% of biotite is retrogressed to chlorite.